Studying the Effect of Diabetes and Hyperglycaemia on Brain Vascular Cells

Gabriel Rocha

Supervisors:

Dr. Zameel Cader

Dr. Hannah Sleven



Submitted to the Graduate School of the University of Oxford for the degree of

DOCTOR OF PHILOSOPHY

June 2024

Nuffield Department of Clinical Neurosciences

Contents

Abstract 4

Introduction: 5

The Blood Brain Barrier In Health and Disease 11

Brain Microvascular Endothelial Cells 13

Pericytes 14

Astrocytes 15

Diabetes And The Brain 16

Diabetes and Atherosclerotic Pathology 18

Global Brain Atrophy 18

Brain regional effects of diabetes 19

Diabetes and Alzheimer Pathology 21

Diabetes Effects on Endothelial Cells - Mechanisms 22

G3P Accumulation and the AGE pathway 23

G3P, DAG, Accumulation, and Protein Kinase C Pathway 24

Fructose-6-phosphate and the Hexosamine Pathway 24

Glucose and the Polyol Pathway 25

Blood Brain Barrier Research Models 26

Thesis Outline 33

Chapter 1: Development of a Novel IPSC-BMEC Differentiation Using Transcription Factor Overexpression 34

Introduction 34

Results 37

Identification of Novel Transcription Factors for the Differentiation of IPSCs into BMECs 37

Lentiviral Delivery Platform Optimization 38

BMEC Differentiation Protocol Development and Optimization 48

Clumped Cells Act as an Endothelial Factory 66

AraC and DAPT are Unable to Resolve Final Culture Contamination due to Toxicity 82

Discussion 92

Chapter 2: Development of a Novel IPSC BMEC Differentiation Protocol Using CRISPR Transcription Factor Gene Activation 98

Introduction 98

RESULTS 100
Transfection Optimization 102
Endothelial Differentiation Using CRISPR Activation 110
DISCUSSION 114
Chapter 3: The Effects of Hyperglycaemia on Primary Mouse BMECs 116
INTRODUCTION 116
RESULTS 117
Barrier Integrity 120
Glucose Consumption 121
Inflammation 123
ROS 126
Nitric Oxide 128
DISCUSSION 130
Chapter 4: Transcriptomic Analysis of the Neurovascular Unit in Diabetic Cortical Tissue 133
INTRODUCTION 133
Challenges in single cell gene expression studies of brain vascular cells 135
RESULTS 137
Protocol Development 137
Sample Selection 138
Sample Processing Optimization: 140
Sample Processing 145
Donor Clinical Details 152
Differential Gene Expression and Pathway Analysis 155
DISCUSSION 161
Concluding Remarks: 169
Methods: 172
SUPPLEMENTAL METHODS 184
Collaboration Declaration / Acknowledgements 203
References 206

Abstract

Type II Diabetes Mellitus (T2DM) is a metabolic disease characterised by insulin resistance and hyperglycaemia. Despite extensive research on the pathology of diabetes in various organs, the effect on the brain's neurovascular unit remains understudied. This neurovascular unit is arguably the fundamental functional unit of the brain and mediates the communication between the systemic circulation and the brain and establishing the blood-brain-barrier (BBB). It is crucial for adjusting the BBB microenvironment by regulating nutrient uptake and toxin removal from the brain. The work in this thesis utilises *in vitro* models and transcriptomic analysis of human post-mortem of diabetic frontal cortex to explore how hyperglycaemia and hyperglycaemia affects brain microvascular endothelial cells (BMECs). Validating mechanistic hypotheses requires relevant BBB models. Existing models range from immortalized cell lines, primary cultures, or human induced pluripotent stem cell (iPSC) models each with several limitations. In this study, forced expression of the transcription factor genes LEF1, ETS1, and MRTFB was investigated as means to improve iPSC-BMEC differentiation. This approach resulted in improved cultures of BMECs with clear endothelial cell identity based on high expression of VE-CADHERIN, PECAM1, as well as expression of CLDN5. Expression of the three transcription genes was investigated using lentiviral over-expression as well as CRISPR-based gene activation, with the latter proving insufficient to robustly induce BMEC identity. Mouse primary BMECs cultures were used to investigate the effects of hyperglycaemia whilst single nuclei RNA sequencing was applied to characterise the molecular state of brain endothelial cells in diabetes. Surprisingly, both approaches found little or no effect on BMECs biology. In contrast hypertension was associated with 1008 differentially expressed genes, indicating increased BBB vulnerability to hypertension. Altered pathways include hypoxia, synaptic health, and axon guidance. This research challenges existing paradigms, suggesting BBB protection from diabetic insults and vulnerability to hypertension. The proposed BMEC differentiation protocol, particularly through forced lentiviral expression, advances the models available for future disease-mechanism research.

Introduction:

Type II diabetes mellitus (T2DM) is one of the world's most prevalent diseases, with approximately 500 million reported cases globally in 2018 [1]. Characterized by insufficient insulin or not being able to respond to insulin (insulin resistance), the immediate consequence is elevated blood glucose levels (hyperglycaemia). Insulin is an important hormone secreted to maintain homeostatic metabolism. Pancreatic β-cells are able to detect changes in plasma glucose levels and release precise amounts of insulin to correct deviations of blood glucose concentrations. β-cells are clustered into islets connected to the vasculature, which is fenestrated to allow for greater nutrient exchange, β-cell nutrient sensing, and rapid insulin secretion into the vasculature [2]. β-cells express two key proteins that allow for precise glucose sensing: GLUT2 and glucokinase. GLUT2 is a glucose transporter, and the only type expressed in pancreatic β-cells. It is mobilized to the plasma membrane in an insulin-independent manner. It has a low glucose substrate affinity, allowing for high glucose influx into β-cells for accurate glucose sensing [3]. While GLUT2 rapidly imports glucose, glucokinase acts as the actual glucose concentration sensor. The conversion of glucose to glucose-6-phosphate leads to an increase in intracellular ATP levels, which closes the ATP-sensitive KATP channel. This closure leads to beta-cell membrane depolarisation and calcium influx through the activation of calcium channels [4], triggering insulin exocytosis [5]. Glucokinase is only expressed in four types of cells: hepatic cells, β-cells, enterocytes, and glucose-sensitive neurons. It has a low affinity for glucose, with its K_M of 6 mM falling around normoglycaemic levels (5.5mM), and also is not inhibited by its product, preventing a negative feedback loop that would reduce glucokinase availability and thus reduce β-cell glucose sensing [6].

Oral ingestion of 75g glucose leads plasma insulin concentrations to rise from basal level (20-30 pM) to elevated levels (250-300 pM). While glucose is primarily responsible for β-cell insulin regulation, amino acids such as alanine, glutamine, and glutamate also have the ability to induce insulin secretion [7]. Additionally, fatty acids, particularly non-esterified fatty acids, can increase

insulin release from β-cells [8]. Ingestion of 75g protein or fat only increases insulin to 50-60pM in humans [9].

Once secreted, insulin can act on several tissues, including muscle [10], adipose tissue, liver, the endothelium [11], the brain [12], kidney [13], gonads [14], and bone [15]. Specifically in the rat CNS, all regions contain varying levels of the insulin receptor, with the olfactory bulb and cerebral cortex displaying highest receptor availability and the pituitary the least [16]. Insulin receptors in these tissues are heterotetramers composed of 2α and 2β glycoprotein subunits [17]. Insulin binds to the extracellular α subunit, which results in a conformational change in the intracellular β subunit, allowing for ATP binding, and subsequent tyrosine kinase activation. This activation allows for phosphorylation of insulin responsive substrates (IRS), which can bind further intracellular signalling molecules to mediate cellular responses to insulin [17].

The cellular effects of insulin release lead to increased glycolysis and reduced gluconeogenesis by dephosphorylation of pyruvate kinases. It is also able to promote conversion of pyruvate into acetyl co-A by activating pyruvate dehydrogenase. This allows for higher flux of substrates into the TCA cycle or for fatty acid synthesis. The increased consumption of glucose leads to a reduction of blood glucose concentration. In liver and muscle, insulin also promotes the uptake and then conversion of glucose to glycogen to further reduce blood glucose concentration. Skeletal muscle in particular acts a glucose sink in response to insulin, with up to 80% of glucose uptake occurring in skeletal myocytes [18]. Insulin triggers the PI3K-AKT signalling pathway, leading to the relocation of GLUT4 to the plasma membrane in skeletal myocytes [19].

The effects of insulin on endothelial cells varies according to their local microenvironment [20]. Brain endothelial cells are responsible for transferring insulin into the brain through the insulin receptor, although insulin receptor knock-out mice are still able to transport insulin (albeit at lower levels) through other insulin receptors such as IGF-1 [21, 22]. Intracellular effects of insulin on brain endothelial cells include release of nitric oxide and intracellular calcium in a bi-phasic manner,

inducing vasoconstriction at insulin concentrations of 0.1ng/ul and vasodilation above 1ng/ul [23, 24].

Insulin can also act through insulin-like growth factor receptors (IGFRs). IGFs are distinct growth hormones that share structural homology to insulin, and can stimulate cell growth, proliferation, and cell differentiation. While insulin affinity to IGFRs is lower than the insulin receptor, this shared overlap in ligand/receptor binding allows for insulin to affect cellular functions beyond glucose metabolism [4].

In addition to the homeostatic role of the pancreas, the hypothalamus also plays a key part through "counter-regulatory responses" (CRRs) mediated glucose-sensing neurons in the hypothalamic ventromedial nucleus. Activation of these hypothalamic neurons increases brain glucose levels through CRRs usually triggered by hypoglycaemia [25]. These CRRs include inhibition of glucose-stimulated insulin release and increased secretion of glucagon and corticosterone. The hormone leptin also has an important role. Its release from adipose tissue signals to the hypothalamus to reduce glucagon secretion from pancreatic α-cells and thereby reducing blood glucose levels [26, 27].

The brain is perhaps the primary consumer of glucose, using up to 20% of the body's glucose. Within the brain, much of the glucose is taken up by astrocytes [28], which is converted to lactate and then shuttled to neurons as their principal energy source. A healthy brain vasculature that is able to provide the brain with sufficient glucose levels is important for ensuring healthy brain function. Brain tissue glucose levels are generally lower than peripheral levels, with ~2.5mM glucose in brain areas (dependent on local activity) compared to 5mM peripherally. Under hyperglycaemic conditions (up to 20mM), the brain glucose concentration rises to 5mM [29]. This may all be a reflection of the heavy consumption of glucose by the brain with the lack of glucose uptake regulatory mechanism – that is if the glucose is available, it is utilised.

Insulin has important functions in the brain, including cognition, memory, nutrient homeostasis, and reproduction [30]. Most brain cells uptake glucose via either GLUT1 or GLUT3, both insulin-independent glucose transporters, indicating that the effects of insulin in the brain are primarily not directly related to cell glucose uptake [31]. In neurons, insulin is involved in neuronal circuitry formation, synaptic health, and dendritic arborization [32]. Lower levels of insulin in the brain have been proposed to lead to Alzheimer's Disease [31], potentially linking the neurodegenerative disease to diabetes. Impairment of insulin delivery to neurons leads to increased neuronal apoptosis via activation of forkhead box O (FoxO) [33].

Systemic Effects of Diabetes

Diabetes insults involve both micro and macrovessels systemically, termed as diabetic panvascular disease (DPD) [34]. Vessels residing in different organs contain different microenvironments that lead to organ-specific injury via differing mechanical and biochemical signals from neighbouring cells. Generally, two systems govern the dynamics of blood vessels: the renin-angiotensin-aldosterone system (RAAS) and the sympathetic nervous system (SNS). RAAS is responsible for controlling blood volume, vascular tone, and blood pressure [35], while the SNS regulates vasoconstriction and vasodilation [36]. Irregularities in these systems due to diabetes affect microvessels and macrovessels in different ways due to their inherent physical and environmental differences. Macroangiopathy is associated with atherosclerosis while microangiopathy results in basement membrane thickening, increase in platelet and red blood cell adhesion, and microthrombosis [34]. Inflammation also accompanies these angiopathic manifestations systemically. The following section will review specific diabetic insults to different extracranial organs in the body.

Heart

Diabetes can lead to diabetic heart disease (DHD), involving coronary artery disease (CAD) and cardiomyopathy. Diabetic patients with DHD have an increased risk of death [37]. Patients experience functional changes in myocardial microvasculature before structural alterations, ultimately leading to

significant macrovascular atherosclerosis. Diabetic cardiomyopathy (DCM) denotes specific anomalies in myocardial structure and function. DCM is characterized by left ventricular hypertrophy, myocardial fibrosis, cell necrosis, and other structural changes, leading to heart failure as the primary injury of chronic cardiovascular complications in diabetes [38]. The myocardium's involvement in the secretion of vasoactive metabolites or neuromodulation contributes to changes in coronary artery wall pressure and endothelial shear stress, leading to atherosclerosis.

The myocardium demands high levels of energy and oxygen, relying primarily on fatty acid oxidation (FAO) and aerobic glucose oxidation as its main energy sources [39]. Insulin resistance contributes to heightened lipid synthesis in hepatocytes and increased lipolysis in adipocytes, resulting in elevated levels of circulating fatty acids and triglycerides [40]. The accumulation of lipids and the lipotoxic effects of fatty acids can disrupt myocardial FAO processes, triggering endoplasmic reticulum (ER) stress, autophagy, and apoptosis [41]. Inflammation triggered by hyperglycaemia upregulates membrane cofactor protein-1 (MCP-1) and NLR family pyrin domain containing 3 inflammasome (NLPR3) expression, leading to fibrosis and cardiac dysfunction [42].

KIDNEY

Diabetic kidney disease (DKD) is the primary factor leading to the development of end-stage renal disease, and up to 40% of patients with diabetes develop DKD [43] [44]. Macrovascular damage includes atherosclerosis and hypertension, which can lead to microvascular damage in glomerular and tubulointerstitial capillaries [45] [46]. Hyperglycaemia also elevates glomerular capillary pressure by RAAS-mediated upregulation of angiotensin II [47]. Further, increased plasma levels of coagulant factors such as kallikrein and thrombin seen in diabetic patients may lead to injury in the kidney vasculature [48].

The kidney also experiences inflammation via the release of cytokines, chemokines, and adhesion molecules in DKD. These responses lead to nephron injury through ultrafiltration, mechanical stress, glycocalyx dysfunction, and endothelial activation through increased expression of

endothelin-1 receptors [49]. Further, inflammation is observed in diabetic kidneys via upregulation of inflammatory markers IL-1, IL-6, IL-18, and TNF-α [50].

Retina

Diabetic retinopathy (DR) is a common microvascular complication in T2DM, with 25.1% of diabetics developing retinal disease [51]. DR is identified by loss of retinal capillary epithelial cells, decreased capillary elasticity, increased vascular permeability, inflammation, and accelerated neovascularization [52].

Elevated levels of VEGF govern the increased neovascularization seen in diabetic patients [53]. A study has found that diabetic patients resistant to diabetic retinopathy contain elevated levels of retinol binding protein 3 (RBP3), and this elevation protects the retina from uncontrolled neovascularization induced by hyperglycaemia and reduces levels of inflammatory cytokine IL-6 [54].

Inflammation in DR is widespread and involves several classical inflammatory marker secretions from various retinal cells. Retinal pigment epithelial and muller cells can release IL-1β, which activates NF-kB and increases oxidative damage to endothelial cells, increasing permeability, vascularization, inflammation through IL-6, and apoptosis [55, 56]. Muller cells can also release TNF-α which promotes cell apoptosis and mitophagy [57].

The blood-retinal-border (BRB) is subject to considerable deterioration through several glycolysis-related pathways such as the diacylglycerol-PKC pathway, polyol pathway, hexosamine pathway and AGE-RAGE pathway [34] (described in depth in Diabetes Effects on Endothelial Cells-Mechanisms section below).

Periphery

Diabetic peripheral vasculopathy (DPVD) includes insults to peripheral arteries and vessels, and is closely associated with large artery atherosclerosis which leads to systemic microangiopathy [58]. Clinical outcomes of DPVD include limb amputation, which occurs when DPVD is accompanied

by diabetic neuropathy and atherosclerosis [59]. Abnormal peripheral neuro-metabolism alters sphingolipid metabolism, leading to peripheral neurotoxicity in patients with hyperglycemia [60]. General atherosclerosis, increased inflammation processes, and neuropathy altogether lead to peripheral infection and ulcer formation, which ultimately may require amputation to limit further damage to the body [34].

In conclusion, diabetes has significant adverse effects on the vasculature of the kidney [61], heart [62], retina [52], and periphery [63]. The effects may be mediated by the elevated levels of glucose or a consequence of impaired insulin secretion or insulin response. In trying to understand the effects of diabetes on the brain, the logical first site to investigate is the brain vasculature, which remains relatively underexplored. This introduction aims to describe how T2DM may detrimentally affect the brain vasculature and overall brain health, beginning with an examination of the BBB in both general health and disease states.

The Blood Brain Barrier In Health and Disease

The brain has a unique vascular supply, with specialized endothelial cells that express tight junctions and transport proteins to selectively control the flow of solutes into and out of the brain through a tight barrier. This barrier tightness was first observed by German scientist Paul Ehrlich in 1885, who injected adult animals with a variety of dyes and observed that all organs, except the brain and spinal cord, were stained [64]. A decade later, Bield and Kraus observed that injecting cholic acids or sodium ferrocyanide directly into the bloodstream did not results in any observable effects on the CNS. However, when the same substances were administered directly into the brain's ventricles, neurological symptoms were observed [65]. This led Lewandowsky to first term this phenomenon as the "Blood Brain Barrier." [66] Finally, in 1967, with the advances in light and electron microscopy, Karnovsky was able to show at an ultrastructural level the localisation of the BBB. Through intravenous injection in mice of horseradish peroxidase (40 kDa), Karnovsky found that

HRP signal was secluded to the first luminal inter-endothelial tight junction in the brain, whereas HRP could freely pass through capillaries in cardiac and skeletal muscle [67]. Karnovsky was able to determine that the barrier was constructed from the plasma membrane and cell bodies of endothelial cells, along with tight junctions between neighbouring cells. These TJs tightly seal the narrow space between adjacent cells, forming continuous rows known as zonulae occludentes. Using freeze fracture techniques, Nagy et al. demonstrated that the tight junctions between endothelial cells in capillaries and venules of the central nervous system (CNS) are organized into 6-8 parallel strands with intricate net-like connections spanning the entire upper circumference of the endothelial cell [68, 69]. Studies ran at the same time also confirmed a distinct relationship between brain endothelial cells and glial cells. Davson and Olendorf observed and suggested that astrocytes, due to their close proximity, could be responsible for the development of the specific BBB [70]. Later studies supported this hypothesis, showing that *in vitro* brain endothelial cells experience a significant increase of tight junctions when co-cultured with astrocytes [71].

Thus, these brain capillary endothelial cells (BMECs), form the blood-brain-barrier (BBB). BMECs have a polarity – a luminal side exposed to the systemic circulation and an abluminal side which interfaces with the parenchyma. The BBB also contains a distinctive basement membrane mainly consisting of collagen IV, laminin, nidogen and perlecan [72]. Notably, the basement membrane in the BBB has laminin α4, mainly produced by pericytes during embryonic development, and astrocytes in adulthood [73], which contributes to barrier integrity. Mice with impaired laminin production develop hydrocephaly, reduction in pericyte coverage, reduced aquaporin 4 (AQP4), and tight junction proteins [74]. Other cells are also critical for the BBB. Pericytes and astrocytic end-feet envelop the abluminal aspect of capillaries. Neurons, oligodendrocytes, and microglia reside in close proximity. This integrated system is referred to as the neurovascular unit, emphasizing the interdependence of the vascular and nervous systems, wherein alterations in one component can significantly impact the other.

Brain Microvascular Endothelial Cells

Brain microvascular endothelial cells (BMECs) play a pivotal role in safeguarding the brain from environmental influences. BMECs are characterized by the absence of fenestrations and close apposition through tight junctions. These tight junctions create a robust barrier preventing paracellular diffusion of molecules and ions. Tight junctions are comprised of transmembrane proteins including CLDNs (CLDN5, CLDN12), Occludin (OCLN), and junctional adhesion molecules (JAMs) (JAM-A, JAM-4). To further fortify the barrier, tight junctions are attached to the endothelial cytoskeleton by the ZO family of cytoplasmic TJ proteins. Mice with ZO-1 deletion observed mislocalization of JAM-A and impaired endothelial angiogenesis [75]. Deletion of ZO proteins in epithelial cells lead to deficient barrier formation, but expression of ZO-1 or ZO-2 alone can re-establish barrier integrity [76].

In addition to tight junctions, adherens junctions are also present in the blood-brain-barrier. PECAM1 (CD31) and VE-CADHERIN (CD144), anchored to the cytoskeleton by catenin molecules, act as transcellular adhesives, further binding endothelial cells together and reinforcing barrier integrity [77]. Notably, several of these proteins are individually found in other vascular tissues throughout the body, but exceptional tightness of the blood brain barrier suggests that a diverse array of junctional proteins are necessary to induce a healthy BBB with sufficient barrier integrity [78].

Brain microvascular endothelial cells play a pivotal role in the central nervous system as they are highly polarized cells that facilitate the transport of essential nutrients, including glucose, lactate, amino acids, and ions into the brain. The precise regulation of nutrient transport by specific transporters such as GLUT1, MCT1, LAT1 (SLC7A5), and Tfr is crucial for maintaining proper neuronal and glial function [79]. Genetic abnormalities affecting these transporters, such as GLUT1 deficiency and SLC7A5 mutations, which can cause brain disorders, underscore the vital role of BMECs in

ensuring adequate nutrient supply to the brain. GLUT1 deficiency is a cause of epilepsy and SLC7A5 mutations are associated with autism spectrum disorder and motor deficits [80, 81].

Beyond nutrient transport, BMECs are equally important in clearing toxins and metabolic waste products from the brain. Efflux transporters, notably P-glycoprotein (PGP) and LRP1, actively contribute to this detoxification process. PGP, a well-studied efflux transporter, plays a crucial role in actively transporting a broad range of hydrophobic compounds out of the brain. PGP is a major reason that many drugs have low CNS bioavailability. Mice with PGP deletion have a significant increase in drug penetrance into the brain due to the impaired ability to pump drugs out [82]. Similarly, LRP1, known for its role in clearing amyloid-beta protein implicated in Alzheimer's Disease, demonstrates the critical function of BMECs in maintaining brain health. LRP1 targeted deletion in the BBB increased amyloid beta levels in mouse brain, leading to spatial learning dysfunction and memory deficits [83].

In summary BMECs form a highly specialized barrier, acting as the gatekeeper to the brain by regulating nutrient transport and facilitating the removal of harmful substances. Any physical or biochemical dysfunction in this barrier can lead to impaired function and severe clinical consequences, emphasizing the significance of preserving the integrity of the blood-brain barrier for overall health.

Pericytes

Brain pericytes are an integral cellular component of the BBB. They play a multifaceted role in regulating various aspects of BBB function and maintaining brain homeostasis. Positioned on capillaries, these cells extend processes that contribute to BBB integrity, phagocytosis, angiogenesis, blood-flow regulation, and modulation of neuro-inflammation [84]. Residing in the abluminal side of the BBB, they are in direct contact with endothelial cells and act as crucial signal mediators between the endothelium and the brain parenchyma.

One notable function of pericytes is their regulatory role in the expression of MFSD2A, a protein essential for BBB formation by controlling vesicular transcytosis [85]. Through this modulation, pericytes actively participate in maintaining the selective permeability of the BBB. The significance of pericytes is further underscored by their involvement in various pathological conditions. Pericyte loss is commonly observed in conditions such as hypoperfusion, stroke, spinal cord injury, and Alzheimer's disease, highlighting their vulnerability to different insults [86-88].

Experimental studies, including global cortical ablation of pericytes, in mice have provided insights into the importance of pericytes and consequences of dysfunction. These studies demonstrated a reduction in cerebral blood flow, emphasizing the crucial role of pericytes in regulating vascular dynamics [87]. Additionally, in Pdgfrb mutant mice, pericyte dysfunction was associated with oligodendrocyte loss in the white matter and increased fibrinogen toxicity to the BBB [89].

Astrocytes

Brain astrocytes, characterized by their distinctive ramified-star shape and extended processes, play a pivotal role in orchestrating communication between the endothelium and neurons. Their extensive processes cover large regional areas, and their specialized "end-feet" located at the end of each process allow simultaneous contact with both endothelial cells and neurons. This strategic arrangement positions astrocytes as crucial signal transducers within the neurovascular unit, actively regulating cerebral blood flow in response to neuronal activity [90] and the development and maintenance of the blood-brain barrier.

The maintenance of BBB integrity by astrocytes, is partly responsible by aquaporin-4 (AQP4)-expression in their end-feet, which is in direct contact with endothelial cells. Mice with AQP4 knockout experience open tight junctions and increased permeability [91]. Further, upregulation of AQP4 improves blood brain barrier integrity following intracerebral haemorrhage by increasing

expression of VE-Cadherin, Claudin-5, Pdgfrβ, and Laminin [92]. However, the exact mechanisms of how AQP4 maintains BBB is unknown [93]. This interaction allows astrocytes to regulate the activity of key protein transporters such as GLUT1 and PGP [94, 95]. In addition to maintenance, astrocytes contribute to the development of the BBB by releasing growth factors, including basic fibroblast growth factor (bFGF), vascular endothelial growth factor (VEGF), and angiopoietin-1 (ANG1). These growth factors play critical roles in promoting endothelial growth, neovascularization, and ensuring barrier stability during development [96].

Astrocyte ablation leads to increased permeability to molecules of varying sizes, such as cadaverine (900Da) and fibrinogen (340kDa) [97]. Further, specific areas of the endothelium close to regions of astrocyte loss experienced a downregulation of ZO-1.

Diabetes And The Brain

Cognitive function has been reported as reduced in diabetic patients, particularly affecting learning, memory, and information processing speed [98-101]. However, the mechanism by which diabetes affects brain function is not clear. There are several potential mechanisms including increased risk of vascular disease and atherosclerosis, increased inflammation, increased brain atrophy and increased incidence of Alzheimer's disease.

Vascular Disease:

There is stronger evidence that diabetes increases risk of brain vascular disease from stroke to small vessel disease [102, 103]. Small vessel disease, identified as the most common cause of vascular cognitive impairment [104], may offer an explanation for the cognitive impairment observed in diabetes. Brain imaging changes in small vessel disease include white matter hyperintensities (WMH), the presence of lacunes, and infarcts [99]. WMHs are small foci of high-intensity signal in T2-

weighted MRIs, signifying the presence of oedema. While some studies report no significant overall difference in WMH volume between diabetic patients and controls [105, 106], others identify an increase [107, 108]. With respect to grey matter microvessels, one study indicates vascular reactivity in the grey matter is reduced [109].

Small, deep lacunar infarcts (areas that have died from loss of blood supply), are more prominent in individuals with T2DM [110]. Furthermore, T2DM is associated with a 1.5-2.5-fold increased risk of at least one infarct upon autopsy [111, 112]. The duration of diabetes is also recognized as a risk factor for lacune incidence, highlighting the potential cumulative effect of diabetes on cerebrovascular health [113]. Whist cerebral infarctions are strongly correlated with perceptual speed, no significant associations with other cognitive domains have been consistently reported [112]. It is therefore not clear if strokes explain the reported association between diabetes and cognitive impairment.

Inflammation:

Inflammation plays a crucial role in the development of small vessel disease, linking proteins associated with diabetes. Markers such as CRP (C-reactive protein), associated with diabetes [114], show a correlation with an elevated risk of WMH and lacunar infarcts [115]. Increased levels of IL-6, IL-1β, and TNF-α are also strong risk factors for incidence of both Type 2 Diabetes and small vessel disease [116, 117]. IL-6 may be elevated years before the onset of T2DM and can induce insulin resistance by impairing phosphorylation of insulin receptor and upregulating SOCS3, an inhibitor of insulin signalling [118]. Similarly, sICAM-1 and sVCAM1, which is dysregulated in diabetes [119], is associated with increased risk of lacunar infarcts [120, 121] and occurrence of future infarcts in diabetic patients [122]. Understanding the inflammatory processes and their associations with cerebrovascular complications in diabetes may help elucidate the impact of diabetes on the brain.

Diabetes and Atherosclerotic Pathology

Atherosclerosis, characterized by the accumulation of plaques on artery walls, is strongly linked to diabetes, especially cerebral atherosclerosis. Autopsy studies of individuals who experienced fatal strokes revealed that T2DM was approximately twice as prevalent as subjects with intracranial stenosis greater than 30% [123]. The relationship between atherosclerosis and Alzheimer's disease-type changes remains an open question, with conflicting findings in the literature. Some studies suggest no association between atherosclerosis and AD-type changes [124, 125], while other propose a potential connection [126, 127]. The complex interplay between diabetes, atherosclerosis, and AD-type pathology requires further investigation to elucidate the mechanisms underlying these associations and their implications for cognitive health.

Global Brain Atrophy

Atrophy, defined as the decrease in the size of an organ, is evident in the brain of individuals with diabetes, as revealed by magnetic resonance imaging (MRI) studies [128, 129]. The duration of diabetes appears to be a contributing factor to brain volume changes, with patients having over 10 years of diabetic history exhibiting increased atrophy compared to those with duration of less than 10 years [113]. However, conflicting findings emerged regarding the association between brain atrophy and cognitive dysfunction [105, 107, 130, 131]. While one study showed that cognitive ability is independent of MRI brain atrophy markers [132], others indicate that grey matter volume, memory, and executive functioning are dependent [133, 134].

The association may be with insulin resistance rather than diabetes more broadly. Investigations involving both healthy individuals and individuals with type II diabetes, increased atrophy was found to be associated with higher insulin resistance irrespective of diabetic diagnosis [135, 136]. Another

study identified specific atrophy of the temporal lobe linked to both increased insulin resistance and decreased cognitive function [136].

The conflicting results underscore the complexity of the relationship between brain atrophy, insulin resistance, and cognitive function in the context of diabetes. Further research is essential to untangle these associations and gain a more comprehensive understanding of the impact of diabetes on brain structure and function.

Brain regional effects of diabetes

Specific regions in the brain appear to be more vulnerable in diabetes to pathology and this includes the hippocampus, hypothalamus, prefrontal cortex, and temporal cortex. The hippocampus is a specialized brain structure in the temporal lobe involved in learning and memory with almost all Alzheimer's patients having a degree of hippocampal atrophy [137]. The hippocampus has reduced volume in T2DM patients and HbA1C levels have been inversely correlated to hippocampal volume [138, 139]. One MRI study reported a two-fold risk of lacunes/infarcts in diabetic hippocampi [110]. High-fat diet mice have increased hippocampal BBB permeability compared to low fat diet mice, and this phenotype is rescued with a mitochondrial carbonic anhydrase inhibitor, topiramate [140]. In rat models, high-fat diets induced a decrease in tight junction proteins Claudin-5 and Claudin-12, as well as increasing permeability to sodium fluorescein (NaF) [141]. Zucker diabetic fatty rats (hyperinsulinemic but normoglycaemic rat model) hippocampal BBB also had a decrease in TJ proteins such as Claudin-5 and Occludin compared to control rats [142] and increased permeability to flourescein.

It has been proposed that brain glucose sensing dysregulation in T2DM is due to hypothalamic dysfunction. Studies of the hypothalamus in mouse, rats, and human find evidence of inflammation in T2DM and obesity [143-145]. In rats, this inflammation occurs from long-chain saturated fatty acids that cross the BBB and activate microglia [146]. The IKKb/NFκB pathway is

activated and enhances expression of pro-inflammatory genes [145, 147]. Further, microglial activation also enhances JNK phosphorylation, which phosphorylates IRS-1 and inhibits insulin signalling [148]. A recent study in mice revealed that Dusp8 (a T2DM risk gene by GWAS) is upregulated in the hypothalamus and acts as a controller for Jnk [149].

Hypothalamic neurons need facilitated access to glucose and hormones from the blood to sense glucose concentrations effectively. The blood brain barrier at the hypothalamus, specifically at the Median Eminence (ME), is specialized and more permeable than in other parts of the brain. [150, 151] Further, this “BBB” contains tanycytes residing immediately adjacent - specialized cells that transfer selected signals such as leptin from the cerebrospinal fluid to the parenchyma [152, 153]. A study in a high fat mouse model observed that the BBB in the hypothalamus is compromised through ROS production with increased permeability to 14C-sucrose. [140]

The prefrontal cortex (PFC) is one of the most complex regions of the brain due to its connections with numerous other cerebral structures. It is involved in emotional behaviour, cognitive support of speech, reasoning and planning. [154] Diabetic humans with neurological phenotypes display difficulty in “attention demanding dual tasks” and show lowered oxygenated haemoglobin in the PFC during exercise [155]. In T2DM patients, overall PFC density [156] and grey matter volume [109] are reduced and associated with impaired visuospatial construction, planning, visual memory, and speed.

Bulk RNA-seq of the Goto-Kakizaki rat, a diabetic model with insulin resistance, identified 22 differentially expressed genes in the prefrontal cortex compared to control rats. [157] Neurotransmission and lipid metabolism genes were the most reported. Of significance, they found a downregulation of ABCA1, a risk gene for T2DM, Alzheimer’s, and dementia. qRT-PCR performed on high-fat diet and streptozotocin-induced diabetic mice revealed a significant increase in inflammatory markers IL-1β, IL-6, and TNF-α specifically in the pre-frontal cortex, highlighting the vulnerability this brain region has to diabetic insults and inflammation [158].

Both reduced volume and cerebral blood flow have been reported in the temporal cortex [129]. A recent bulk RNA-seq transcriptomic study was performed on Brodmann areas 21/22, both involved with learning and language, of patients with self-reported T2DM [159]. Cells of the neurovascular unit (endothelial cells, astrocytes, and neurons) were isolated using laser capture microdissection. Compared to controls, 912, 2202, and 1227 genes were differentially expressed in neurons, astrocytes, and endothelial cells, respectively. Interestingly, the genes identified for the endothelial samples contained classical diabetic manifestations such as insulin signalling (n=12), fluid shear stress and atherosclerosis (n=9) and AGE-RAGE signalling (n=10).

Diabetes and Alzheimer Pathology

There are widely reported associations between diabetes and Alzheimer's disease [160] but causal relationship remains debated [161]. The association between diabetes and Alzheimer's disease (AD) pathology remains inconclusive, with varying results reported in studies. While some studies have found an increase in AD-type pathological changes, such as amyloid plaques and neurofibrillary tangles (NFTs), with age, no clear association was established in diabetic patients [162]. In contrast, another study reported that diabetics carrying APOE e4 allele may show increased incidence of neurovascular insults. While diabetics without the APOE e4 allele showed higher incidence of infarcts compared to controls, and controls with APOE e4 alone was associated with higher number of neurofibrillary tangles in the cortex and hippocampus, the combination of both showed a significantly higher incidence of hippocampal neuritic plaques, cortical and hippocampal NFTs, and an elevated risk of cerebral amyloid angiopathy [163]. However, this association with the APOE e4 allele has not been consistently validated in other studies [112]. Surprisingly, one study found that diabetes was associated with fewer neuritic plaques and NFTs compared to non-diabetic controls [164]. The inconsistent findings highlight the complexity of the relationship between diabetes and Alzheimer's pathology, suggesting that cognitive dysfunction in diabetic patients may arise from processes distinct from AD.

Diabetes Effects on Endothelial Cells - Mechanisms

Endothelial cells from the heart and retina exhibit significant changes in key metabolic genes upon exposure to hyperglycaemia [165, 166]. One notable change is the inhibition of GAPDH [167]. GAPDH is primarily found in the cell's cytosol where its main function is to convert glyceraldehyde-3-phosphate (G3P) into 1,3-biphosphoglycerate in the glycolysis pathway. Cytosolic GAPDH can trigger release of cytochrome c, leading to cellular apoptosis. GAPDH can also be modified via nitric oxide-mediated S-nitrosylation and mobilize to the nucleus, where it can regulate DNA repair, telomere formation, nuclear membrane assembly, and mRNA destabilization [168]. Furthermore, the potent vasoconstrictor endothelin-1 is increased upon GADPH downregulation, suggesting that GAPDH may also have effects on blood flow dynamics [169], perhaps mediating the observed reduced blood flow in diabetes.

In bovine aortic endothelial cells exposed to hyperglycaemia, GAPDH inhibition is linked to an increase in mitochondria-derived reactive oxygen species (ROS) [166, 170, 171]. The proposed mechanism involves an overworked tricarboxylic acid (TCA) cycle from high glucose levels, leading to an excess of electron donor molecules such as NADH and FADH2. This imbalance of electron donor molecules affects the mitochondrial membrane potential, resulting in an increased production of ROS from complex III [172]. It was proposed that the increase in intracellular ROS activates poly(ADP-ribose) polymerase (PARP), to inhibit GAPDH activity.

The inhibition of GAPDH would be expected to increase substrates that precede the GAPDH reaction in glycolysis. Accumulation of substrates is prevented by shuttling them to other glycolysis-linked pathways. There have been four such pathways identified to be affected in endothelial cells from GAPDH downregulation:

G3P Accumulation and the AGE pathway

Advanced glycation end products (AGEs) result from the covalent attachment of a sugar to proteins through a process called glycation. Intracellularly, a common metabolite precursor to AGEs is methylglyoxal (MG), which can be produced from glyceraldehyde 3-phosphate (G3P) in glycolysis. This occurs through the conversion of dihydroxyacetone phosphate (DHAP) into MG by methylglyoxal synthase. In the mouse kidney, increased levels of MG have been associated with inflammation, as evidenced by the overexpression of inflammatory markers such as Ang2, VCAM, and ICAM. This inflammatory response increases sensitivity to TNF-α [173], which is commonly upregulated in hyperglycaemia [174].

MG on cultured immortalized human endothelial cell lines results in a dose-dependent decrease in trans-endothelial electrical resistance (TEER) [175]. This effect is mitigated when cells are exposed to N-Acetylcysteine (NAC), a precursor to glutathione (GSH), highlighting the role of NAC in protecting endothelial barrier integrity. Conversely, inhibiting glyoxalase (the enzyme that produces GSH) exacerbates the effects of MG on TEER levels, as GSH production and its antioxidant effects are compromised.

The receptor for advanced glycation end products (RAGE) is implicated in generating reactive oxygen species through the activation of NFκB and p21ras [176]. In endothelial cells, AGE binding alters the expression of various genes, including VCAM1, PAI1, and VEGF. VCAM1 and PAI1 play roles in inflammation and blood clot clearing [177, 178], while changes in VEGF expression may contribute to increased vascular permeability and angiogenesis [175]. Furthermore, hyperglycaemia-induced ROS upregulates RAGE expression, creating a positive feedback loop where elevated AGE levels lead to increased receptor expression, resulting in heightened ROS activation [179, 180].

G3P, DAG, Accumulation, and Protein Kinase C Pathway

Protein kinase C (PKC) is a group of serine/threonine-related protein kinases that play various roles in modulating membrane structure, regulating transcription, mediating immune responses, and influencing cell growth [181]. PKC can be activated by diacylglycerol (DAG), a product synthesized from glycerol-3-phosphate (G3P) [182]. In diabetes, total DAG levels are elevated in vascular tissues, including the rat retina [183] and heart [184].

In the mouse retina, PKC activation recruits Shp-1, which dephosphorylates PDGFRb, ultimately leading to pericyte death and neurovascular dysfunction [185]. PKC activation in cultured human brain endothelial cells through exposure to TNF-α results in a reduction of tight junction protein ZO-1 and a decrease in TEER values. Treatment with PKCδ inhibitor rescues ZO-1 levels and TEER values to similar levels observed in control cells [186]. However effects of PKC may be tissue specific since in the kidneys, diacylglycerol and associated PKC activation, may have nephroprotective effects [187].

Fructose-6-phosphate and the Hexosamine Pathway

Fuctose-6-phosphate, the second product of glycolysis, is typically converted to fructose 1,6-biphosphate. However, an alternative pathway involves the conversion to glucosamine 6-phosphate by the enzyme GFAT (glutamine:fructose-6-phosphate amidotransferase), and this pathway has been observed to be upregulated in diabetic rat aortic endothelial cells [188]. Glucosamine 6-phosphate is further metabolized into UDP-N-Acetylglucosamine (UDP-GlcNAc), which serves as a major substrate for the formation of O-GlcNAc-modified proteins. This modification is catalysed by OGT (O-GlcNAc transferase) [189].

Elevated levels of O-GlcNAc are considered significant contributors to the pathology of vascular and metabolic diseases such as hypertension and diabetes [190]. In the context of

hyperglycaemia, elevated levels of O-GlcNAc induced in isolated human umbilical endothelial cells (HUVECs) can activate inflammation markers such as VCAM1 and ICAM1 [191].

Glucose and the Polyol Pathway

In the polyol pathway, aldose reductase (AR) catalyses the conversion of glucose to sorbitol using NADPH as a cofactor. Subsequently, sorbitol is converted to fructose by sorbitol dehydrogenase (SORD) using NAD+ as a cofactor. In the context of diabetes, overexpression of AR in the retina of streptozotocin-induced hyperglycaemic mice has been associated with a decrease in levels of glutathione (GSH). Interestingly, a subsequent downregulation of SORD in the same transgenic mouse allowed GSH levels to rise significantly. This suggests that SORD, by influencing the levels of GSH, may play a role in controlling oxidative damage [192]. Mouse models have demonstrated that inhibitors of AR can be effective in preventing diabetic complications, including cataracts, neuropathy, and nephropathy [193].

In summary GAPDH directly or through changes in flux of associated metabolic pathways represents an important candidate by which deleterious effects of diabetes may be mediated. However, the hypothesis implicating GAPDH in brain endothelial dysfunction has some limitations that should be considered. First, much of the evidence comes from studies utilizing animal models, so relevance to human physiology remains to be established. Additionally, a significant portion of the research has been conducted in non-brain endothelial cells, raising questions about the direct applicability of the findings to the BMEC environment. Moreover, most of the information regarding GAPDH downregulation and its impacts on various metabolic pathways originates from a single laboratory. While their work provides valuable insights, scientific findings are typically strengthened by independent validation from multiple research groups.

Blood Brain Barrier Research Models

Selecting an appropriate model is crucial when investigating disease mechanisms, and this is particularly challenging when studying the blood-brain barrier due to its complex microenvironment. Establishing *in vitro* models of the BBB involves creating conditions that mimic the intricate interactions between various cell types, including endothelial cells, pericytes, and astrocytes.

Vasculogenesis begins from angioblast precursors, who establish the perineural vascular plexus (PNVP) in the head mesenchyme enveloping the neural tube [194]. Endothelial precursor cells form blood vessels of the PNVP and are established by E8.7 in mice [195]. This occurs when endothelial cell precursors, which express VEGFR2 (KDR), migrate from neighbouring lateral plate and pre-somitic mesoderm regions in response to VEGFA gradient generated within the neuroepithelium due to hypoxia[194]. Following, these blood vessels undergo angiogenesis where newly sprouted blood vessels invade the growing brain. This invasion is directed by a spatial pattern of signalling pathways including the Wnt/β-catenin, Notch, and VEGF [196-198], which signal through the canonical pathways to promote BBB specification. Vessels invade the hindbrain before the forebrain due to higher concentrations of Wnt, BMP, and FGF in the hindbrain [199]. The vessels continue growing through the lateral and ventral areas of the brain, following a VEGF gradient. The dorsal region is the last to be populated by migrating angioblasts [197]. This process begins at gestational week 8 in humans, and reaches a peak in activity at around 35 weeks [200, 201]. Endothelial invasion is possible due to tip cells, specialised endothelial cells located at the front of sprouting vessels. These cells are abundant in VEGFR2, which allows for growth along the VEGFA gradient produced by neuroepithelial cells in the developing brain [202]. Other proteins involved in endothelial cell fate include NRP1 and TIE2. NRP1 is a VEGFR2 co-receptor and is required for lateral capillary branching [203]. TIE2 selectively controls angiogenesis in response to angiopoietins secreted by endothelial cells or pericytes [204].

Several key transcription factors regulate the endothelial fate, including ETS, FOX, GATA, SMAD. ETS factors are comprised of a large family of TFs including ETV2, FLI1, ERG, and ETS1. ETV2 is a strong mesoderm activator and is the only ETS TF whose genetic ablation leads to a complete loss of vasculogenesis, leading to death [205]. It peaks in expression during early embryogenesis in endothelial progenitor cells rather than in mature ECs. Its role is likely related to regulation expression of VEFGR2 receptors [206], important for angiogenesis and endothelial tip-cell migration. ETV2 can also further activate other endothelial ETS TF factors such as FLI1, ETS1, ETS2, ERG, and FEV [207].

Important FOX TFs involved in endothelial specification include FOXC1 and FOXC2. They are both expressed early in embryogenesis and are involved in angiogenesis through DLL4-mediated NOTCH signalling downstream of VEGF [208]. FOXC factors can also work synergistically with ETV2 to bind FOX:ETS motifs within endothelial gene enhancers [209]. This promotes expression of imperative endothelial identity genes such as FLK1, FLT4, TAL1, CDH5, TIE2, and NOTCH4 [210].

GATA consists of six TFs which have roles in the development of hematopoietic stem cells and EC specification. GATA2 is able to interact with ETV2 and promote expression of VEGFR2 for endothelial angiogenesis [211]. In fact, all VEGFR2 EC enhancers contain essential GATA-binding motifs, increasing its effectiveness in regulating expression of the essential endothelial receptor [212]. While GATA3 and GATA6 have been reported to upregulate TIE2 in HUVEC cells [213], neither TF is strongly expressed in the developing endothelium [214].

SMAD proteins serve as the transcriptional regulators for the TGFβ superfamily. Both TGFβ and BMP can activate expression of downstream SMAD proteins. SMADs are expressed early in embryogenesis, although not exclusively by endothelial cells, and deletion of Smad4 or Smad1/5 lead to erratic angiogenesis that leads to death by E10.5 [215]. Specifically, Smad1/5 binding in endothelial cells have several targets including Id1, Hey1, Hey2, Hes1, and Jag1 (Notch pathway genes) [216].

Upon reaching maturity, the transcription factors most expressed in the CNS include FOXL2, FOXF1, ETS1, FLI1, and LEF1 [217]. ATAC-seq revealed that the most well expressed TF in the brain compared to peripheral endothelial cells is LEF1, which is a strong activator of the Wnt pathway [218]. Neighbouring cells also promote endothelial TF expression. For example, pericyte-derived CDH2 activity on the endothelium can upregulate cellular adhesion molecules such as Ctnnd1 and WNT signalling regulated genes such as Ccnd1, Ptma, and Ctnnb1. CDH2 can further induce Lef1 expression and Wnt target Axin2 [219, 220]. SMCs express Itgb1, which can drive expression of Rad51, a protein responsible for vascular maintenance through DNA damage protection [221].

In summary, endothelial cell differentiation *in vivo* is largely governed by a wide array of expressed transcription factors and secreted factors from neighbouring cells. Figure Intro.1 shows simplified diagram of the development of the endothelium.

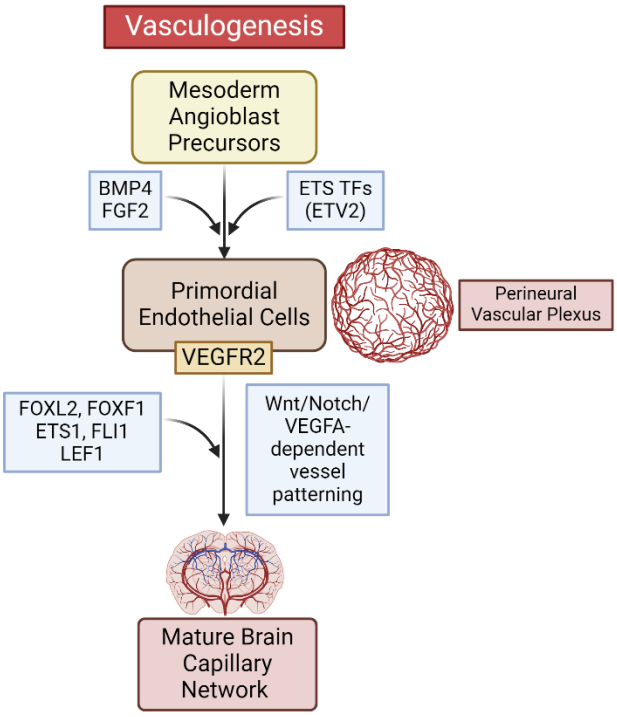


Figure Intro.1 – Simplified Diagram of the Developing Endothelium

Mesoderm angioblast precursor cells are differentiated into primordial endothelial cells through growth factors BMP4 and ETS transcription factors. These cells invade the developing parenchyma through Wnt, Notch, and VEGFA gradients and form mature endothelial cells expressing transcription factors FOXL2, FOXF1, ETS1, FLI1, and LEF1.

Through investigation of the sequential steps that allow endothelial progenitor cells to arise from mesoderm in the PNVP have helped researchers mimic this development *in vitro* with IPSCs. Namely, the activation of the Wnt pathway, induction of VEGFR2, and NOTCH early in the differentiation is vital to determining an endothelial fate. The most important factor to produce early in differentiation is VEGFR2, as this receptor will allow for further proliferation of endothelial cells. While some published protocols involve a mesoderm induction through activation of WNT/β-catenin [222], some go directly to a dual neural/endothelial induction trough an "unconditioned medium" including 0.1mM β-mercaptoethanol to promote nestin expression in undifferentiated cells, leading to a "brain-like" environment [223]. Subsequent change to an endothelial cell culture medium and exposure to BMEC-inducing agents such as retinoic acid improve endothelial cell fate thereafter, and diminish the presence of neural cell types. The final seeding onto collagen IV/fibronectin allows for the final purification of the culture. The latter protocol is not a conventional differentiation towards one single cell fate, which may have detrimental effects to the resulting phenotype (discussed below). A summary provided by Workman et al. [224] denotes different published differentiation protocols currently available (Figure Intro.2)

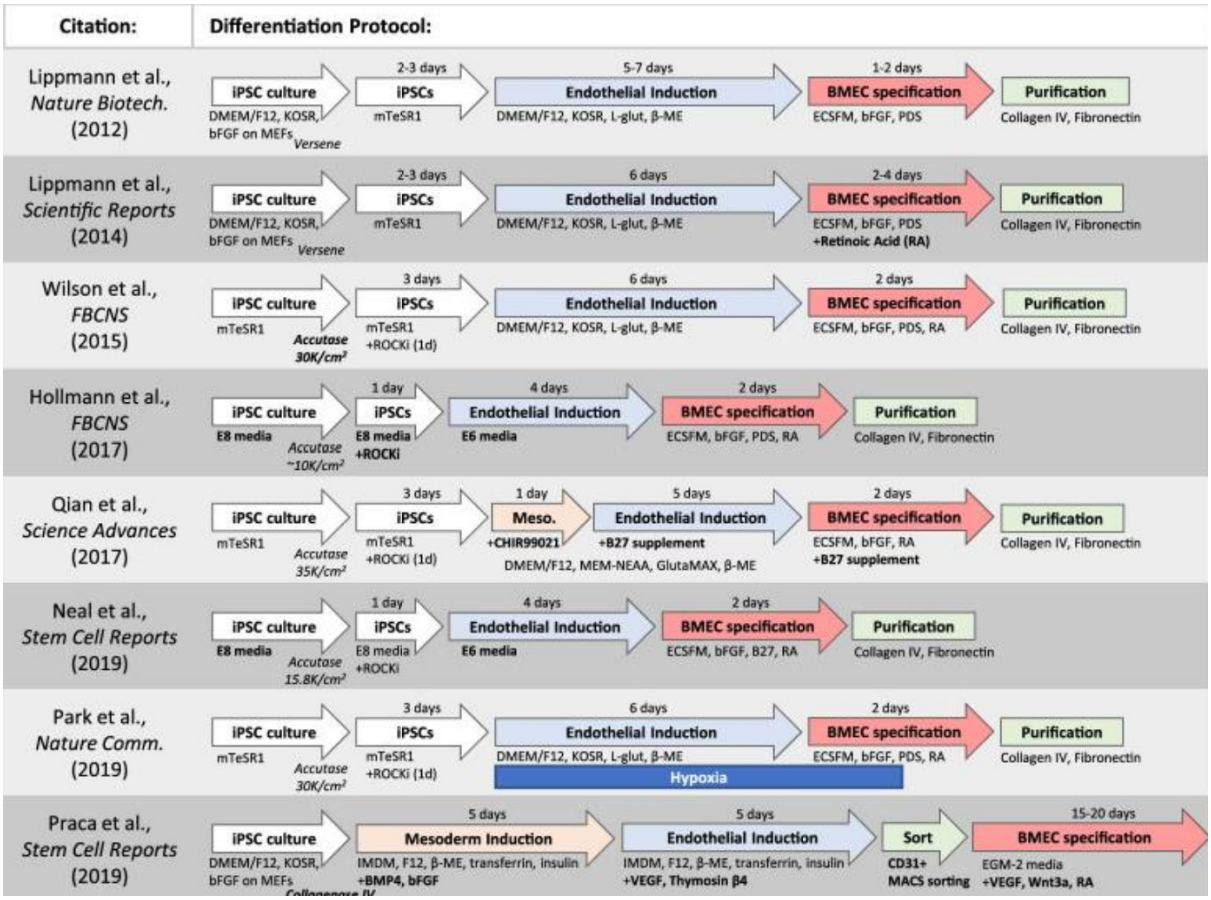


Figure Intro.2 – Available Published Protocols for Brain Microvascular Endothelial Cell Differentiation

Published protocols for the differentiation of IPSCs into brain microvascular endothelial cells. Typical approaches include a dual neural/endothelial differentiation followed by endothelial specification and purification, while others introduce a mesoderm intermediate stage. Image taken from Workman et al. [224]

Innovative approaches, such as the use of primary cells in co-culture systems or the development of more sophisticated *in vitro* models, are continually being explored to improve the relevance and reliability of BBB research in the context of diseases like diabetes. It has been over 40 years since the first reported isolation and *in vitro* culture of murine brain endothelial cells, where researchers identified through alkaline phosphatase staining that filtering and spinning brain homogenates at specific density gradients yielded a capillary enrichment pellet that was viable for cell expansion [225]. While this is a valuable approach, it comes with its own set of challenges.

Isolating and purifying these different cell types from mice is a demanding process, and it necessitates using many animals to obtain sufficient quantity of each cell type. This not only raises ethical considerations but also practical challenges in terms of resources and time. Immortalized cell lines offer a more accessible and reproducible approach to study BBB function *in vitro*. However, these Immortalization can alter the cellular phenotype, potentially masking or introducing diabetic-like phenotypes that may not be representative of the primary cells [226].

The development of protocols for differentiating human induced pluripotent stem cells (iPSCs) into brain microvascular endothelial cells represent a significant advancement in overcoming the challenges associated with immortalised cell lines and murine *in vitro* models [222, 223, 227, 228]. These protocols aim to create a more human-relevant physiological system for studying the BBB and associated diseases.

The original protocol allowed spontaneous undirected differentiation which yielded cells with brain endothelial identity [223]. Subsequent steps aimed to enrich for endothelial cells with subsequent maturation by seeding cultures onto fibronectin/collagen matrices and using platelet-poor plasma-derived bovine serum in the culture medium. Additional optimizations were then developed[223, 227, 229, 230], such as the introduction of retinoic acid to enhance the barrier properties of endothelial cell monolayers.

Cells differentiated using this method were reported to express key markers indicative of brain capillary endothelial cell identity, including PECAM1, VE-CADHERIN, GLUT1, CLDN5, OCLN, and ZO1. These proteins are essential for the formation of tight junctions which underlie integrity of the BBB. TEER measurements of the monolayers were exceptionally high (ranging from 2,940 $\Omega*cm^2$ in early studies [227] to 8,000 $\Omega*cm^2$ in more recent studies [228]), indicating the formation of a tight barrier.

In recent years, concerns have been raised about the fidelity of this differentiation protocol [231, {Lippmann, 2020 #481, 232]. Previous unpublished work in the Cader lab identified expression

of the epithelial marker E-CADHERIN in differentiated cells, suggesting that the generated cells may represent an endo-epithelial cell hybrid rather than pure endothelial cells. Recent evidence from a study utilising thorough bulk and single-cell RNA sequencing also indicates an epithelial hybrid phenotype [231], with expression of epithelial genes, including CDH1, CDH3, CLDN4, and KRT7. This hybrid phenotype could contribute to the very high TEER values observed in culture, which differ significantly from TEER values for primary mouse endothelial cell monolayers.

THESIS OUTLINE

The research approach I have taken involves a dual strategy to investigate the effects of diabetes and hyperglycaemia. Chapters 1 and 2 aim to develop a novel iPSC-derived BMEC protocol by activating three transcription factors through lentiviral overexpression or CRISPR activation for more physiological gene expression levels. The goal was to address limitations in current IPSC models, to provide an improved *in vitro* representation of BMECs. The model will enable future studies to focus on targets identified from chapters 3 and 4 to delve deeper into the intricate pathways and molecular interactions involved in diabetes.

Chapter 3 employs a murine model for *in-vitro* analysis of glucose modulation and endothelial cell response, while chapter 4 focuses on diabetic human post-mortem brain single nuclei RNA-sequencing analysis. This dual strategy balances experimental control and clinical relevance. Both of these chapters aimed to identify key disease mechanisms related to pathological effects on the brain endothelial cells, with a particular focus on inflammation.

Chapter 1: Development of a Novel IPSC-BMEC Differentiation Using Transcription Factor Overexpression

Introduction

Claims that current techniques and protocols can differentiate IPSCs into brain microvascular endothelial cells are controversial. Whilst widely used in the field due to the excellent barrier properties, variations of the Lippman small molecule-based protocol results in endothelial-epithelial hybrid cells. An in depth analysis through bulk and single cell RNA-seq identified that cells differentiated using current methods express key epithelial markers including TRPV6, EPCAM, and CLDN4 [231]. This limits the use of these protocols for investigation of disease relevant mechanisms.

These small molecule-based differentiations include 1% platelet-derived bovine serum [223, 227, 228, 230], however, including serum can increase batch to batch variability dependent on serum fabrication. These differentiation protocols start with the removal of bFGF, necessary for IPSC maintenance, and then move to E6 medium containing insulin and human transferrin, as it has been shown to help IPSCs differentiate into neuroectoderm. Small molecules are also used to help drive IPSC differentiation to a mesoderm intermediate via CHIR99021, a glycogen synthase kinase 3b inhibitor and Wnt pathway agonist [233]. Despite a decade of optimization on this protocol, as it stands, it is still unable to produce brain endothelial cells without expression of epithelial markers.

An alternative approach to using small molecules to achieve differentiation into a desired cell type is to use expression of key transcription factors. A recent study identified ETV2, ERG, and FLI1, as three transcription factors necessary for endothelial identity acquisition in IPSCs [234]. These factors were identified from a previous study with differentiated endothelial cells from hESCs, in which micro-array profiling was performed to identify such transcription factors. Results indicated that the ETS family of transcription factors, specifically ETV2, ERG, and FLI1, are essential inducers of vascular identity and angiogenesis [235, 236]. When these genes were over-expressed via lentiviral

delivery in induced pluripotent stem cells (iPSC), after 16 days in culture, the arising cells robustly improve existing protocols by increasing expression of key endothelial genes KDR, VWF, and CLDN5, whilst suppressing expression of epithelial genes TRPV6, EPCAM, and CLDN4[234]. Despite the improved shift from an epithelial to endothelial lineage, certain transport genes such as SLCO1A2, MFSD2A, and ABCB1 (PGP) were absent in the final endothelial culture and thus the cells resembled generic endothelial cells rather than brain endothelial cells [234].

The Cader Lab had also investigated a unique small molecule-based differentiation protocol, but despite RNA-seq results showing expression of key endothelial markers OCLN and CLDN5, it also showed expression of epithelial marker E-CADHERIN. Previous work done by Dr. Satyan Chintawar in the Cader lab starting from generic endothelial cell (not brain) differentiation method [237] was developed to try to induce differentiation into brain capillary endothelial cells. iPSC are first patterned into mesodermal progenitors using LY294002 (a PI3K inhibitor/Wnt activator commonly used in cardiomyocyte differentiation that also suppresses DVL (dishevelled))[238], and BMP4 (a strong mesoderm activator proven to work best together with a WNT activator (in this case, LY294002)). The cells are then exposed to SB43154 to inhibit TGF-β to promote differentiation to mesenchymal-like cells and has previously been shown to increase proliferation of endothelial cells [239]. Lastly, the cells are exposed to LY294002 alone until day 5 when they achieve mesodermal cell identity. The cell culture medium is changed to ESFM, and cells are exposed to Wnt7a, retinoic acid (RA), forskolin, and VEGF. Wnt7A has previously been reported to support endothelial differentiation by upregulating expression of LEF1, APCDD1, and ZIC3 [240]. Retinoic acid is commonly used in neuronal differentiation, but can also regulate β-catenin expression [241] and enhance adherens and tight junction expression in endothelial cultures [227]. RA has been added to the original Lippman protocol [223] as it increased adherens and tight junction expression in cultures [227, 233]. Forskolin activates adenylyl cyclase to increases intracellular cAMP, previously shown to stabilize tight barrier function [242, 243]. Lastly, VEGF is a potent endothelial inducer and increases barrier functionality. VEGF secreted by mesenchymal stem cells drives differentiation of vascular progenitor cells to

endothelial cells [244]. Forskolin can also act as a VEGF inducer, and both together can promote angiogenesis [245]. The final stage allows the endothelial cells to mature by removing VEGF and adding angiopoietin-1 (ANG1) and sonic hedgehog protein (SHH). The removal of VEGF allows the endothelial cells to reduce proliferation and migration [246]. ANG1 is secreted by pericytes and has vasculoprotective effects including vessel stability [247]. SHH is secreted by astrocytes and aids in endothelial maturity by upregulating tight junction proteins [248]. Both factors also decrease vascular permeability to inflammatory mediators and leukocytes, decreasing inflammation in the BBB. This unique small molecule-based differentiation protocol yielded cells that express key endothelial markers such as CLDN5, VE-CADHERIN, and PECAM1, but also showed expression of epithelial marker E-CADHERIN.

In order to improve current protocols for the differentiation of brain microvascular endothelial cells, I hypothesized that overexpression of novel key transcription factors in IPSCs in conjunction with small molecule directed differentiation and maturation, would yield a homogenous culture of BMEC cells with a brain-specific identity and do not express epithelial markers. My specific aims are to:

- Identify novel transcription factors for BMEC-like cell specification and validate lentiviral delivery for transcription factor overexpression
- Optimise transcription factor-based differentiation protocol for robust and homogenous differentiation of BMEC-like cells
- Validate BMEC-like cell identity with immunocytochemistry for key BMEC markers as well as absence of epithelial markers
- Validate BMEC-like cell functionality through barrier integrity tests and vessel-formation assays
- Validate brain-specific endothelial identity through transporter expression and transport assays

RESULTS

Identification of Novel Transcription Factors for the Differentiation of IPSCs into BMECs

In order to identify transcription factors specifying brain endothelial cell fate, we collaborated with Professor del Sol in the University of Luxembourg, who leads a bio-informatic research group developing single cell sequencing analysis methods. They identified a novel combination of three transcription factors that could direct the differentiation of IPSC into BMECs. By using their computational tool for identification of synergistic transcription [249], they were able to identify three key transcription factors that may confer capillary brain microvascular endothelial cell identity. They used mouse vascular single-cell RNAseq data from Vanlandewijck et al. [250] to perform pseudotemporal analysis via Monocle3 and identify target genes highly expressed in brain endothelial cell clusters (arterial, venous and capillary) but not in other cell types. They further narrowed the target genes by focusing solely on the brain capillary endothelial cells, to identify LEF1, ETS1, and MRTFB (MKL2) as three key transcription factors (Supplementary Figure 1.1). LEF1 and ETS1 have been previously associated with endothelial identity [234], while MRTFB has not been studied in this context.

Lymphoid enhancer-binding factor 1, or LEF1, has been implicated in endothelial cell invasion and maturation through the Wnt/β-catenin pathway activation [251, 252]. Exposing human endothelial cells to Wnt3A increases β-catenin, LEF1, and MMP2 expression, allowing for endothelial invasion and proliferation to occur [251]. Specifically, LEF1 allows $FLI1A^{+}$ vascular progenitor cells to achieve an endothelial cell fate [253]. ETS Proto-Oncogene 1, or ETS1, is highly expressed in endothelial cells and regulates growth factors such as vascular endothelial growth factor (VEGF), receptors such as KDR and TIE2, and metalloproteinases such as MMP9, all involved in angiogenesis and cellular migration [254-256]. Furthermore, inhibition of ETS1 exacerbates blood brain barrier dysfunction in multiple sclerosis mouse models, suggesting its expression is imperative for a healthy

BBB [257]. While vascular reports on myocardin-related transcription factor-B (MRTFB) are scarce, some report that this TF is necessary for maturation of coronary vessels through epicardium motility and epithelial-to-mesenchymal transition of epicardium derived progenitor cells [258]. In embryonic mice, *Brg1* promotes transcription of *Mrtfb*, which in turn increases embryonic capillary integrity [259].

Lentiviral Delivery Platform Optimization

Cells Transduced with Polycistronic and rtTA Viruses Express Key Transcription Factors

A lentiviral construct (Figure 1.1A) was designed, containing a polycistronic sequence of LEF1, ETS1, and MRTFB (MKL2) cDNA, and the mVenus mitochondrial reporter. The expression of the three transcription factors is governed by a doxycycline/tetracycline dependent promoter – the TetON system, where doxycycline initiates transcription. Therefore, expression of the transcription factors is dependent on co-transduction with an rtTA virus. The lentivirus constructs (including rtTA3) were packaged into lentiviral particles by Dr. Ryan Beveridge at the Weatherall Institute of Molecular Medicine.

Virus functionality was first validated by co-transducing HEK cells with the polycistronic virus construct and rtTA3 virus (Figure 1.1B). Four different viral titres, 0.5ul, 1ul, 2ul, 4ul of the 3xTF lentiviral construct were assessed along with 1.5ul rtTA3 virus per 22K cells per cm2. Four days after transduction and doxycycline exposure at 4mg/ml, HEK cells were fixed and stained for LEF1, ETS1, and MRTFB separately and overlayed with the mVenus signal. HEK cells had a strong expression for mVenus and all three transcription factors at a volume of 2ul virus (n=1), indicating that the virus was indeed synthesized and assembled properly (Figure 1.2).

The rtTA virus does not have a reporter and it was not possible to determine the efficiency of rtTA transduction, which might then limit the efficiency of transcription factor expression. To overcome this issue, a tagBFP-rtTA virus construct with a puromycin selection cassette

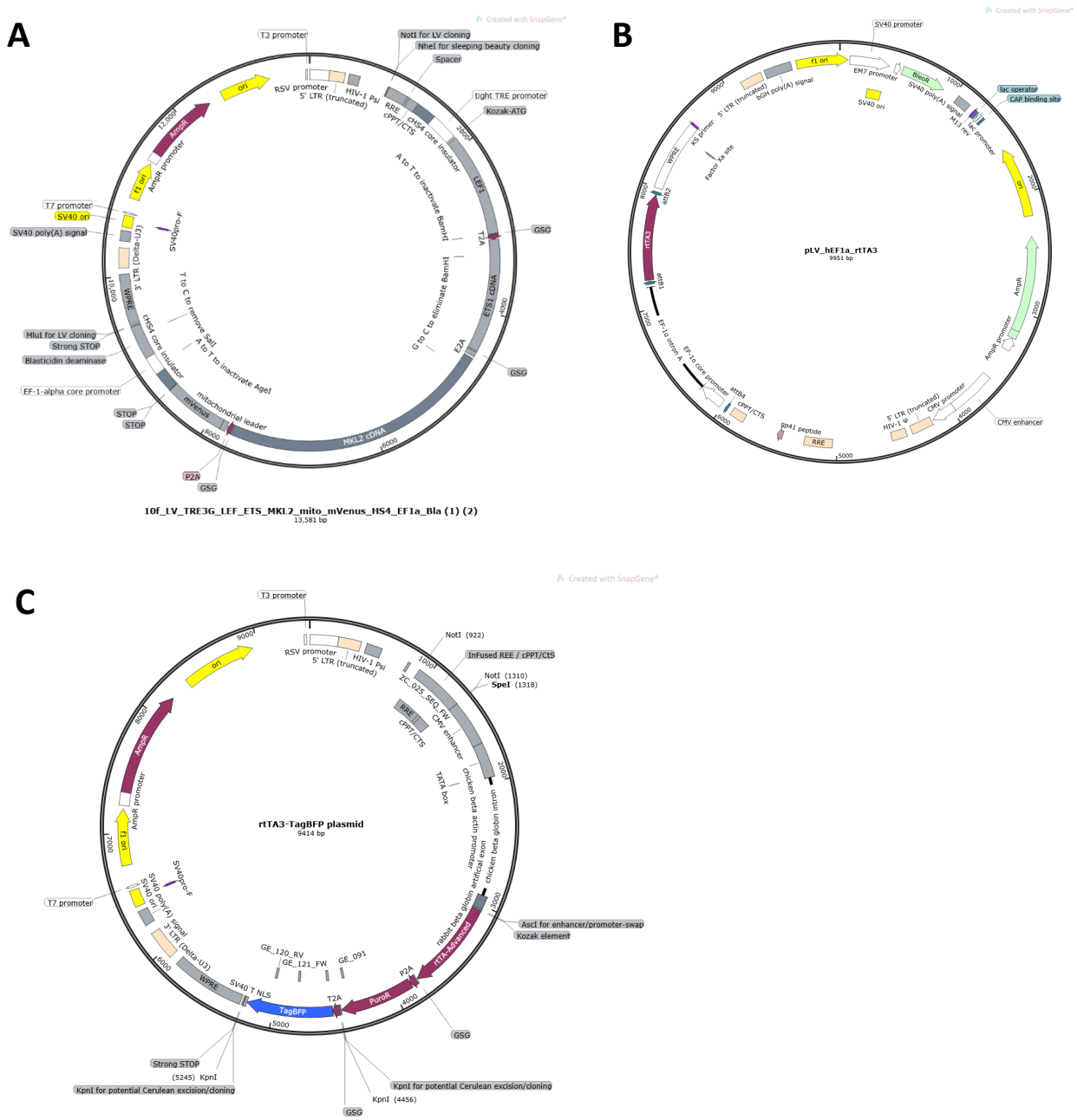


Figure 1.1 – Plasmid Maps used in IPSC-BMEC Differentiation

A- Plasmid map of polycistronic virus construct with LEF1, ETS1, and MRTFB cDNA. This construct also has an mVenus mitochondrial reporter.

B- Plasmid map of rtTA3 used for pilot experiments in endothelial differentiation

C- Plasmid map of rtTA-tagBFP used for subsequent differentiations. This construct has a tagBFP reporter, although visualising this reporter was challenging.

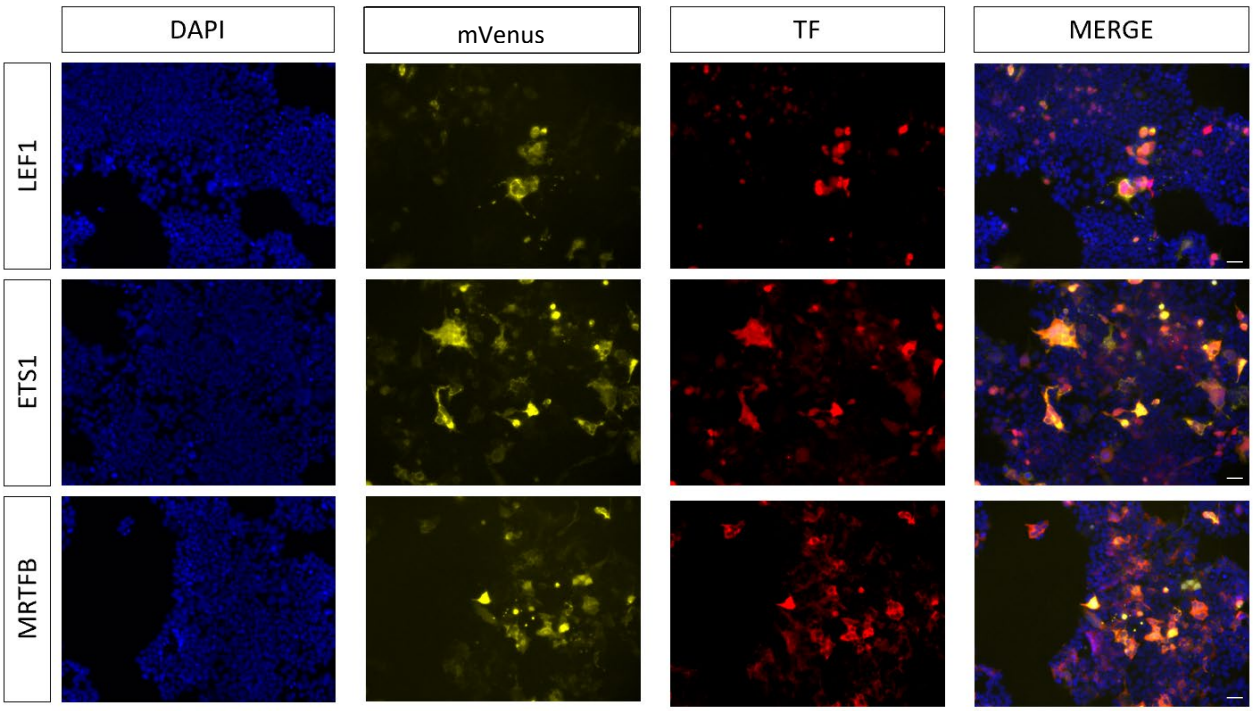


Figure 1.2 – Establishment of the Polycistronic Virus Platform for Brain Microvascular Endothelial Cell Differentiation

HEK cells transduced with rtTA3 and polycistronic TF virus were fixed and stained for LEF1, ETS1, and MRTFB. Results show co-localization of the transcription factors the mVenus reporter. Scale bars, 50um. (n=2 biological replicates)

(Figure 1.1C) was assessed. iPSCs were transduced with different viral titres of tagBFP-rtTA (0,1,4, 8ul, and 12ul) and blue fluorescent protein (tagBFP) expression was monitored for 5 days using live-cell imaging and a tagBFP 2.0 light cube (Ex 392/23, Em 447/60). Fluorescence was not detected in the 0, 1, 4, and 8ul virus conditions, and a small proportion of cells were showing expression in the 12ul condition (Supplementary Figure 1.2). However, there was significant toxicity with 12ul virus, and only few cells remained in culture after 5 days.

Despite the low apparent transduction efficiency which may relate to low fluorescent protein expression not detected on the light microscope, we sought to assess whether the virus nevertheless was functional with respect to rtTA activity. 2ul tagBFP-rtTA and 2ul polycistronic transcription factor virus were co-transduced in IPSCs and treated with puromycin for 2 days and doxycycline for 5 days.

Surprisingly, cells that were mVenus positive (indicating that the transcription factors were being expressed) were negative for tagBFP (n=2) (Figure 1.3A). This indicates that although the reporter fluorescent protein was not visible, the functional rtTA part of the construct was working as intended. Furthermore, this confirmed that a lower volume of tagBFP-rtTA virus was sufficient to induce expression, while avoiding toxicity problems seen in higher volumes. I therefore elected to continue with the tagBFP-rtTA virus rather than the rtTA virus since the former had a puromycin selection cassette.

To confirm optimal viral titres for IPSCs, cells were transduced with 2.0ul tagBFP-rtTA per 22K cells per cm^2 and 0, 0.5, 1, 2, 4, and 8ul of the polycistronic TF virus. 5 days post transduction, with dox induction, 4.0ul virus had the largest proportion of cells showing mVenus signal (n=2) (Figure 1.3B). Cells transduced with 8.0ul of virus experienced significant toxicity and cell death (not shown). Cells were also stained for LEF1, ETS1, and MRTFB separately. ETS1 and MRTFB was present in mVenus expressing and non-expressing cells (Supplementary Figure 1.3) with no apparent differences in signal intensity in iPSC endogenously expressing the TF versus transduced iPSC. LEF1 was only expressed in transduced cells, making this also a reliable marker for transduction efficiency. Using $LEF1^+$ cells over total $DAPI^+$ nuclei, the estimated transduction efficiency was low at 4 %.

Polybrene increases transduction efficiency, but at the cost of cellular toxicity.

To improve transduction efficiency, the addition of polybrene was investigated. Polybrene (hexadimethrine bromide) acts as a neutralization agent for the charge repulsion between viral particles and the cell surface, potentially allowing more virus to integrate into the cell [260]. IPSCs were exposed to vehicle, 5ug/ml polybrene, or 5ug/ml polybrene with a 1-minute centrifugation at 200g, either at a low (43ul) or high (86ul) virus load of CMV-GFP supernatant obtained from Dr. Ryan Beveridge. The CMV-GFP virus supernatant was previously confirmed to not induce toxicity in IPSCs. Polybrene led to an increase in both number of GFP+ cells and their signal intensity (n=2), with

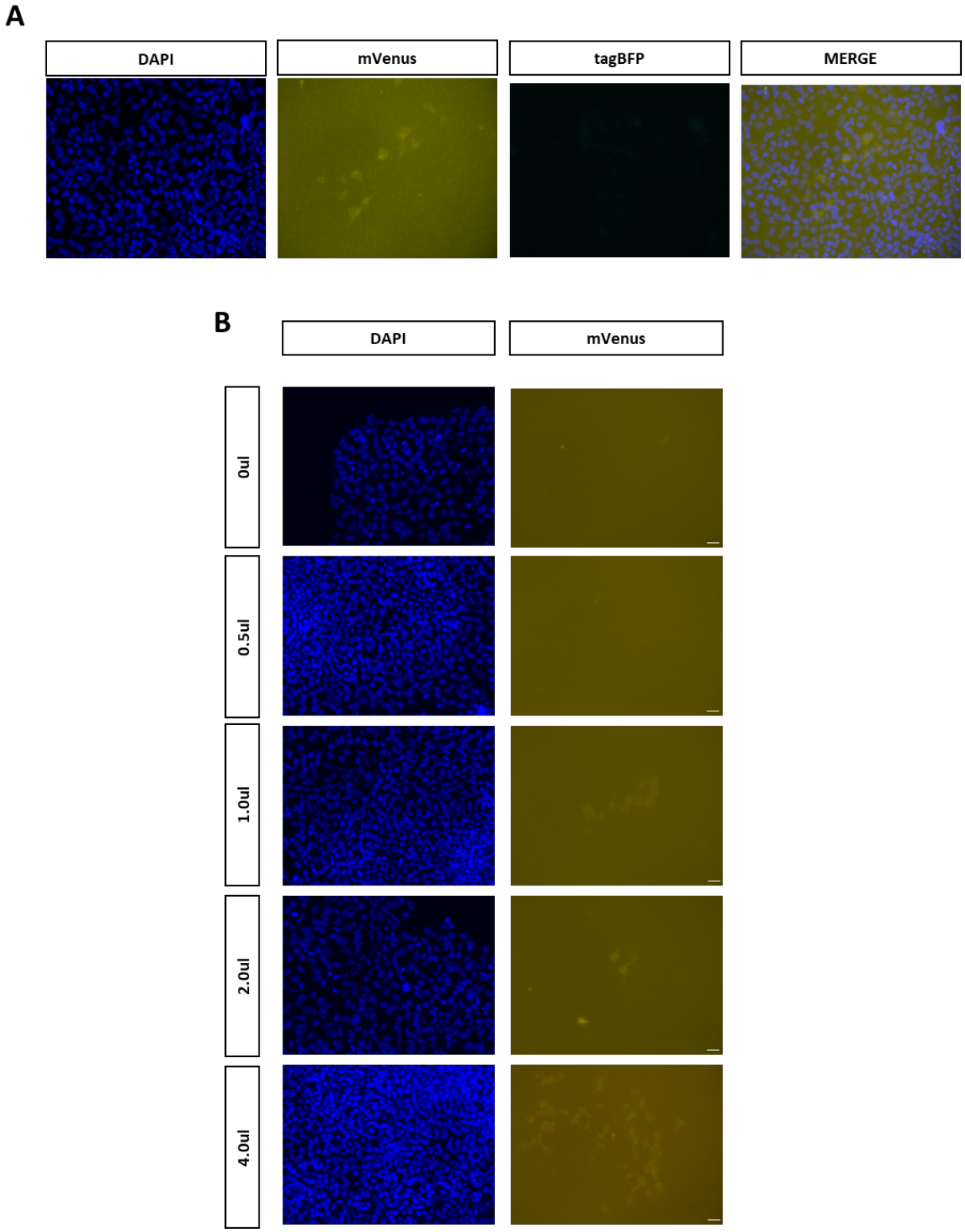


Figure 1.3– Polycistronic and rtTA-tagBFP virus optimization
A- Live imaging done on IPSCs transduced with tagBFP- rtTA and polycistronic TF virus show that despite no tagBFP expression, its functionality in activating transcription factor expression is working. Cells positive for mVenus are negative for tagBFP indicating co-transduction of viruses in each positive cell.
B- IPSCs transduced with tagBFP- rtTA and polycistronic virus at different volumes show increased mVenus signal in higher volumes while not compromised cell toxicity. Scale bars, 50um. (n=2 biological replicates)

slightly better transduction when polybrene was combined with brief centrifugation (Supplementary Figure 1.4A).

To evaluate polybrene toxicity in IPSCs, a dose-dependent toxicity curve of polybrene (without virus) was constructed. iPSCs were plated at 22K/cm^2 and were treated the following day with 0, 1, 2, 3, 4, 5, 6, 7, and 8 ug/ml polybrene. Cells were fixed either at 6 hours or 20 hours, stained for DAPI and counted using ImageJ analyse particles feature. Compared to the no-polybrene control, polybrene concentrations up to 3ug/ml showed no toxicity either at 6 or 20 hours post exposure. There is mild to moderate toxicity at 4 and 5ug/ml, and these two conditions show that longer exposure to polybrene caused greater toxicity, especially at 5ug/ml. Concentrations above 5ug/ml (6, 7, and 8ug/ml) show considerable toxicity (n=1) (Supplementary Figure 1.4B).

Finally, to test how polybrene performs when transducing both rtTA and the polycistronic TF virus, IPSCs were seeded at 22K/cm2, and transduced with 5ug/ml polybrene (+spin) at 2.0ul tagBFP-rtTA and 4ul of the polycistronic transcription factor virus. Unfortunately, once all three components of transduction (polybrene, rtTA, and transcription factor virus) were introduced to the culture, widespread toxicity and cell death was visible by day 2 post transduction (not shown). Therefore, although initial results with the CMV-GFP virus showed promise in increasing transduction efficiency, polybrene was not used further with the polycistronic TF virus and tagBFP-rtTA.

Stable Cell Line Greatly Improves LEF1 and mVenus (GFP) Expression

Given to low transduction efficiency and toxicity associated with polybrene, I decided to establish a stable cell line. iPSCs were transduced with the polycistronic TF construct and selected with blasticidin. To identify optimal blasticidin concentration for selection, an antibiotic kill curve was established using 0, 0.5, 1, 2, 4, and 8ug/ml blasticidin on IPSCs transduced with the polycistronic virus, or control non-transduced IPSC. After four days of selection, percentage cell confluency (total cell area divided by total vessel area) was used as a surrogate for cell survival. In

non-transduced IPSCs, there was no apparent effect on cell survival at 0.5 and 1ug/ml blasticidin, but almost complete loss of cells at ≤2ug/ml. There was no loss of cells transduced with the polycistronic virus at all blasticidin concentrations (Figure 1.4A). The concentration of 4ug/ml was chosen for subsequent blasticidin selection in IPSCs.

To develop a polyclonal stable cell line, IPSCs were seeded at 22k/cm^2 and 4ul of the polycistronic transcription factor virus was added the following day. The cells were allowed to grow to confluency, and subsequently split at a density of 22K/cm^2 using accutase to disaggregate clumped cells. The cells were then subject to a further 11 days of Blasticidin 4ug/ml selection, which included 2 cell culture passages.

Cells were then split and seeded at 22K/cm^2 and transduced with 2.0ul of tagBFP-rtTA. To control for endogenous expression of transcription factors, half of the transduced wells were exposed to doxycycline and half were not. Cells were then allowed to grow to confluency, split at 22K/cm^2 and subjected to puromycin at 0.25ug/ml selection for three days. The resulting culture was then fixed and stained with Anti-LEF1 and Anti-GFP to assess transcription factor expression. Anti-GFP was used as I found the mVenus signal in previous experiments was faint relative to high background fluorescence. Expression of LEF1 was markedly increased in cultures exposed to doxycycline and co-localized with GFP signal (Figure 1.4B). Cells not exposed to doxycycline had no LEF1 or GFP signal. Common for polyclonal stable cell lines, levels of expression varied between cells, but a high proportion of cells (82.3%) were positive for LEF1/GFP.

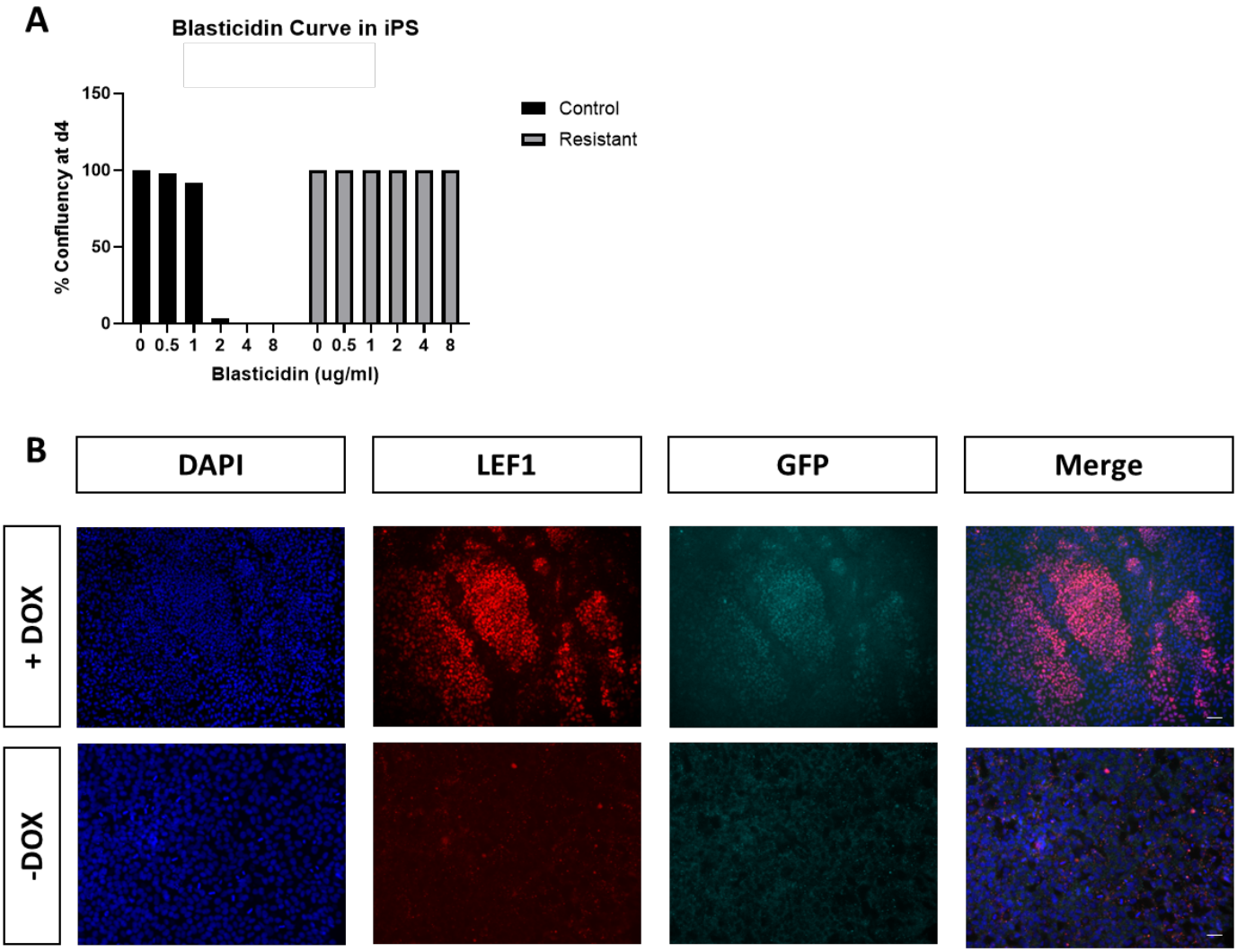


Figure 1.4 – Stable Cell Line Generation

A- Blasticidin exposure to control and resistant IPSCs optimization. Blasticidin has minimal toxicity in control IPSCs after four days of exposure up to 1ug/ml, almost complete selection at 2ug/ml, and total selection at 4 and 8ug/ml. In the other hand, IPSCs transduced with the polycistronic virus to induce Blasticidin resistance survived all concentrations of Blasticidin, suggesting the Blasticidin resistance part of the construct is functionally active and transcribed correctly. (n=1)

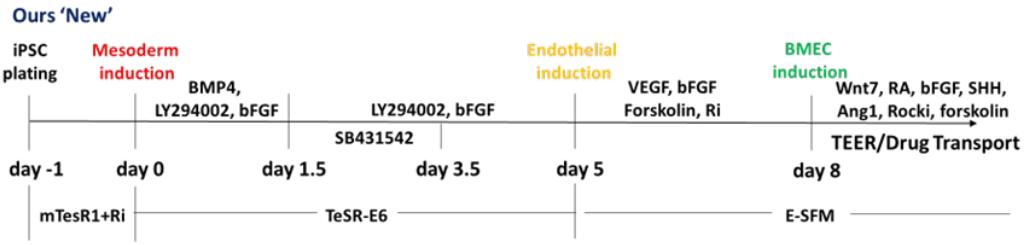
B- Stable cell line generation of IPSCs transduced with the polycistronic virus for the transcription factors. LEF1 was chosen as a marker due to its absence of endogenous expression in untransduced IPSCs. The stable cell line exposed to doxycycline has increased GFP staining that co-localizes with LEF1, indicating correct expression of the transcription factor in transduced cells. The stable cell line not exposed to doxycycline is negative for GFP and LEF1, validating that doxycycline-dependent transcription of the transcription factor c. Scale bars, 100um. (n=3 biological replicates)

Small molecule based BMEC protocol yields highly heterogenous cultures

SBAD0201 cells were differentiated without TF activation using the protocol developed by Dr Chintawar (Figure 1.5A), and were fixed and stained for CLDN5, VE-CADHERIN, OCLN, LEF1 and ETS1. This protocol produced an extremely heterogeneous population of cells, with staining of VE-CADH and CLDN5 present in spaces where cells were clumped (n=1) (Figure 1.5B). However, OCLN was not expressed anywhere in the culture. A large proportion of cells did not express CLDN5 and VE-CADH, and the lack of OCLN expression indicated that significant improvements to this protocol would be required to produce a homogenous culture of brain capillary endothelial like cells. Interestingly, there was no co-localization of LEF1 expression and VE-CADH or CLDN5, but cells with strong ETS1 expression clearly co-localize with both VE-CADH and CLDN5. This supported the hypothesis that ETS1 is necessary for brain capillary endothelial cell identity.

To understand the dynamics of expression of LEF1, ETS1, and MRTFB in the original protocol, gene expression was assessed at day 5 (mesoderm stage), day 8 and day 12 (Supplementary Figure 1.5A). As expected, LEF1 exhibited the greatest upregulation, as it is the only transcription factor not endogenously expressed by IPSCs. Although to a variable degree, LEF1 is upregulated 45 log-fold by day 5 (n=3) and remains highly expressed by the end of the protocol at day 12, with a 53.78 log-fold upregulation. MRTFB was upregulated 2.49 log-fold by day 5 and maintained throughout the remainder of the differentiation. ETS1 expression is reduced at the mesodermal stage, but then upregulated from day 8-12 with 4.70 log-fold increase by day 12. All target gene expressions were normalized to actin, which showed a stable expression through the differentiation (Supplementary Figure 1.5B).

A


Ours 'New'
iPSC plating
Mesoderm induction
BMP4, LY294002, bFGF
LY294002, bFGF
SB431542
Endothelial induction
VEGF, bFGF Forskolin, Ri
BMEC induction
Wnt7, RA, bFGF, SHH, Ang1, Rocki, forskolin
TEER/Drug Transport
day -1
day 0
day 1.5
day 3.5
day 5
day 8
mTesR1+Ri
TeSR-E6
E-SFM

B

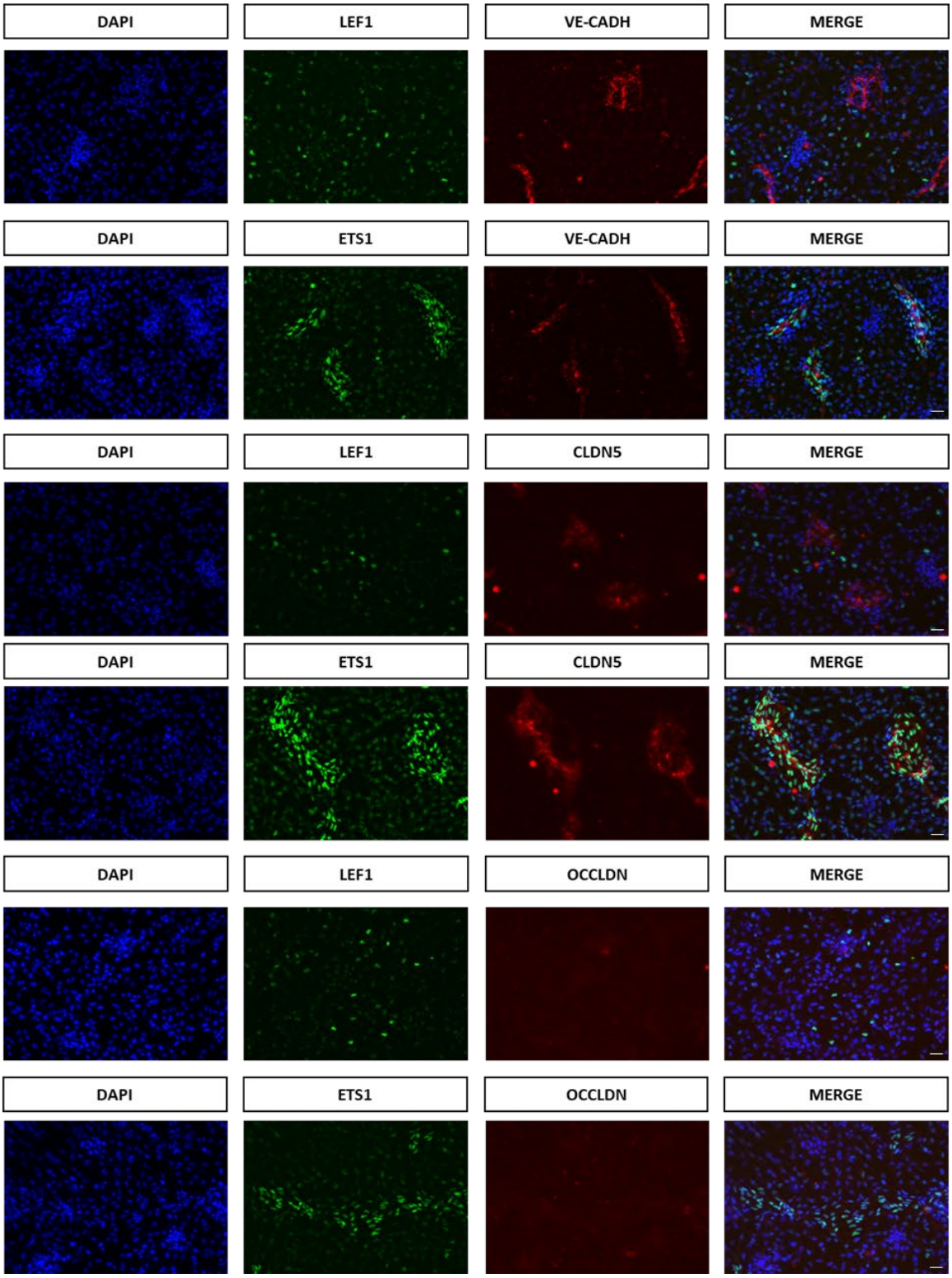

DAPI
LEF1
VE-CADH
MERGE
DAPI
ETS1
VE-CADH
MERGE
DAPI
LEF1
CLDN5
MERGE
DAPI
ETS1
CLDN5
MERGE
DAPI
LEF1
OCCLDN
MERGE
DAPI
ETS1
OCCLDN
MERGE

Figure 1.5 – Original Brain Microvascular Endothelial Cell Differentiation without Transcription Factor Overexpression
A- Original protocol design
B- Immunocytochemistry to check endogenous levels of transcription factors LEF1 and ETS1 and BMEC markers VE-CADHERIN, CLDN5, and OCCLDN. While expression of LEF1 is sporadic throughout the culture, it does specifically co-localize with endothelial markers VE-CADHERIN and CLDN5. On the other hand, cells with high ETS1 signal do co-localize with VE-CADHERIN and CLDN5 signal. OCCLDN was absent from the original cultures, and therefore does not co-localize with any transcription factors. Scale bars, 50um. (n=2 biological replicates)

BMEC Differentiation Protocol Development and Optimization

Activating Transcription factor in IPSC does not yield BMECs

The stable iPSC polycistronic TF line was transduced with rtTA-tagBFP and selected using puromycin at 0.25ug/ml for 3 days. To assess if TF activation in iPSC was sufficient to confer BMEC identity, cells were split to 30K cells/cm^{2,} and the next day the media was changed to either EGM2 or ESFM with doxycycline to initiate TF expression. Different additives to support endothelial cell differentiation were included in each media (Table 1.1). The cells were allowed to grow for three days, passaged at 1:2 split, fixed four days later, and stained for VE-CADHERIN, CLDN5, and OCLN together with ETS1, LEF1, and MRTFB, (Figure 1.6A - 1.12A).

Table 1.1

Basal Media	*Media #*	*Day 1-3 media components*	*Day 4-7 Media components*
EGM2	*1 (Figure 1.6)*	*bFGF + VEGF*	*Same formulation -VEGF + Ang1 and SHH*
	2 (Figure 1.7)	*bFGF + VEGF + Forskolin*	
	3 (Figure 1.8)	*B FGF + VEGF + Forskolin + Wnt7A*	
ESFM	*4 (Figure 1.9)*	*bFGF + VEGF + Forskolin*	*Same formulation – VEGF + Ang1 and SHH*
	5 (Figure 1.10)	*bFGF + VEGF + Forskolin + Wnt7A*	
	6 (Figure 1.11)	*bFGF + VEGF + Forskolin + RA*	
	7 (Figure 1.12)	*bFGF + VEGF + Forskolin + RA + Wnt7A*	

Overall, in all conditions, very few cells expressed both VE-CADHERIN and CLDN5 (except Media 7 that sees upregulation of VE-CADHERIN expression) (Figure 1.6B-1.12B). ESFM (medias 4-7,

Figure 1.9B-1.12B) was superior to EGM2 (medias 1-3, Figure 1.6B-1.8B) with respect to VE-CADHERIN expression as seen with the positive signal in the cell membrane. OCLN staining was positive for all conditions (1-7), but undifferentiated IPSCs serving as a negative control also stain positive for this marker (Supplementary Figure 1.6). Unlike the small molecule-based protocol, LEF1 expression was completely absent except in media 7, which contained Wnt7A and RA. Both ETS1 and MRTFB expression varied between conditions and did not show a consistent pattern of expression based on media formulations. High ETS1 cells did not show discrete co-localization with VE-CADHERIN as previously seen.

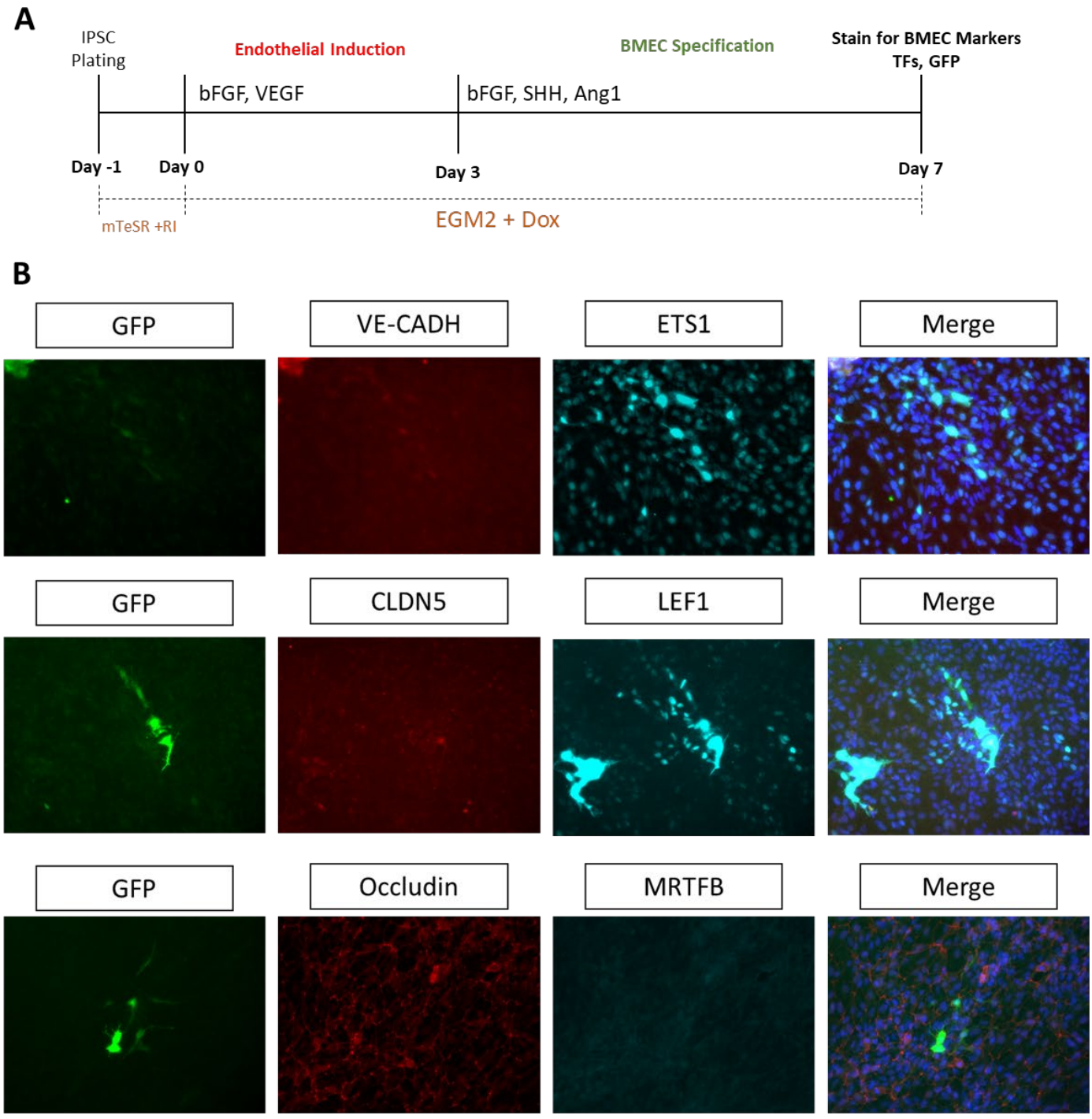


Figure 1.6– Direct Differentiation of IPSCs to BMECs without a Mesodermal Stage
A – Schematic of the protocol performed (EGM2+bFGF+SHH+Ang1)
B- Immunocytochemistry of differentiated cells under with media 1(EGM2: bFGF and VEGF -> bFGF, SHH, Ang1). Cells grown in this media express Occludin but lacked VE-CADHERIN or CLDN5 expression. Merged image contains DAPI channel. Scale bars, 50um. (n=1 biological replicate)

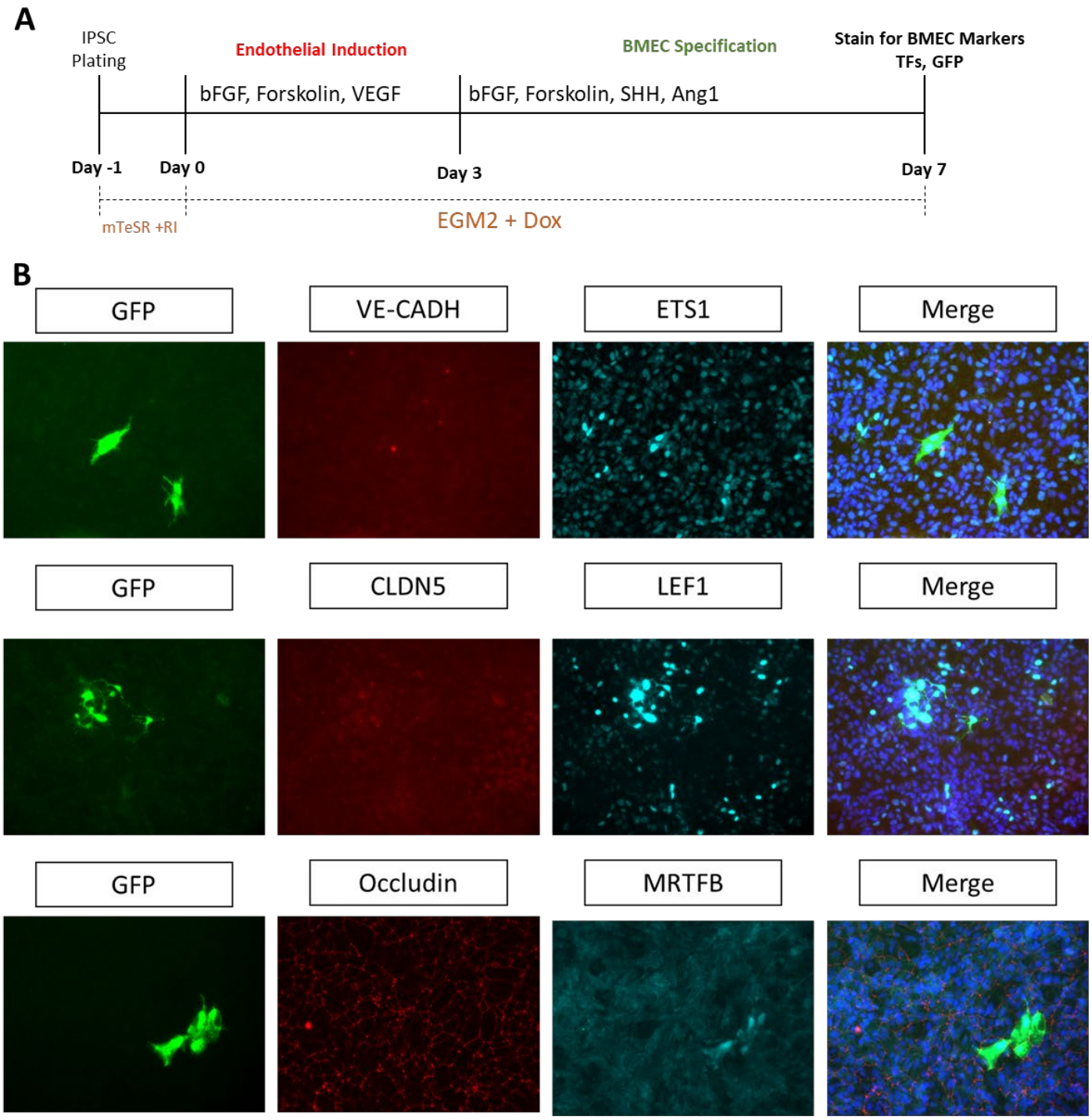


Figure 1.7 – Direct Differentiation of IPSCs to BMECs without a Mesodermal Stage
A – Schematic of the protocol performed (EGM2+bFGF+Forskolin+SHH+Ang1)
B- Immunocytochemistry of differentiated cells under with media 2 (EGM2: bFGF, Forskolin, and VEGF -> bFGF, Forskolin, SHH, and Ang1). Cells grown in this media express Occludin but lacked VE-CADHERIN or CLDN5 expression. Merged image contains DAPI channel. Scale bars, 50um. (n=1 biological replicate)

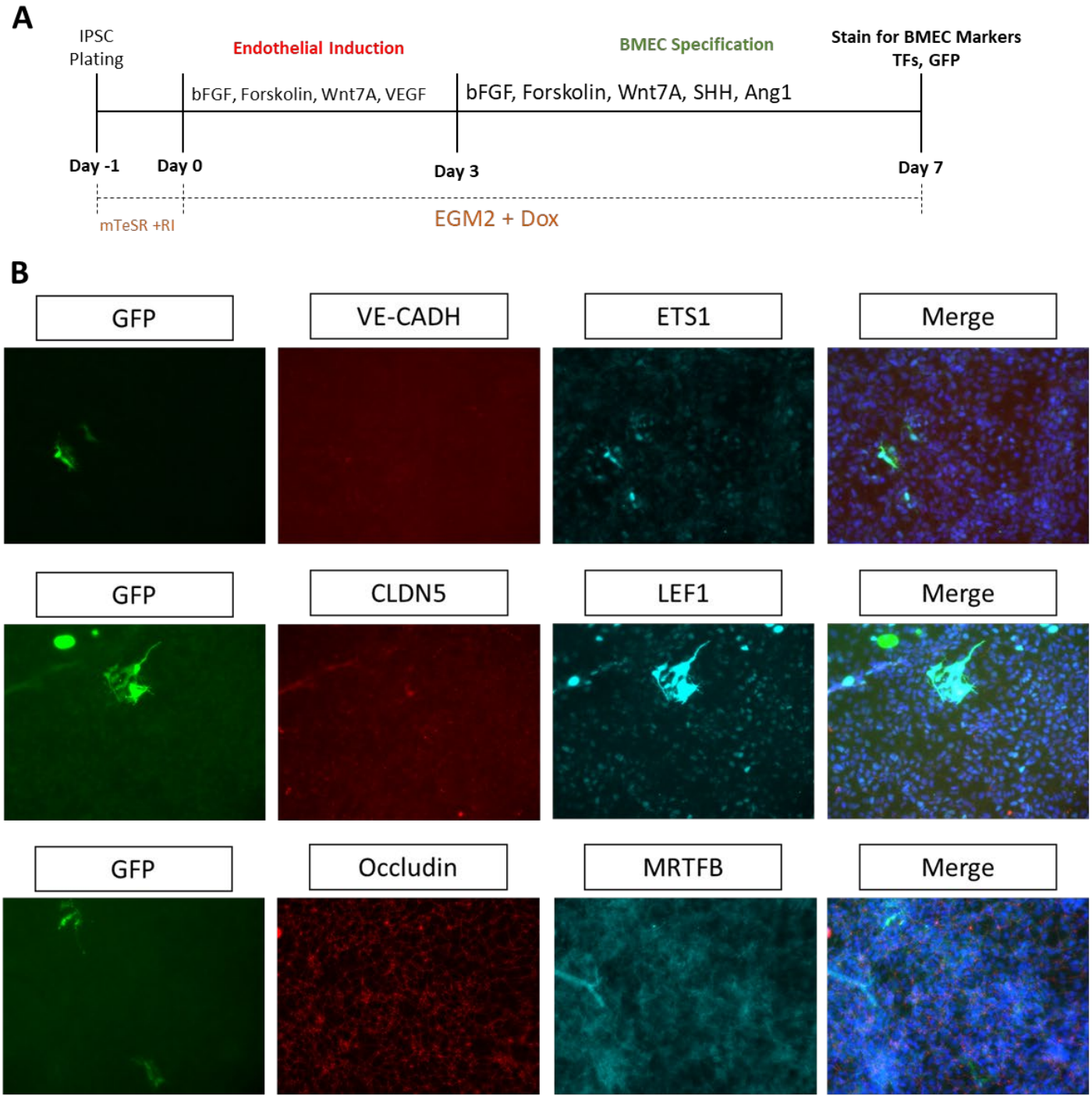


Figure 1.8– Direct Differentiation of IPSCs to BMECs without a Mesodermal Stage
A – Schematic of the protocol performed (EGM2+bFGF+Forskolin+Wnt7A+SHH+Ang1)
B- Immunocytochemistry of differentiated cells under with media 3 (EGM2: bFGF, Forskolin, Wnt7A and VEGF -> bFGF, Forskolin, Wnt7A, SHH, and Ang1). Cells grown in this media express Occludin but lacked VE-CADHERIN or CLDN5 expression. Merged image contains DAPI channel. Scale bars, 50um. (n=1 biological replicate)

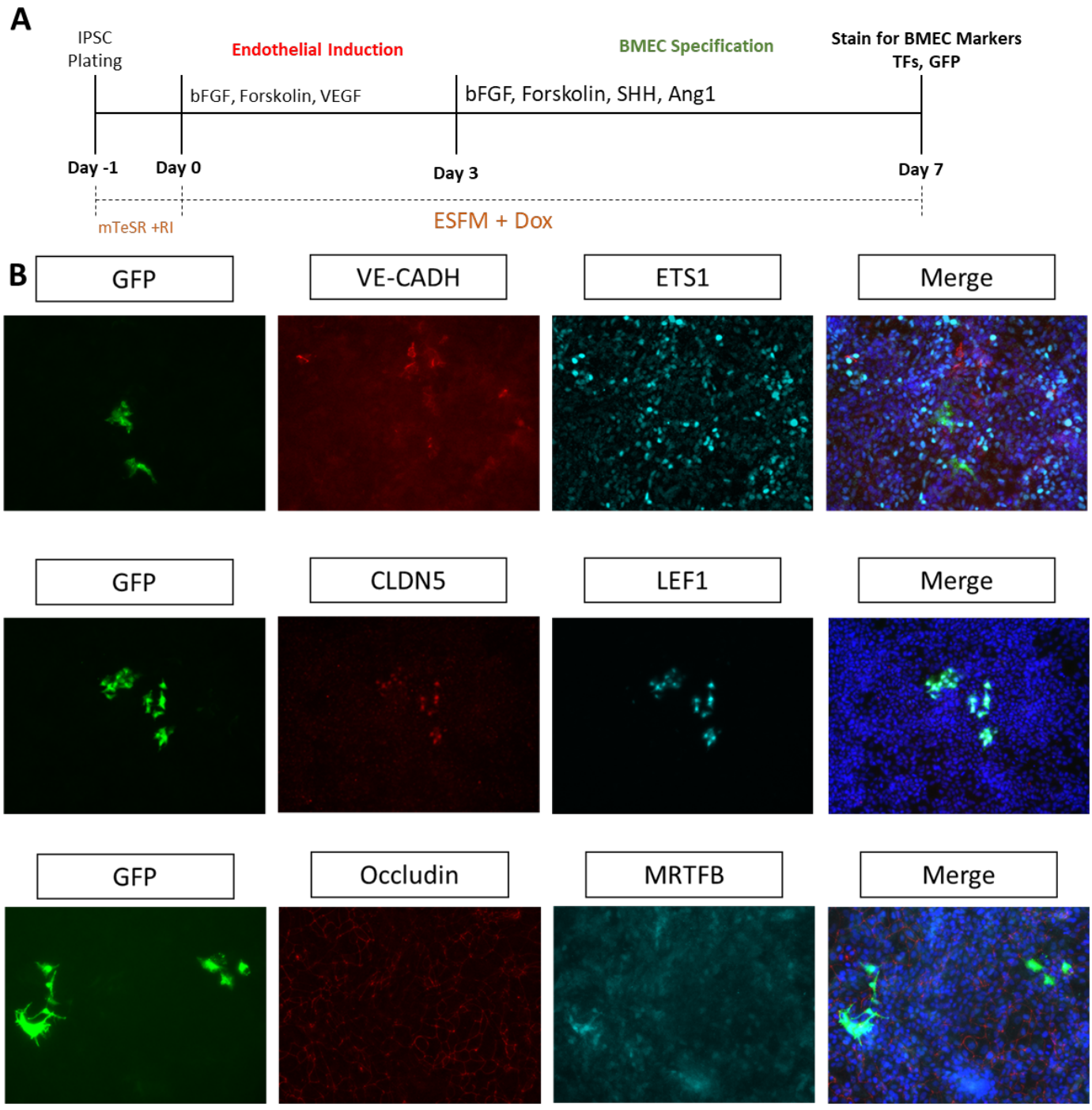


Figure 1.9 – Direct Differentiation of IPSCs to BMECs without a Mesodermal Stage
A – Schematic of the protocol performed (ESFM+Forskolin+SHH+Ang1)
B- Immunocytochemistry of differentiated cells under with media 4 (ESFM: bFGF, Forskolin, and VEGF -> bFGF, Forskolin, SHH, and Ang1). Cells grown in this media express Occludin, have few patches of VE-CADHERIN+ cells, but still lack proper CLDN5 expression. Merged image contains DAPI channel. Scale bars, 50um. (n=1 biological replicate)

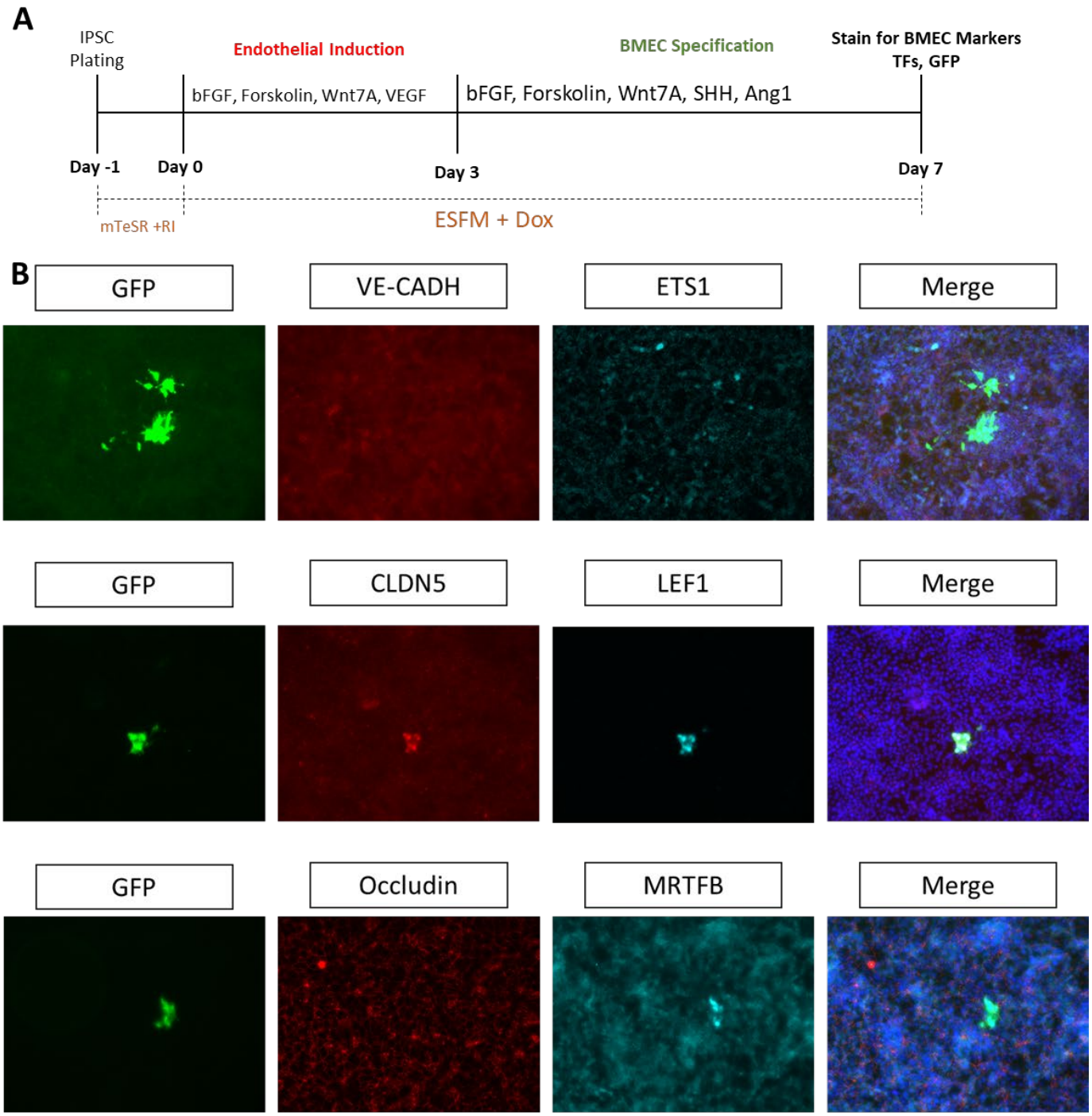


Figure 1.10 – Direct Differentiation of IPSCs to BMECs without a Mesodermal Stage
A – Schematic of the protocol performed (ESFM+bFGF+Forskolin+Wnt7A+SHH+Ang1)
B- Immunocytochemistry of differentiated cells under with media 5 (ESFM: bFGF, Forskolin, Wnt7A and VEGF -> bFGF, Forskolin, Wnt7A, SHH, and Ang1). Cells grown in this media express Occludin, have few patches of VE-CADHERIN+ cells, but still lack proper CLDN5 expression. Merged image contains DAPI channel. Scale bars, 50um. (n=1 biological replicate)

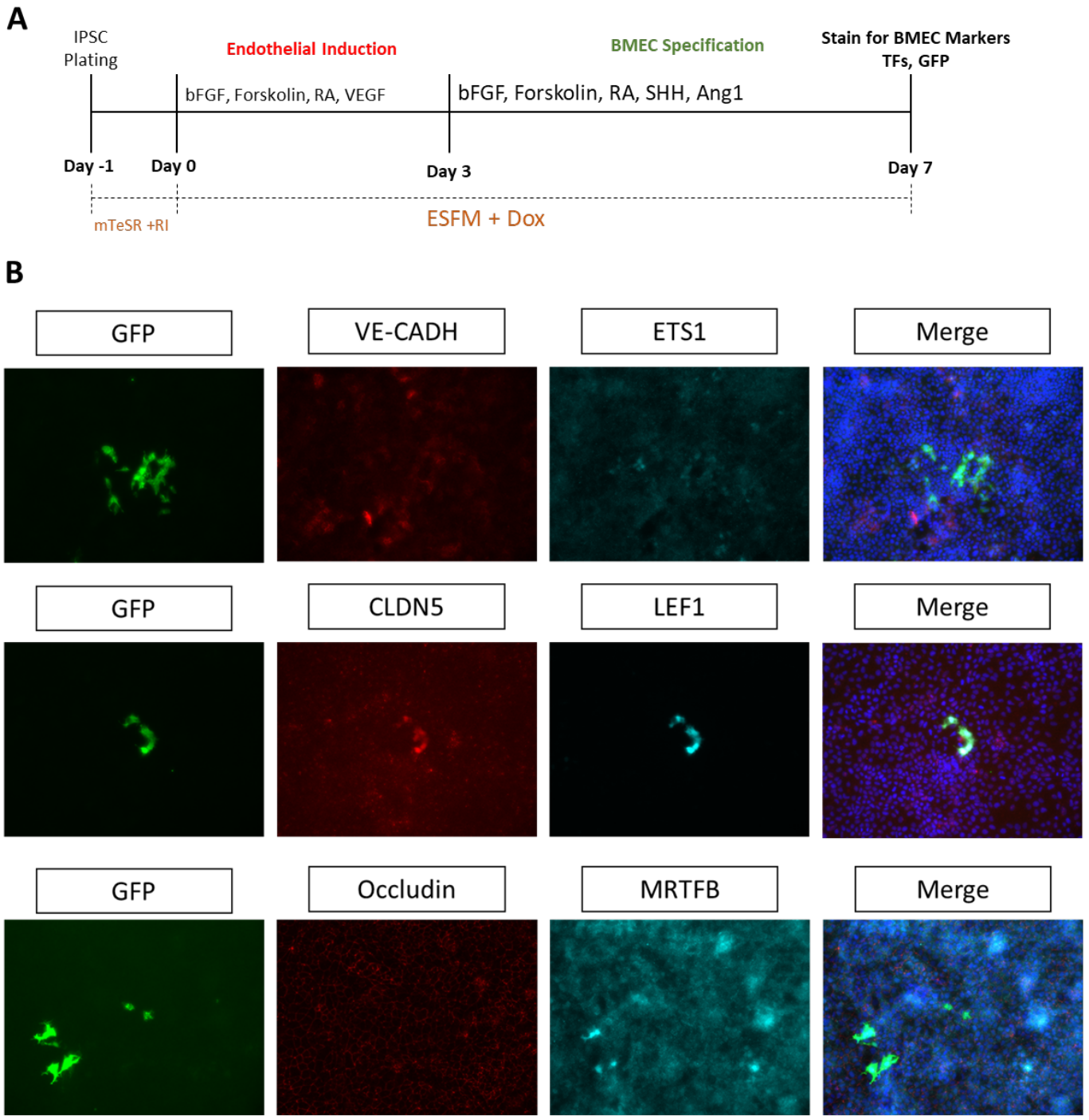


Figure 1.11 – Direct Differentiation of IPSCs to BMECs without a Mesodermal Stage
A – Schematic of the protocol performed (ESFM+bFGF+Forskolin+RA+SHH+Ang1)
B- Immunocytochemistry of differentiated cells under with media 6 (ESFM: bFGF, Forskolin, RA and VEGF -> bFGF, Forskolin, RA, SHH, and Ang1). Cells grown in this media express Occludin, have few patches of VE-CADHERIN+ cells, but still lack proper CLDN5 expression. Merged image contains DAPI channel. Scale bars, 50um. (n=1 biological replicate)

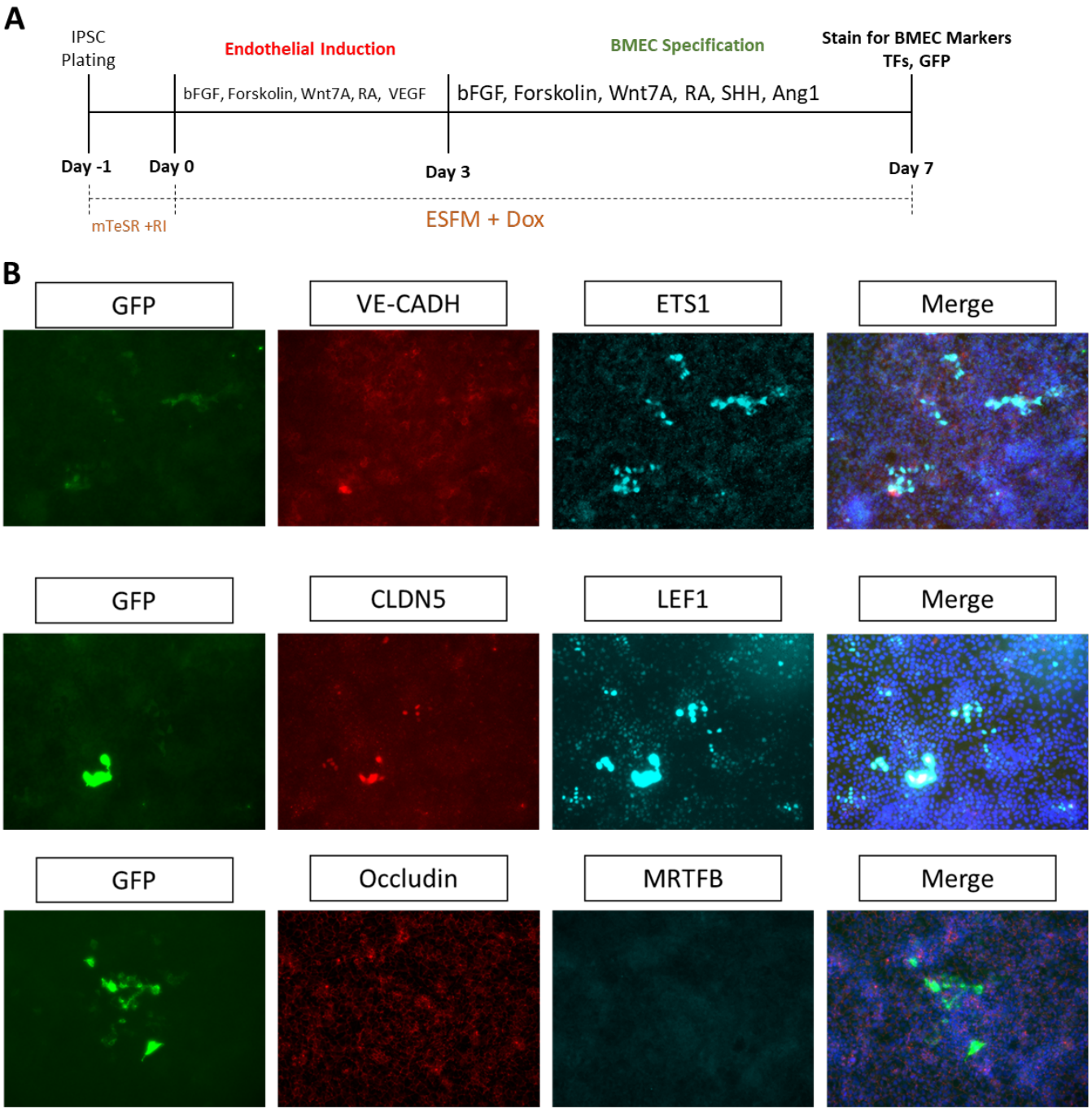


Figure 1.12 – Direct Differentiation of IPSCs to BMECs without a Mesodermal Stage
A – Schematic of the protocol performed (ESFM+bFGF+Forskolin+Wnt7A+RA+SHH+Ang1)
B- Immunocytochemistry of differentiated cells under with media 7 (ESFM: bFGF, Forskolin, Wnt7A, RA and VEGF -> bFGF, Forskolin, Wnt7A, RA, SHH, and Ang1). Cells grown in this media express Occludin, have high proportion of cells expressing VE-CADHERIN, but still lack proper CLDN5 expression. Cells grown in this media experienced the highest expression of LEF1 in untransduced (GFP-) cells. Merged image contains DAPI channel. Scale bars, 50um. (n=1 biological replicate)

Introducing a Mesoderm Intermediate and Transcription Factor Expression Greatly Increases BMEC Fate and Yield

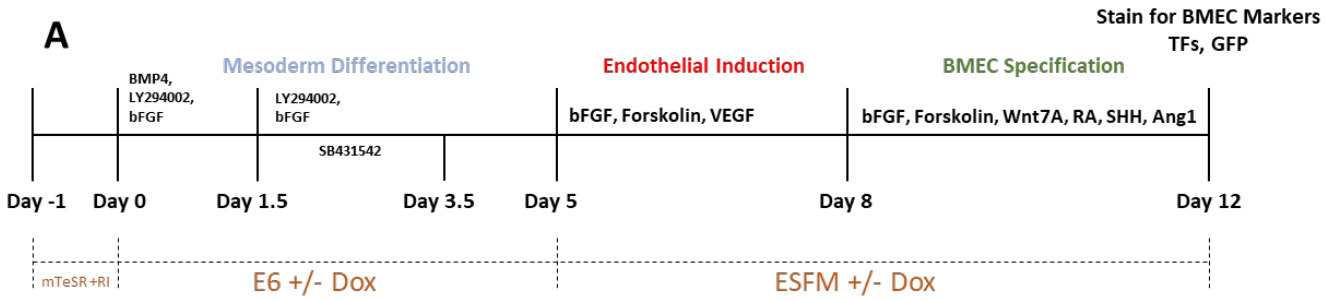
I next investigated TF expression in mesoderm patterned iPSC. The stable cell line was taken to the mesodermal stage as described above with TF activation via doxycycline. A number of different conditions (Table 1.2) were investigated including cells not exposed to doxycycline as a control. At day 12, cells were fixed and stained for key endothelial markers, LEF1, ETS1, MRTFB and Anti-GFP (Figure 1.13A-1.16A).

Table 1.2

Media #	*Day 5-8 media (ESFM)*	*Day 8-12 Media*
1 (Figure 1.13)	*bFGF+Forskolin+VEGF (+/-dox)*	*bFGF + Forskolin + Wnt7A + RA + Ang1 + SHH*
2 (Figure 1.14)	*bFGF+Forskolin+VEGF+Wnt7A (+/-dox)*	
3 (Figure 1.15)	*bFGF+Forskolin+VEGF+RA (+/-dox)*	
4 (Figure 1.16)	*bFGF+Forskolin+VEGF+Wnt7A+RA (+/-dox)*	

TF activation on mesoderm patterned iPSC led to a significant improvement in all conditions when compared to TF activation in iPSC with no mesoderm patterning. Cells in media 1 have very low CLDN5 expression, but VE-CADHERIN and PECAM1 expression was strong with localization to the cell membrane (Figure 1.13B). LEF1, ETS1, and MRTFB expression is upregulated with widespread GFP signal in comparison to TF activation in iPSC (Figure 1.6-1.12). Further, the control differentiation without TF activation (DOX^- condition) resulted in sporadic signal of VE-CADHERIN and PECAM1, while the expression in DOX^+ condition is more widespread and indicates a higher proportion of cells with endothelial marker expression.

Media 2 containing Wnt7A showed a marginal increase in CLDN5 signal but not localized to the membrane (Figure 1.14B). VE-CADHERIN expression was less jagged and more robustly expressed in each cell than in media 1, indicating that Wnt7A addition to the media may have beneficial effects in the differentiation.


A
Stain for BMEC Markers
TFs, GFP
Mesoderm Differentiation
Endothelial Induction
BMEC Specification
BMP4,
LY294002,
bFGF
LY294002,
bFGF
SB431542
bFGF, Forskolin, VEGF
bFGF, Forskolin, Wnt7A, RA, SHH, Ang1
Day -1
Day 0
Day 1.5
Day 3.5
Day 5
Day 8
Day 12
mTeSR +RI
E6 +/- Dox
ESFM +/- Dox

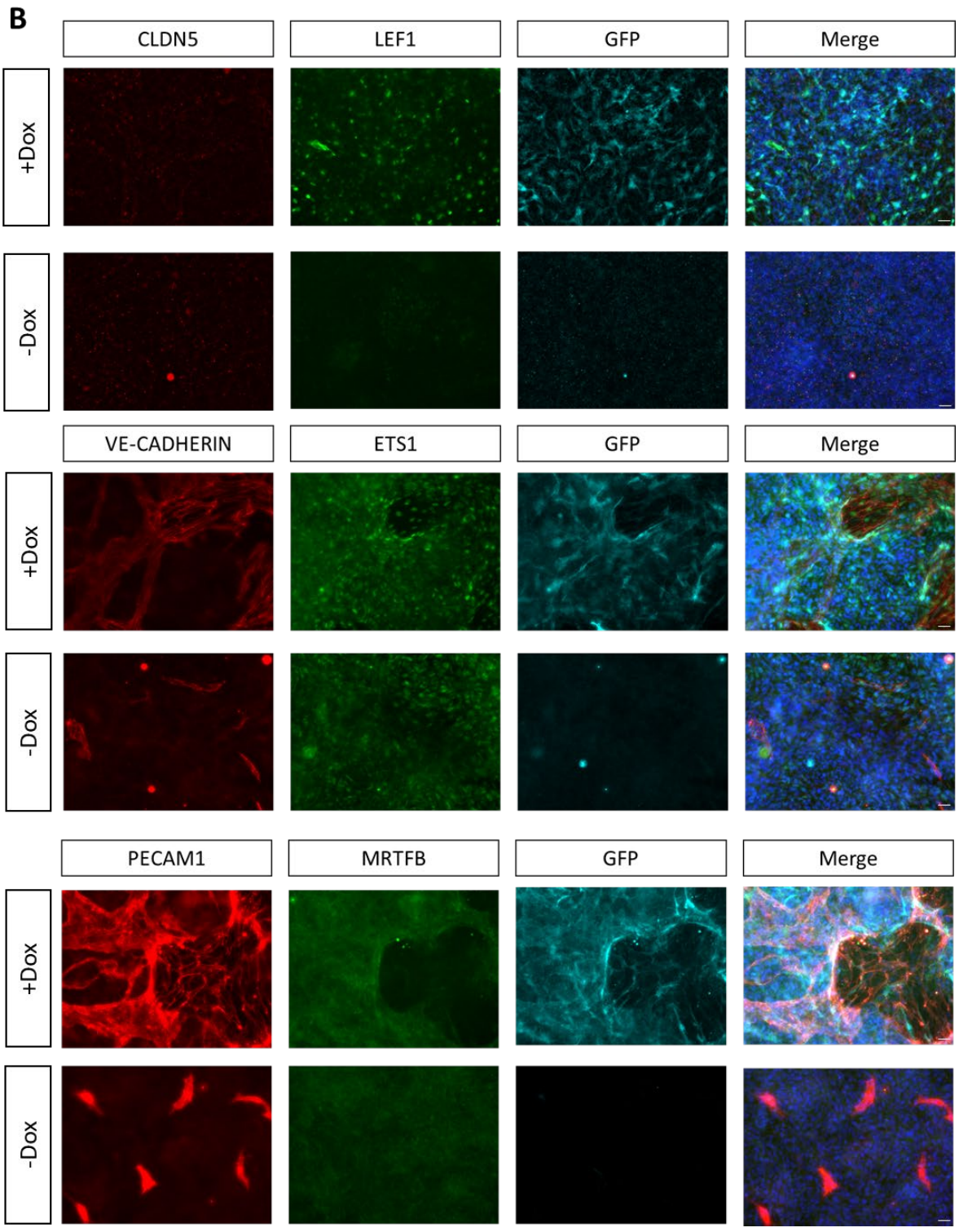

B
CLDN5
LEF1
GFP
Merge
+Dox
-Dox
VE-CADHERIN
ETS1
GFP
Merge
+Dox
-Dox
PECAM1
MRTFB
GFP
Merge
+Dox
-Dox

Figure 1.13 - Direct Differentiation of IPSCs to BMECs with a Mesodermal Stage
A- Schematic of the protocol performed with endothelial induction modulation (bFGF+Forskolin+VEGF)
B- Immunocytochemistry of BMEC markers CLDN5, VE-CADHERIN, PECAM1 and transcription factors LEF1, ETS1, and MRTFB under media 1(bFGF, Forskolin, VEGF). Dox+ cells assembled into a 'double-layer' and show expression of VE-CADHERIN and PECAM1. Dox- cells show a smaller proportion of VE-CADHERIN and PECAM1+ cells. Neither dox conditions express CLDN5. Scale bar, 50um. (n=2 biological replicates)

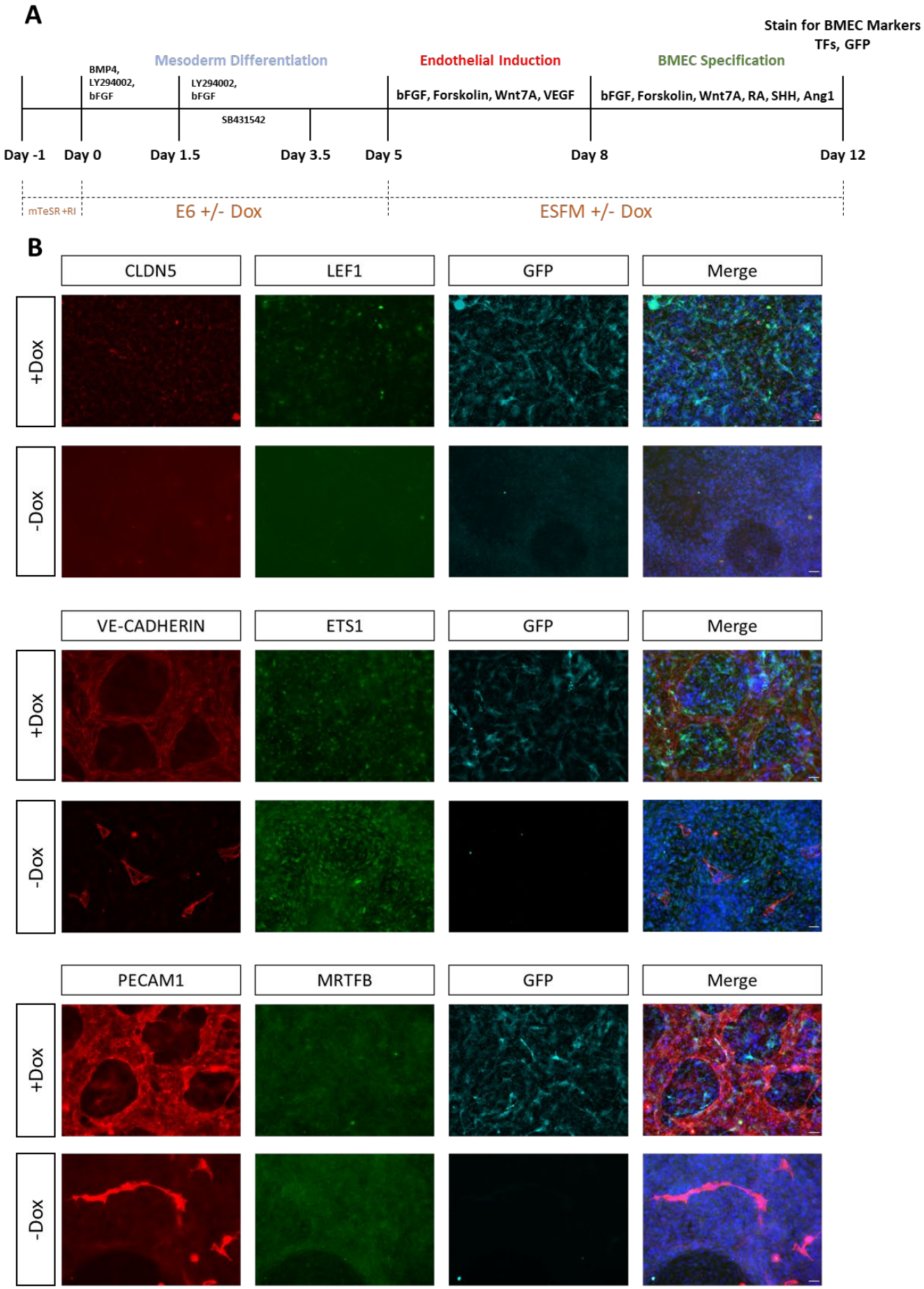

A
Stain for BMEC Markers
TFs, GFP
Mesoderm Differentiation
Endothelial Induction
BMEC Specification
BMP4,
LY294002,
bFGF
LY294002,
bFGF
SB431542
bFGF, Forskolin, Wnt7A, VEGF
bFGF, Forskolin, Wnt7A, RA, SHH, Ang1
Day -1
Day 0
Day 1.5
Day 3.5
Day 5
Day 8
Day 12
mTeSR +RI
E6 +/- Dox
ESFM +/- Dox
B
CLDN5
LEF1
GFP
Merge
+Dox
-Dox
VE-CADHERIN
ETS1
GFP
Merge
+Dox
-Dox
PECAM1
MRTFB
GFP
Merge
+Dox
-Dox

Figure 1.14 - Direct Differentiation of IPSCs to BMECs with a Mesodermal Stage
A- Schematic of the protocol performed with endothelial induction modulation (bFGF+Forskolin+Wnt7A+VEGF) B- Immunocytochemistry of BMEC markers CLDN5, VE-CADHERIN, PECAM1 and transcription factors LEF1, ETS1, and MRTFB under media 2(bFGF, Forskolin, Wnt7A, VEGF). Dox+ cells assembled into a 'double-layer' and show expression of VE-CADHERIN and PECAM1. Dox- cells show a smaller proportion of VE-CADHERIN and PECAM1+ cells. Dox+ condition shows a faint signal for CLDN5 while Dox- does not show any signal. Scale bar, 50um. (n=2 biological replicates)

The best outcomes were in cells grown in Medias 3 and 4 with cells showing robust VE-CADHERIN and PECAM1 expression (Figure 1.15B-1.16B). These media differed from Media 1 and 2 with respect to retinoic acid addition, which appeared to lead to better monolayer formation. The presence of Wnt7A (Media 4) led to a subtle increase in expression of CLDN5. RA did not seem to help DOX^- conditions, showing` similar appearances in media without RA. Further, the DOX^- conditions resulted in greater cell proliferation, with 67.15% DAPI coverage compared to 49.5% for DOX^+. Therefore, ESFM media containing bFGF, forskolin, VEGF, Wnt7A and RA was chosen as to progress further optimization rounds.

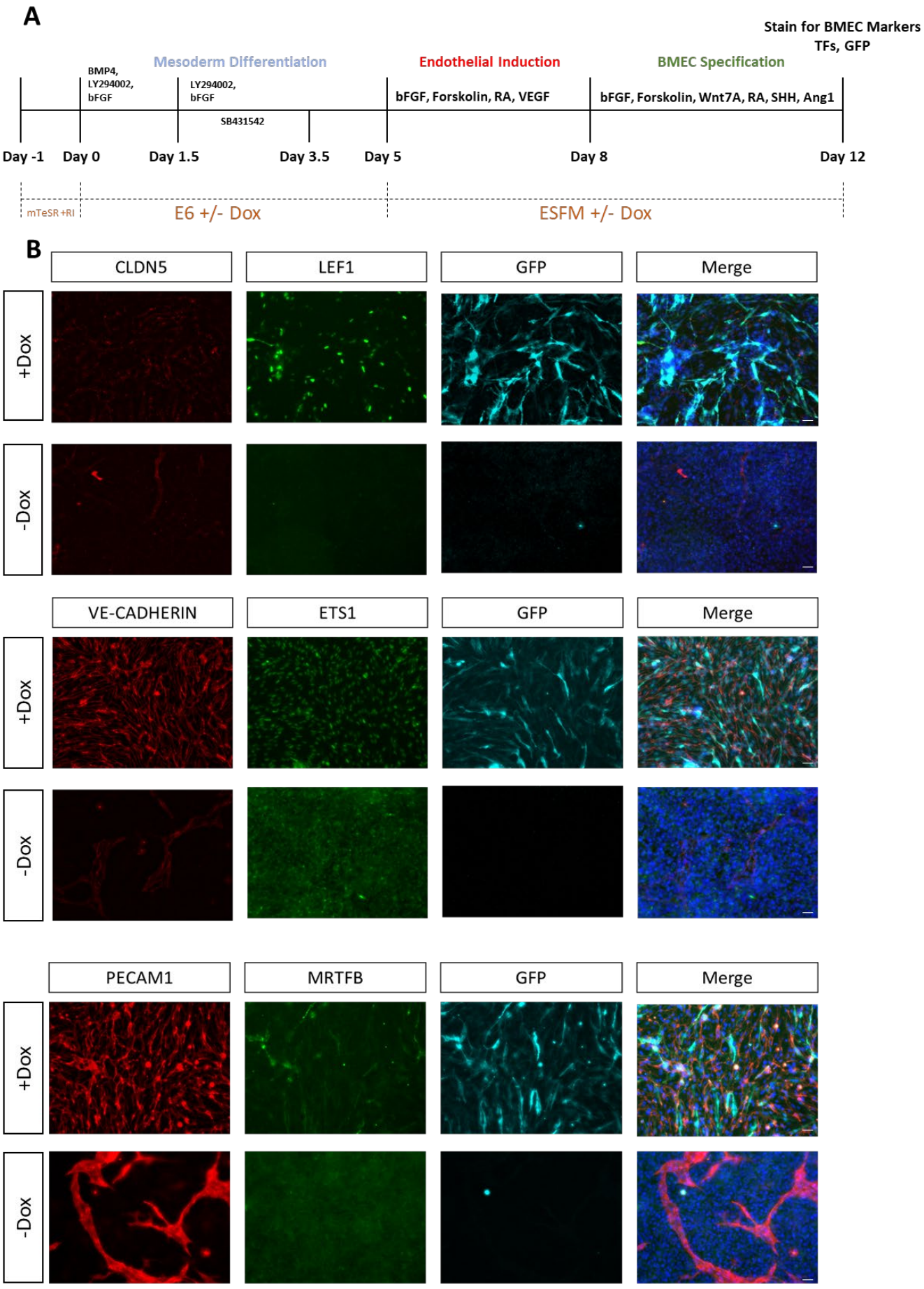

A
Stain for BMEC Markers
TFs, GFP
Mesoderm Differentiation
Endothelial Induction
BMEC Specification
BMP4,
LY294002,
bFGF
LY294002,
bFGF
SB431542
bFGF, Forskolin, RA, VEGF
bFGF, Forskolin, Wnt7A, RA, SHH, Ang1
Day -1
Day 0
Day 1.5
Day 3.5
Day 5
Day 8
Day 12
mTeSR +RI
E6 +/- Dox
ESFM +/- Dox
B
CLDN5
LEF1
GFP
Merge
+Dox
-Dox
VE-CADHERIN
ETS1
GFP
Merge
+Dox
-Dox
PECAM1
MRTFB
GFP
Merge
+Dox
-Dox

Figure 1.15 - Direct Differentiation of IPSCs to BMECs with a Mesodermal Stage
A- Schematic of the protocol performed with endothelial induction modulation (bFGF+Forskolin+RA+VEGF)
B- Immunocytochemistry of BMEC markers CLDN5, VE-CADHERIN, PECAM1 and transcription factors LEF1, ETS1, and MRTFB under media 3(bFGF, Forskolin, RA, VEGF). Dox+ cells form a single monolayer and show expression of VE-CADHERIN and PECAM1. Dox- cells show a smaller proportion of VE-CADHERIN and PECAM1+ cells. Dox+ condition shows a faint signal for CLDN5 while Dox- does not show any signal. Scale bar, 50um. (n=2 biological replicates)

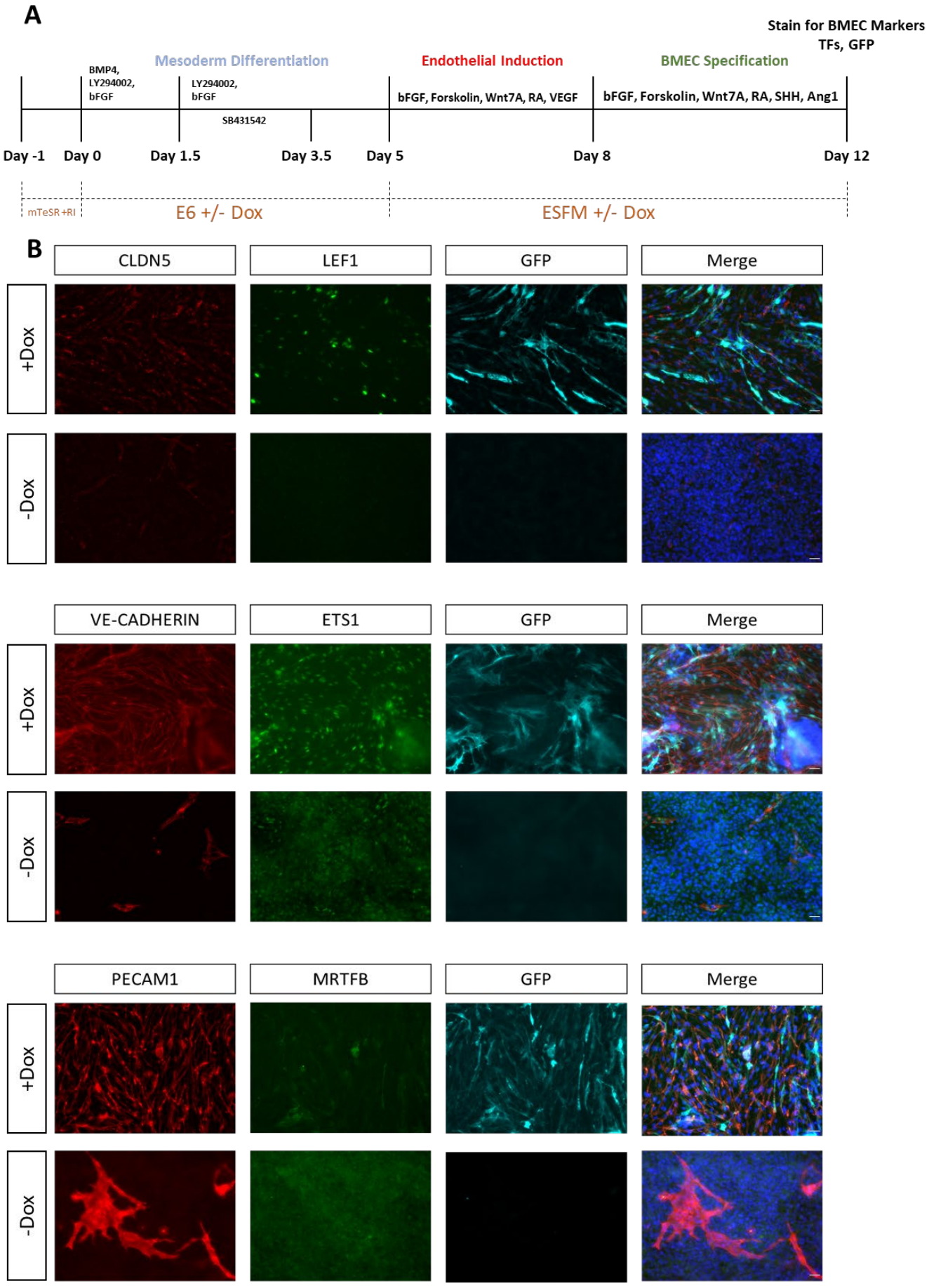

A
Stain for BMEC Markers
TFs, GFP
Mesoderm Differentiation
Endothelial Induction
BMEC Specification
BMP4,
LY294002,
bFGF
LY294002,
bFGF
SB431542
bFGF, Forskolin, Wnt7A, RA, VEGF
bFGF, Forskolin, Wnt7A, RA, SHH, Ang1
Day -1
Day 0
Day 1.5
Day 3.5
Day 5
Day 8
Day 12
mTeSR+RI
E6 +/- Dox
ESFM +/- Dox
B
CLDN5
LEF1
GFP
Merge
+Dox
-Dox
VE-CADHERIN
ETS1
GFP
Merge
+Dox
-Dox
PECAM1
MRTFB
GFP
Merge
+Dox
-Dox

Figure 1.16 - Direct Differentiation of IPSCs to BMECs with a Mesodermal Stage
A- Schematic of the protocol performed with endothelial induction modulation (bFGF+Forskolin+VEGF)
B- Immunocytochemistry of BMEC markers CLDN5, VE-CADHERIN, PECAM1 and transcription factors LEF1, ETS1, and MRTFB under media 4(bFGF, Forskolin, Wnt7A, RA, VEGF). Dox+ cells form a single monolayer and show expression of VE-CADHERIN and PECAM1. Dox- cells show a smaller proportion of VE-CADHERIN and PECAM1+ cells. Dox+ condition shows a faint signal for CLDN5 while Dox- does not show any signal. Scale bar, 50um. (n=2 biological replicates)

Cells grown in media 3 and 4 reduced the cells to a monolayer with sporadic large 'clumps' of cells (Supplementary Figure 1.7). Whilst the images were slightly diffuse due to different focal planes in the culture, the cells exhibited strong expression of CLDN5, VE-CADHERIN, PECAM1 and GFP. This suggests that the "clumps" may provide the best conditions for differentiation into BMECs (Figure 1.17).

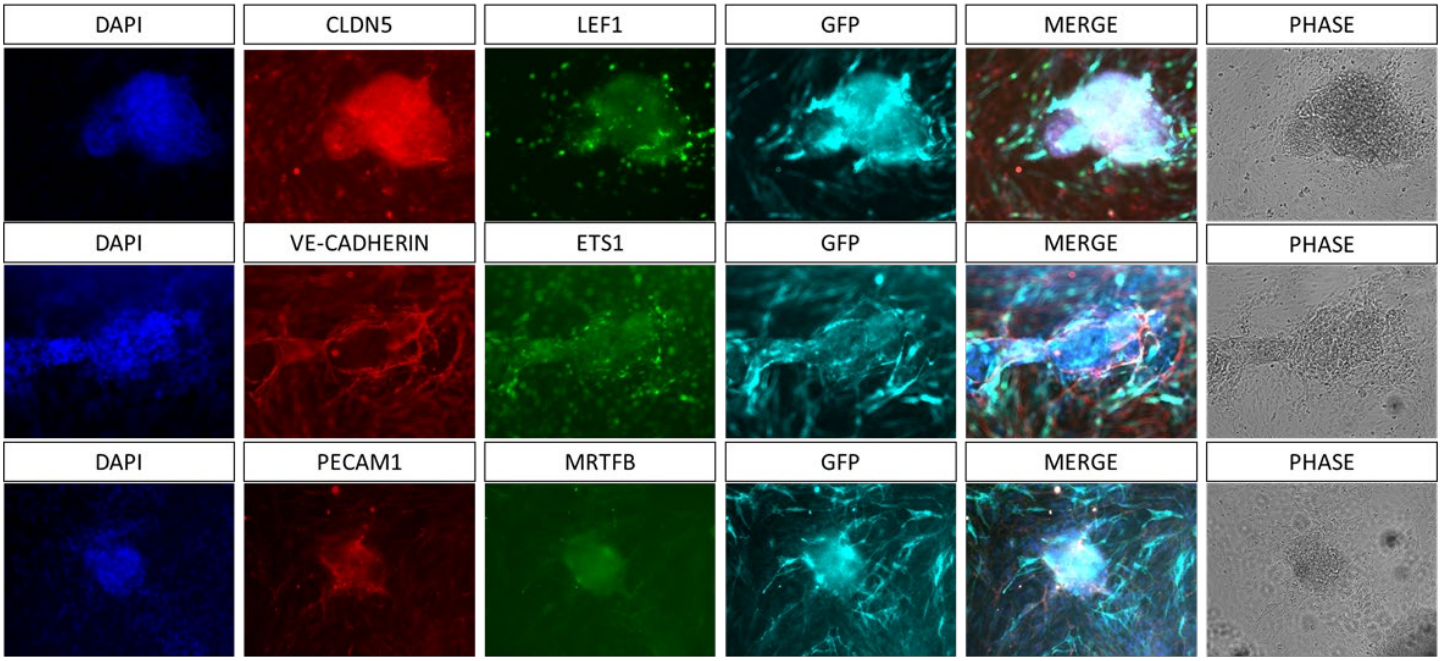


Figure 1.17 – Clump-focused immunocytochemistry of cells grown under media 4.
F- Immunocytochemistry of clumps at day 12 show strong expression of BMEC markers, transcription factors, and GFP. (n=2 biological replicates)

Clumped Cells Act as an Endothelial Factory

To determine whether cells in the clumps were dividing endothelial progenitors or maturing post-mitotic endothelial cells, the culture was further stained with KI67. Cells in clumps were mostly $KI67^{+}$ while cells in the monolayer below had a considerably higher proportion of $KI67^{-}$ cells (Figure 1.18). This led to a hypothesis that these clumps may serve as endothelial progenitor factories, which produce mature, KI67- endothelial cells that may then migrate away.

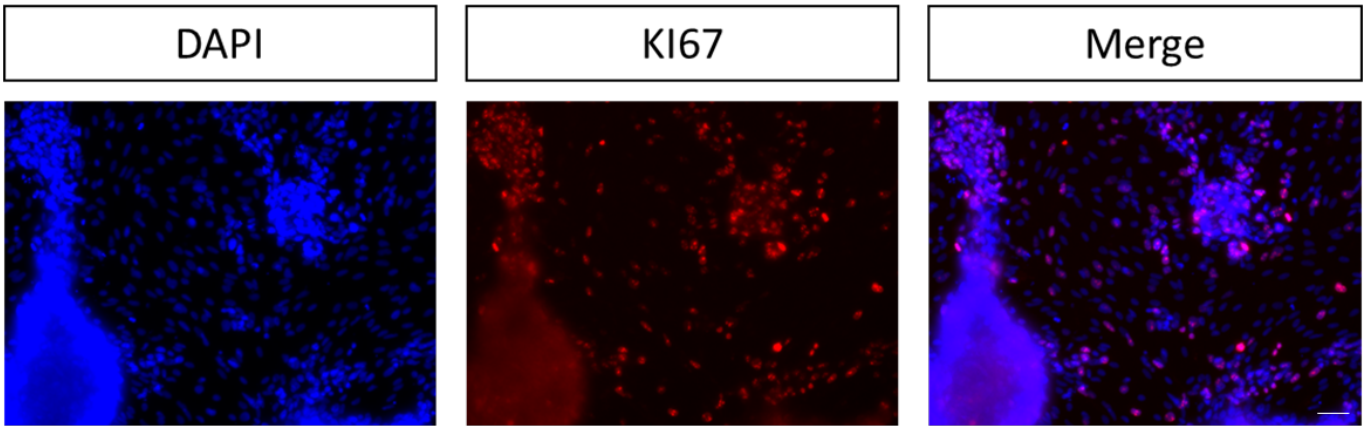


Figure 1.18 – Analysis of Formed Clumps in BMEC Differentiation Including Wnt7A and RA
A- Immunocytochemistry of clumps at day 12 show while clumped cells are positive for KI67, cells in the monolayer below are mostly KI67-. Scale bar, 50um. (n=3 biological replicates)

To test this hypothesis, RELESR, a gentle dissociating reagent, was employed to dissociate any single cells while keeping clumps intact. By using differential centrifugation at a low speed of 35g for 1 minute, heavy clumps formed by day 8 of the protocol pelleted to the bottom of a tube while single cells remain suspended in the supernatant. Repeating this process three times during passage allowed the resulting culture to be remarkably enriched with clumps and have few single cells.

Clumps and single cells were then seeded into separate multi-well plates and cultured for at least 4 days. Single-cells harvested from the supernatant of the differential centrifugation did not assemble into a homogenous monolayer and did not express VE-CADHERIN and PECAM1 (Supplementary Figure 1.8).

After seeding the clumps, a monolayer is formed around them with cells expressing PECAM1, VE-CADHERIN, and CLDN5 (Figure 1.19A). Furthermore VE-CADHERIN^{+} cells in this monolayer were KI67^{-}, suggesting they had entered a maturation stage (Figure 1.19B). Lastly, seeding isolated clumps in growth-factor-reduced (GFR) Matrigel matrix allowed endothelial cells to grow out and form vessel-like structures (Figure 1.20A,B). These structures expressed CLDN5 and VE-CADHERIN. These results indicate that cells growing out of clumps are endothelial. Interestingly, CLDN5 expression was highly expressed in a 3D culture compared to monolayer differentiations, suggesting cells preferentially differentiate to BMECs in 3D culture.

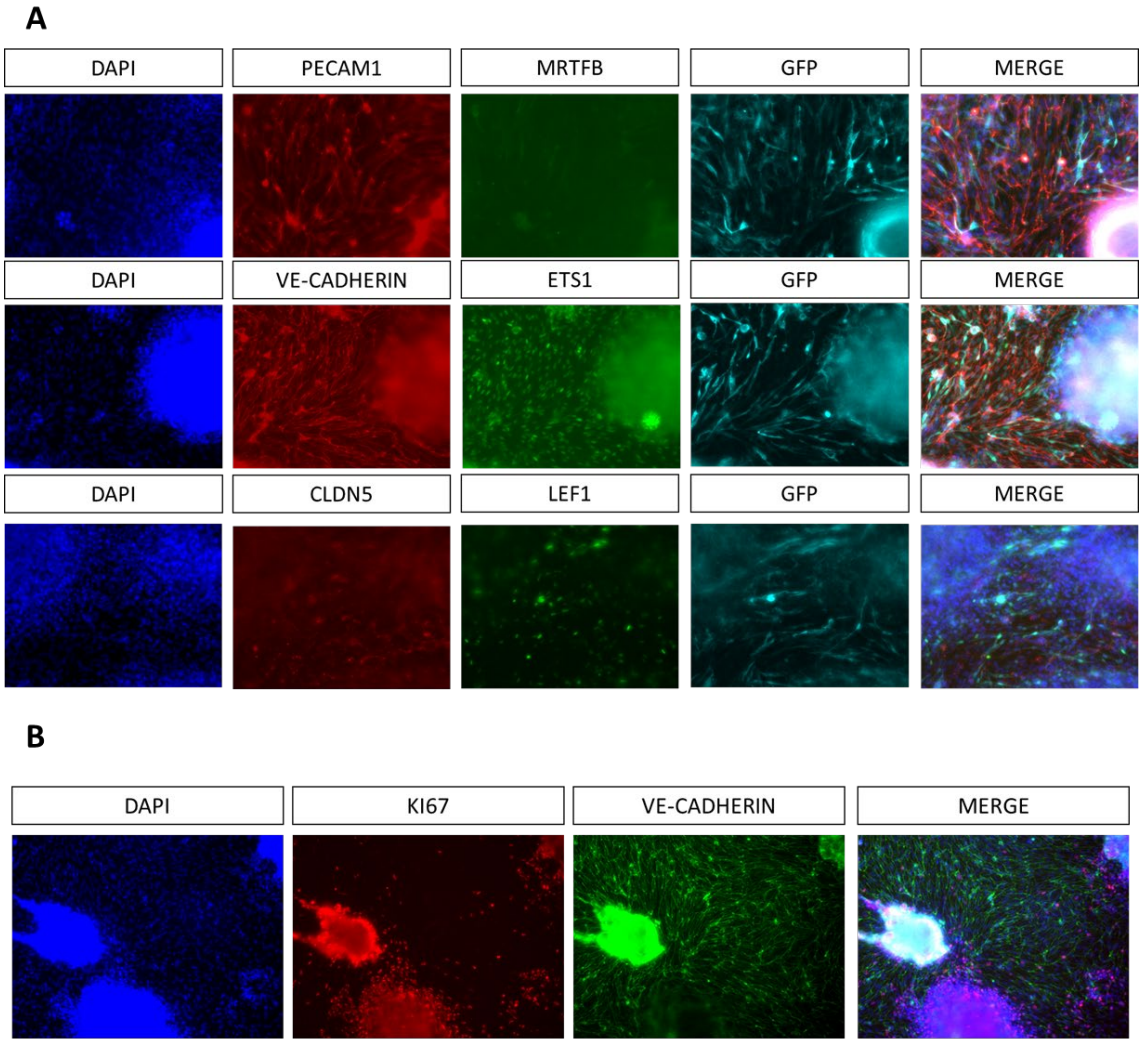


Figure 1.19 – Analysis of Formed Clumps in BMEC Differentiation Including Wnt7A and RA
A- Immunocytochemistry of BMEC markers, transcription factors, and GFP of isolated clumps show clumps give rise to BMEC cells. Scale bar, 50um. (n=2 biological replicates)
B- Immunocytochemistry of clumps at day 12 of VE-CADHERIN and KI67 show that VE-CADHERIN+ cells in monolayer below are mature and KI67-. Scale bar, 50um. (n=2 biological replicates)

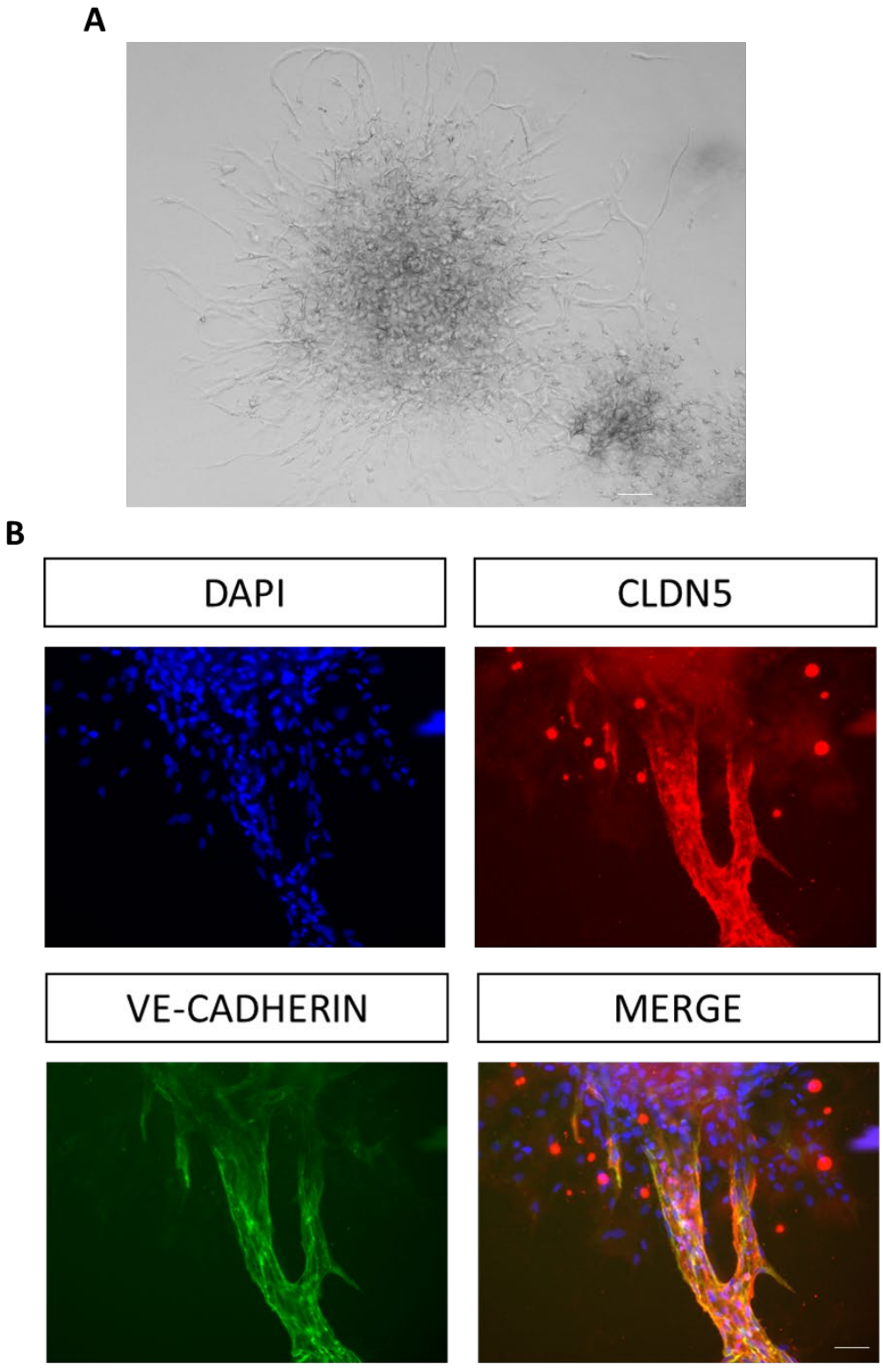


Figure 1.20 – Analysis of Formed Clumps in BMEC Differentiation Including Wnt7A and RA
A-Phase image of isolated clump. Image taken at 10X. Scale bar, 100um.
B- Immunocytochemistry of isolated clumps seeded in GFR Matrigel give rise to large vessel-like structures with strong expression of CLDN5 and VE-CADHERIN. Scale bar, 50um. (n=3 biological replicates)

Ang1, SHH, and Wnt3A do not Improve BMEC Fate

To try to improve BMEC maturation and barrier formation, time in culture was increased from 12 to 16 days (Figure 1.21-1.25A). The addition of ANG1 and SHH, which *in vivo* are produced by pericytes and astrocytes, was also evaluated. Furthermore, Wnt7A was replaced by Wnt3A in certain medias as some protocols use Wnt3A [222]. Lastly, the effect of extended VEGF exposure was tested. A summary of these conditions is given in table 1.3.

Table 1.3

Media	*Day 5-8 Media*	*Day 8-16 Media*
1 (Figure 1.21)	*bFGF+Forskolin+VEGF+Wnt7A+RA*	*bFGF+Forskolin+Wnt7A+RA+Ang1+SHH*
2 (Figure 1.22)		*bFGF+Forskolin+Wnt7A+RA*
3 (Figure 1.23)		*bFGF+Forskolin+Wnt3A+RA+Ang1+SHH*
4 (Figure 1.24)		*bFGF+Forskolin+Wnt3A+RA*
5 (Figure 1.25)		*bFGF+Forskolin+VEGF+Wnt7A+RA*

Immunocytochemistry reveals that the addition of Ang1 and SHH do not change VE-CADHERIN or PECAM1 expression (n=2) (Figure 1.21-1.22). Wnt3A also resulted in no change in expression of PECAM1, VE-CADHERIN, and CLDN5 (Figure 1.23-1.24). Lastly, extending VEGF exposure induces subtle morphological changes to endothelial cells (Figure 1.25), whereby the cells were not as elongated and homogenous.

A necessary condition of a successful differentiation to endothelial rather than epithelial cells, is absence of E-CADHERIN expression. Across all conditions, there was minimal to no E-CADHERIN staining, confirming that differentiated cells are not a hybrid endothelial-epithelial cells as seen in other protocols (Figure 1.21-1.25). The differentiation protocol is capable of producing E-CADHERIN^{+} cells, as evidenced by the small clusters present in the cultures, but importantly, these E-CADHERIN^{+} cells do not co-localize with endothelial marker PECAM1. This confirms that these E-CADHERIN^{+} cells are a separate population of cells. Based on these results, subsequent experiments did not include Ang1, SHH, Wnt3A or extended VEGF exposure.

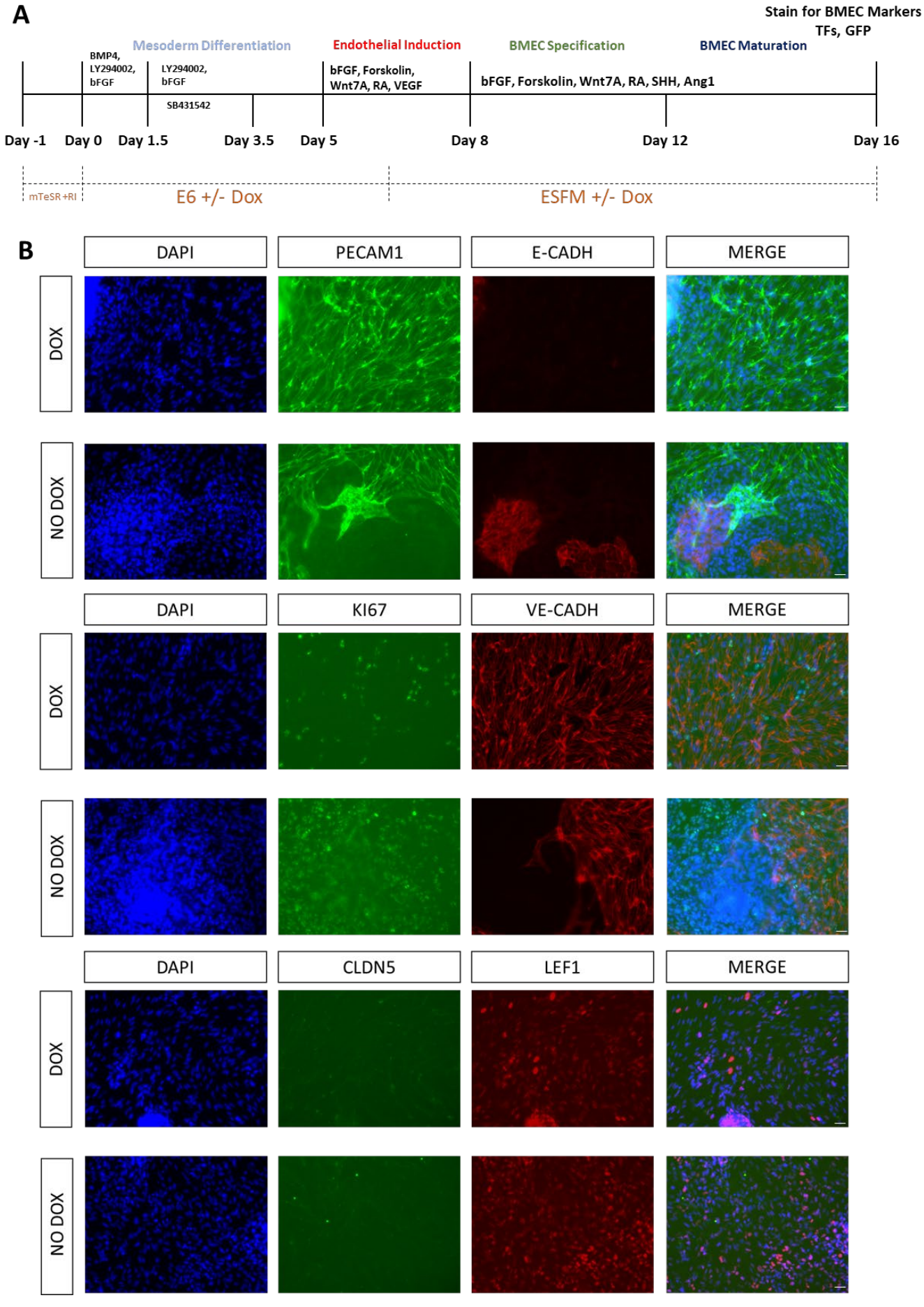

A
Stain for BMEC Markers
TFs, GFP
Mesoderm Differentiation
Endothelial Induction
BMEC Specification
BMEC Maturation
BMP4,
LY294002,
bFGF
LY294002,
bFGF
SB431542
bFGF, Forskolin,
Wnt7A, RA, VEGF
bFGF, Forskolin, Wnt7A, RA, SHH, Ang1
Day -1
Day 0
Day 1.5
Day 3.5
Day 5
Day 8
Day 12
Day 16
mTeSR+RI
E6 +/- Dox
ESFM +/- Dox
B
DAPI
PECAM1
E-CADH
MERGE
DOX
NO DOX
DAPI
KI67
VE-CADH
MERGE
DOX
NO DOX
DAPI
CLDN5
LEF1
MERGE
DOX
NO DOX

Figure 1.21 – Optimization of maturation media (control media)
A- Schematic of protocol used with BMEC specification modulation (bFGF+Forskolin+Wnt7A+RA+SHH+Ang1)
B- Immunocytochemistry of day 16 BMEC markers, KI67, LEF1, and epithelial marker E-CADHERIN under media 1 (bFGF+Forskolin+Wnt7A+RA+Ang1+SHH). Dox conditions show higher proportion of cells express PECAM1, VE-CADHERIN, and CLDN5 than no Dox conditions. There is reduced KI67 expression in Dox conditions. E-CADHERIN expression is absent in dox conditions, while no dox contains patches of E-CHADERIN+ cells. Scale bar, 50um. (n=2 biological replicates)

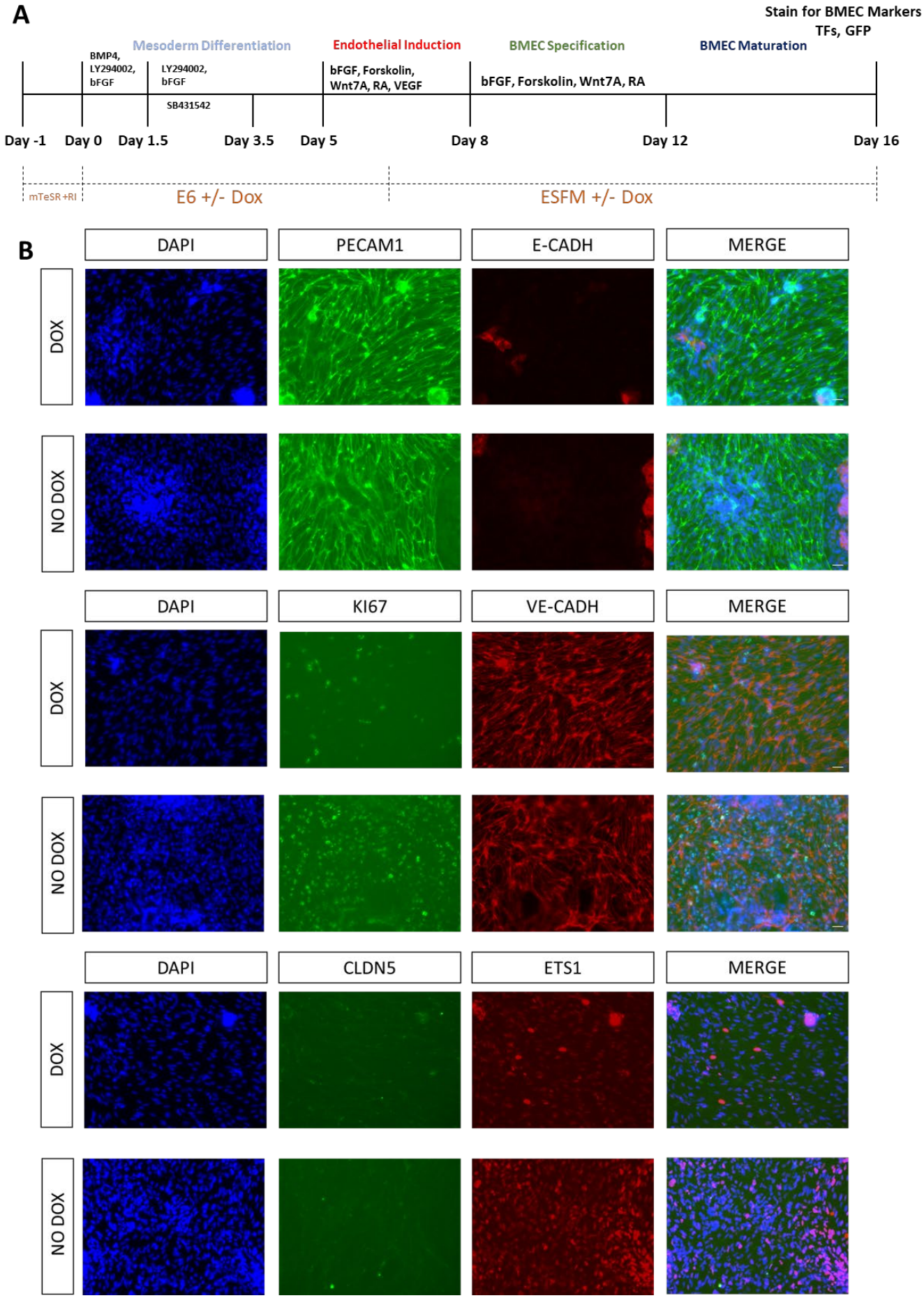

A
Stain for BMEC Markers
TFs, GFP
Mesoderm Differentiation
Endothelial Induction
BMEC Specification
BMEC Maturation
BMP4,
LY294002,
bFGF
LY294002,
bFGF
SB431542
bFGF, Forskolin,
Wnt7A, RA, VEGF
bFGF, Forskolin, Wnt7A, RA
Day -1
Day 0
Day 1.5
Day 3.5
Day 5
Day 8
Day 12
Day 16
mTeSR+RI
E6 +/- Dox
ESFM +/- Dox
B
DAPI
PECAM1
E-CADH
MERGE
DOX
NO DOX
DAPI
KI67
VE-CADH
MERGE
DOX
NO DOX
DAPI
CLDN5
ETS1
MERGE
DOX
NO DOX

Figure 1.22 – Optimization of maturation media (SHH and Ang1 removal)
A- Schematic of protocol used with BMEC specification modulation (bFGF+Forskolin+Wnt7A+RA)
B- Immunocytochemistry of day 16 BMEC markers, KI67, LEF1, and epithelial marker E-CADHERIN under media 3 (bFGF+Forskolin+Wnt7A+RA). Dox conditions show higher proportion of cells express PECAM1, VE-CADHERIN, and CLDN5 than no Dox conditions. There is reduced KI67 and E-CADHERIN expression in Dox conditions. Scale bar, 50um. (n=2 biological replicates)

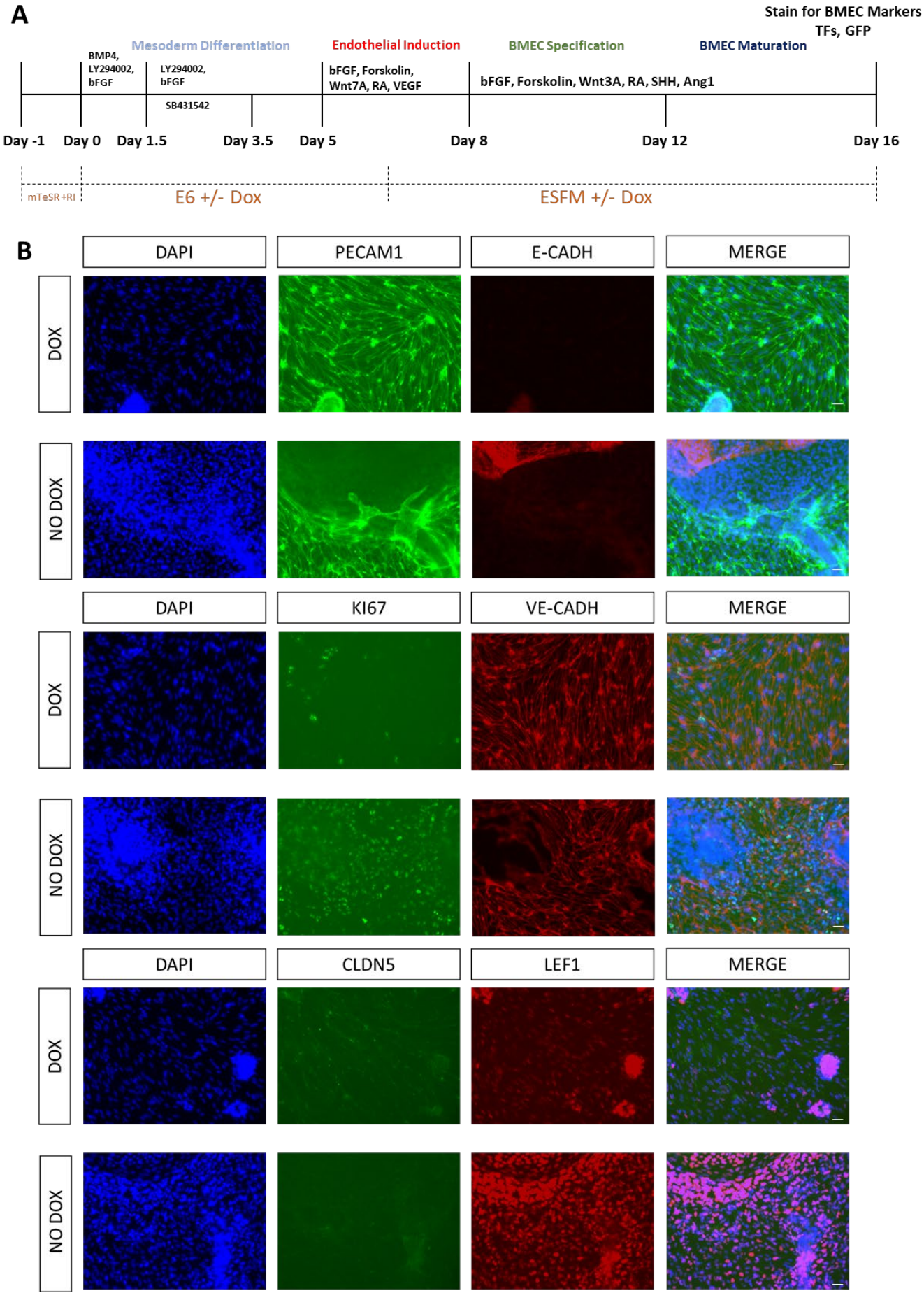

A
Stain for BMEC Markers
TFs, GFP
Mesoderm Differentiation
Endothelial Induction
BMEC Specification
BMEC Maturation
BMP4,
LY294002,
bFGF
LY294002,
bFGF
SB431542
bFGF, Forskolin,
Wnt7A, RA, VEGF
bFGF, Forskolin, Wnt3A, RA, SHH, Ang1
Day -1
Day 0
Day 1.5
Day 3.5
Day 5
Day 8
Day 12
Day 16
mTeSR+RI
E6 +/- Dox
ESFM +/- Dox
B
DAPI
PECAM1
E-CADH
MERGE
DOX
NO DOX
DAPI
KI67
VE-CADH
MERGE
DOX
NO DOX
DAPI
CLDN5
LEF1
MERGE
DOX
NO DOX

Figure 1.23 – Optimization of maturation media (control media with Wnt3A In lieu of Wnt7A)
A- Schematic of protocol used with BMEC specification modulation (bFGF+Forskolin+Wnt3A+RA+SHH+Ang1)
B- Immunocytochemistry of day 16 BMEC markers, KI67, LEF1, and epithelial marker E-CADHERIN under media 3 (bFGF+Forskolin+Wnt3A+RA+Ang1+SHH). Dox conditions show higher proportion of cells express PECAM1, VE-CADHERIN, and CLDN5 than no Dox conditions. There is reduced KI67 expression in Dox conditions. E-CADHERIN expression is absent in dox conditions, while no dox contains patches of E-CHADERIN+ cells. Scale bar, 50um. (n=2 biological replicates)

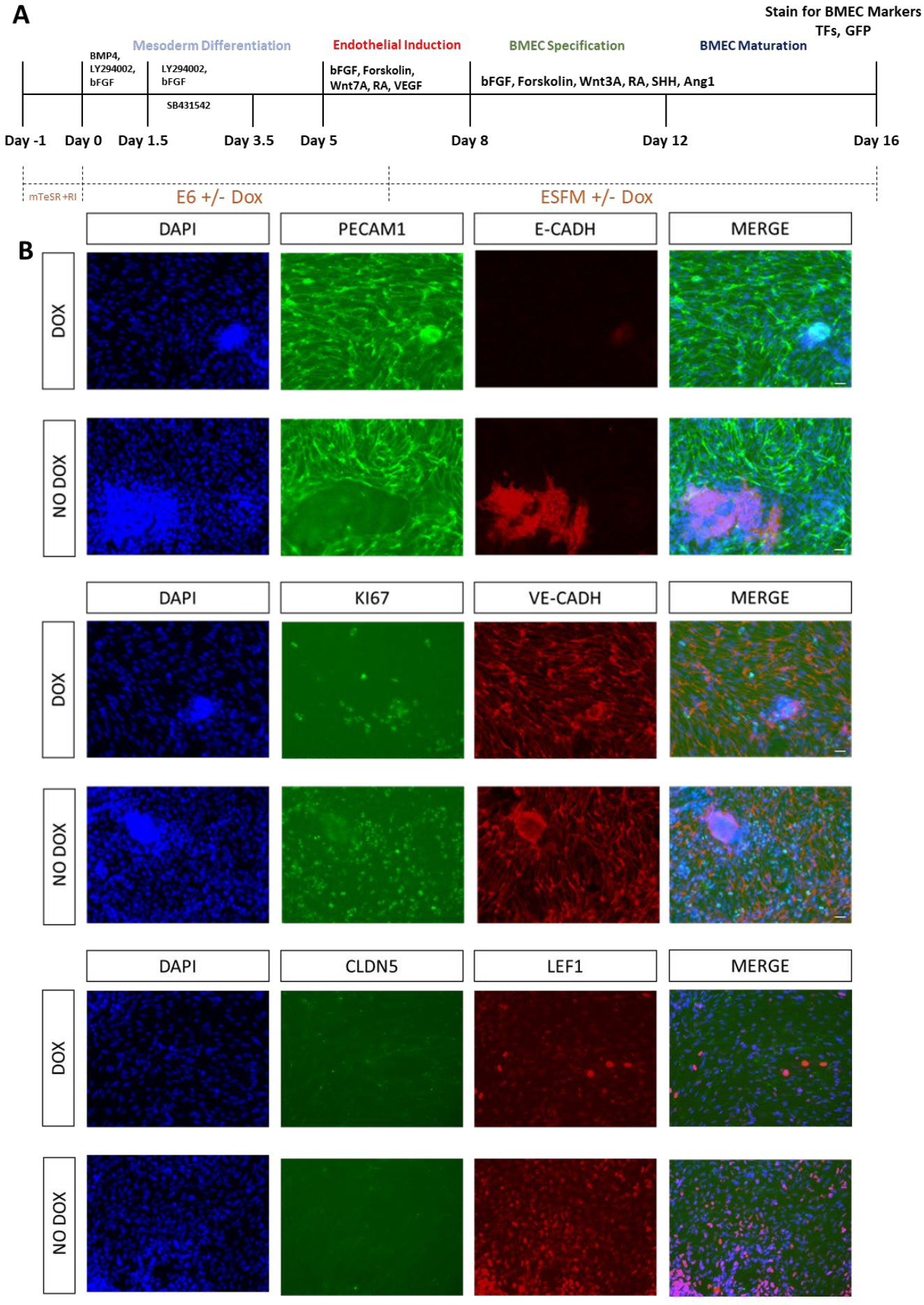

A
Stain for BMEC Markers
TFs, GFP
Mesoderm Differentiation
Endothelial Induction
BMEC Specification
BMEC Maturation
BMP4,
LY294002,
bFGF
LY294002,
bFGF
SB431542
bFGF, Forskolin,
Wnt7A, RA, VEGF
bFGF, Forskolin, Wnt3A, RA, SHH, Ang1
Day -1
Day 0
Day 1.5
Day 3.5
Day 5
Day 8
Day 12
Day 16
mTeSR+RI
E6 +/- Dox
ESFM +/- Dox
B
DAPI
PECAM1
E-CADH
MERGE
DOX
NO DOX
DAPI
KI67
VE-CADH
MERGE
DOX
NO DOX
DAPI
CLDN5
LEF1
MERGE
DOX
NO DOX

Figure 1.24 – Optimization of maturation media (Wnt3A in lieu of Wnt7A and removal of SHH and Ang1)
A- Schematic of protocol used with BMEC specification modulation (bFGF+Forskolin+Wnt3A+RA)
B- Immunocytochemistry of day 16 BMEC markers, KI67, LEF1, and epithelial marker E-CADHERIN under media 4 (bFGF+Forskolin+Wnt3A+RA). Dox conditions show higher proportion of cells express PECAM1, VE-CADHERIN, and CLDN5 than no Dox conditions. There is reduced KI67 expression in Dox conditions. E-CADHERIN expression is absent in dox conditions, while no dox contains patches of E-CHADERIN+ cells. Scale bar, 50um. (n=2 biological replicates)

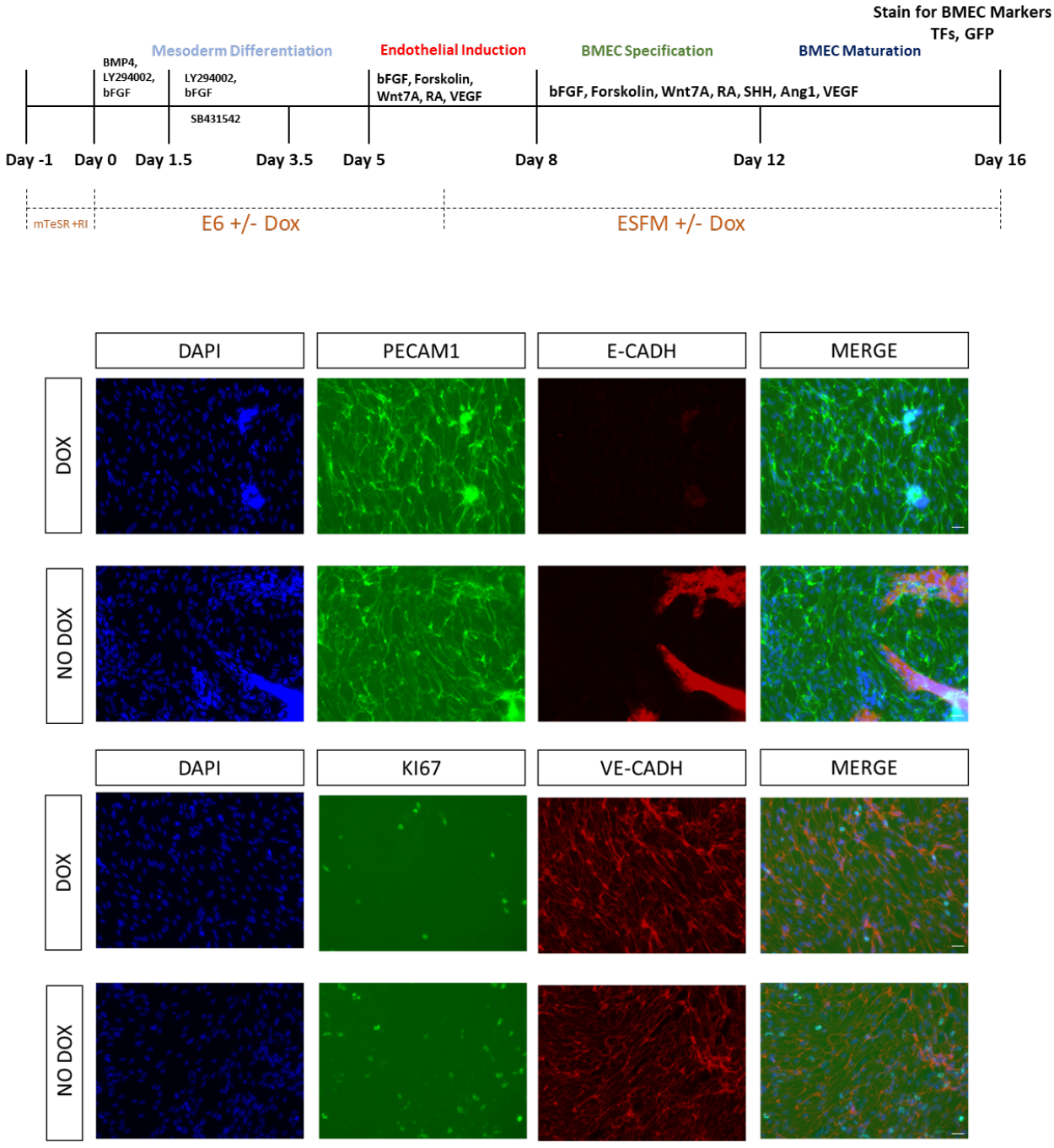


Figure 1.25 – Optimization of maturation media (VEGF extension)
A- Schematic of protocol used with BMEC specification modulation (bFGF+Forskolin+Wnt7A+RA+SHH+Ang1+VEGF)
B- Immunocytochemistry of day 16 BMEC markers, KI67, LEF1, and epithelial marker E-CADHERIN under media 1 (bFGF+Forskolin+Wnt7A+RA+VEGF+Ang1+SHH). Dox conditions show higher proportion of cells express PECAM1, VE-CADHERIN, and CLDN5 than no Dox conditions. There is reduced KI67 expression in Dox conditions, but no dox condition KI67 expression is reduced from medias 1-4. E-CADHERIN expression is absent in dox conditions, while no dox contains patches of E-CADHERIN+ cells. Scale bar, 50um. (n=2 biological replicates)
Note*: CLDN5/LEF1 image for media 5 is not shown as source image was not located, but based on laboratory notes, there was no difference in CLDN5 expression compared to other media conditions.

B27, CAMP, Dexamethasone, or RO-20-1724 do not Improve BMEC Fate

To improve tight junction formation, further optimizations were undertaken (Supplementary Figure 1.9-1.13). First, B27 (Supplementary Figure 1.10)- a media additive commonly used in neuronal differentiation, was used to investigate whether this would encourage cells to attain a brain endothelial status rather than a generic vascular phenotype. Second, additives typically included in the mouse brain endothelial cell culture - cAMP (312.5uM) , dexamethasone (0.5uM), and RO 20-1724 (175uM) were added, as they have been shown to increase barrier integrity in mouse brain endothelial cells [261].

These changes did not affect CLDN5 expression in comparison to control (Supplementary Figure 1.9-1.13). Media containing B27 was associated with reduced CLDN5 expression. cAMP, dexamethasone or RO 20-1724 had no effect on CLDN5 expression or localisation.

I noted that in this experiment there was a strong CLDN5 expression in all conditions, including controls. However, this round of optimization yielded a poor clump-enrichment step, yielding a low proportion of successfully differentiated BMEC cells. The additive exposure lengthened the differentiation time to 16 days, which may have enabled CLDN5 to better localize into the membrane. However, the previous differentiations extended to 16 days did not result in CLDN5 expression. It is also possible that non-BMEC cells present in culture were required for expression and localisation of CLDN5 signal. However previous differentiations with high proportion of non-BMEC cells had no increase in CLDN5 signal. Due to no differences seen between medias with additives and control, no investigated additives were included in subsequent optimizations.

BMECs sorted through MACS Greatly Improves Homogeneity of Final Culture

I found substantial variation between each differentiation in the clump enrichment-step. Differentiated cells strongly express VE-CADHERIN in all differentiations with robust expression by day 12. Cells were therefore subjected to magnetic-activated cell sorting (MACS) for VE-CADHERIN positive cells (Figure 1.26A). There were clear morphological differences between VE-CADHERIN^{+} and

VE-CADHERIN$^-$ cells following MACS, with VE-CADHERIN$^+$ cells showing an elongated morphology while VE-CHADERIN$^-$ were amorphous (Supplementary Figure 1.14).

Following MACS sorting, CLDN5 expression in the purified cells (MACS$^+$) was increased in comparison to non-differentiated cells (MACS$^-$). However, MACS$^+$ CLDN5 expression is similar to expression without MACS sorting from previous experiments. Despite an increase in purity, there is still a small proportion of VE-CADHERIN$^-$ cells that contaminate the VE-CADHERIN$^+$ population. As these cells are still in their replicative cycle, the contamination becomes more apparent with time, yielding small patches of VE-CADHERIN$^-$ cells in the final culture (Figure 1.26B). Fortunately, these cells are void of E-CADHERIN staining and show no epithelial phenotype (Figure 1.26C). Lastly, no cells in culture express OCLN (Figure 1.26C), still leaving room for improvement in the protocol.

Repeated MACS sorting showed variability in MACS efficiency. The manufacturer's protocol recommended incubation with antibody at 4C to prevent non-specific binding. The interval centrifugation steps were performed at room temperature, and so I changed this to centrifugation to 4C. This resulted in a more homogenous final BMEC population. Further, increasing the MACS separation time to ensure all cells went through the column increased culture purity. With these optimisations, the subsequent cultures used for RNA and protein analysis were considerably less variable and visibly more homogenous.

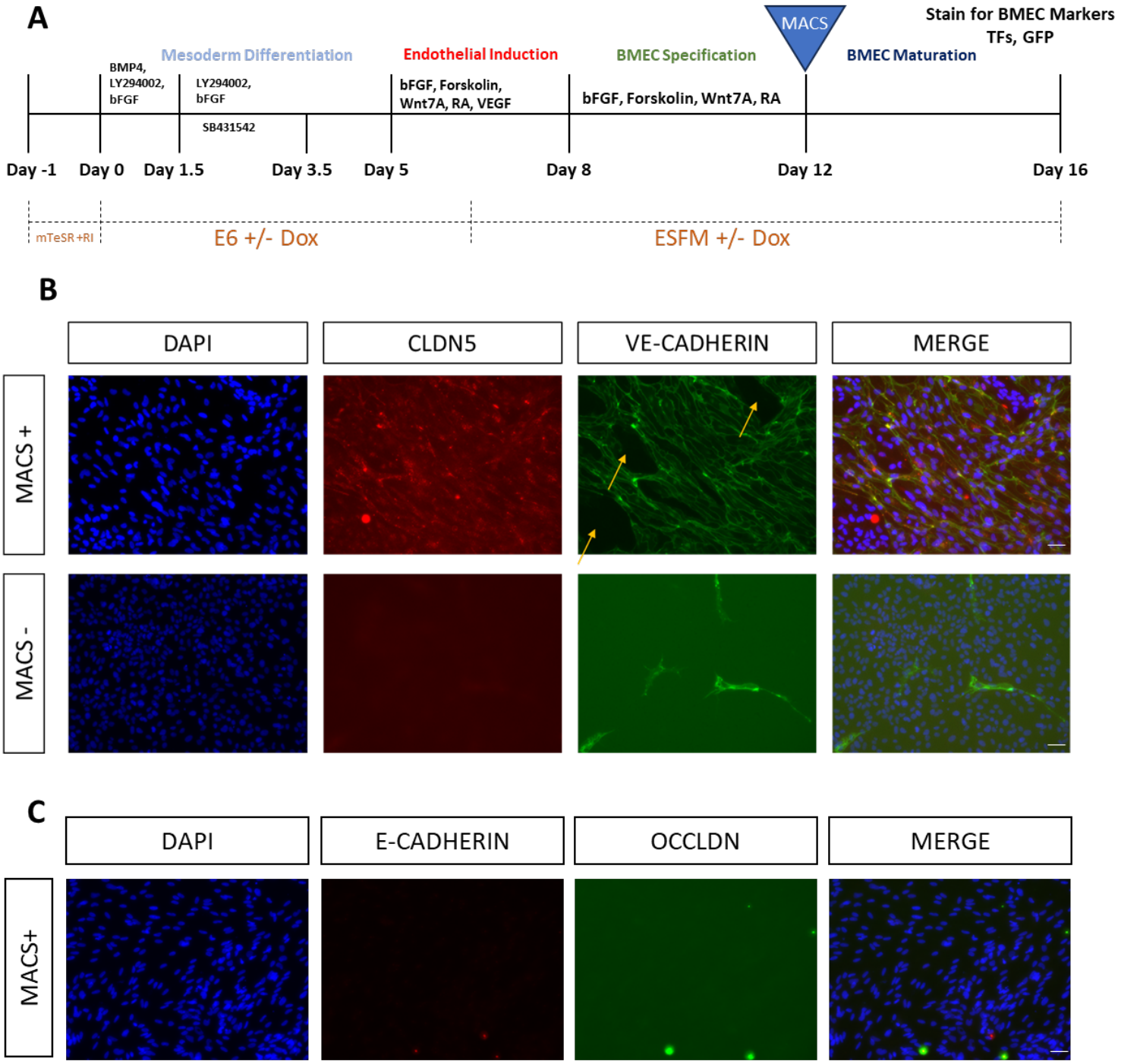
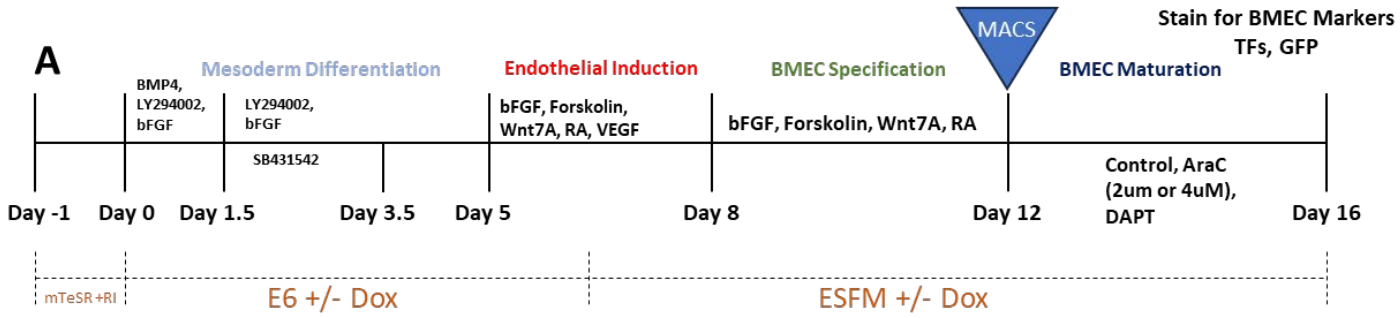


Figure 1.26– VE-CADHERIN+ MACS Sorted Cells Are Able to Purify Cultures and Form a Monolayer Void of Clumps
A- Schematic of the protocol used with MACS sort added.
B- Immunocytochemistry of MACS+ and MACS- cells show increased yield in MACS+ of differentiated cells, although holes are still formed by contaminating VE-CADHERIN- cells. Cells in MACs+ fraction express CLDN5 although do not show clear membrane staining seen in VE-CADHERIN panel. MACS- fraction has no CLDN5 signal, and low proportion of VE-CADHERIN+ cells. Scale bar, 50um.
C- Immunocytochemistry of MACS+ cultures showing no epithelial signature in endothelial cells through negative E-CADHERIN staining, but also a lack of tight junction protein expression of OCCLDN. Scale bar, 50um. (n=3 biological replicates)

AraC and DAPT are Unable to Resolve Final Culture Contamination due to Toxicity

VE-CADHERIN$^-$ cells may replicate and overtake the final culture, thus AraC at two different concentrations and DAPT were tested to either kill dividing cells or arrest the cell-cycle and prevent cells from dividing. Compared to control media, all conditions were detrimental to BMEC health (n=2) (Figure 1.27A-B). AraC at 2uM was unable to kill dividing cells as DAPI$^+$ nuclei still populate areas where VE-CADHERIN signal is absent. AraC at 4uM caused cell death that permitted surviving cells to become sparse as seen in the DAPI channel compared to control media. DAPT induced less toxicity but changed cell morphology from elongated to amorphous. The signal intensity of VE-CADHERIN also changed, with cells containing a diffused background stain, decreased membrane signal, and areas of high signal intensity.

A summary of all differentiation optimisation can be found in table 1.4. In summary the differentiation protocol I developed shows a significant improvement over the original protocol designed by Dr. Satyan Chintanwar. The final culture yielded robust and consistent expression of VE-CADHERIN and PECAM1. While CLDN5 expression is low, its expression is more homogenous than in the original protocol. More work is needed to induce tight junction expression of OCLN.



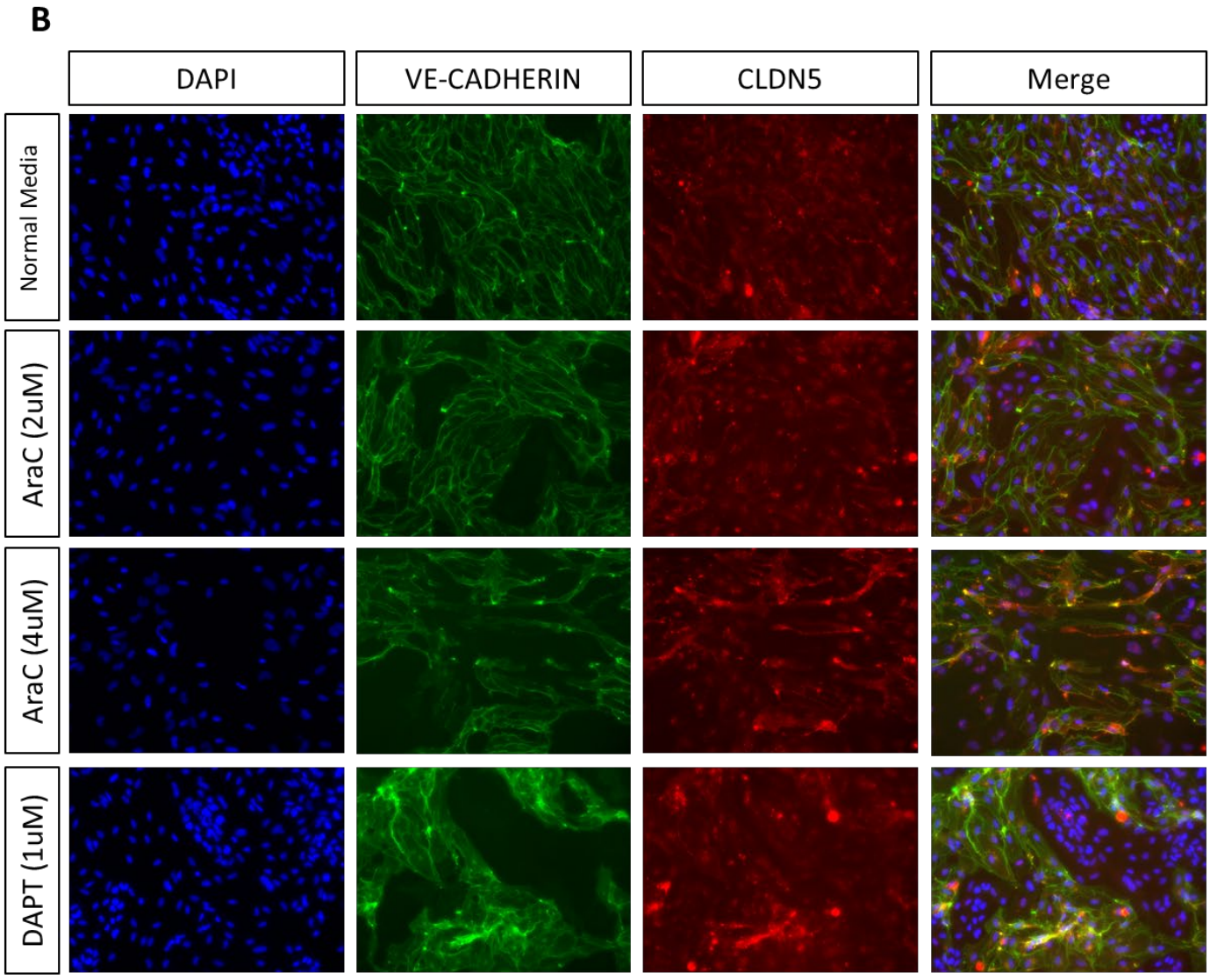


Figure 1.27 – VE-CADHERIN+ MACS Sorted Cells Are Able to Purify Cultures and Form a Monolayer Void of Clumps
A-Schematic of protocol with conditions on day 13-16.
B- Immunocytochemistry of different chemical agents (AraC and DAPT) to control cell proliferation of contaminating VE-CADHERIN- cells show insufficient selection at 2uM of AraC, toxic effects at 4uM of AraC, and large morphological changes upon exposure to DAPT at 1uM. Scale bar, 50um. (n=2 biological replicates)

Table 1.4 – Summary of Differentiation Experiments

Differentiation	Protocol Step Inclusion	Conditions Tested	n	Results	Figure
1	No Mesoderm	· Day 5-12 media compositions ·EGM2 vs ESFM ·Wnt7A, RA, and Forskolin modulation	n=1	·ESFM better than EGM2 in VE-CADHERIN induction No conclusive results on factor modulation	Figures 1.6-1.12
2	Mesoderm	·Day 5-8 media compositions ·Wnt7A and RA modulation	n=2	·Wnt7A and RA yield better BMECs than conditions without VE-CADHERIN and PECAM1 signal attained, low CLDN5 signal	Figures 1.13-1.16
3	Mesoderm + Clump Enrichment	·Clump Enrichment	n=2	·Clump enrichment increases yield and allows for better spatial organization of BMECs	Figure 1.19
4	Mesoderm + Clump Enrichment	·Increased protocol duration to 16 days ·Day 8-16 media composition (Ang1/SHH, Wnt7A vs Wnt3A, VEGF)	n=2	·Longer protocol duration did not change immunocytochemistry results ·Ang1/SHH, or Wnt3A had no change to results ·Little to no E-CADHERIN signal ·Cells positive for E-CADHERIN and not positive for PECAM1	Figures 1.21-1.25
5	Mesoderm + Clump Enrichment	·Day 8-16 media composition (B27, CAMP, Dexamethasone, RO-20-1724)	n=2	·No change across conditions, but CLDN5 signal localization ameliorated, even in control media ·B27 reduced CLDN5 signal intensity	Supp Figures 1.9-1.13
6	Mesoderm + Clump Enrichment + MACS	·MACS sorted VE-CADH+ cells vs VE-CADH- cells	n=2	·VE-CADH+ cells show better PECAM1 and CLDN5 staining, but CLDN5 staining still low No OCLN signal	Figure 1.26
7	Mesoderm + Clump Enrichment + MACS	·AraC and DAPT modulation	n=2	·AraC and DAPT are ineffective or toxic to cells	Figure 1.27

Gene Expression

Gene expression for three main endothelial genes (VE-CADHERIN, PECAM1, and CLDN5) was performed using qRT-PCR at 4 time points: day 0 (IPSC), day 5 (mesoderm end stage), day 8, (immature endothelial cells), and day 16 for MACS-sorted VE-CADHERIN$^+$ (MACS$^+$, mature BMECs) and VE-CADHERIN$^-$ cells (MACS$^-$, non-differentiated cells). In accordance with immunocytochemistry data, both VE-CADHERIN and PECAM1 are highly expressed at day 16 MACS cells (3.19+/-0.22 log normalized fold change and 4.99+/-0.26 log normalized fold change in comparison to iPSC, respectively, n=3) (Figure 1.28A,B). MACS$^-$ conditions had a log fold change of 0.19+/-0.24 log normalized fold change for VE-CADHERIN and 2.15+/-0.68 log normalized fold change for PECAM1. At day 5, cells did not express any endothelial markers, while at day 8 VE-CADHERIN and PECAM1 have started to be expressed and show an upregulation in comparison to IPSCs. CLDN5 shows upregulation only in day 16 MACS$^+$ cells (1.80+/-0.21 log normalized fold change) (Figure 1.28C) but were not expressed in MACS$^-$ cells (-0.35+/-0.30 log normalized fold change) or at day 8 (-0.43+/-0.44 log normalized fold change).

Gene expression of additional endothelial genes was assessed to compare gene expression of MACS$^+$, MACS$^-$, and IPSCs (Figure 1.29A-E). Firstly, in MACS+, KDR (VEGF receptor) and von-willembrand factor (VWF) had significant upregulation (0.93+/-0.02 and 1.00+/-0.30 log normalized fold change, respectively) in comparison to IPSCs. In MACS-, cells had a downregulation of KDR (-.90+/-0.36 log normalized fold change) and VWF (-0.22+/- 0.38). Glucose transport protein SLC2A1 (GLUT1) had the highest expression at the IPSC stage, with MACS$^+$ cells showing a downregulation of -0.40+/-0.09 log normalized fold change and MACS$^-$ cells showing a further downregulation of -0.73+/-0.02 log normalized fold change. In accordance with immunocytochemistry results, OCCLUDN shows a significant downregulation in both MACS$^+$ (-0.88+/-0.02 log normalized fold change) and MACS$^-$ (-0.91+/-0.08-fold change) cells. IPSCs may not be the ideal control to compare expression of SLC2A1 and OCLN. Although PGP in MACS$^+$ is upregulated in comparison to IPSCs (0.57+/-0.28 log normalized fold change), MACS$^-$ cells showed greater upregulation (0.87+/-0.22 log normalized fold

change). All gene expressions were normalized by housekeeping gene Actin which showed stable expression throughout the differentiation (Supplementary Figure 1.15).

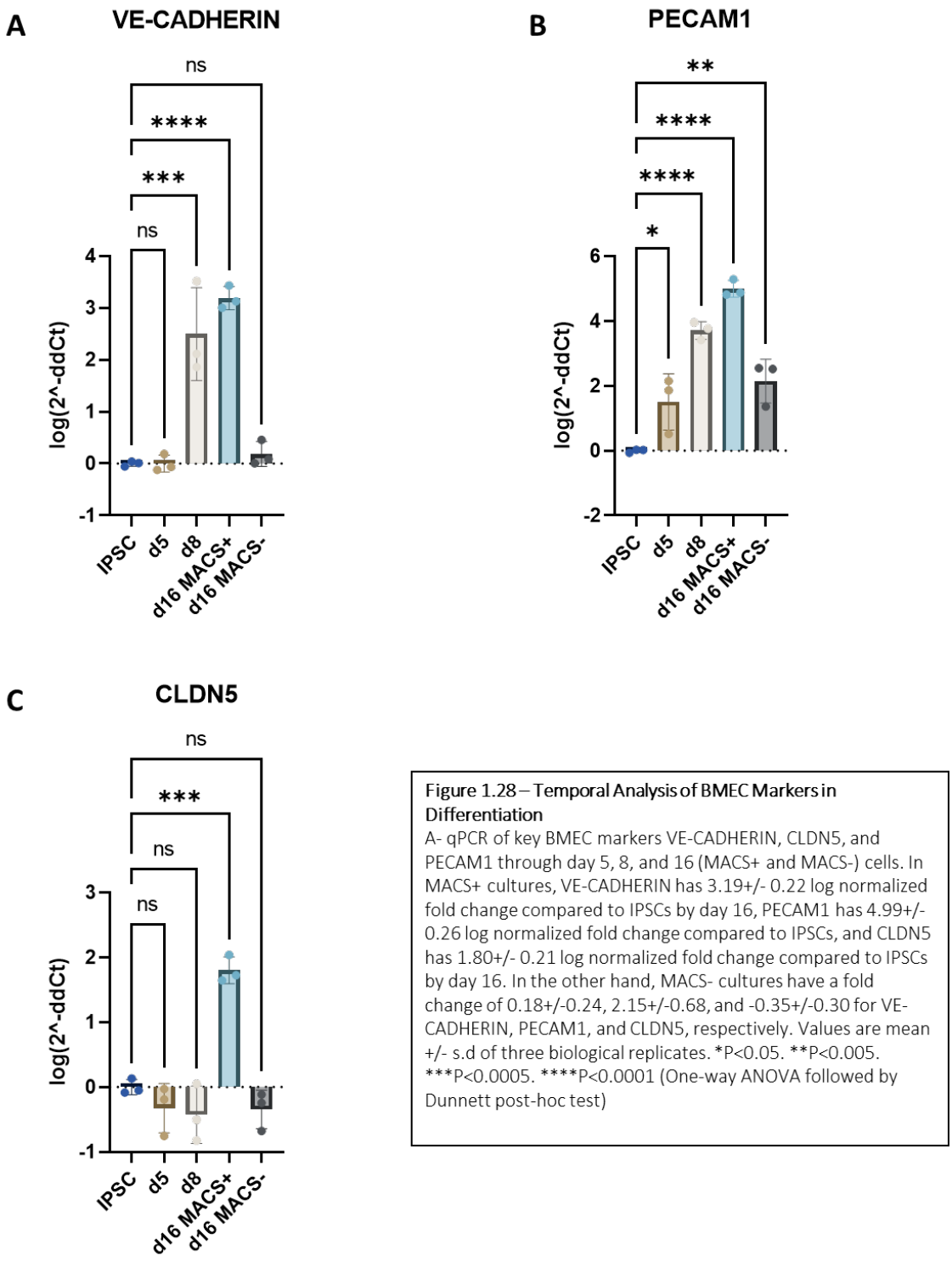


Figure 1.28 – Temporal Analysis of BMEC Markers in Differentiation
A- qPCR of key BMEC markers VE-CADHERIN, CLDN5, and PECAM1 through day 5, 8, and 16 (MACS+ and MACS-) cells. In MACS+ cultures, VE-CADHERIN has 3.19+/- 0.22 log normalized fold change compared to IPSCs by day 16, PECAM1 has 4.99+/- 0.26 log normalized fold change compared to IPSCs, and CLDN5 has 1.80+/- 0.21 log normalized fold change compared to IPSCs by day 16. In the other hand, MACS- cultures have a fold change of 0.18+/-0.24, 2.15+/-0.68, and -0.35+/-0.30 for VE-CADHERIN, PECAM1, and CLDN5, respectively. Values are mean +/- s.d of three biological replicates. *P<0.05. **P<0.005. ***P<0.0005. ****P<0.0001 (One-way ANOVA followed by Dunnett post-hoc test)

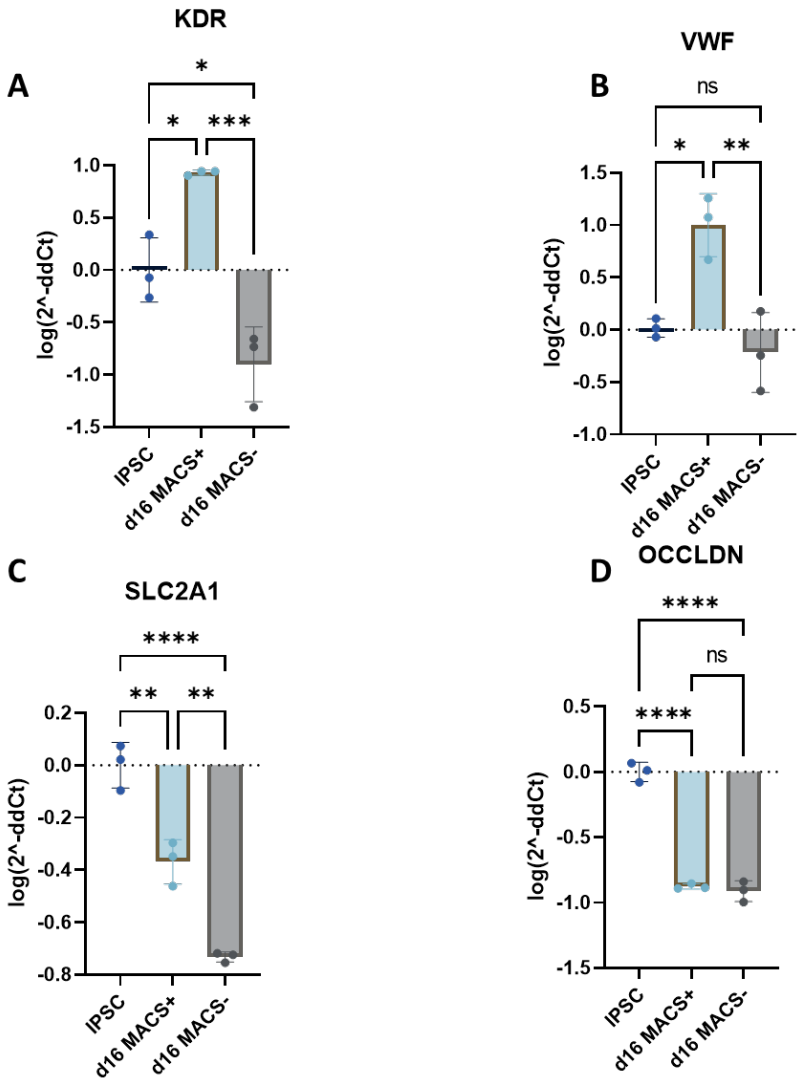


Figure 1.29- qPCR of other BMEC markers at day 16 for MACS+ and MACS-.
A- KDR sees an upregulation to a log normalized fold change of 0.93+/- 0.02 in MACS+, and downregulation to a log normalized fold change of -.90+/-0.36 in MACS- conditions.
B- VWF sees an upregulation to a log normalized fold change of 1.00+/-0.30 in MACS+, and downregulation to a log normalized fold change of -0.22+/-0.38 in MACS- conditions.
C- SLC2A1 sees a downregulation in both conditions to a log normalized fold change of -0.37+/-0.09 and -0.73+/-0.02 in MACS+ and MACS-, respectively.
D- OCCLDN sees a downregulation in both conditions to a log normalized fold change of -0.88+/-0.02 and -0.91+/-0.08 for MACS+ and MACS-, respectively.
E- PGP sees an upregulation in both conditions to a log normalized fold change of 0.57+/-0.28 and 0.87+/-0.22 in MACS+ and MACS- cultures, respectively
Values are mean +/- s.d of three biological replicates. *P<0.05. **P<0.005. ***P<0.0005. ****P<0.0001 (One-way ANOVA followed by Tukey post-hoc test)

CLDN5 Protein Expression

CLDN5 expression was assessed using western blot. A faint band at ~19KDA was detected only in MACS$^+$ cells but not in MACS$^-$ cells (Supplementary Figure 1.16). Due to time and sample constraints, the western blot was not further optimized to improve the CLDN5 signal. Further, technical errors resulted in a bubble placed in the middle two lanes of the blot, making quantification of the housekeeping gene unreliable. Therefore, no quantification was performed for this blot.

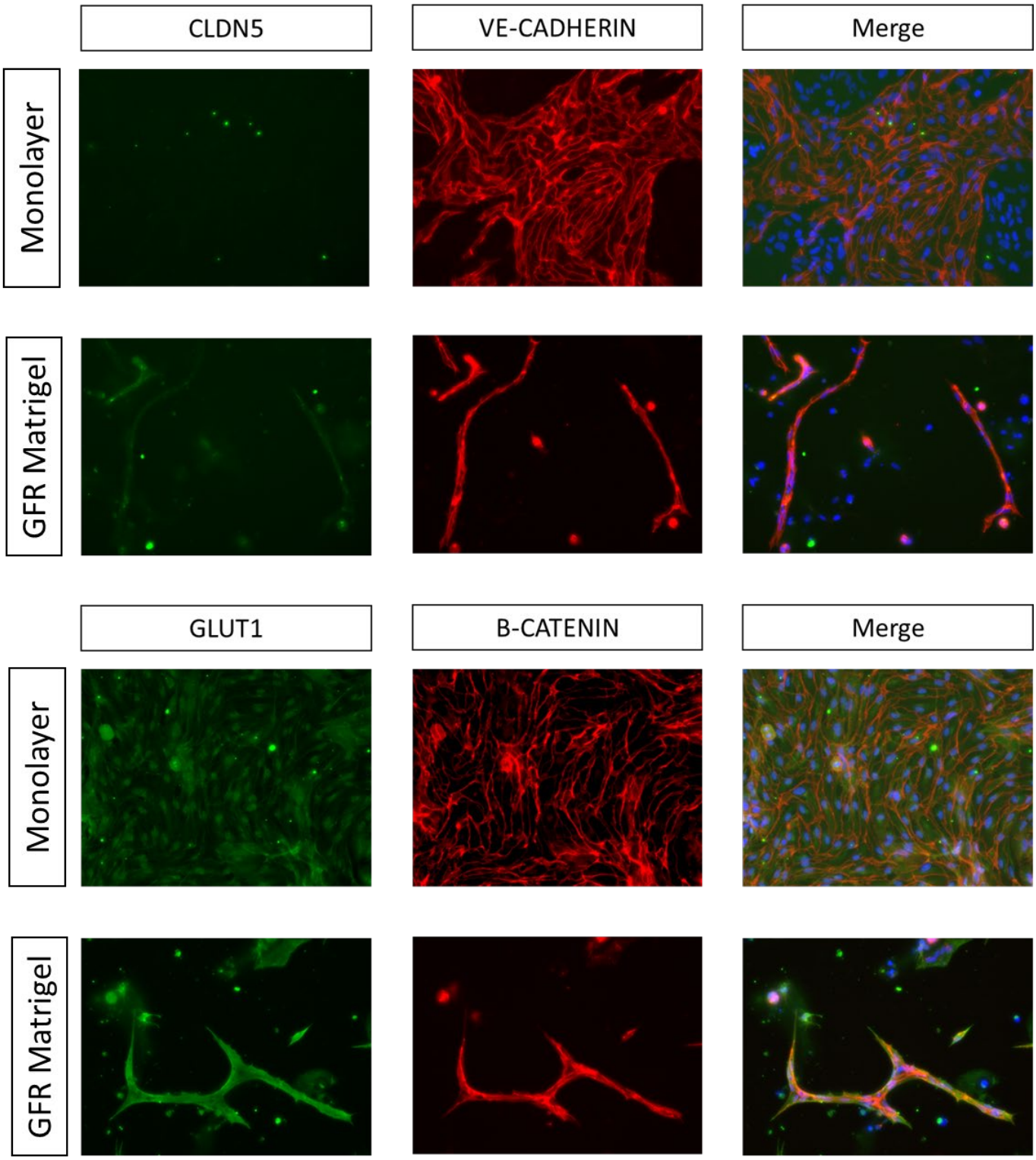
Matrigel 3D culture

MACS-sorted Cells were seeded in GFR-Matrigel and after four days of maturation they were fixed and stained for endothelial markers. Much like the clumps seeded in GFR Matrigel (Figure 1.20), MACS$^+$ cells seeded in GFR Matrigel also form vessel-like structures, but in this case, they resembled capillaries rather than larger vein/artery-like structures (Figure 1.30A). Compared to cells seeded in a monolayer in parallel, expression of CLDN5 in GFR Matrigel was evident, co-localizing with the VE-CADHERIN signal. Other markers such as PECAM1, ZO-1, SLC2A1, and b-CATENIN were also well-expressed in these capillary cultures. PGP and OCCLUDIN signal were negative in these cultures (Figure 1.30B).

Barrier properties

To measure barrier integrity of the BMEC cells, trans-endothelial electrical resistance (TEER) measurements were performed on day 16 of MACS$^+$ and MACS$^-$ cells cultured as a monolayer in a transwell insert. TEER measurements of MACS+ cells were significantly greater than MACS- cells, at 50+/-16 Ω*cm2 compared to 18+/-14 Ω*cm2 (Figure 1.31).

A


CLDN5
VE-CADHERIN
Merge
Monolayer
GFR Matrigel
GLUT1
B-CATENIN
Merge
Monolayer
GFR Matrigel

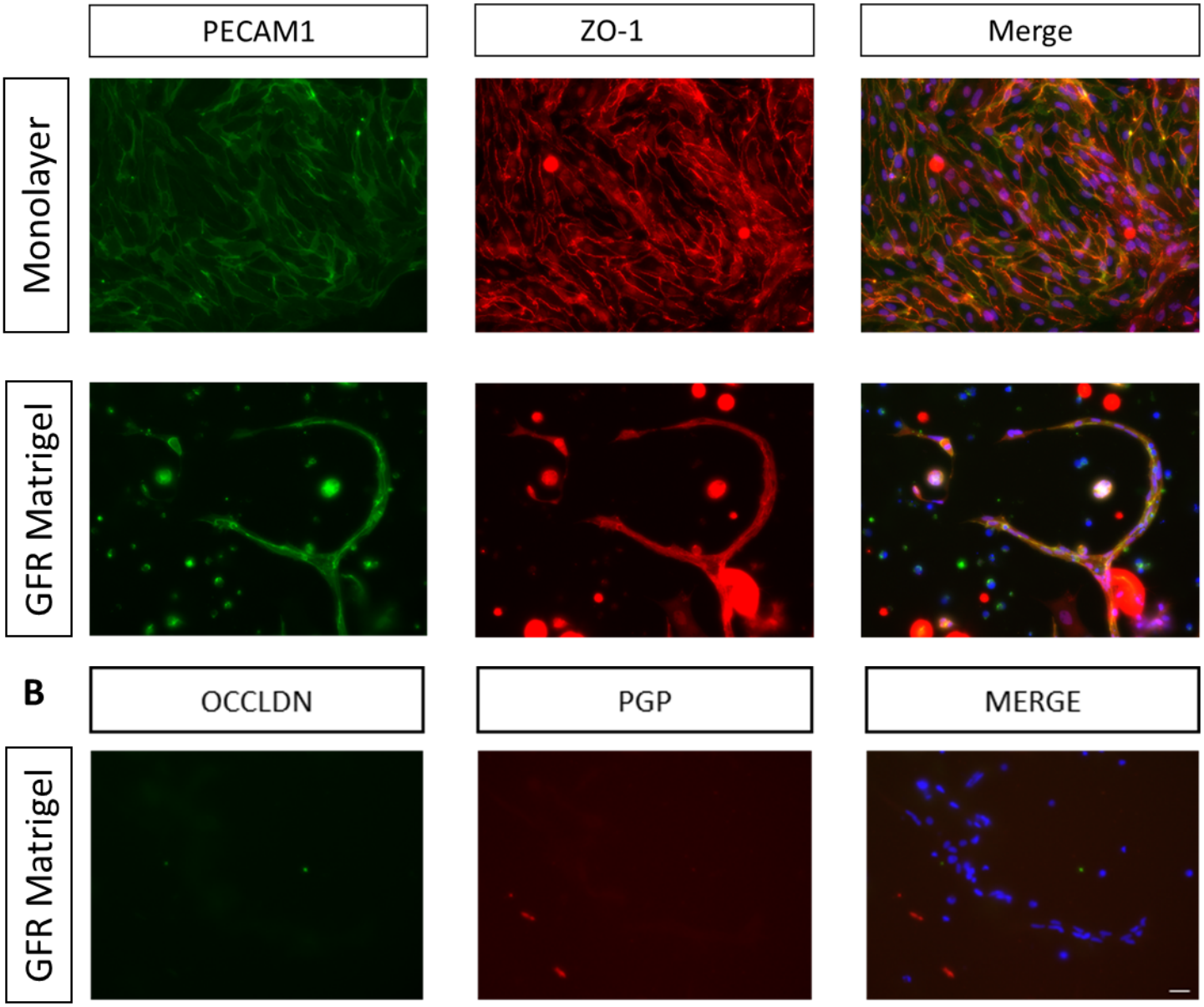


Figure 1.30 - MACS Sorted Cells Seeded in GFR Matrigel Matrix Assemble into Capillary-Like Structures
A- Immunocytochemistry of VE-CADHERIN+ MACS sorted cells seeded in GFR Matrigel and monolayer formats for CLDN5, VE-CADHERIN, GLUT1, B-CATENIN, PECAM1, and ZO-1. Merge image contains DAPI channel.
B- Immunocytochemistry of VE-CADHERIN+ MACS sorted cells seeded in GFR Matrigel show OCCLDN and PGP signal is absent. Scale bars, 50um. (n=2 biological replicates)

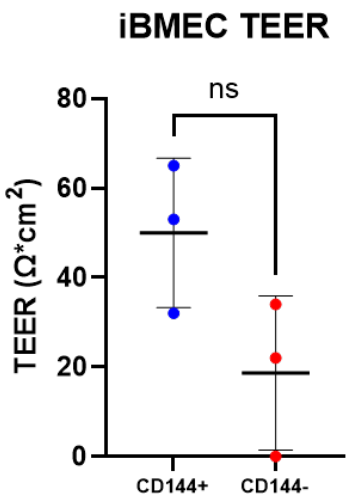


Figure 1.31 – Differentiated BMECs Is a Functionally Weak Barrier
A- Values for TEER for MACS+ and MACS- differentiated endothelial cells. MACS+ cells have an average TEER of 50.0+/-16.7 ohms*cm2 and MACS- have an average TEER of 18.3+/-14.1 ohms*cm2. Values are mean +/- s.d of three biological replicates. *P<0.05. (Student's unpaired t-test) (n=3 biological replicates)

DISCUSSION

The success of this protocol, using lentiviral overexpression of LEF1, ETS1, and MRTFB combined with small molecule directed differentiation, can be judged using several different criteria. Firstly, in terms of endothelial protein marker expression, the cell identity of the final product of the differentiation is endothelial, as evidenced by robust expression of VE-CADHERIN and PECAM1. qPCR results also demonstrate a strong endothelial phenotype, with VE-CADHERIN and PECAM1 being strongly upregulated in the final $MACS^+$ culture in comparison to IPSCs, and $MACS^-$ cultures. The $MACS^+$ cells also express GLUT1, B-CATENIN, and ZO-1 by immunocytochemistry and show relative upregulation of KDR (VEGF receptor), VWF, and CLDN5 $MACS^-$ cells showed an upregulation of VE-CADHERIN and PECAM1 relative to iPSC, which is likely due to VE-$CADHERIN^+$ cells not captured during the MACS process carried through to the $MACS^-$ culture.

All target genes were normalized to housekeeping gene β-Actin which showed minimal gene expression changes throughout the protocol. A pilot panel of housekeeping genes including β-Actin, GAPDH, ribosome small subunit (18S), 20S proteasome subunit beta-1 (PMM-1), ribosomal RNA (rRNA), ribosomal protein L13a (RPL13A), Ubiquitin C (UBC), and hypoxanthine guanine phosphoribosyl transferase (HPRT) would have increased confidence in precise gene expression results to minimize housekeeping gene fluctuations. While Actin proved to be stable enough for confident significance testing across genes, the addition of one extra housekeeping gene per experiment would fortify the result integrity. A published panel on housekeeping genes assayed on *ex-vivo* bovine endothelial cells demonstrated the optimal number of reference genes to be two, highlighting that PMM-1 was the most stable in monocultures [262]. However, the researchers indicate that different experimental conditions (such as co-cultures) can change the optimal reference gene. Considering the significant changes in IPSC and bovine endothelial cells, a panel for my differentiation would still have been necessary to optimize qPCR results.

Despite a clear positive result of key-membrane markers in immunocytochemistry assays, analyses on different signal levels from different conditions could have fortified conclusions or identified subtle changes between varying conditions. Although experiments were tailored towards increased activation of tight junction markers CLDN5 and OCLN, precise analyses of VE-CADHERIN, PECAM1, ZO1, etc. would have been informative towards choosing the correct path forward to prevent future optimisations on expression of these markers. Precise analysis of membrane-bound staining proved to be technically difficult due to the narrow signal that would require meticulous area selection to prevent background noise. However, dissociating the final culture and utilising flow-cytometry would have been an excellent tool to provide discrete values of expression.

A key feature of this protocol compared to previously published protocols is the absence of E-CADHERIN staining. Interestingly, small clusters of E-CADHERIN$^+$ cells arose prior to day 12, but these clusters are separate to the VE-CADHERIN$^+$/PECAM1$^+$ cell population. The clump isolation step at day 8, and MACS sort at day 12 eliminates this small group of E-CADHERIN$^+$ cells.

The endothelial like cells produced by this protocol are able to form vessel-like structures. Endothelial clumps arise at day 8 and can be isolated to form large vessel-like structures in GFR Matrigel (Figure 1.20). Similarly, by adding single-cells isolated after MACS, the cell self-assemble into thinner capillary-like structures in GFR Matrigel (Figure 1.30). Furthermore, CLDN5 expression increases in the vessel structures and is already apparent by Day 12 in comparison to the weak CLDN5 expression in monolayers. This might suggest a 3D environment (the Matrigel or the cell-cell interactions) is required for expression of this protein. Additional qRT-PCR and Western blotting studies should be performed on the cells to investigate this. Nevertheless, and despite the apparent improvement in cell identity toward a brain like endothelial cell, there remain challenges with the 3D cultures. For example, OCLN remains absent, indicating further work for the accurate expression of all tight junction markers. It should also be noted that the 3D cultures are not long term viable, with cell death evident after 4 days in culture.

GFR Matrigel is rich in extracellular matrix proteins, including collagen IV, heparin sulfate proteoglycan, laminin, and entactin/nidogen. GFR Matrigel used in the 3D cultures differs from Matrigel used in the monolayer culture as it is treated with ammonium sulfate to reduce the numbers of growth factors bound to the matrix components. Furthermore, Matrigel is not a defined substrate and batch to batch variations can lead to large difference in tight junction expression and TEER measurements [263]. GFR Matrigel was used in lieu of regular Matrigel for 3D studies to minimize batch-to-batch variations and increase basement membrane definition. A further study investigating both GFR and regular Matrigel could be useful in identifying specific compounds that may help or hinder vessel formation and protein expression.

CLDN5 gene expression is increased at day 16 $MACS^+$ cells compared to day 8 cells and iPSCs, suggesting that the further maturation period is important in monolayer cultures. Protein expression of CLDN5 in monolayer cultures however was weak. Typical CLDN5 staining should look akin to VE-CADHERIN and PECAM1, with localization to the cell membrane. But here, CLDN5 staining in the monolayer was jagged and faint. Furthermore, western blots results exhibit a weak CLDN5 band. Hence it is likely that CLDN5 translation and trafficking to the membrane requires activation of additional signalling pathways.

The lack of OCLN and weak expression of CLDN5 indicates that the proteins required to form tight junctions are insufficient. This is corroborated by the low TEER measurements, with a mean 50 Ω*cm2. Published protocols have reported a wide range of values, from 60 Ω*cm2[222] to 4678 Ω*cm2 [230]. However, high TEER values are only described with protocols that produces endothelial-epithelial hybrid cells [223, 227, 236]. The high TEER may be driven by the epithelial identity since epithelial cells are expected to have elevated TEER resistances [264]. Whilst it is not possible to measure TEER values in the human brain endothelial cell barrier with current technology, a value of 50 Ω*cm2 does not indicate a tight barrier and is likely lower than *in-vivo* values. Few studies have attempted to measure *in vivo* TEER measurements by injecting a glass electrode to

pulse current through a pial vessel in the brain surface, and another glass electrode adjacent to measure the current resistance. Using this technique, average TEER values for frog capillaries ranged from 1870 Ω*cm2[265] to 2000 Ω*cm2[266]. Average TEER values for arterial microvessels in rats was 1490 Ω*cm2, although individual readings ranged from as low as 500 Ω*cm2 to 5900 Ω*cm2[267]. Both mentioned experiments were published in 1985 and 1990, raising the question as to why such measurements have not been optimized and adapted to different systems. While these values may serve as indicators of a potential *in vivo* value for humans, pia mater vessels may have different physical characteristics to parenchymal vessels since they are on the surface of the brain and have fewer neuronal interactions [268]. Although time constraints did not permit for these experiments to be carried out, investigating barrier tightness by analysing its permeability would have been informative. Dextran or sodium-fluorescein permeability provide another quantifiable characteristic of barrier integrity. Further work is needed to increase protocol robustness and reproducibility.

Optimizations, including addition of Ang1 and SHH, to improve CLDN5 or OCLN expression failed to do so. Other factors such as Wnt3A, B27, cAMP, dexamethasone, and RO 20-1724 also failed to show significant differences to CLDN5 expression compared to control media. Co-cultures of endothelial cells with pericytes and astrocytes show increased TEER measurements [269], likely indicating high expression of tight junction markers. There is a possibility that direct or proximal contact between the three cell types may be necessary for increase barrier integrity, rather than the sole addition of the two secreted factors.

Further studies are also required to improve OCLN and CLDN5 expression. For example GLP-1 activation, through activation of cAMP/PKA, has been reported to promote OCLN expression [270]. Despite forskolin increasing intracellular cAMP concentrations, other compounds may have a higher capacity of modulating cAMP expression to appropriately induce OCLN and CLDN5. Modulating the coating matrix of the endothelial cells may also be beneficial, for example, by using fibronectin,

collagen IV, or laminin. Collagen IV is able to stabilize CLDN5 in the BBB through b1-integrin signalling pathway.[271] Collagen and fibronectin are also commonly used as cell culture substrates in *ex-vivo* murine endothelial cell cultures [261, 272] Despite Matrigel already containing collagen IV, laminin, and trace amount of fibronectin, a more defined culture substrate could help elucidate how the ECM may help endothelial cells express and stabilize tight junction proteins

An unresolved challenge is the contamination of VE-CADHERIN$^-$ cells in the final VE-CADHERIN$^+$ population separated by MACS. AraC and DAPT were trialled to kill off dividing cells or arrest the cell cycle of diving cells, but both had negative effects on the overall culture compared to untreated cells. Contamination by VE-CADHERIN$^-$ cells may relate to technical issues with MACS and addressing these could improve the purity. Firstly, cell loading onto the column or the column size could be optimised as overloading can lead to clogging of the MACS separation column. Secondly, VE-CADHERIN antibody binding is temperature sensitive, and by reducing the temperature to 4C to include the spin steps, purity improved presumably due to reduced non-specific binding. VE-CADHERIN$^-$ cells are mitotic, meaning that any contamination will grow with time, which then becomes an increasing problem if the culture timeline is extended for maturation purposes. Addition of AraC after allowing more time to stabilise after MACS could reduce this problem.

Future optimisations should include re-design of the viral constructs and transductions. The polycistronic virus ensures each cell will express all three transcription factors but results in a large plasmid size of 13,581 base pairs that makes transduction less efficient. This necessitated creation of a stable cell line, which took time to produce and validate. Generating a monoclonal stable cell line rather than polyclonal could also help with consistency of results.

The requirement for each of the three transcription factors should be assessed in future experiments and this may allow a reduced viral construct size. ETS1 is strongly associated with BMEC markers in the culture produced. LEF1 expression was more sporadic and not consistently showing an association with the BMEC markers VE-CADHERIN or PECAM1. MRTFB is highly expressed in both

IPSCs and endothelial cells. Therefore, there is an argument that LEF1 upregulation may not be necessary and that endogenous upregulation through Wnt7A and RA may be enough to attain an endothelial phenotype. Similarly, MRTFB is expressed throughout the entire protocol, and a further lentiviral overexpression may also not be necessary.

Not all VE-CADHERIN^{+} cells stained for GFP. This could either represent cells not expressing the transcription factor constructs or expressing weakly. This may indicate that differentiating cells that strongly express the transcription factors, may be secreting factors that allow for endothelial identity acquisition of unstransduced cells. Performing a micro array analysis of cytokines and growth factors in doxycycline^{+} and doxycycline^{-} cultures at different stages of the differentiation may be informative to this question.

One of the original aims included validation of key brain-endothelial specific targets that could serve as transport mechanisms for drugs and biologics (transport targets). Given that these assessments of transport function require a barrier with high integrity and tightness, transport assays were not performed.

Overall, a novel BMEC differentiation protocol has been presented in this chapter. The new protocol activates LEF1, ETS1, and MRTFB, isolates the endothelial clumps from the heterogenous culture, and enriches VE-CADHERIN^{+} cells. The protocol demonstrates increased homogeneity and cellular arrangement compared to the original small molecule differentiation protocol. The arising cells express endothelial markers including PECAM1, VE-CADHERIN, CLDN5, and ZO-1, but does not express OCLN. Functionally, they are able to create vessels under a GFR Matrigel matrix but are unable to form a tight layer when cultured in a monolayer as seen from TEER results and immunocytochemistry of tight junction markers. My work has progressed current protocols, but additional work is required to improve tight junction formation and barrier integrity.

Chapter 2: Development of a Novel IPSC BMEC Differentiation Protocol Using CRISPR Transcription Factor Gene Activation

Introduction

In the previous chapter, a novel protocol for the differentiation of brain microvascular endothelial cells was established. However tight junction expression and localization of CLDN5 and OCLN are either inadequate or missing, resulting in a lack of a tight barrier indicated by low TEER values. Therefore, approaching the protocol from different technical angles could yield better results.

Activating transcription factors by cDNA delivery through lentiviruses, leading to over-expression of these factors, is an established approach to achieve differentiation to specific target cell types. However, with the growth of the CRISPR technology, the scientific field has been studying its capability of driving IPSC differentiation via the activation of specific transcription factors at physiological levels. Originally produced for genetically modifying DNA base pairs, the Cas9 protein is guided by gRNA to cleave the DNA at specific locations. By modifying the Cas9 enzyme through point mutations in its endonuclease domain, the modified enzyme becomes unable to cleave DNA, and allows for either activation or inhibition of gene transcription [273]. Over the past decade, CRISPR activation (CRISPRa) technology has improved to facilitate gene activation. Since the first synthesis of the modified Cas9, termed dead Cas9 (or dCas9), many further modifications have been made to increase the platform's ability to induce gene expression by the fusion of the dCas9 enzyme with activator domains. Activator domains represent a group of proteins capable of recruiting and accelerating transcription preinitiation complex (PIC) to a specific promoter. In this chapter, CRISPR activation using SAM (Synergistic Activation Mediator) will be used [274].

The original CRISPRa dCas9 enzyme functioned solely with one activator protein fused to it, namely VP64. On the other hand, SAM was developed by the finding that upon binding of the sgRNA to the dCas9 enzyme, small loops in the sgRNA (tetraloop and stem loop 2) protrude out of the enzyme and are free of any interactions. This now provided a genomic space to fuse further activator

proteins to facilitate the recruitment of activator proteins [274]. The fused protein consists of MS2, P65, and HSF-1. MS2 is a bacteriophage coat protein able to bind to RNA molecules, in this case, the sgRNA. P65 and HSF-1 are transcriptional activation proteins derived from the NF-kB and HSF-1 protein, respectively. In unison with VP64, the dCas9 complex can bind to a specific promoter region of a gene (usually around 300bp upstream of the transcription start site) and successfully initiate enhanced expression of such gene through activation of several cellular transcription machineries.

With the help of Dr. David Knapp, from the University of Oxford, a new platform utilizing CRISPRa for the differentiation of IPSCs into brain microvascular endothelial cells was explored. By activating the three key transcription factors identified in the previous chapter, LEF1, ETS1, and MRTFB, I hypothesize that this could help drive the differentiation of IPSCs into BMECs. In contrast to the previous cDNA delivery through lentivirus, this platform could help cells attenuate their transcription factor expressions to more physiological levels, as CRISPRa would only enhance transcription of such factors, whereas lentiviral delivery of cDNA results in overexpression. My specific aims are to:

- Establish a CRISPRa IPSC platform able to activate genes of interest
- Identify sgRNA sequences able to upregulate LEF1, ETS1, and MRTFB
- Determine if endothelial differentiation is improved upon CRISPR activation compared to lentiviral cDNA delivery

RESULTS

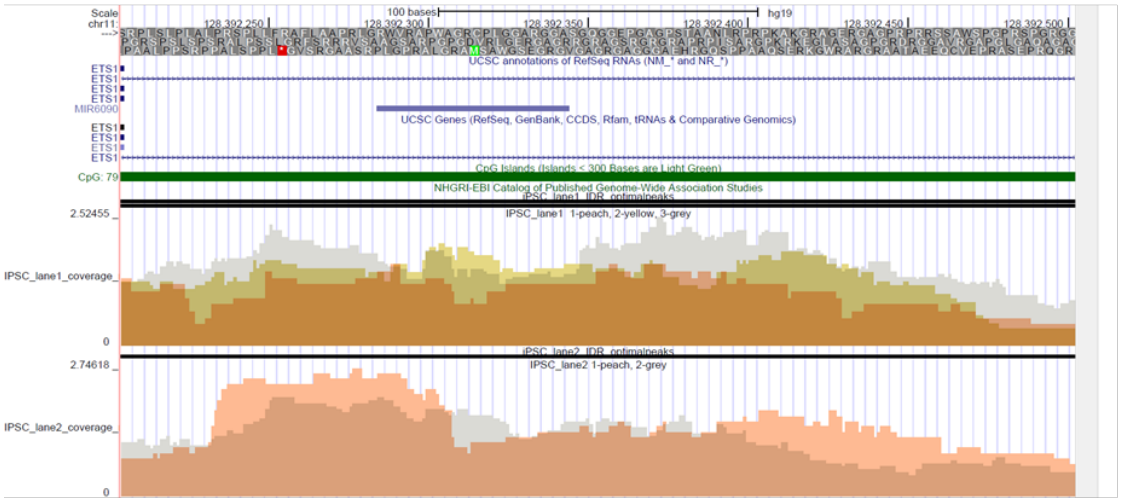
As CRISPRa functions by the direct attachment of the dCas9 complex to the genome, I validated that the promoter regions of the LEF1, ETS1, and MRTFB are epigenetically open. Previous ATAC-Seq experiments in IPSCs done in the Cader lab by Dr. Adam Handel revealed the regions 300 base pairs upstream of the transcription start site of LEF1, ETS1, and MRTFB are widely open for protein interactions (Figure 2.1). This indicates that recruiting dCas9 to these locations is possible and will not be interfered by highly coiled regions of DNA and histones.

To establish a successful CRISPR platform, sgRNA sequences must be optimized, as the precise location and binding of the dCas9 complex is highly dependent on sgRNA efficacy. While most protocols use the TSS as a guide to identify sgRNA binding sites, I sought to investigate whether targeting the protein-coding site (PCS) for genes where the TSS and PCS are distant could yield for gene activation. The TSS and PCS of LEF1 and ETS1 were near each other (<1000 kbp). On the other hand, these two locations for MRTFB were separated by over 60,000 base pairs, warranting sgRNA design targeting both distinct sites. The online tool E-CRISP[275] was utilised to synthesize 4 sgRNAs per transcription factor targeting the TSS, and a further 2 solely for MRTFB targeting the PCS (Table 2.1). A scrambled sgRNA sequence was also provided by Dr. David Knapp.

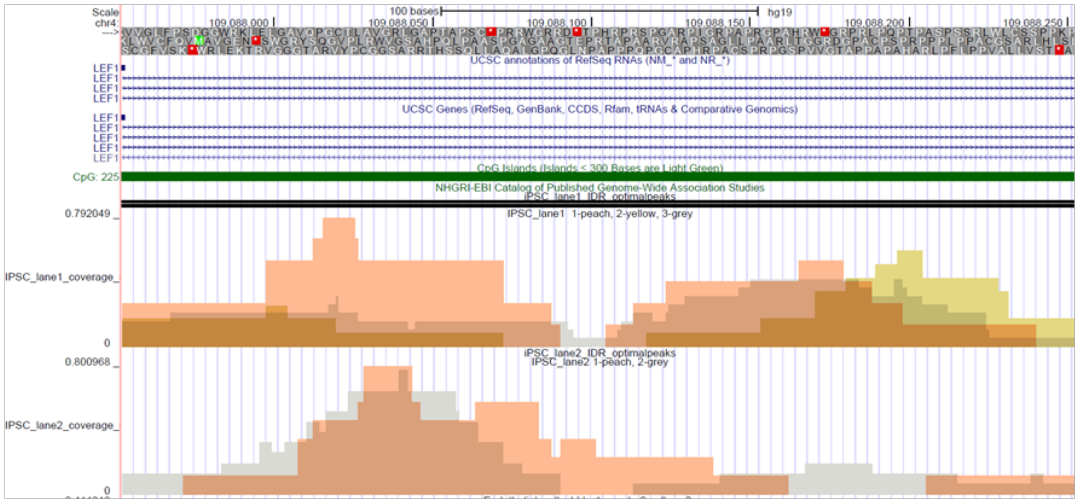
Table 2.1

sgRNA	Sequence
LEF1-1	GCCAAGGAGAGCTAGAGG
LEF1-2	GCGCCTGGAGGGAAGGATC
LEF1-3	AGCCAAGGAGAGCTAGAGG
LEF1-4	GCGGGCAAAGCGTGCCTTT
ETS1-1	GGAGATTGGCCGCGGTGCT
ETS1-2	GTTCCTTTCGCTTTGGGCCG
ETS1-3	GTTTCGCTTTGGGCCGCGGG
ETS1-4	GTAAAGAGGAGGGGAGAGCG
MRTFB-1	GCCGAGCCGCTTCTAGCCT
MRTFB-2	GGGCTTGACCCTTGAGGCG
MRTFB-3	GGGCTTGACCCTTGAGGC
MRTFB-4	GTGCGCATGCGCATGTCCG
MRTFB-5 (PCS)	GTTACACTCCCTGTTGCCAG
MRTFB-6 (PCS)	GACTCCCTGTTGCCAGTGGC
Scramble	GCACTACCAGAGCTAACTC

ETS1



LEF1



MRTFB

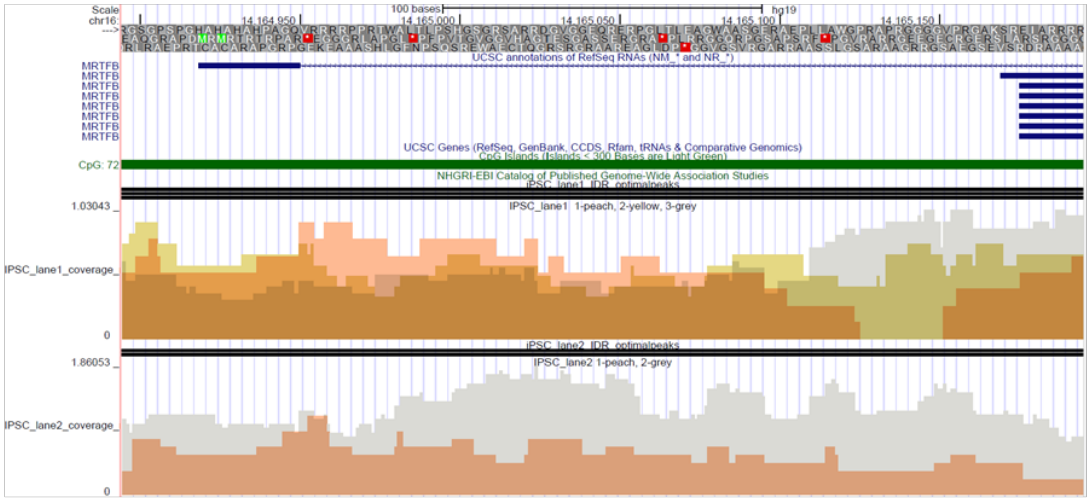


Figure 2.1 – ATAC-seq of IPSCs show open promoter regions of genes LEF1, ETS1, and MRTFB in the regions 300bp upstream of TSS. LEF1 contains regions that have low coverage, but do not consistently show epigenetic closure across both IPSC replicates (lane1 and lane2).

Testing these sgRNAs into an IPSC platform would entail transfection of four separate plasmids donated by Dr. David Knapp: p222_U6-placeholder, p284_U6-short-tracrRNA-MS2, SAM_dCas9_VP63, and p326_SAM (Supplementary Figure 2.1). P222 serves as the backbone to insert the individual sgRNAs for each gene. p284 codes for the scaffolding containing the MS2 linker proteins. SAM_dCas9_VP64 codes for dCas9 and activator protein VP64. p326 codes for the SAM activator proteins needed to increase the efficacy of gene activation. P222's Bbs1 sites located on either end of the placeholder sequence were utilized to insert the sgRNA sequences by restriction site digest and cloning. The correct insertion of each sequence was verified using sanger sequencing of the purified plasmids.

Transfection Optimization

To optimize transfection conditions, a pilot transfection optimization was performed on IPSCs using an EGFP plasmid. Two transfection reagents, LT-1 and LipoSTEM, were used. LT-1 works through reverse transfection, where cells are split and seeded directly into a medium containing the LT-1/plasmid complex. LipoSTEM works through standard forward transfection, where cells are seeded on day 0 and only transfected the next day. Each transfection reagent was further divided into three seeding densities, three plasmid loads, and 2 transfection reagent volume groups (Table 2.2). IPSCs were transfected and allowed to grow for three days, where they were then fixed and stained with DAPI to allow for cell quantification via EGFP expression.

Table 2.2

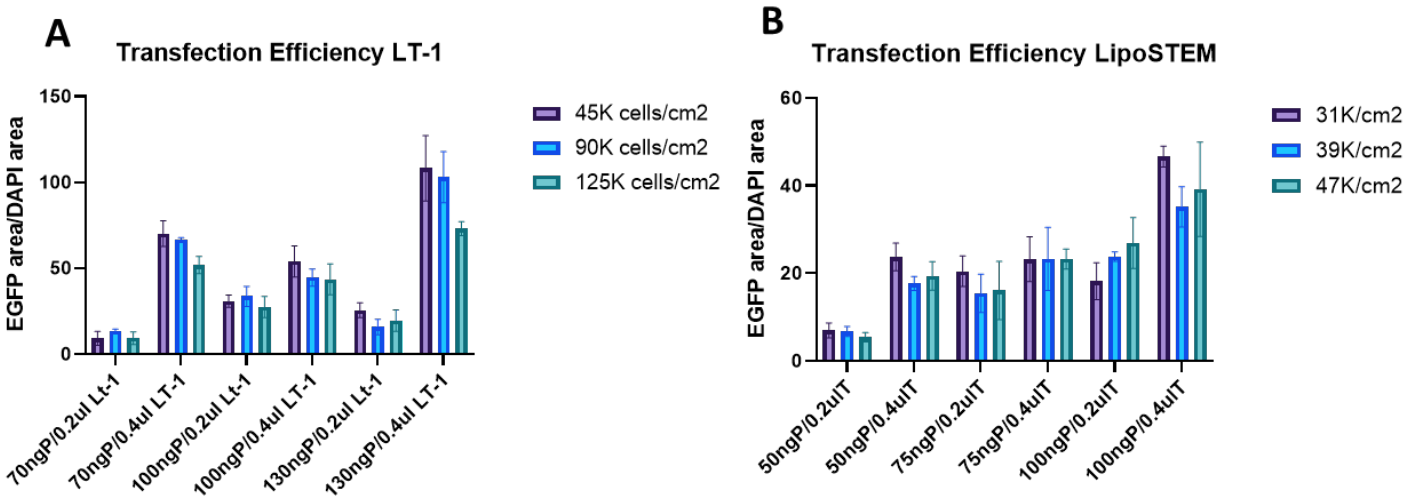
	Plasmid Load in 96 well-plate	*Transfection Reagent Volume in 96-well plate (uL)*
LT-1 *(45K cell/cm²)* *(90K cell/cm²)* *(125K cell/cm²)*	*70 ng*	*0.2*
		0.4
	100ng	*0.2*
		0.4
	130ng	*0.2*
		0.4
LipoSTEM *(31K cell/cm²)* *(39K cell/cm²)* *(47K cell/cm²)*	*50ng*	*0.2*
		0.4
	75ng	*0.2*
		0.4
	100ng	*0.2*
		0.4

Results were quantified by measuring the total EGFP area divided by DAPI area since counting $DAPI^+$ nuclei individually was not reliable due to cell clumping. Both LT-1 and LipoSTEM show that increasing plasmid load and transfection reagent volume increase transfection efficiency, while seeding density is the factor that least influences transfection efficiency (Figure 2.2A-B).

LT-1 showed highest efficiency in wells that received 130ng plasmid and 0.4ul LT-1. Seeding densities of 45K/cm^2 and 90K/cm^2 showed highest efficiency of 108.16 +/-18.99 and 102.88 +/- 14.88 EGFP/DAPI ratio, respectively, while 125K/cm^2 had a decrease in efficiency of 73.01 +/- 4.122 (n=3).

LipoSTEM behaved in similar ways, with higher plasmid loads and transfection reagent volume increasing efficiency, while density had less of an effect. Cells transfected with 100ng of EGFP and 0.4ul LipoSTEM had transfection efficiency of 46.64 +/- 2.4, 35.12 +/- 4.60, and 39.18 +/- 10.74 EGFP/DAPI ratio, for 31, 39, and 47K cells/cm^2 seeded, respectively. Representative images of transfections at highest plasmid load (130ng and 100ng for LT-1 and LipoSTEM, respectively) are shown in Figure 2.2C.

With these results, the chosen transfection conditions for further experiments were 0.4ul LT-1, 130ng plasmid, and 45K cells/cm^2 seeded.



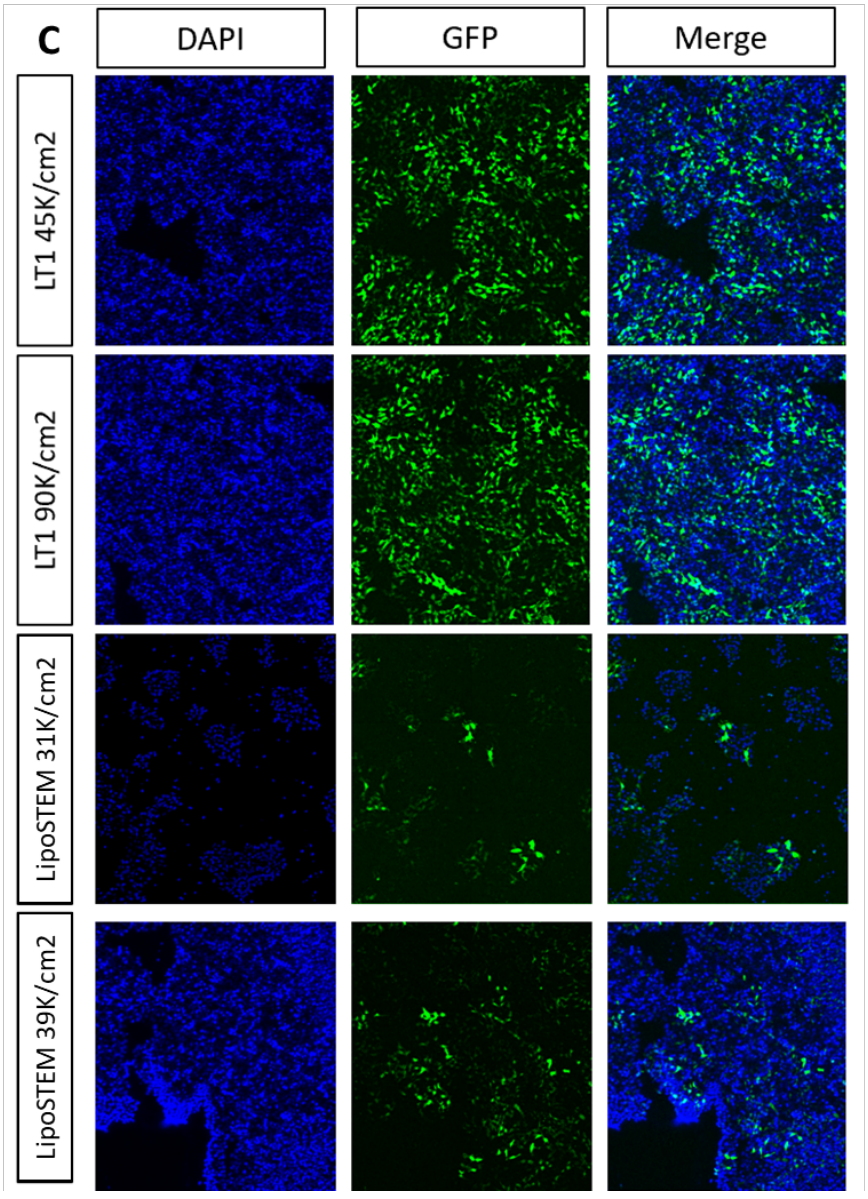


Figure 2.2 – Transfection Condition Optimization in IPSCs

A- Transfection efficiency of LT-1 for different amount of LT-1, plasmid load, and seeding density. n=3 biological replicates. Measurements were taken by dividing EGFP area by DAPI area.

B- Transfection efficiency of LT-1 for different amount of LT-1, plasmid load, and seeding density. Measurements were taken by dividing EGFP area by DAPI area. n=3 biological replicates.

C- Representative images of two high efficiency conditions from each LT-1 and LipoSTEM reagents. Scale bar, 100um. (n=3 biological replicates, each with 3 technical replicates)

sgRNA Screen

To decrease the number of plasmids to go into each transfection, as well as to increase the load of each individual plasmid, a monoclonal stable cell line was generated that contained all of the necessary features from p326 (dCas9 and activator proteins). A Sleeping Beauty transposon including such features was obtained by Dr. David Knapp and transfected together with a transposase to integrate the DNA into IPSCs. The cells were grown to confluency, split at 22K/cm^2, and selected with puromycin at 0.25ug/ml for three days. The cells were then split again and sparsely seeded at 7K/cm^2, and after colonies started to form, they were picked and re-seeded in a 96 well plate. Upon expansion, each well was then further split 1:2 in replicates across two 96 well plates, where one plate served for immunocytochemistry check for dCas9, and the other to allow for further expansion based on dCas9 immunocytochemistry results. Out of 48 colonies seeded, 19 stained positively for dCas9. Signal intensity for dCas9 was measured via imageJ and the 9 colonies with highest intensity (n=1) (Figure 2.3A) were assessed with qPCR to check for dCas9 expression (Figure 2.3B). The three colonies with highest ICC and qPCR results were chosen for further expansion, with colony H9.1 being the colony with highest scores for both assays. (Figure 2.3C).

To determine gene activation with the sgRNA constructs assembled previously, each separate construct (including control sgRNA) was transfected into the generated monoclonal cell line and checked for its respective transcription factor expression via qPCR. Equimolar amount of P222 and p284 totalling to 650ng were transfected with 2.0ul LT-1 with 85.5K cells (scaled to a 24 well plate condition). Cells were allowed to grow for four days, and RNA was taken for qPCR of LEF1, ETS1, and MRTFB to determine which sgRNA had highest capacity to upregulate gene expression.

sgRNA LEF1-1 upregulated LEF1 gene expression the highest with an average of 0.59+/-0.08 log-normalized fold change compared to control sgRNA (p=0.0094) (Figure 2.4A). sgRNA ETS1-1 upregulated expression of ETS1 with an average of 0.23+/-0.03 log-normalized fold change, although not significantly (p=0.0.211) (Figure 2.4B). Lastly, sgRNA MRTFB-1 upregulated expression

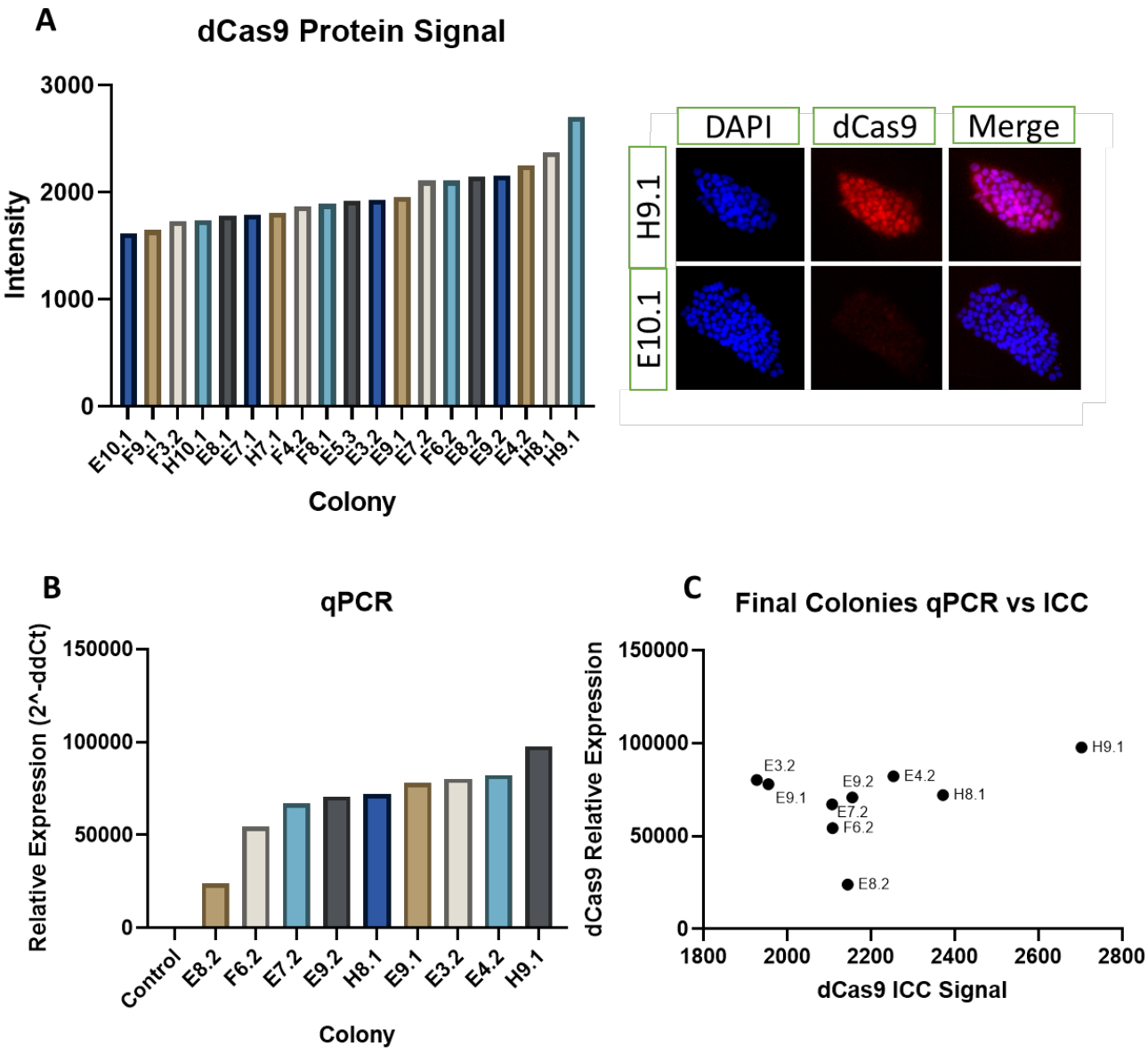


Figure 2.3 – Development of a monoclonal stable cell line including dCas9 and activator proteins
A- Signal intensity of dCas9 captured by immunocytochemistry and of stained colonies. (n=1 biological replicate)
B- Relative expression of dCas9 in top 9 scoring colonies based on immunocytochemistry results (A). (n=1 biological replicate)
C- X/Y plot of ICC and qPCR scores for top 9 colonies.

of MRTFB with an average of 0.26+/-0.1 log-normalized fold change (Figure 2.4C). sgRNAs targeting the PCS (MRTFB-5 and MRTFB-6) did not show significant activation compared to control, and comparing MRTFB-1 and MRTFB-6 (highest TSS and PCS targeting sgRNAs) yielded non-significant results between themselves (p=0.97). Therefore, no conclusion can be drawn on which region is best to target, despite MRTFB-1 targeting the TSS having a higher mean activation. The three target genes were normalized to actin.

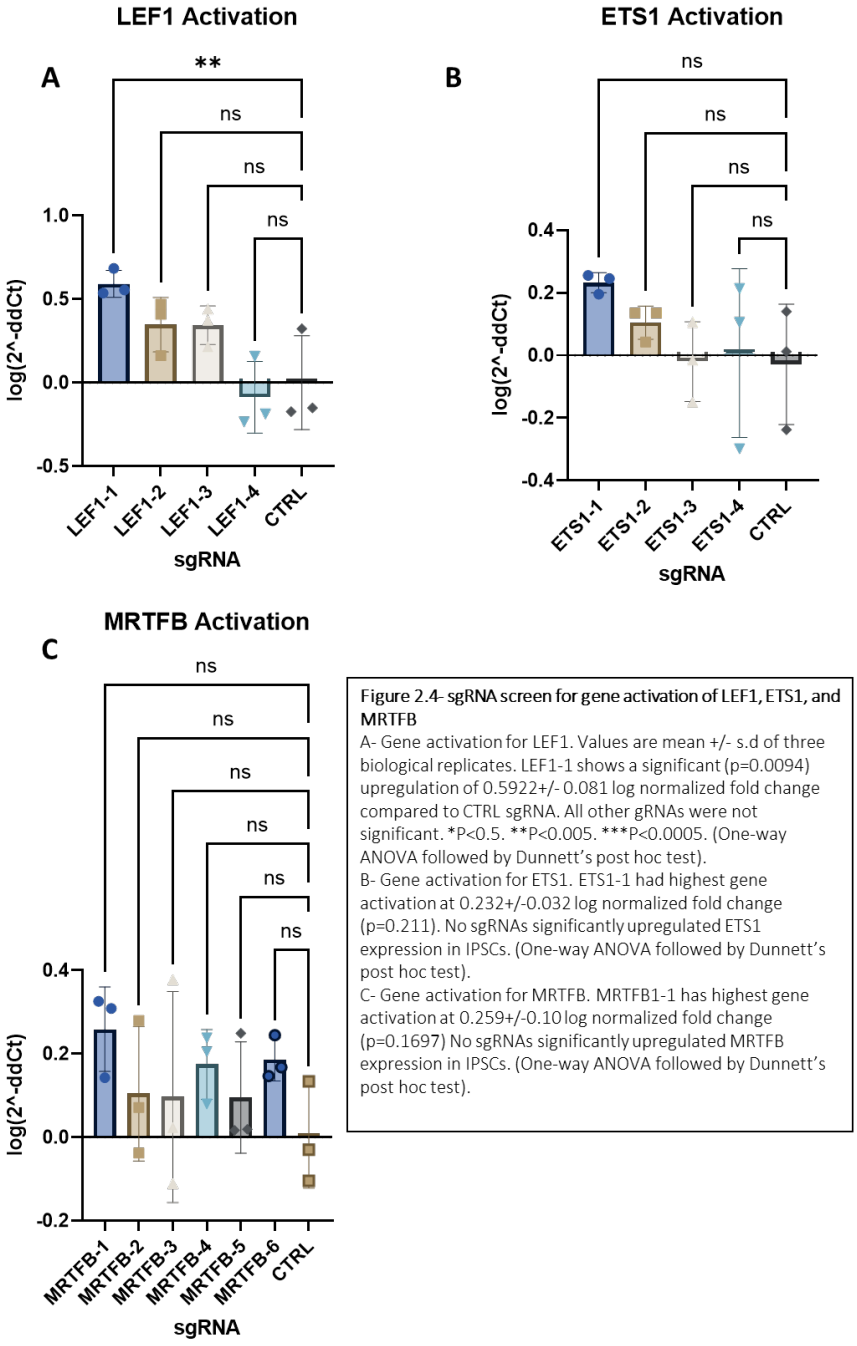


Figure 2.4- sgRNA screen for gene activation of LEF1, ETS1, and MRTFB

A- Gene activation for LEF1. Values are mean +/- s.d of three biological replicates. LEF1-1 shows a significant (p=0.0094) upregulation of 0.5922+/- 0.081 log normalized fold change compared to CTRL sgRNA. All other gRNAs were not significant. *P<0.5. **P<0.005. ***P<0.0005. (One-way ANOVA followed by Dunnett's post hoc test).

B- Gene activation for ETS1. ETS1-1 had highest gene activation at 0.232+/-0.032 log normalized fold change (p=0.211). No sgRNAs significantly upregulated ETS1 expression in IPSCs. (One-way ANOVA followed by Dunnett's post hoc test).

C- Gene activation for MRTFB. MRTFB1-1 has highest gene activation at 0.259+/-0.10 log normalized fold change (p=0.1697) No sgRNAs significantly upregulated MRTFB expression in IPSCs. (One-way ANOVA followed by Dunnett's post hoc test).

Viral Construct Assembly

Next, a single viral plasmid construct containing the three chosen sgRNAs, the scaffold sequence necessary for CRISPR activation, and Blasticidin resistance gene for antibiotic selection of transduced cells was synthesized. Five separate ~300base pairs DNA sequences were synthesized by IDT genestring and ligated using HiFi assembly (Golden Gate Assembly) to produce a single double stranded DNA with flanked ends complimentary to XhoI sites. A backbone plasmid provided by Dr. David Knapp was digested using XhoI enzyme, and the assembled genestring was ligated to the backbone plasmid. The plasmid was used for bacterial transformation and then purified.

The resulting plasmid construct was digested with XhoI and BamHI to determine if the number of cut products were accurate and of the predicted sizes. The original backbone plasmid contained BamHI while the synthesized plasmid did not, so under the same digest conditions it was expected that the control plasmid would result in three bands while the newly synthesized plasmid would have only two (Figure 2.5A). Visualizing the digested plasmids indicated all selected colonies had the correct number of bands (2) while the original control plasmid had 3 bands (Figure 2.5B). Two colonies produced bands that were of incorrect sizes whilst six colonies produced correct size products.

As a further validation, IPSCs were transfected with the six plasmids correctly assembled as described above, a positive control plasmid including Blasticidin deaminase (BSD) and untransfected IPSCs lacking BSD. All six plasmids and positive control had an upregulation of BSD compared to the negative control IPSCs (n=1), indicating that the plasmid is expressing the protein as expected (Figure 2.5C).

One colony was subsequently picked to undergo a final validation as it was the plasmid with highest transformation yield. The plasmid was sequenced using 13 different primers targeting different regions of the plasmid. While all sgRNA and scaffold sequences were validated to have the correct sequence, two extra base pairs were sequenced in the EF-1α promoter region (two extra

cytosine residues in positions 2989 and 3696), and one wrong base in the Blasticidin gene at position 4159 (C->T) (Figure 2.5D). Despite these point mutations, the qPCR results indicate that the EF-1α promoter and BSD gene were correct, and this plasmid was used to synthesize lentivirus particles.

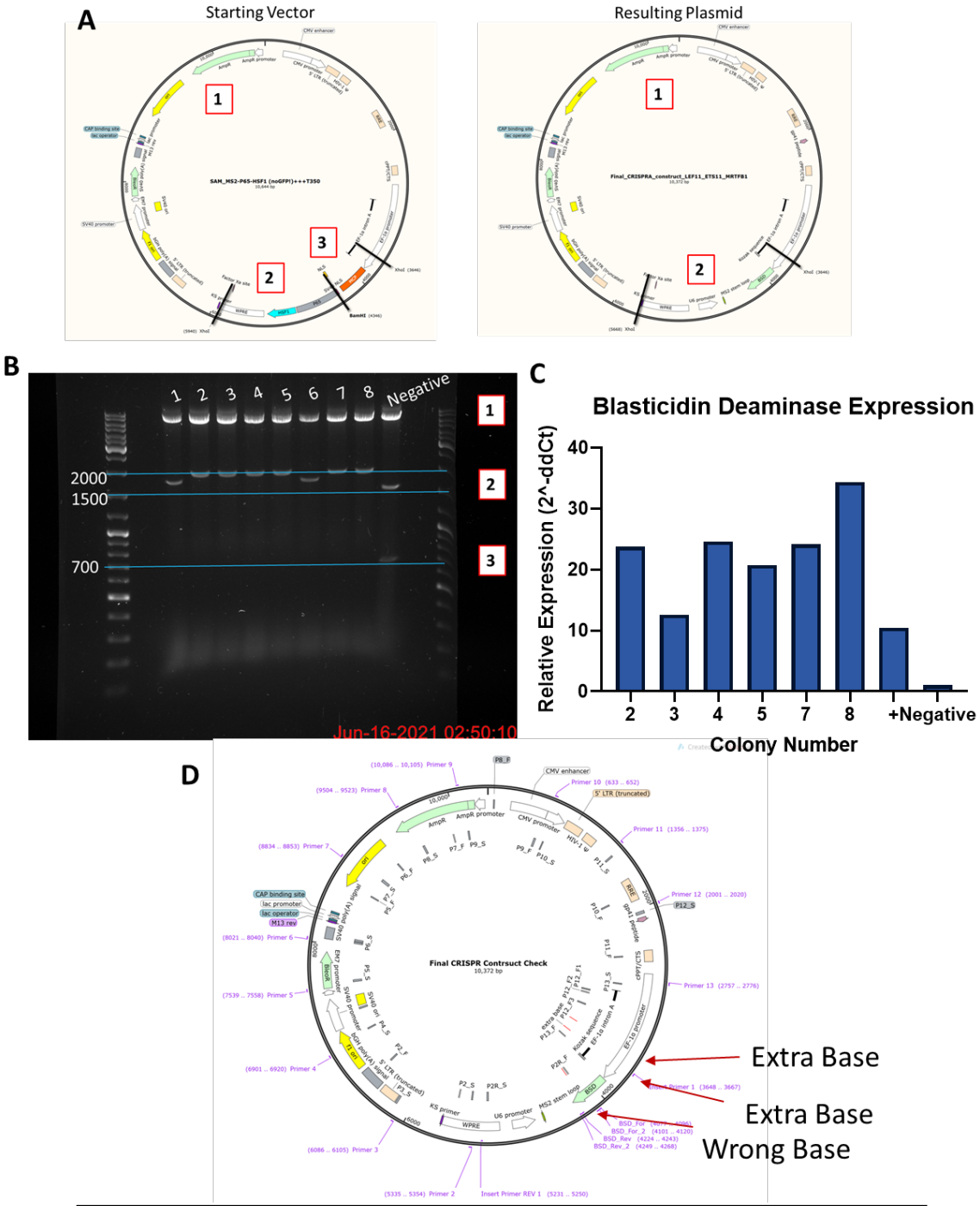


Figure 2.5– Plasmid assembly for chosen sgRNAs via Golden Gate Assembly
A- Backbone (initial) and resulting plasmid maps after golden gate assembly
B- Gel electrophoresis of resulting transformed colonies and backbone (negative control) after XhoI and BamHI restriction digest.
C- qPCR for Blasticidin deaminase expression in 6 validated colonies, positive control BSD plasmid, and negative control untransfected IPSCs
D- Summary results of primer sequencing screen for colony 5

Lentivirus was produced by Dr. Ryan Beveridge. The virus was then transduced at different amounts (0,0.01, 0.02, 0.05, 0.1, 0.15, and 0.2ul) into the monoclonal cell line containing dCas9 and activator proteins previously generated, selected with Blasticidin for 5 days, and stained for LEF1 to validate protein expression. LEF1 activation was highest with 0.2ul of virus with an average of LEF1 signal intensity of 1528 +/- 24.68 (n=3, $p<0.0001$) (Figure 2.6A-B). No difference was seen in ETS1 and MRTFB conditions due to the endogenous expression of both factors in IPSCs.

Endothelial Differentiation Using CRISPR Activation

To determine whether CRISPR activation would yield a better brain capillary endothelial fate than through forced transcription factor overexpression, the CRISPRa cell line was differentiated using the protocol developed in chapter 1 The monoclonal CRISPRa cell line was seeded at 22K/cm2 and the next day transduced with the sgRNA/scaffold virus at 1ul (scaled to 24 well plate) and selected with Blasticidin for 5 days. The cells were then split and seeded at 30K/cm2 and then differentiated. In parallel, cells with the polycistronic over-expression cassette were also differentiated to provide a comparison.

The CRISPRa cell line yielded a significantly lower number of VE-CADHERIN$^+$ cells after MACS on day 12, with 4.6% +/- 2.3% compared to 16.2% +/- 1.9% in the TF over-expression cell line (n=3, $p=0.0027$, unpaired t-test) (Figure 2.7A). CRISPRa cultures at day 16 also had a smaller proportion of endothelial marker staining compared to lentiviral overexpression. CLDN5 staining was reduced, VE-CADHERIN and ZO-1 stained a smaller proportion of cells, and PECAM1 staining showed a lack of cellular organization seen in the TF overexpression line. Interestingly, small patches of OCLN signal were picked up in the CRISPRa cultures, but this co-localized with E-CADHERIN staining, indicating the stained cells are not of a true endothelial identity. No E-CADHERIN or OCLN signal was detected in the TF overexpression cultures. Calponin (CCN1) and β-CATENIN were detected in both cultures, but the CRISPRa cells had a more diffuse signal for CCN1 and lower intensity in b-CATENIN staining (Figure 2.7B).

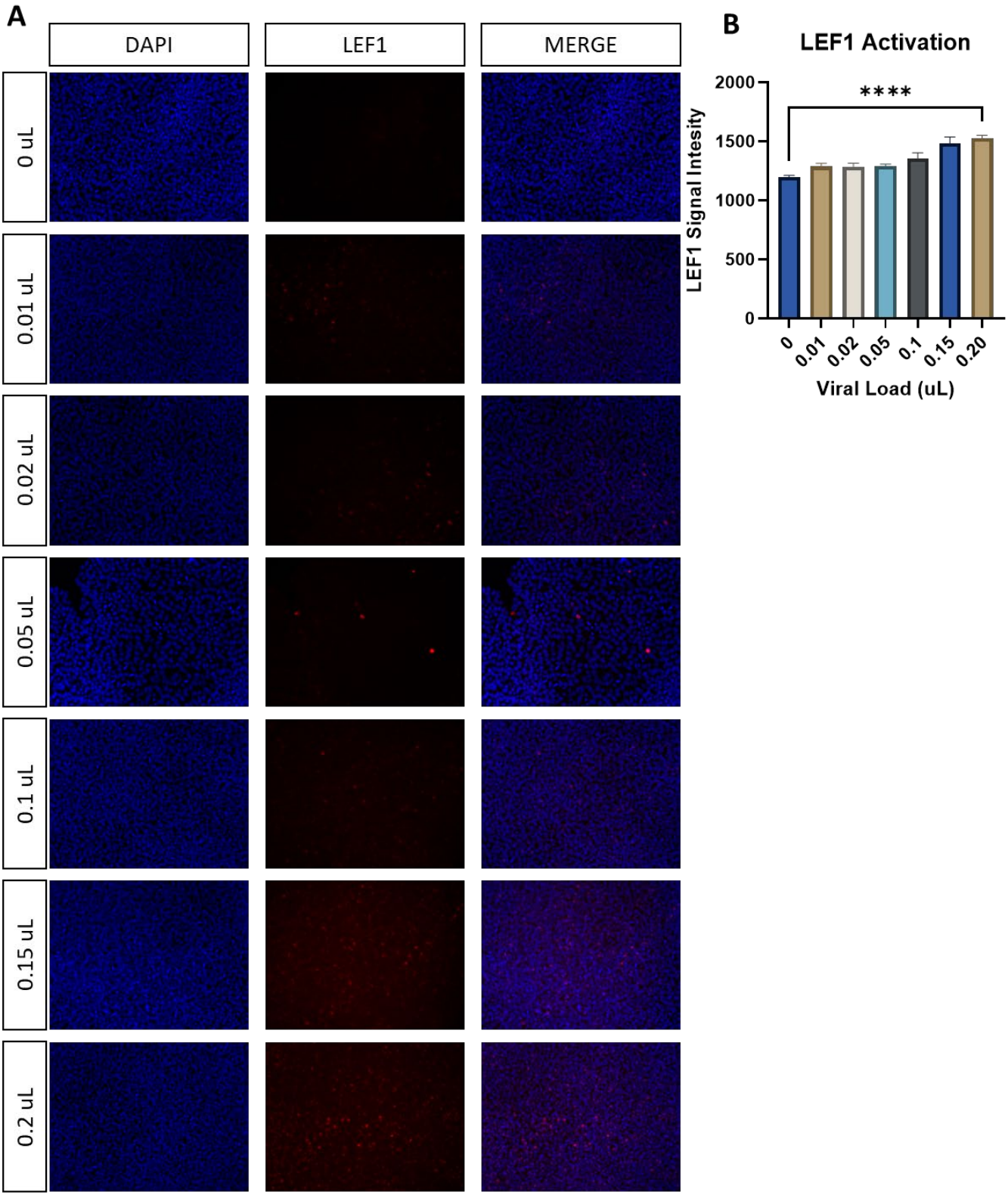
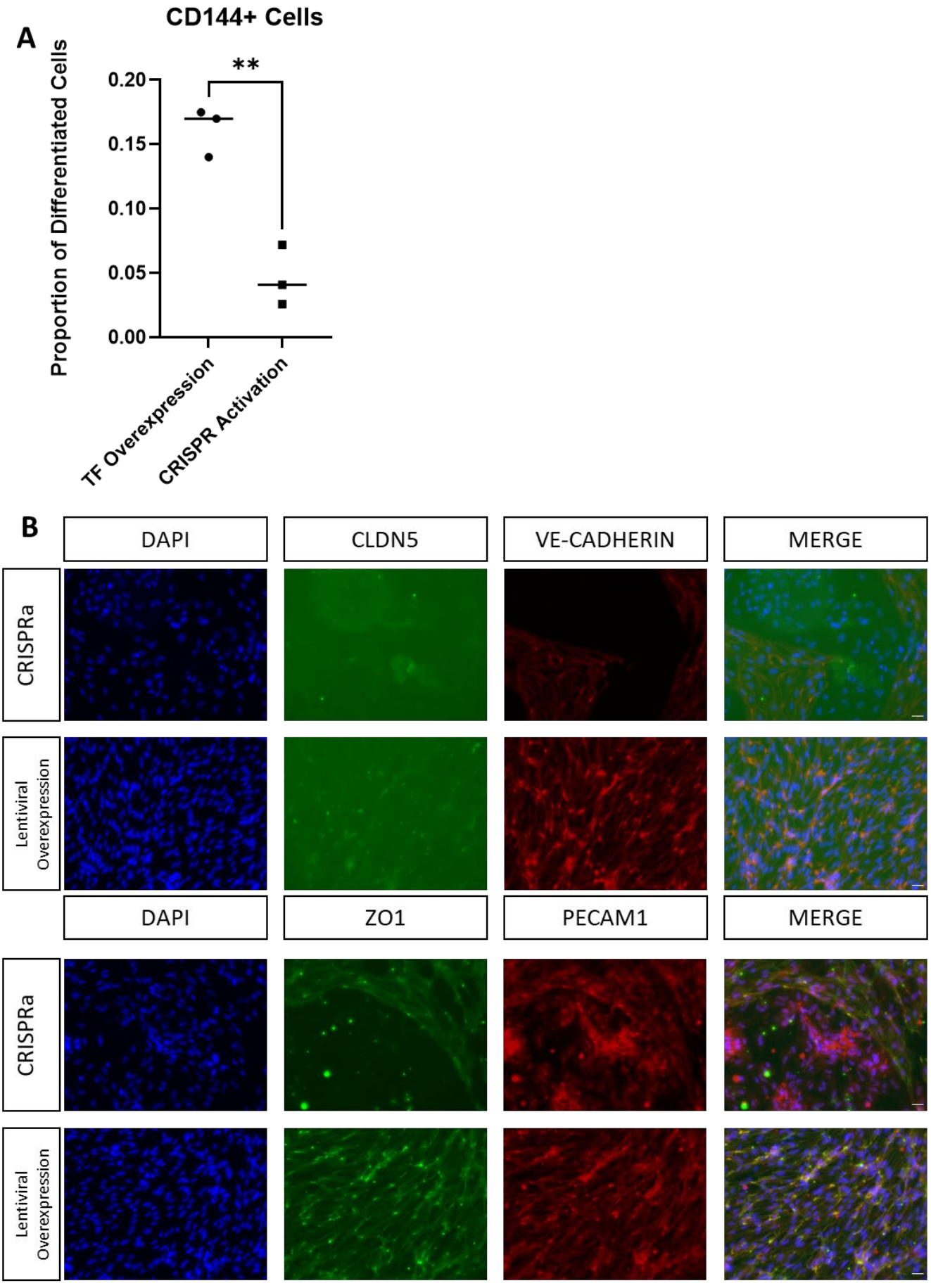


Figure 2.6– LEF1 is Activated by transduction of newly synthesized sgRNA virus
A- Representative images of cultures transduced with varying amounts of virus (n=3)
B- LEF1 signal intensity based on varying viral loads in uL. Values are mean +/- s.d of three biological replicates. *P<0.05. **P<0.005. ***P<0.0005.****P<0.0001 (Student's paired t-test)


A
CD144+ Cells
Proportion of Differentiated Cells
**
0.20
0.15
0.10
0.05
0.00
TF Overexpression
CRISPR Activation
B
DAPI
CLDN5
VE-CADHERIN
MERGE
CRISPRa
Lentiviral Overexpression
DAPI
ZO1
PECAM1
MERGE
CRISPRa
Lentiviral Overexpression

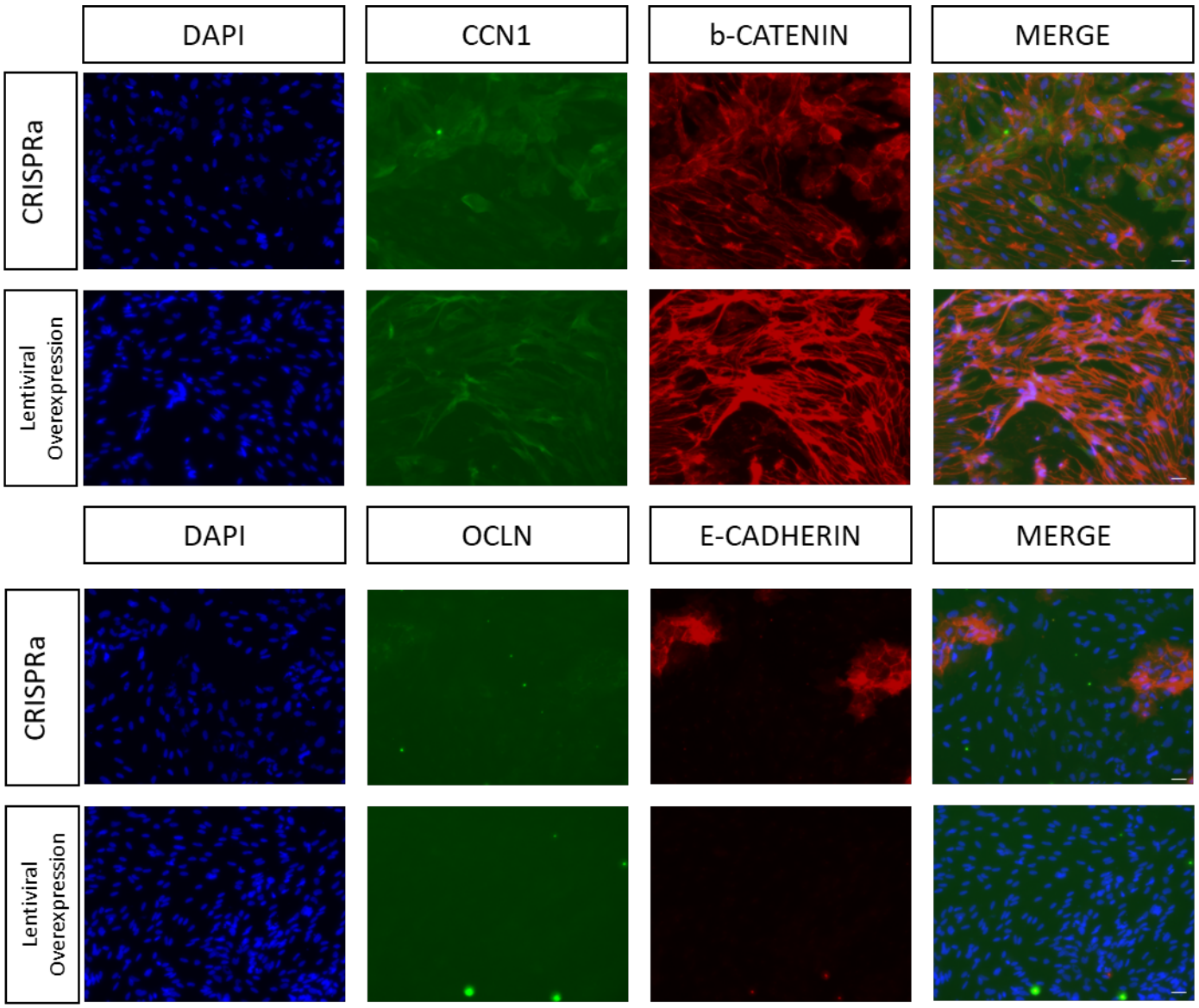


Figure 2.7– Brain Endothelial Cell Differentiation Comparison of CRISPRa and Lentiviral Overexpression Protocols
A- Proportion of VE-CADHERIN+ cells separated during MACS at day 12 of the protocol for TF Overexpression and CRISPRa protocols. TF overexpression significantly produces a higher proportion of VE-CADHERIN+ cells, with 16.17 +/- 1.8% of total cells staining positively for VE-CADHERIN while CRISPRa stained for 4.6% +/- 2.3% of cells ($p=0.0027$). Values are mean +/- s.d of three biological replicates. **P<0.005. (Student's unpaired t-test)
B- Representative images for both platforms for CLDN5, VE-CADHERIN, ZO1, PECAM1, CCN1, B-CATENIN, OCLN, and E-CADHERIN . Scale bar, 50um. (n=3 biological replicates)

Discussion

The CRISPRa technology was employed to investigate whether physiological gene activation rather than a forced overexpression would improve the differentiation from IPSCs to endothelial cells. A CRISPRa cell line was developed and used to identify specific gRNAs to activate expression of LEF1, ETS1, and MRTFB. CRISPR activation is being used as a tool to differentiate stem cells into neurons[276-278], and I hypothesized it could be employed into an endothelial differentiation model as well. However, IPSCs under CRISPR TF gene activation had significantly lower VE-CADHERIN^{+} proportion of differentiated cells, reduced expression of markers such as CLDN5 and b-CATENIN, and diminished cellular organization seen in the TF overexpression model.

An interesting finding was that OCCLUDIN expression was only detect in cells expressing E-CADHERIN. Occludin is considered a key marker for tight junctions and was absent in differentiations described in chapter 1. With previous results showing that VE-CADHERIN and E-CADHERIN do not co-localize, these E-CADHERIN/OCLN^{+} cells are not endothelial. These cells also show a distinct morphological difference from VE-CADHERIN^{+} cells; while VE-CADHERIN shows an elongated cell body, E-CADHERIN/OCLN cells are more round, with typical “cobblestone” patterning discussed in several publications of endothelial differentiations that stain positively for OCLN [223, 227, 279].

IPSCs have the capacity to differentiate into several different “endothelial” cell identities. In my experiments, I have seen VE-CADHERIN^{+}/PECAM1^{+}/CLDN5^{+}/OCLN^{-}/E-CADHERIN^{-} population, and a separate OCLN^{+}/E-CADHERIN^{+} population. Other publications indicate the differentiated endothelial cells are OCLN^{+}/PECAM1^{+}/CLDN5^{+}/VE-CADHERIN^{+}, but representative images from these studies show a diffuse signal of PECAM1 and VE-CADHERIN through the cell, rather than the membrane localization seen in my protocol. Further, published protocols do not show evidence for lack of E-CADHERIN staining in their cultures. Differentiated endothelial cells from published protocols may thus have a significant composition of the non-endothelial E-CADHERIN^{+} cell population. This is

supported by transcriptomic studies of the Lippman protocol that show E-CADHERIN expression[234].

The CRISPR activation cell line may not have been able to effectively differentiate into brain capillary endothelial cells because expression levels of the required transcription factor were not sufficiently increased. I found that LEF1 was significantly upregulated but ETS1 and MRTFB showed only a small relative increase. Differentiation into mesoderm as employed in my protocol may alter the epigenetic landscape of the transcription factors. If promoter regions of the three TFs close during the differentiation, the activation potential of dCas9 could have been blocked or substantially limited. ETS1 and MRTFB already show expression in iPSC whilst LEF1 expression is absent. At the mesoderm stage ETS1 expression reduces. Hence there are likely to be transcriptional signalling mechanisms that could easily over-ride any activation induced by CRISPRa in the critical stages.

This contrasts with studies using CRISPRa to achieve neuronal differentiation. Hence CRISPR activation of ASCL1 and NGN2 enables differentiation into excitatory and inhibitory cortical neurons [277, 280]. This may have been more successful because these transcription factors are stronger identity determinants or perhaps because iPSC have an innate tendency to differentiate into neurons.

In conclusion, CRISPR activation of LEF1, ETS1 and MRTFB is currently not competent to differentiate IPSCs into brain capillary endothelial cells. A detailed characterisation of the epigenetic and transcriptional landscape will be required to progress this work. This will help identify pioneer TFs that are sufficiently robust to drive differentiation to endothelial cell fate despite other signals that may be present in culture.

Chapter 3: The Effects of Hyperglycaemia on Primary Mouse BMECs

Introduction

The consequences of hyperglycaemia on endothelial cells have been studied in several different cell lines, including bEnd3, hCMEC, HUVEC, etc. [281-287]. However, such cells lines are either derived through immortalisation of brain endothelial cell lines, which may have several non-physiological properties (bEnd3 and hCMEC), or endothelial cells that are from a different non-brain tissue (HUVECs, aortic endothelial cells). Nevertheless, the most consistent results arising from these different cellular models is that hyperglycaemia at 25mM glucose leads to inflammatory changes. Increased ROS, inflammatory markers such as TNF-α, IL-1β, and IL-6, and reduced nitric oxide (NO) availability are key pathways that have been previously reported.

The mechanisms by which these pro-inflammatory pathways are activated was proposed two decades ago from studies of porcine aortic endothelial cells, where it was suggested that glucose overloads the cellular respiration mechanism leading to increased ROS, reducing GAPDH availability, and an increased flux of glycolytic intermediates into separate pro-inflammatory pathways [166, 170]. Although these mechanisms have been extensively discussed in review papers [172, 288-290], there has been little advance in validating them in brain endothelial cells.

To better understand the effects of hyperglycaemia on brain microvascular endothelial cells, I used primary mouse brain endothelial cell cultures. Protocols to isolate brain microvascular endothelial cells have only been optimized and published in the past decade, and to my knowledge, no studies have been performed directly investigating the effects of hyperglycaemia in this model.

I hypothesize BMECs exposed to elevated levels of glucose in the media will exhibit markers of increased inflammation. My aims are:

- Establish murine *primary* brain endothelial cell cultures
- Investigate the effect of media glucose on glucose consumption and lactate production
- Investigate the effect of media glucose on expression of pro-inflammatory markers and mitochondrial ROS levels
- Determine whether media glucose affects brain endothelial cell barrier integrity

RESULTS

Primary brain microvascular endothelial cells were grown by sacrificing C57/Bl6 mice and isolating their brain microvessels. Once cultures had stabilised, they were then maintained under different glucose concentrations in the media (5.5mM, 15mM, and 25mM) (Figure 3.1A) [261]. Immunocytochemistry was performed for key endothelial markers CLDN5 and PECAM1 (CD31) to check for culture purity, differences in marker intensity, and cellular proliferation.

All cells showed high PECAM1 signal, but CLDN5 signal intensity varied from cell to cell (Figure 3.1B). Across all three glucose concentrations (5.5mM, 15mM, and 25mM), there was no significant difference in mean signal intensity of either PECAM1 or CLDN5 (Figure 3.2A,B). Cells under 15mM glucose had a significantly greater number of cells at 4 days in culture. The average cell count (number of DAPI nuclei/ mm^2) in 15mM glucose was 1349+/-147 cells/mm^2 compared to 781+/-178 mm^2 in 5.5mM ($n=3$, $p<0.05$). This could reflect increased proliferation or improved survival. Cells grown in 25mM glucose had 1051 cell/ mm^2, which was not significantly different compared to other conditions (Figure 3.2C).

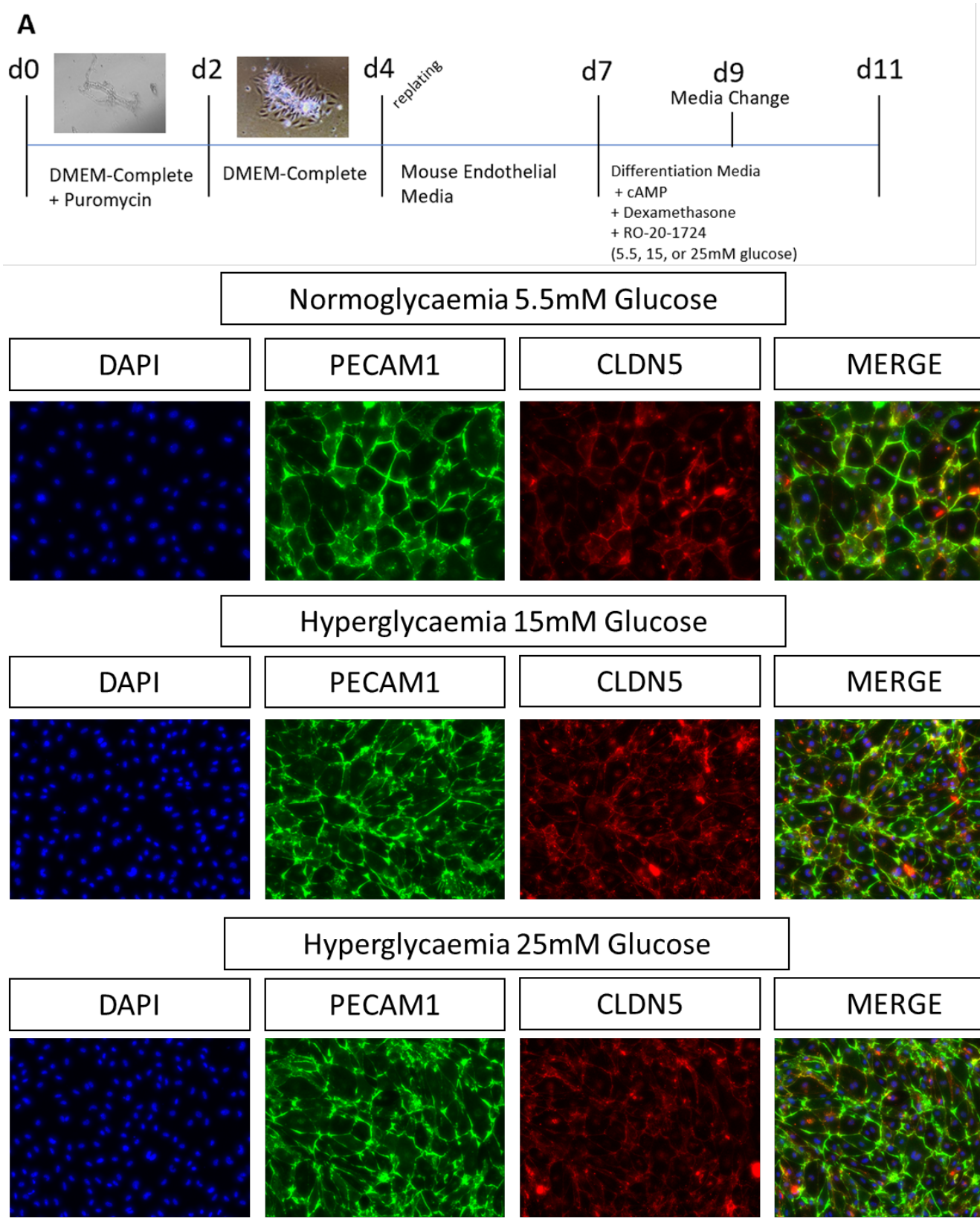


Figure 3.1 – Establishment of *ex-vivo* murine Brain Microvascular Endothelial Cell Culture
A- Experimental design
B- Immunocytochemistry of BMEC markers PECAM1 and CLDN5 under different concentrations of media glucose (n=3, 5.5mM, 15mM, 25mM). Scale bar = 50um. (n=3 biological replicates)

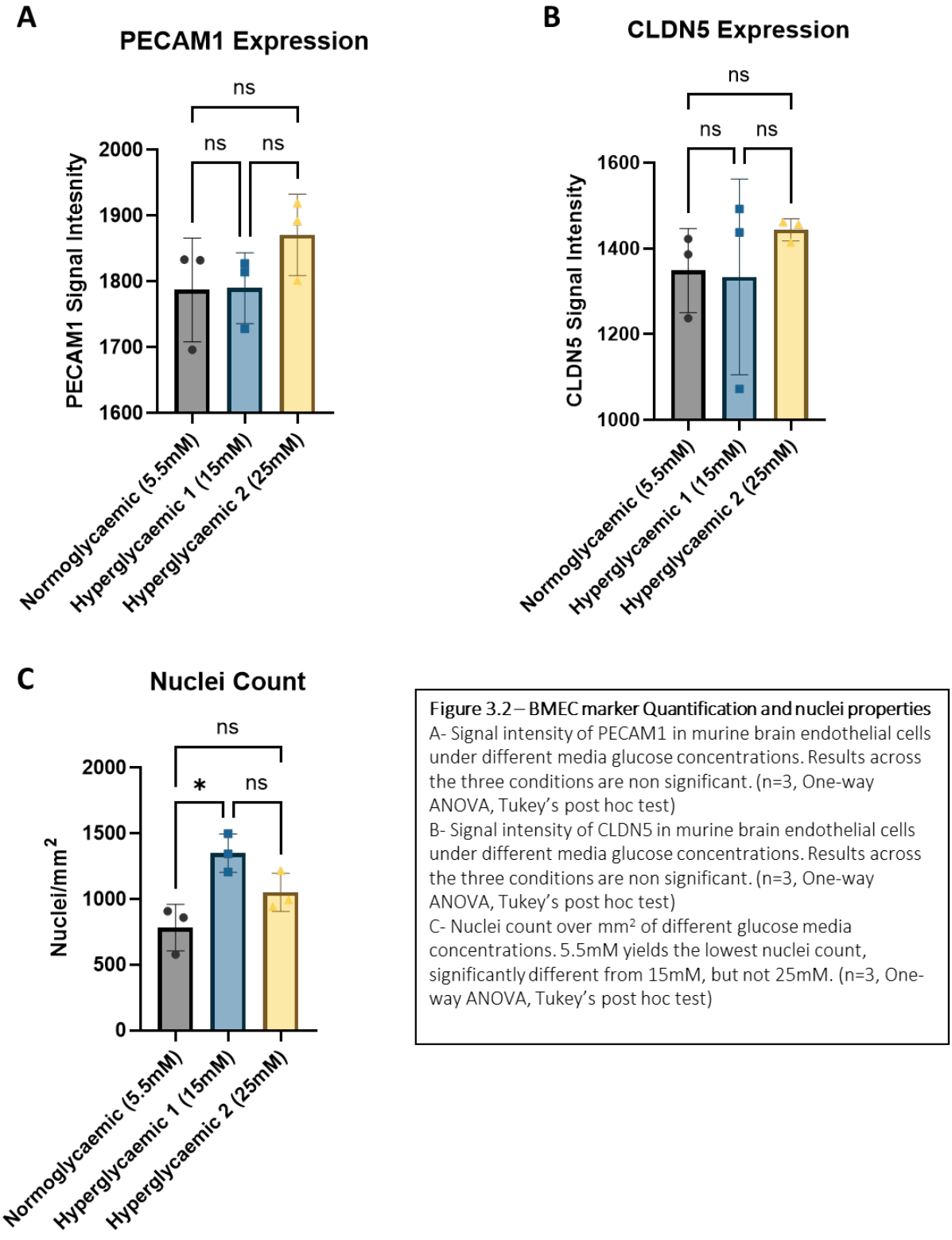


Figure 3.2 – BMEC marker Quantification and nuclei properties
A- Signal intensity of PECAM1 in murine brain endothelial cells under different media glucose concentrations. Results across the three conditions are non significant. (n=3, One-way ANOVA, Tukey's post hoc test)
B- Signal intensity of CLDN5 in murine brain endothelial cells under different media glucose concentrations. Results across the three conditions are non significant. (n=3, One-way ANOVA, Tukey's post hoc test)
C- Nuclei count over mm^2 of different glucose media concentrations. 5.5mM yields the lowest nuclei count, significantly different from 15mM, but not 25mM. (n=3, One-way ANOVA, Tukey's post hoc test)

The media used in this protocol contains cAMP, dexamethasone, and RO-20-1724, which have all been identified to reduce inflammation via inhibition of pro-inflammatory cytokines and ROS production [291-293]. Since these additives could mask inflammatory phenotypes, I investigated

whether cells would survive and maintain barrier integrity without them. Without the additives, there were sparse nuclei staining, disruption of the confluent monolayer of cells and lower proportion of cells staining for both CLDN5 and PECAM1 (Supplementary Figure 3.1). Hence it was not possible to perform experiments without these agents.

Barrier Integrity

I next investigated endothelial barrier integrity by measuring trans-endothelial electrical resistance. BMECs were exposed to normoglycaemic (5.5mM) or hyperglycaemic (15mM) media for four days (with a media change at day 2) and trans-endothelial electrical resistance (TEER) measurements were taken at day 4. Cells in 5.5mM glucose showed TEER values of 187+/-9 $\Omega*cm^2$ and in 15mM glucose showed 183 +/-18 $\Omega*cm^2$ (Figure 3.3, n=3, not significant, student's t-test). These results are in accordance with immunocytochemistry results, where junctional markers CLDN5 had non-significant differences in signal intensity.

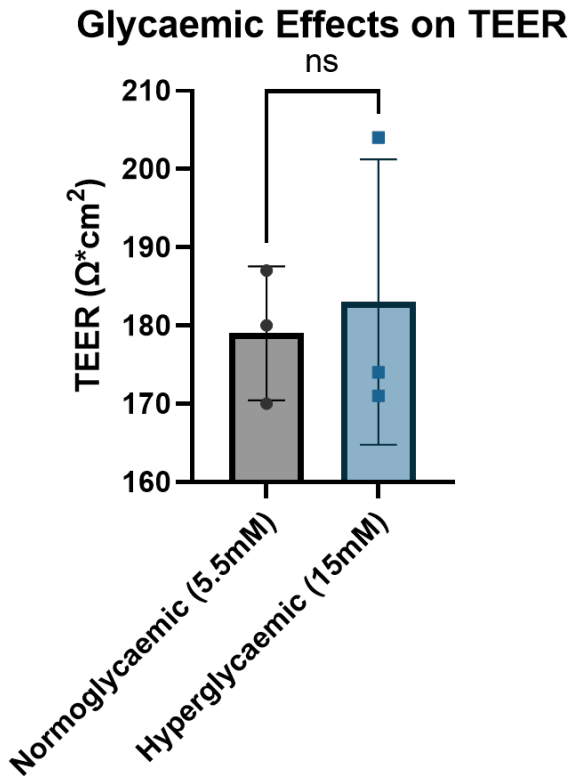


Figure 3.3- TEER measurement of murine brain endothelial cells exposed to 5.5mM or 15mM media glucose concentration
Cells exposed to 5.5mM glucose had an average TEER of 187+/- 8.54 Ω*cm2 and cells exposed to 15mM had an average TEER of 183+/- 18.25Ω*cm2. There is no statistical significance between both results (n=3, unpaired student's t-test)

Glucose Consumption

To assess glucose consumption, media glucose measurements were taken after 2 days of cell culture. The supernatant was assayed using the KDBio GlucCell Meter. Cells grown in 5.5mM glucose had a starting concentration of 5.6+/-0.1mM glucose and after 2 days it reduced slightly to 5.4+/-0.1mM. Cells grown in 15 mM glucose had an initial measurement of 15.13+/- 0.057mM and after 2 days this reduced to 12.83+/-0.12mM (Figure 3.4A). Calculating the total amount of glucose consumed under both conditions, there was a significantly greater glucose consumption in hyperglycaemic (82.33+/- 2.99ug) compared to normoglycaemic condition (6.70+/-0.06ug) (Figure 3.4B)

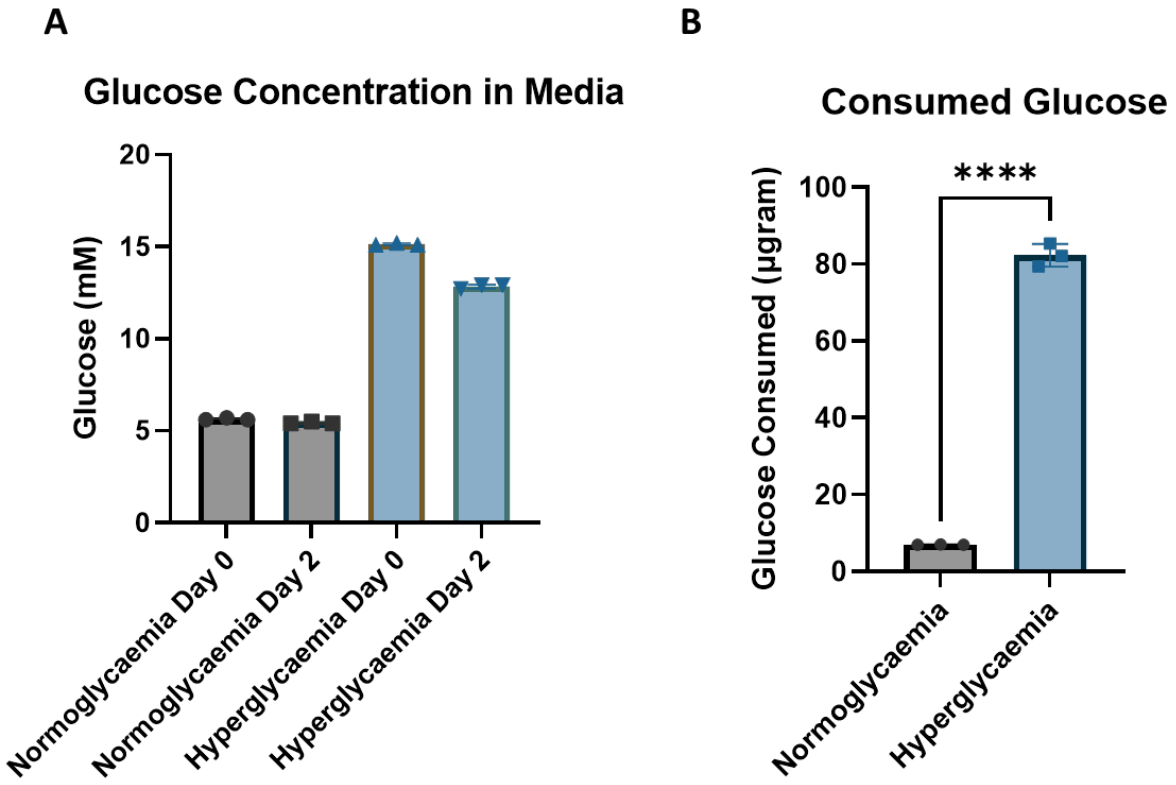


Figure 3.4A-B- Murine brain endothelial cells do not experience hypoglycaemia under experimental conditions and uptake more glucose under hyperglycaemic media

A- Glucose levels measured by GlucCell meter before and after 2 days of cell exposure. Normoglycaemic media prior to exposure averaged 5.63+/- 0.057mM and after 2 days averaged 5.43+/-0.05mM. Hyperglycaemic media prior to exposure averaged 15.13+/- 0.057mM and after 2 days averaged 12.83+/-0.12mM (n=3).

B- Total glucose consumed by cells in normoglycaemic media averages 6.699+/-0.06ug and hyperglycaemic media averages 82.33+/- 2.975ug. The results are statistically significant (n=3, $p<0.0001$, unpaired student's t-test)

To investigate whether increased glucose consumption is being metabolized into lactate, a lactate assay was employed on the media after 2 days in culture. Lactate media concentrations had an average of 300.5+/- 69.03 ng/ul and 365.1+/-32.10 ng/ul in normoglycaemic (5.5mM) and hyperglycaemic (15mM) media, respectively (Figure 3.5, n=3, not significant, unpaired student's t-test).

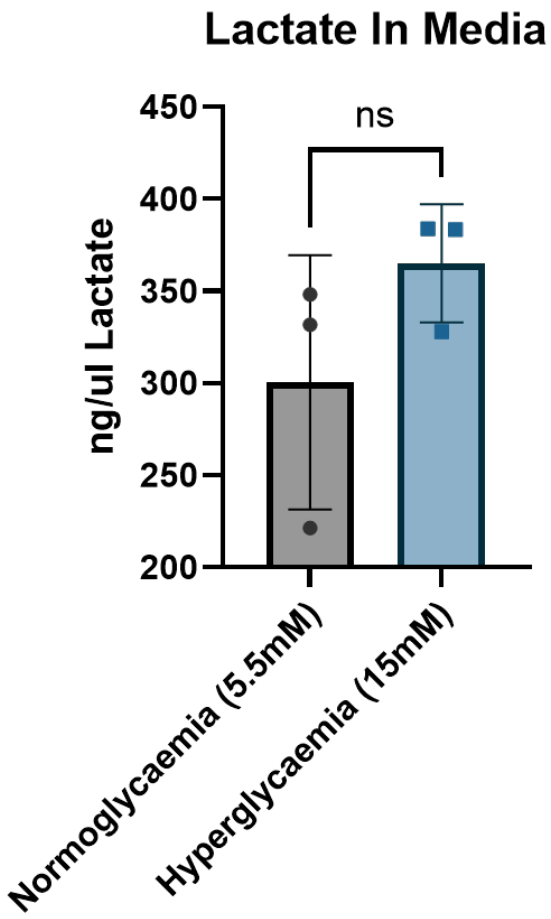


Figure 3.5- Cells under hyperglycaemic media do not produce more lactate than cells in normoglycaemic media
Lactate measurements from the media supernatant two days after exposure to cells. Normoglycaemic media averaged 300.5+/-69.03 ng/ul lactate and hyperglycaemic media averaged 365.1+/- 32.10 ng/ul lactate (n=3, not significant, unpaired student's t-test)

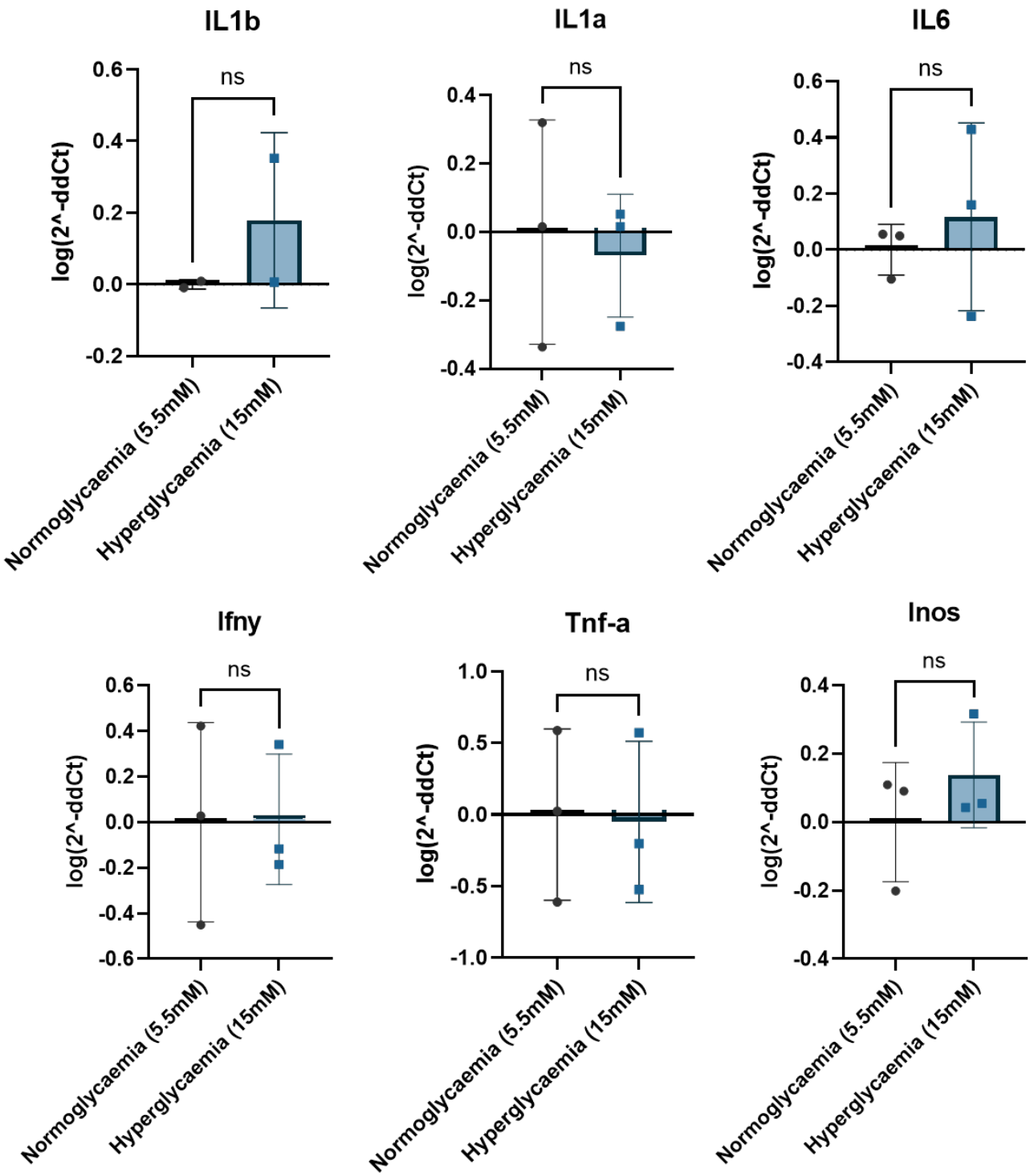
Inflammation

. Mouse brain endothelial cells cultures under differing glucose concentrations (5.5mM and 15mM) were assayed using qPCR panel of inflammatory and diabetes-associated markers (Table 3.1).

Table 3.1: List of qPCR targets

Marker	**Potential Diabetes Mechanism**
IL1β	Endothelial inflammatory marker
IL1α	Endothelial inflammatory marker
IL6	Endothelial inflammatory marker
Ifnγ	Endothelial inflammatory marker
Tnf-α	Endothelial inflammatory marker
iNos	NO availability marker
Gapdh	Proposed target of ROS generated by hyperglycaemia
Icam	BBB cell adhesion molecule
Vcam	BBB cell adhesion molecule
Crp	Diabetes-associated molecule/Inflammatory Marker
Mcp1	Diabetes-associated molecule
Pai1	Hypertension-associated Molecule

No markers showed any significant differences between normoglycaemic media and hyperglycaemic media (Figure 3.6). There was a trend of upregulation (iNos, Mcp1, Pai1, Crp, and Il6) or downregulation (Gapdh). However, no marker consistently showed the same directional change in expression across all three biological replicates. All target genes were normalized to Actin as Gapdh was a target gene that I hypothesized could have had changes in expression. Actin had stable expression across both glycaemic levels and therefore was deemed as an appropriate housekeeping gene (Supplementary Figure 3.2).


IL1b
ns
log(2^-ddCt)
0.6
0.4
0.2
0.0
-0.2
Normoglycaemia (5.5mM)
Hyperglycaemia (15mM)
IL1a
ns
log(2^-ddCt)
0.4
0.2
0.0
-0.2
-0.4
Normoglycaemia (5.5mM)
Hyperglycaemia (15mM)
IL6
ns
log(2^-ddCt)
0.6
0.4
0.2
0.0
-0.2
-0.4
Normoglycaemia (5.5mM)
Hyperglycaemia (15mM)
Ifny
ns
log(2^-ddCt)
0.6
0.4
0.2
0.0
-0.2
-0.4
-0.6
Normoglycaemia (5.5mM)
Hyperglycaemia (15mM)
Tnf-a
ns
log(2^-ddCt)
1.0
0.5
0.0
-0.5
-1.0
Normoglycaemia (5.5mM)
Hyperglycaemia (15mM)
Inos
ns
log(2^-ddCt)
0.4
0.2
0.0
-0.2
-0.4
Normoglycaemia (5.5mM)
Hyperglycaemia (15mM)

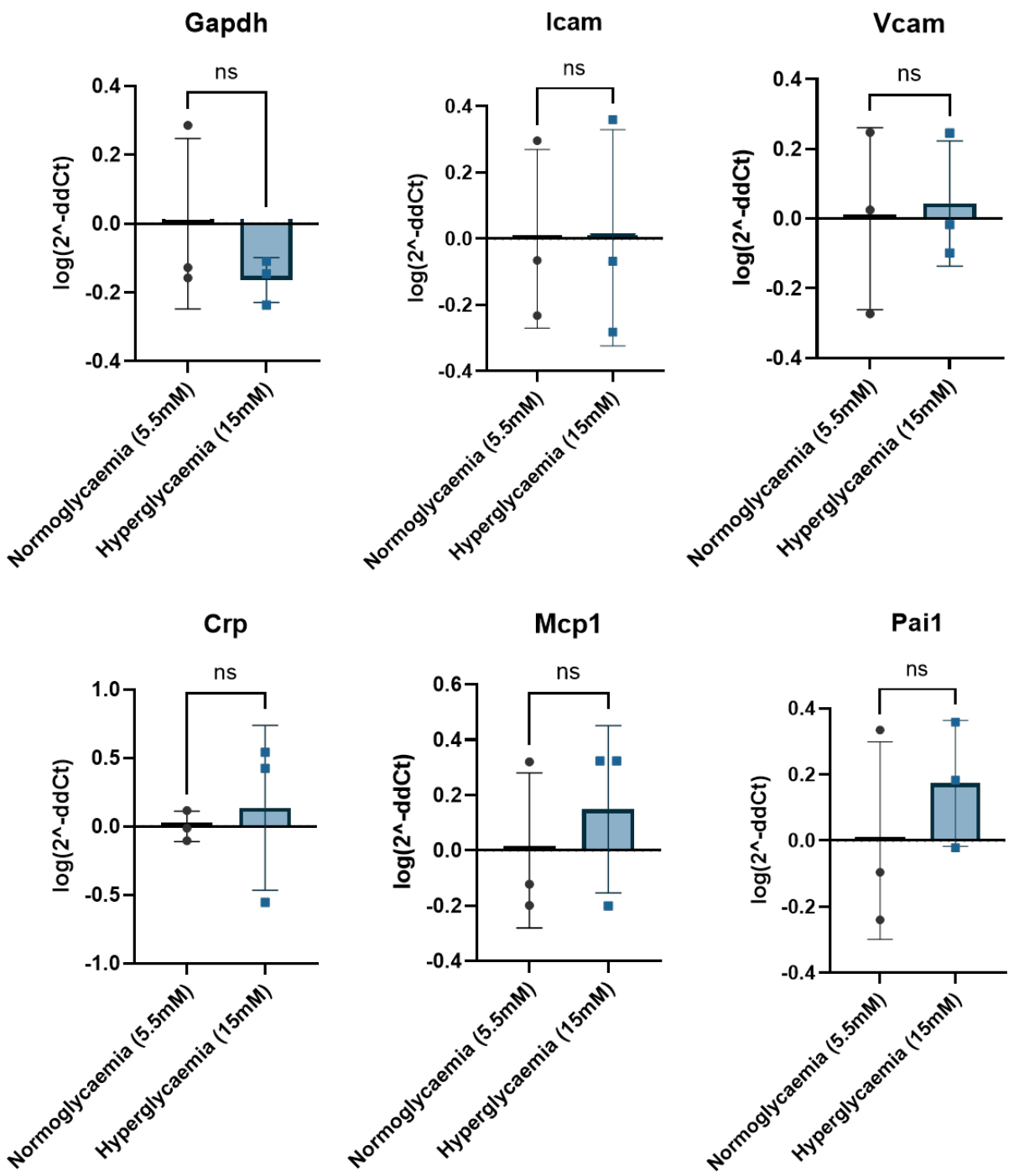


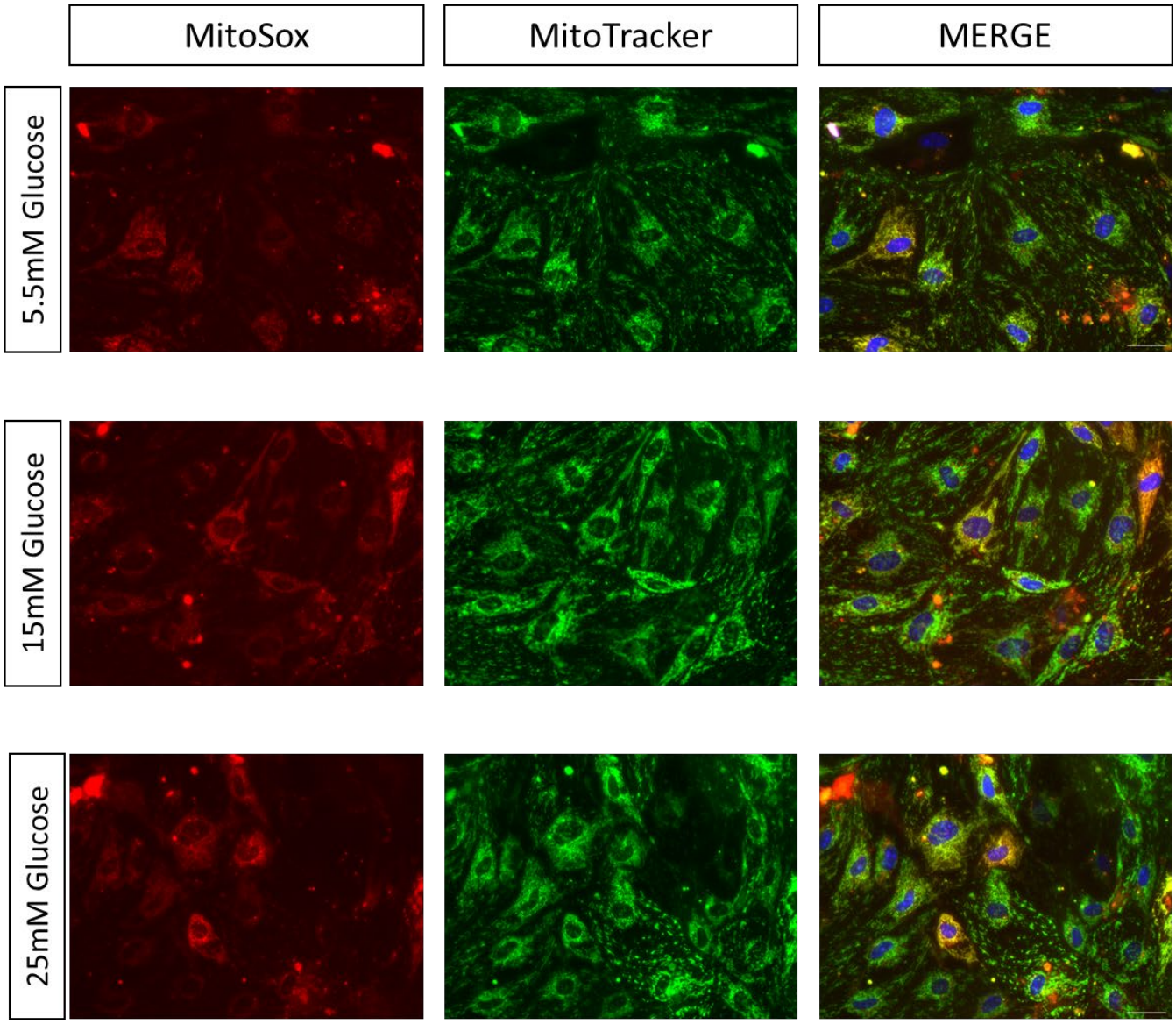
Figure 3.6- qPCR of inflammatory, diabetic, and hypertension-related genes
qPCR results mouse endothelial cells exposed to 5.5mM or 15mM glucose for IL1b, Il1a, IL-6, IFNy, TNF-a, Inos, Gapdh, Icam, Vcam, Crp, Mcp1, and Pai1 normalized to b-Actin. No significance was found across any gene assayed.

ROS

To test the hypothesis posited by Du et al [166, 170] that increased mitochondrial ROS levels represents the primary insult by hyperglycaemia, I employed a live-cell mitochondrial ROS assay in conjunction with mitochondrial staining via MitoTracker Green to measure levels of mitochondrial ROS under different media glucose conditions.

To optimize assay conditions, cells were exposed to 20, 100, or 200nM of MitoTracker Green reagent and Hoechst for live-nuclei staining. Cells under 20 and 100nM showed clear distinct signal in the cells' cytoplasm. However, upon increasing concentration to 200nM, aberrant staining was seen, with a diffuse signal in the cell's cytoplasm (Supplementary Figure 3.3). To minimise toxicity, I elected to move forward with 20nM of MitoTracker Green. Cells were then exposed to 1, 3, or 5ul of the Mitosox reagent along with Mitotracker Green at 20nM and Hoechst. Cells at 1, 3, and 5uM show distinct signal of ROS that co-localize with Mitotracker Green, confirming that the ROS signal is of mitochondrial origin (Supplementary Figure 3.4). However, in the 5uM condition a few cells showed a high intensity across the nucleus and cell body, indicating toxicity from the Mitosox reagent. Therefore, I elected to perform the glycaemic experiments with 1uM Mitosox reagent to prevent any toxicity. Image analysis was performed using ImageJ, overlaying MitoTracker Green signal over the ROS image to ensure ROS measurements were localised to the cell's mitochondria. The results were then normalized to the background.

ROS signals were 1.39+/-0.26, 1.79+/-0.89, and 1.60+/-0.50 for 5.5mM, 15mM, and 25mM media glucose, (Figure 3.7, n=4, 5.5 and 15mM, n=3, 25mM) with no significant differences across all three condition (One-way ANOVA, Tukey's post-hoc test).



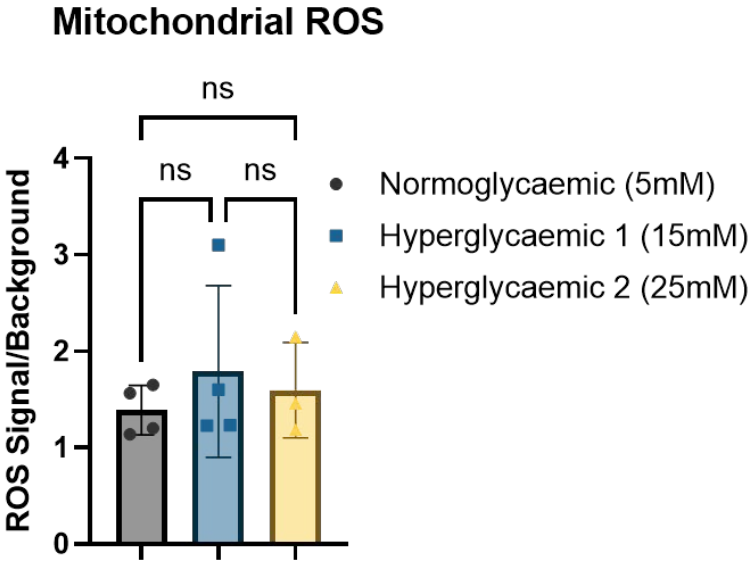
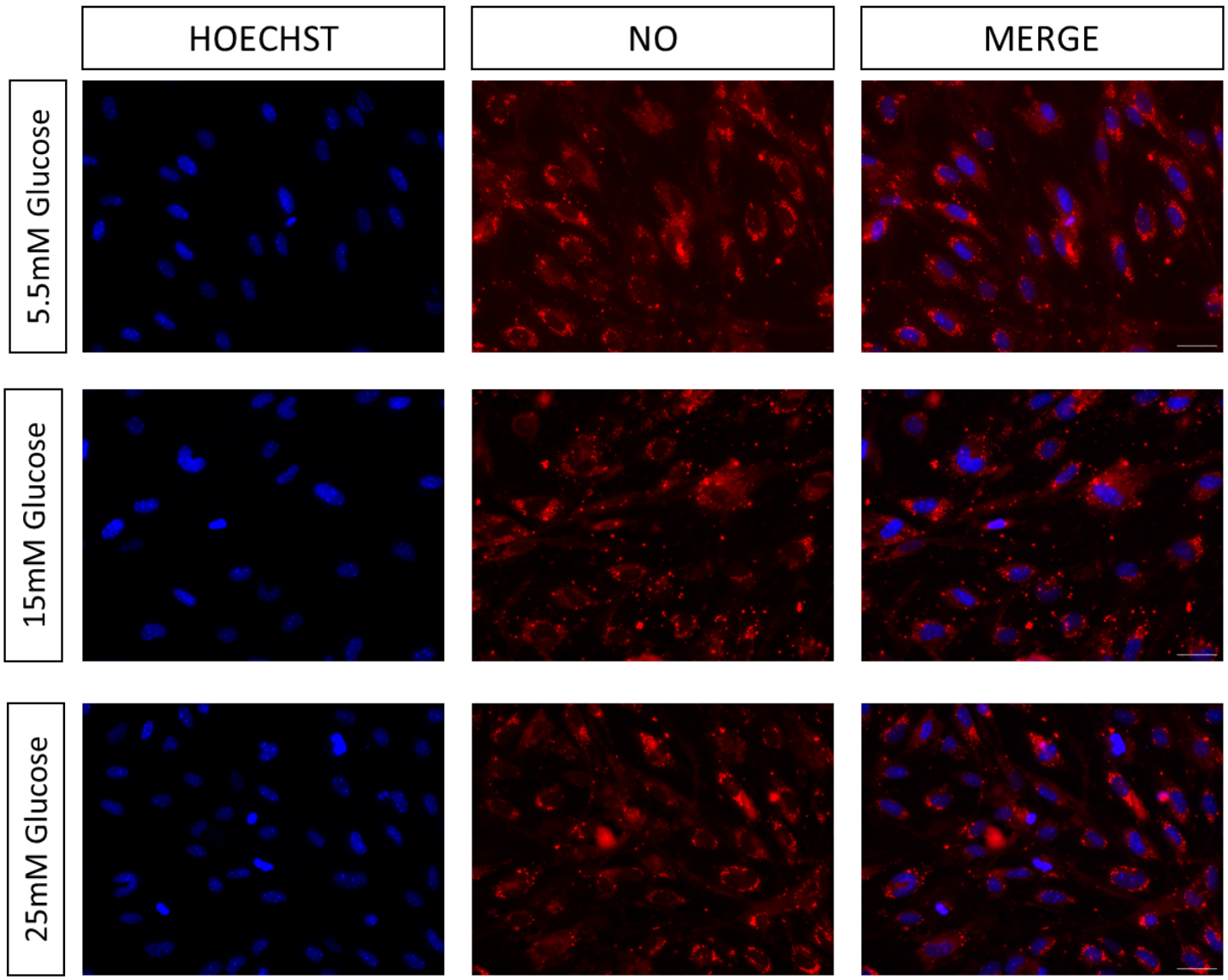


Figure 3.7- Murine brain endothelial cells do not have increased mitochondrial ROS under hyperglycaemia
Live-staining of endothelial cells showing ROS signal (red) and mitochondria (green). Merged image contains Hoechst staining. Analysis done via ImageJ indicates no statistical difference in ROS signal intensity across different glucose concentrations. (n=4, 5.5mM and 15mM, n=3 25mM, One-way ANOVA, Tukey's post-hoc test, not significant)

Nitric Oxide

To investigate whether hyperglycaemia could lead to impaired NO production, I employed a live-cell stain for NO based on the ROS/RNS Detection Kit (Enzo). Cells were exposed to L-Arginine, an NO inducer, at 0, 1mM, 2mM, or 3mM concentrations to first validate the assay. Images were analysed by using the Gaussian blur filter and image calculator in ImageJ to detect specific puncta in cells. The number of puncta was then normalized by number of nuclei in the field. Upon exposing cells to L-Arginine, the expected increase in puncta counts, was observed (n=1) (Supplementary Figure 3.5).

Cells cultured 5.5mM, 15mM, and 25mM were assayed for NO production after four days. No significance was found between conditions (Figure 3.8, n=3, one-way ANOVA, Tukey's post-hoc test).



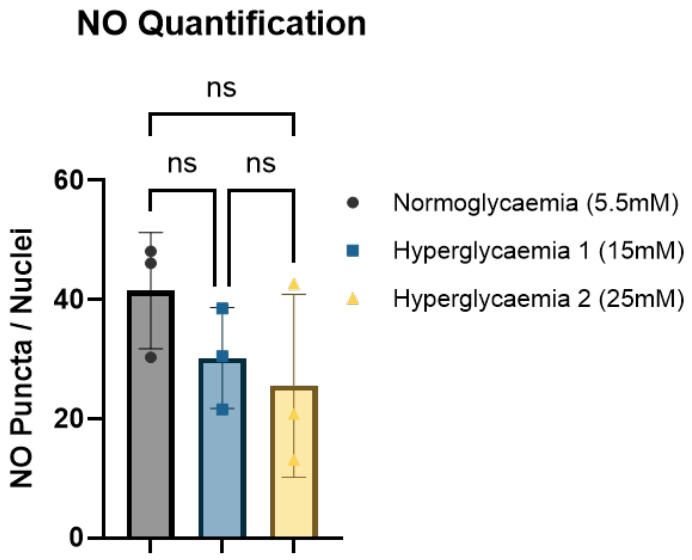


Figure 3.8- Murine brain endothelial cells trend to lower NO per cell with increasing media glucose concentrations

Live-cell imaging of NO puncta (red) and Hoechst. Analysis done via imageJ show a slight, but non-significant, reduction in NO puncta per nuclei with increasing media glucose concentration. (n=3, One-way ANOVA, Tukey's post-hoc test).

Discussion

My investigation of media glucose on mouse brain endothelial cells is not in agreement with previous published studies. The commonly used model of diabetes and hyperglycaemia is the streptozotocin-based diabetic mouse and rat models, which models Type I Diabetes, but induces hyperglycaemia also seen in type II diabetes. In the mouse and rat, it has been reported in this model that brain endothelial cells cause progressive blood brain barrier breakdown by deregulating genes related to angiogenesis, inflammation, and vasoconstriction (including eNOS, TNF-α, Tgfβ1, and Vcam1)[294], reduction of tight junction proteins zonula occludens (Zo-1) and Occludin (Ocln)[295], upregulation of receptor for advanced glycation end products (RAGE)[296], and increase in reactive oxygen species[297]. Streptozotocin is a toxin able to kill pancreatic beta-cells. However it has not been established if streptozotocin has direct effects on brain endothelial cells and the BBB [298]. Previous studies have also suggested altered NO using *in vitro* models [286, 299]. Cultured retinal endothelial cells exposed to 15 and 25mM glucose experience a reduction in NO synthesis likely due to an upregulation of the protein kinase C (PKC) pathway[300]. The study also found that advanced glycated end products (AGEs) also lead to a reduction in NO availability via a downregulation of eNos. Additionally, inhibition of NO in isolated mouse brain endothelial cells inhibits insulin transport into endothelial cells, further implicating NO to an insulin-based pathology as seen in type II diabetes [301].

I found that murine brain endothelial cells were largely unaffected by increasing levels of glucose. Cells exposed to 15mM glucose did not show an increase in key inflammatory gene expression, mitochondrial ROS, or NO production. In accordance with the lack of pro-inflammatory changes, the endothelial junctional protein expression and barrier properties as indicated by TEER were also unchanged. This indicates that either glucose does not affect the cell's phenotype due to intrinsic protective capabilities, or due to environmental factors.

It was not possible to exclude cAMP, dexamethasone, and RO-20-1724 from cultures as endothelial cells became non-viable. However, these factors have anti-inflammatory properties and may have concealed phenotypic differences associated with varying glucose concentrations.

Several genes assayed using qRT-PCR had high cT values (30) indicating very low baseline expression. This may have partly arisen from the low input RNA (150ng) used in these experiments. Endothelial cells have low RNA amount [302] and since the number of endothelial cells that can be successfully recovered and cultures is also small, recovery of sufficient RNA for experiments remains a challenge. Experiments could have thus benefited from increasing the number of biological replicates to overcome the greater variance associated with lowly expressed genes.

Hyperglycaemic media appeared to lead to a significant increase in cell numbers. This may be a consequence of cell proliferation or increased cell viability. Future studies should directly assess for these possibilities. The increased number of cells may then partly explain the apparent increase in glucose consumption and amount of glucose uptake by the cells. Nevertheless, whilst there are around 2-fold more cells in hyperglycaemic conditions, there was a 12-fold greater glucose uptake. The amount of lactate in the media did not change suggesting that despite the increased uptake, glucose may be directed to other pathways than glycolysis. It would be informative in future studies to assay glycolytic intermediate pathways. These include the polyol, AGE/RAGE, PKC, and hexosamine pathways discussed in the introduction [172]. Further studies into the pentose phosphate pathway could also elucidate whether glucose is being shuttled into this pathway, increasing nucleotide synthesis and NAPDH production.

My results are aligned with a study of the hyperglycaemic $Ins2^{AKITA}$ mice[303]. This mouse line contains a point mutation in the Ins2 gene causing pancreatic beta-cell loss, leading to hyperglycaemia. $Ins2^{AKITA}$ mice did not show any changes in gene expression related to inflammation and there were no effects in tight junction formation or altered BBB permeability. The $Ins2^{AKITA}$ mice had a significant downregulation of glucose transporter Slc2a1, which might suggest that glucose

uptake would be reduced in these mice although this has not been directly examined. With respect to NO production, a study of NO in forearm arteries of diabetic patients versus controls showed no difference [304].

In conclusion, primary murine brain endothelial cells appear to unaffected by elevated glucose in the media. This contrasts with other studies suggesting elevated glucose is pro-inflammatory. It is possible that inclusion of cAMP, dexamethasone, and RO-20-1724 opposed any inflammatory changes. It is also possible that inflammatory changes require other cell types that would normally be present in brain tissue such as mural cells, astrocytes, and microglia. There was evidence that endothelial cells did adapt to increased glucose by increased glucose uptake or consumption. There was no corresponding significant increase in lactate levels or ROS. Further studies are required to understand how brain endothelial metabolism may change with increased glucose availability.

Chapter 4: Transcriptomic Analysis of the Neurovascular Unit in Diabetic Cortical Tissue

Introduction

Molecular analysis of human tissues provides a direct examination of molecular changes induced by diabetes. Recent advances in single-nuclei RNA sequencing (snRNA-seq) have revolutionized the ability to delineate precise transcriptomic landscapes of individual cell types in a complex tissue, affording researchers novel insights into the molecular mechanisms of diseases. This technological advancement serves as a crucial bridge, enabling the identification of key disease targets that can be subjected to hypothesis-driven testing for subsequent validation using in vitro and in vivo models.

Several transcriptomic analyses have been done for diabetic humans[305] in adipose tissue [306, 307], whole blood [308, 309], pancreatic islet cells [310, 311], PBMCs [312], and neutrophils [313, 314]. The common output of the above articles notes changes in lipid metabolism (PPAR signalling pathway, fatty acid degradation, AMPK signalling pathway), increased inflammation (HIF-1α pathway) and immune response (T-lymphocyte and granulocyte activation, pro-inflammatory cytokine production).

Notably, there has also been one research investigating the effects of diabetes in human cubital endothelial cells purified via CD144 microbeads [315]. This study highlighted 51 upregulated DEGs and 96 downregulated DEGs. Upregulated gene pathways included TGF-β and cyclin-D1, while downregulated gene pathways included oxidative phosphorylation and androgen signalling. The study also provided data from HUVECs exposed to high glucose and reported that there were significantly more DEGs captured *in vitro* than *ex-vivo*, shedding light to potential limitations of *in vitro* transcriptomic studies.

A noticeable disparity exists between studies conducted in non-brain tissues and those specifically focused on the brain. Few hippocampus transcriptomic studies have been done in animal

models. A mouse model with a high fat diet identified 886 DEGs in mice receiving the diet for 11 weeks and fewer after 19 weeks (111). Significantly altered processes included increases in inflammatory pathways such as MAPK and lipid metabolism dysfunction [316]. In diabetic rats (induced by selective breeding and by modifying glucose tolerance [317]) identified 30 genes were differentially expressed in diabetic hippocampi. Ten of the thirty genes were related to "oxidative stress/DNA damage/cell cycle" while two were related to "insulin/growth hormone secretion." [157] This study also demonstrated that streptozotocin-treated rats (reflective of a type I diabetes and hyperglycemia model) did not yield any significant differentially expressed genes, suggesting that expression changes in the rat impaired glucose tolerance diabetic model (perhaps better reflecting type II diabetes) induce expression changes distinct from loss of insulin o hyperglycaemia.

Transcriptomic datasets of the neurovasculature in the context of diabetes are notably scarce. To the best of my knowledge, only a singular study has been conducted thus far, utilizing laser capture microdissection from post-mortem human tissue with a limited sample size of n=6 diabetic and n=6 controls [159], which is under-powered to detect biologically relevant findings and has a significant risk of false-positive findings. RNA extracted from captured cells for each major cell type were then analysed using microarrays. This study utilised the lateral temporal cortex from patients with self-reported T2DM and minimal AD neuropathology (low Braak scores). The study successfully captured transcriptomic profiles of endothelial cells, neurons, and astrocytes; however, the inclusion of pericytes was notably absent. The authors acknowledged the likelihood of pericytes being integrated into the "endothelial" cluster owing to their physical adjacency to blood vessels. KEGG pathway analysis of DEGs in the endothelial fraction identified several diabetes-related altered pathways including insulin signalling, fluid shear stress and atherosclerosis, and AGE-RAGE signalling. Further immunohistochemical analysis of the brain tissues revealed positive AGE staining for endothelial cells, astrocytes, and neurons, as well as positive staining of IGF1Rβ in endothelial cells. However, the study did not undertake immunohistochemical analyses of control cases, preventing any comparative quantification to be performed.

The absence of a sufficiently sized neurovascular RNA sequencing dataset in type II diabetes highlights a critical gap in the field. Given that diabetes is widely held to affect endothelial cell function, then gene expression data from the neurovascular cells would help in understanding the effects on the brain. It may also pave the way for therapeutic interventions that improve brain vascular health and thereby brain health.

Challenges in single cell gene expression studies of brain vascular cells

A significant challenge in transcriptomic neurovascular research is obtaining a substantial yield of brain endothelial cells suitable for meaningful bioinformatic analyses. Traditional protocols involving the homogenization of whole brain matter typically result in ~1% representation of endothelial nuclei [318-320]. This inefficiency arises from the inadequacy of conventional homogenization techniques, such as douncing, to effectively disintegrate the basement membrane of cerebral vessels and release endothelial nuclei for subsequent sequencing. Consequently, there is a need for endothelial-enrichment procedures aimed at augmenting the proportion of vascular nuclei within the sequenced samples.

While published protocols exist for endothelial enrichment [321, 322], they often fall short in achieving adequate purification. Conventional protocols typically employ dextran, a glucan that is highly viscous at 16% concentration, facilitating the separation of heavy vessels, allowing them to settle, while lighter single-cell masses remain in the supernatant following a high-speed centrifugation. However, this method results in parenchymal cell contamination to persist at a substantial level. In response to this limitation, researchers have turned to laser capture microdissection (LCM) as a method to manually isolate and extract endothelial cells for sequencing [159, 323, 324]. Despite generating sequencing data of high quality, the utilization of LCM is hindered by low throughput, its labour-intensive nature, and time-consuming protocols.

The absence of an effective protocol for isolating endothelial cells prompted Dr. Hannah Sleven, a researcher in the Cader lab to first remove myelin and then parenchymal cells (as a parenchymal fraction) before subjecting the brain homogenates to the dextran spin to produce a pure vascular fraction, with an endothelial cell enrichment of up to 80% (manuscript in prep). Importantly, this approach allows parenchymal nuclei to be sequenced in parallel with the vascular pellet, enabling a comprehensive investigation of neurovascular coupling interactions at a molecular level.

While 10X technology allows researchers to analyse nuclei at the single-nuclei level by isolating each nuclei in individual compartments, it also has relatively low throughput, limiting number of samples to be analysed depending on lane capacity of the sequencer. On the other hand, SPLiT-seq [325] operates by barcoding individual nuclei in designated wells, followed by pooling and redistributing them into additional wells. This process is iterated three times, effectively minimizing the likelihood of two nuclei sharing the same barcodes to statistically insignificant levels. cDNA is generated through an in-cell reverse transcription, and samples are identified via well-specific barcoded primers and unique molecular identifiers (UMI). Following the sequencing process, the assembly of each transcriptome involves combining reads that share an identical four-barcode combination. This process allows for more samples to be processed at once, and Split-seq kits are now available and can process as much as 96 samples at once. A SPLiT-seq kit (Parse Biosciences) allows fixing and freezing nuclei after sample processing and prior to library preparation, which enables processing of large numbers of samples. Once libraries are prepared and sequenced, quality checks are undertaken to exclude any nuclei with poor quality- based on poor number of gene counts and high proportion of mitochondrial genes. Following, data normalization is employed to remove technical variation while preserving inter-sample biological variation for subsequent gene analysis. This is typically done by dividing the raw UMI count by the total detected RNAs in each cell and performing a log transformation. The UMI normalization reduces technical variation from sequencing depth while the use of log transformation mitigates the impacts of outliers in gene

expression and prevents influence of high-abundance genes in subsequent analysis [326]. Nuclei are then clustered into subpopulations that represent individual cell types through expression of key cell markers. Different resolutions can be used, where higher resolutions identify more detailed subpopulations while lower resolutions merge closely related cell types into broader clusters. Lastly, pseudobulk values are obtained by combining expression values from nuclei within the same cell cluster type. Identifying differentially expressed genes (DEGs) using pseudobulk is valuable as it ensures trustworthy statistical tests, as the samples align with units of replication. Treating each nucleus as an independent sample can result in an underestimation of variance and false-positive results through small p-values.

Results

Protocol Development

My contribution to the protocol development was digestion of the vascular fraction with collagenase II to thereby release endothelial nuclei and subsequent confirmation of identity through the application of signal-amplification by exchange reaction fluorescent *in situ* hybridization (SABER-FISH) techniques [327, 328].

Crude tissue homogenates (prepared using a Dounce homogeniser) were divided into two samples: one subjected to digestion with collagenase II and the other left untreated. Samples were subject to SABER-FISH staining for specific markers, including CLDN5, ATP10A, and FLT1 (indicative of endothelial cells), as well as PDGFRB, PTH1B, and NOTCH3 (representing pericytes).

In the untreated sample, endothelial staining was evident along the vessel wall, with no observable puncta staining in the nucleus of the released nuclei. In contrast, the digested sample revealed staining of released nuclei for both endothelial and pericytic markers (Supplementary Figure 4.1), confirming the successful release of endothelial and pericytic cells from the basement membrane.

Sample Selection

The initial phase of the study involved the identification and procurement of post-mortem brain pre-frontal cortex samples from donors diagnosed with type II diabetes and matched controls. To achieve this, a targeted search was conducted on the Netherland's Brain Bank (NBB) and UK Brain Banks websites using the query "Type II Diabetes." Results were subsequently filtered to exclude cases with moderate and severe small vessel disease (SVD). Severe SVD was excluded to avoid the transcriptome simply reflecting end-stage vascular degeneration as the goal of this study was to study how diabetes affected vascular biology. Pre-frontal cortex was chosen as it has been implicated by imaging studies in diabetes and is relatively abundant in brain banks to be able to obtain sufficient numbers of samples for the study.

The search yielded a limited number of samples, with only four identified from the NBB. In contrast, a more extensive cohort of 102 samples was identified across the Newcastle, Bristol, and Edinburgh brain banks. The distribution of samples reflects the challenging nature of obtaining post-mortem brain tissue specific to T2DM, emphasizing the need for careful curation due to the abundance in co-morbidities seen in diabetic patients.

Samples were then filtered to exclude significant large territory stroke, brain cancer, brain infections (encephalitis, meningitis), neurodegenerative processes, including Alzheimer's, Parkinson's, progressive supranuclear palsy (PSP), amyotrophic lateral sclerosis (ALS) and Creutzfeldt-Jakob disease (CJD). Neurodegenerative disorders were excluded due to their potential to induce non-diabetic-associated degeneration.

Following these exclusions, a cohort of 25 donors with Type II Diabetes remained, comprising 9 females and 16 males, with an average age of 78 years. Considerable variability persisted within the diabetic group, encompassing factors such as medication regimens, lifestyle, smoking and alcohol intake status, and brain pH. Notably, hypertension emerged as a prevalent co-morbidity within the diabetic group, with 8 diabetic donors also having hypertension.

Controls, chosen with the same exclusion criteria as diabetic donors, were paired with the diabetic donors, and matching where possible for sex, age, and hypertension across the cohort. This yielded a control group of 25 individuals, comprising of 11 females and 14 males, with an average age of 79.96 years. Of these, 8 donors from the diabetic and control groups were diagnosed as hypertense. Table 4.1 summarised all donors and their subgroups.

Table 4.1 – Randomized cohort based on brain bank diagnosis of diabetic, hypertense, and control donors used in the study.

DIABETIC				**CONTROL**			
Sample	**Age**	**Sex**	**Bank**	**Sample**	**Age**	**Sex**	**Bank**
1	93	F	Bristol	2	87	F	Bristol
3	83	M	Bristol	5	89	F	Newcastle
4	71	M	Bristol	11	99	F	Newcastle
6	74	M	Newcastle	12	92	F	Bristol
9	80	F	Newcastle	14	78	M	Bristol
10	69	F	Newcastle	18	78	M	Newcastle
16	86	F	Newcastle	24	84	F	Netherlands
19	80	F	Newcastle	26	82	M	Bristol
20	70	M	Bristol	28	82	M	Netherlands
21	88	M	Newcastle	29	78	F	Newcastle
23	75	M	Newcastle	30	73	M	Bristol
25	86	M	Netherlands	34	65	F	Newcastle
38	82	F	Bristol	37	101	F	Netherlands
39	85	F	Netherlands	41	64	M	Newcastle
43	89	F	Netherlands	42	67	M	Newcastle
46	65	M	Newcastle	45	88	M	Newcastle
49	78	M	Bristol	47	85	M	Bristol
DIABETIC/HYPERTENSION				**CONTROL/HYPERTENSION**			
8	84	M	Edinburgh	7	91	M	Newcastle
17	73	M	Newcastle	13	71	F	Newcastle
27	71	M	Newcastle	15	68	M	Edinburgh
31	69	M	Edinburgh	22	97	M	Newcastle
32	71	F	Edinburgh	33	73	F	Edinburgh
36	60	M	Edinburgh	35	61	M	Edinburgh
44	84	M	Newcastle	40	86	F	Newcastle
50	91	M	Newcastle	48	60	M	Edinburgh

Samples were coded and blinded for processing, ensuring an unbiased approach in the execution of the protocol across the 50 (25 diabetic, 25 control) preparations, with two samples processed per preparations.

Sample Processing Optimization:

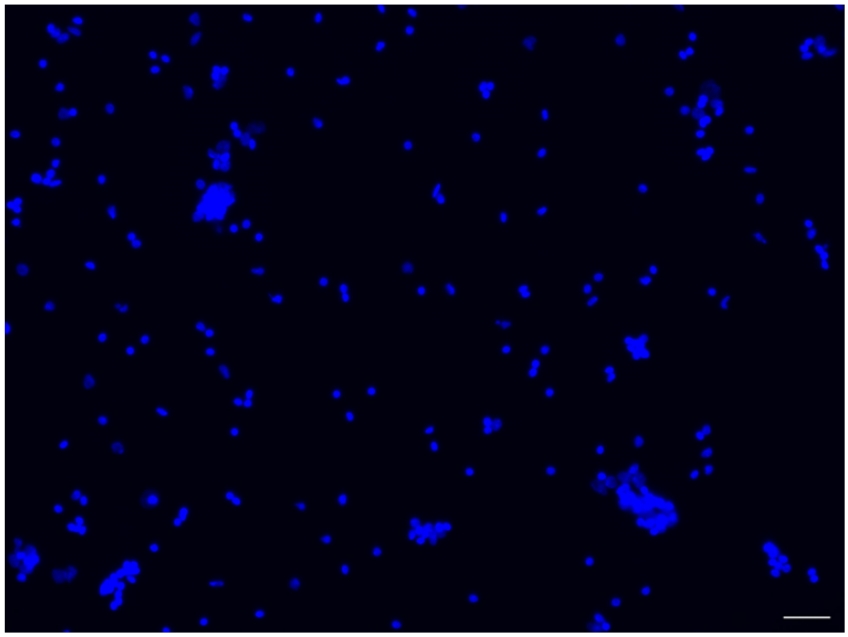
In a preliminary investigation, nuclei were crudely isolated, homogenized using a dounce homogenizer, and subsequently passed through a 1.0M sucrose bed to segregate nuclei from myelin. The sucrose step was introduced to emulate FACS sorting typically employed for purifying nuclei preparations. This protocol resulted in the formation of exceptionally large clumps of nuclei (Figure 4.1A), which could lead to multiple nuclei acquiring identical barcodes. By carefully looking at the nuclei sample during each step of the fixation protocol, cells clumping occurred after the permeabilization and final step spins of the protocol. After measuring clump sizes via ImageJ, many clumps were smaller than 40um but larger than 5um. I therefore reduced the filter pore size to 5um, where a considerable drop in clump abundance was seen (Figure 4.1B).

A pilot nuclei isolation and fixation was then performed using the full vascular and parenchymal isolation protocol. Briefly, the frontal cortex tissue was minced using razor blades over dry ice to maintain a cold temperature and prevent tissue degradation, the tissue was subsequently homogenized and subjected to multiple centrifugation spins to deplete myelin and separate the parenchymal and vascular fraction.

The parenchyma underwent treatment with triton-x, followed by homogenization to release parenchymal nuclei from the cells. The vascular fraction underwent a dextran spin and additional filtration using 100, 40, and 20 um filters. Subsequently, vessels were treated with collagenase II and homogenised to release endothelial nuclei (Figure 4.2A-B). Both parenchymal and vascular nuclei were then subjected to the 5um filter and then fixed. The vascular fraction had 54.75% of recovered nuclei (based on nuclei count prior to fixation) with 11.4% identified as clumped. In contrast, the parenchyma fraction yielded 10.55% with 11.1% classified as clumped nuclei (Supplementary Figure 4.2). Despite the relatively low yield observed in the parenchyma fraction, it was still sufficient for subsequent sequencing.Upon confirmation of adequacy of nuclei preparation for SPLiT-seq, a pilot

A

Manufacturer's Protocol – 40um Filter



B

Modified Protocol – 5um Filter

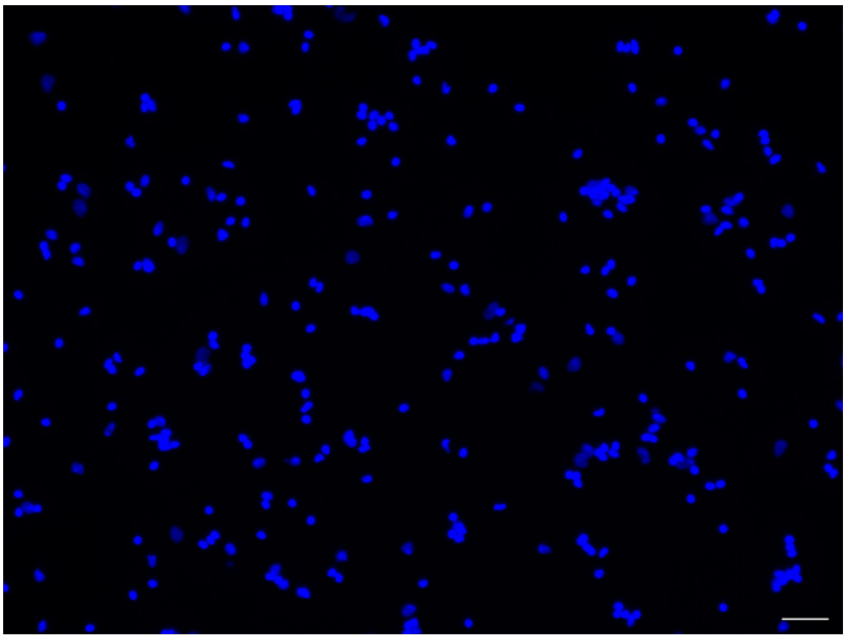


Figure 4.1– Reducing filter pore size decreases proportion of nuclei clumped in Parse fixation
A- Image of nuclei stained with DAPI at end of Parse fixation protocol following manufacturer's guidelines
B- Image of nuclei stained with DAPI at end of Parse fixation with filter modification from 40um to 5um reduces proportion and size of clumps in final nuclei suspension. Scale bar = 1000um.

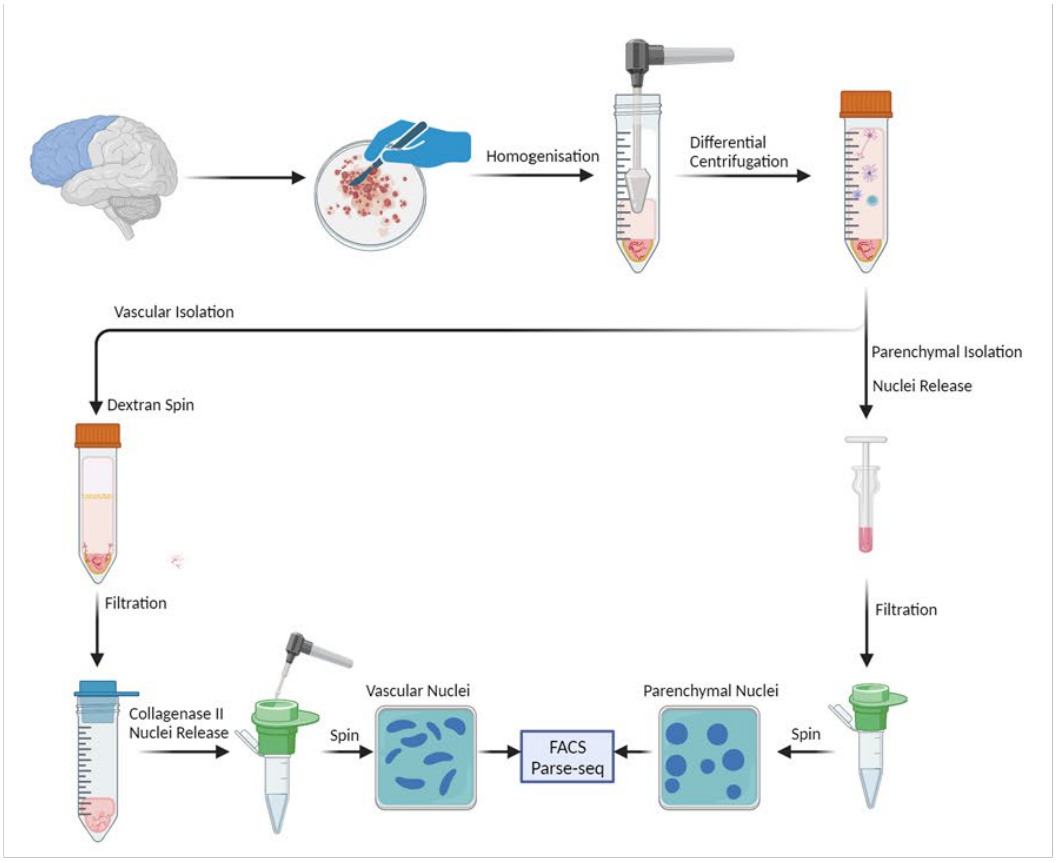


Figure 4.2– Human post-mortem isolation of vessels protocol for snRNA-seq
A- Schematic of protocol
B- Phase image shows significant vessel enrichment at mid-point of protocol, with little contamination of parenchymal cells and myelin. Scale bar = 50um.

experiment was undertaken to compare the 10X and Parse sequencing technologies – to ensure sequencing quality using SPLiT-Seq was a high as 10X. Following vascular and parenchymal nuclei isolation and FACS sorting, the samples were split into two. One set of nuclei were captured on 10X chips and then sequenced whilst the other set of nuclei were prepared using the SPLiT-Seq barcoding and library preparation followed by sequencing.

The estimated number of cells captured using the 10X platform were 11,413 and 6,071 for parenchymal and vascular samples, respectively. In parallel, for Parse sequencing, the estimated cell captures amounted to 4,662 for parenchymal samples and 10,265 for vascular samples (Figure 4.3A). Mean reads per cell using the 10X platform were 5,356 and 10,182 for parenchymal and vascular, respectively. Parse sequencing yielded 35,636 and 22,657 mean reads per cell in parenchymal and vascular samples, respectively (Figure 4.3B). Lastly, quality check of with Q30 bases (sequencing quality score based on the estimated probability of the base read being wrong) indicated 96.8% and 96.9% of barcodes were accurately sequenced in 10X for parenchymal and vascular samples, respectively. Parse Q30 scores (based on third round of barcoding) were 94.8% and 94.8% in parenchymal and vascular samples, respectively (Figure 4.3C). These results confirmed that both technologies are feasible for the sequencing of post-mortem nuclei isolated with our vessel-enrichment protocol.

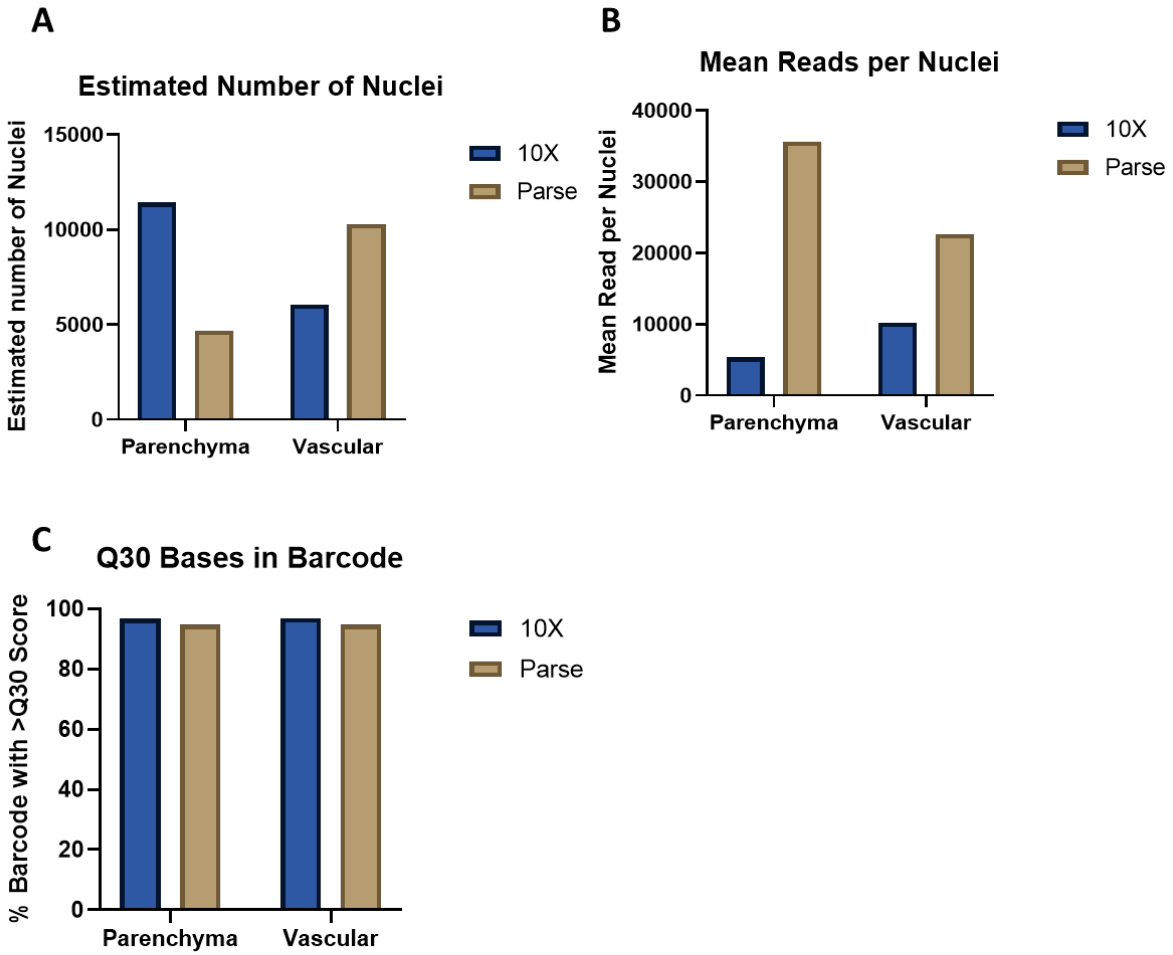


Figure 4.3–Quality Check of Isolated Vascular and Parenchymal Nuclei from 10X and Parse technologies
A- Estimated number of nuclei captured in the parenchymal compartment was 11,413 and 4,662 for 10X and Parse, respectively. Estimated number of nuclei captured in the vascular compartment was 6,071 and 10,265 for 10X and Parse, respectively.
B- Mean reads per nuclei in the parenchymal compartment was 5,356 and 35,636 for 10X and Parse, respectively. Mean read per nuclei in the vascular compartment was 10,182 and 22,657 for 10X and Parse, respectively.
C- Percent of barcodes with QC score >30 in the parenchymal compartment was 96.8% and 94.8% for 10X and Parse, respectively. Percent of barcodes with QC score >30 in the vascular compartment was 96.9% and 94.8% for 10X and Parse, respectively.

Sample Processing

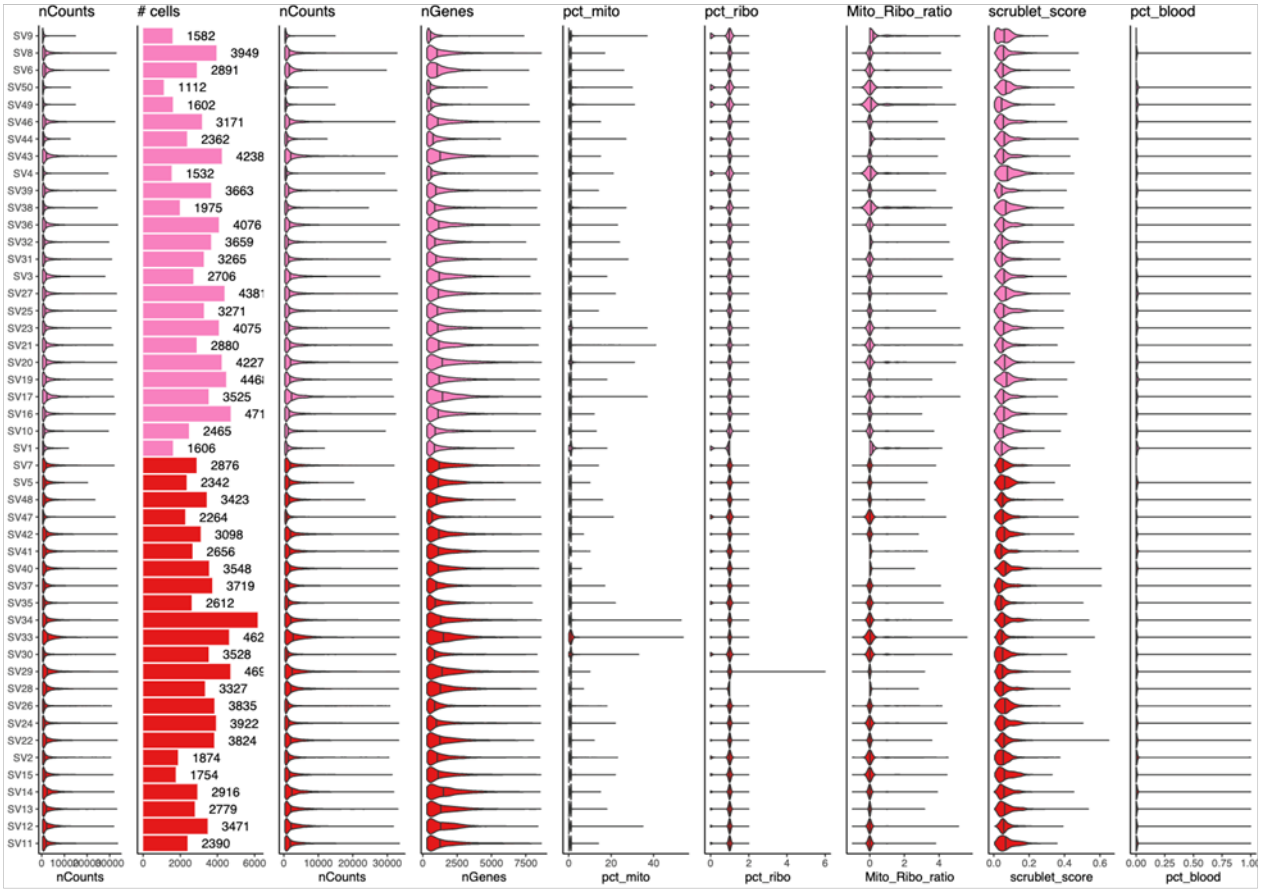
Upon achieving satisfactory results with Parse during the pilot phase, the processing of the entire set of 50 samples was completed. 48 out of the 50 samples yielded enough nuclei to proceed with barcoding and sequencing. The subsequent steps, including barcoding and library preparation, were executed by Dr. Anandhakumar Chandran from Novo Nordisk to yield 16 sub-libraries (8 vascular and 8 parenchymal). 2 vascular and 2 parenchymal libraries were then sequenced using NovaSeq6000 at NovoGene. Parse's comprehensive analysis pipeline by Novo Nordisk was employed for read alignment, transcript counting, and sample deconvolution - the data was then returned to the Cader group for further analysis.

The resulting dataset comprises a total of 268,367 nuclei, with 153,035 originating from the vascular fraction and 115,332 from the parenchymal fraction. Quality check was performed on the samples and showed that 44 samples had adequate number of captured nuclei, nCounts, nGenes, and low percent mitochondrial genes, successfully passing the check (Figure 4.4A-B, provided by Cesar Prada). An initial clustering and cell type annotation was also conducted by Dr Cesar Prada at Novo Nordisk (Supplementary Figure 4.3). Four samples did not meet the quality check criteria and I conducted further analysis to understand this failure, revealing a low number of annotated vascular cells captured within the sequenced nuclei from the vascular fraction (Supplementary Figure 4.4).

Upon inspection of the annotation results, 5 clusters: ExNeuron_1, In_Neuron_0, Endo_1, SMC_0, and Endo_6 (boxed in Supplementary Figure 4.3) could not be robustly annotated due to a lack of cluster specific marker identification in these clusters. Clusters Ex_Neuron_1 and In_Neuron_0 demonstrated a substantial number of nuclei from samples that failed the quality check, with 12.87% and 24.42%, respectively (Supplementary Figure 4.5).

Further investigation into the cluster composition of each individual failed sample revealed a distinct skew towards clusters In_Neuron_0, Ex_Neuron_1, and Astro_0, with a limited

A


Parenchyma
nCounts
cells
nCounts
nGenes
pct_mito
pct_ribo
Mito_Ribo_ratio
scrublet_score
pct_blood

B


Vascular
nCounts
cells
nCounts
nGenes
pct_mito
pct_ribo
Mito_Ribo_ratio
scrublet_score
pct_blood

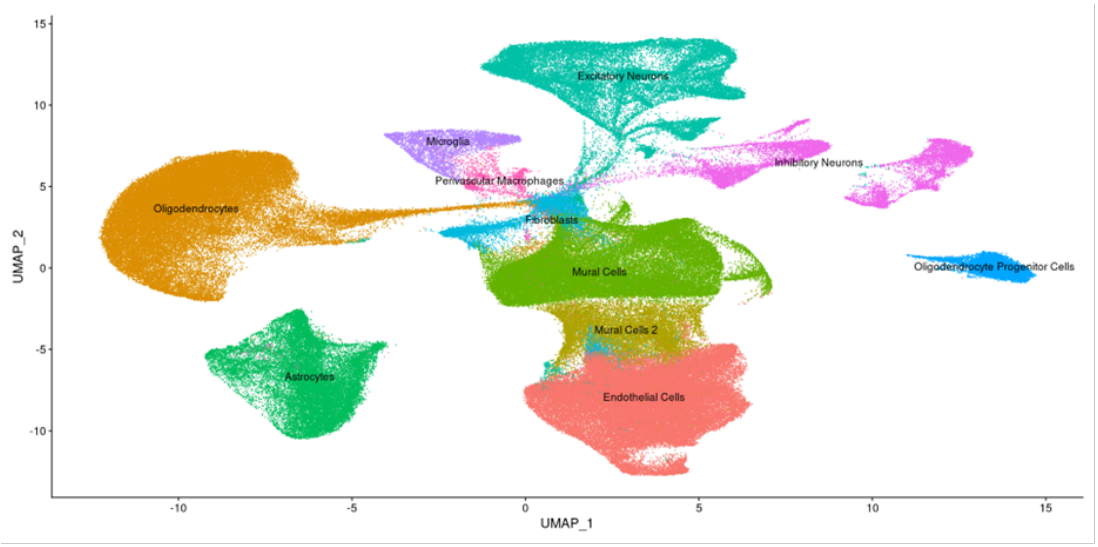
Figure 4.4–Quality Check of Isolated Vascular and Parenchymal from Type II Diabetes and Control patients
A- QC for all parenchymal samples showing high number of nuclei captured, nCounts, and nGenes, and low mitochondrial and blood contamination.
B- QC for all vascular samples showing high number of nuclei captured, nCounts, and nGenes, and low mitochondrial and blood contamination. Four samples were flagged due to low nuclei numbers and high mitochondrial contamination (Samples 1, 4, 9, and 49).
Image provided by Cesar Prada, Novo Nordisk.

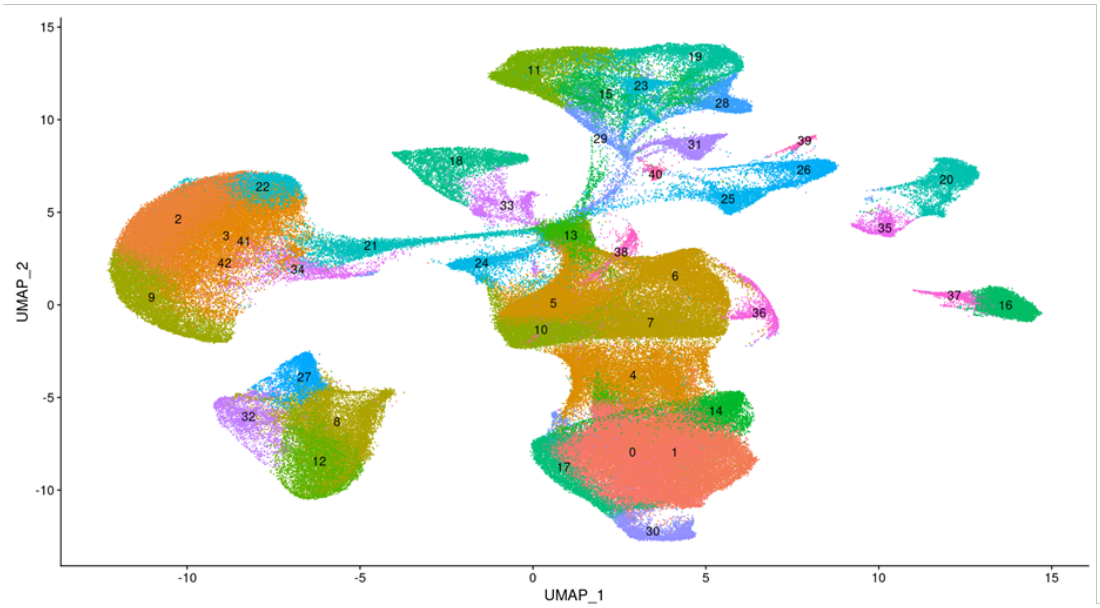
representation of vascular clusters such as Endo and Peri (Supplementary Figure 4.6). These four samples were therefore removed from the dataset.

In an effort to uncover potential tissue characteristics contributing to the aberrant sequencing observed in the failed samples, an analysis based on the year of death and the brain bank source was conducted, focusing on nuclei retrieval and the cell population within the vascular fraction. Despite low r^2 values of 0.1287 and 0.0491 for parenchymal and vascular fractions, respectively, an interesting trend emerged when examining samples based on the year of death. Specifically, samples provided before 1995 exhibited low parenchymal nuclei capture (Supplementary Figure 4.7). Furthermore, an analysis based on brain bank source revealed a significant bias in astrocyte and neuron contamination within the vascular sample. Notably, the Bristol brain bank appeared to contribute the most to parenchyma contamination in the vascular fraction. Strikingly, three out of the four samples that failed quality check were sourced from Bristol brain bank. This observation suggests that tissues obtained more than 15 years ago or sourced from the Bristol brain bank are less likely to be sufficient quality for snRNAseq using our protocol.

Upon the removal of the four samples from analysis, cell type clustering, annotation, and differential gene expression analysis of pseudobulk expression was performed by Hope Han from the Cader lab. This process identified 11 main clusters, further delineated into 43 sub-clusters (Figure 4.5). The cell annotation was carried out manually by leveraging the top 20 markers genes from each cluster, referencing PanglaoDB [329].

The eleven clusters encompass a diverse array of cell types, including astrocytes, endothelial cells, fibroblasts, microglia, mural cells, mural cells 2 (hybrid endothelial/mural cells), excitatory





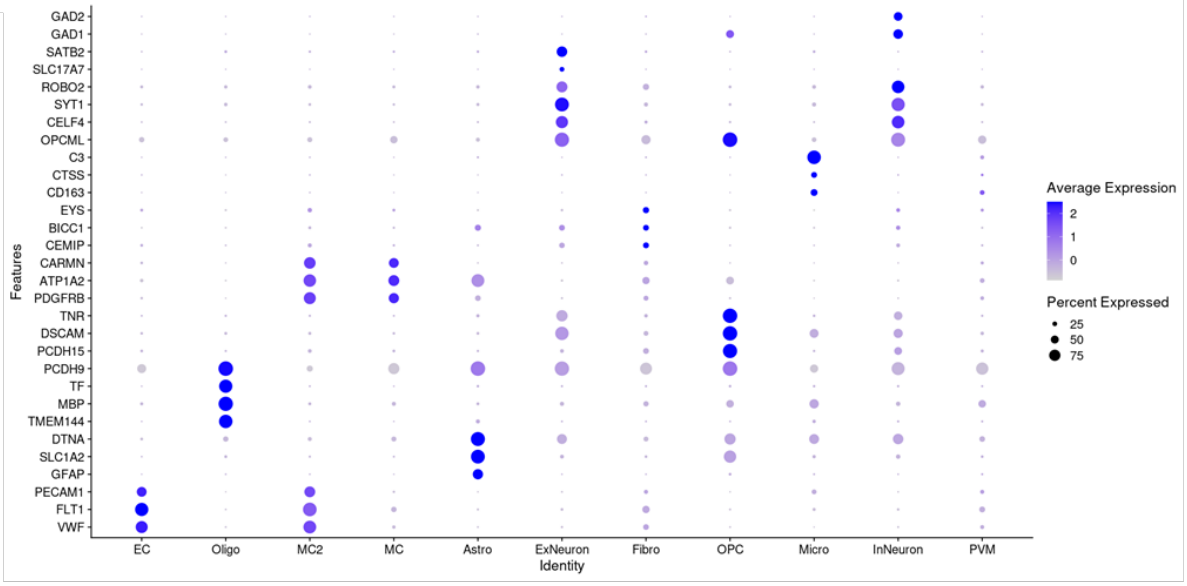


Figure 4.5– New UMAP Plot with removal of four QC-fail samples
Upon removal of donors 1, 4, 9, and 49, samples were re-clustered and annotated by Hope Han. Eleven clusters were identified, with 40 sub-clusters. Dot plot shows top marker expression for each cluster.

neurons, inhibitory neurons, oligodendrocytes, oligodendrocyte progenitor cells (OPC), and perivascular macrophages. Notably, the vascular cluster is further compartmentalized into arterial, capillary, and venous groups, offering a nuanced understanding of endothelial cell diversity (Figure 4.6). Arterial endothelial cells, identified by VEGFC and ALPL, occupy the lower section of the vascular cluster while capillary endothelial cells, marked by MFSD2A and SLC7A5, populate the middle section. Venous endothelial cells, characterized by IL1R1 and NR2F2, are situated in the upper section. Additionally, annotating the UMAP plot with donor IDs reveals no significant donor bias across all clusters (Supplementary Figure 4.8).

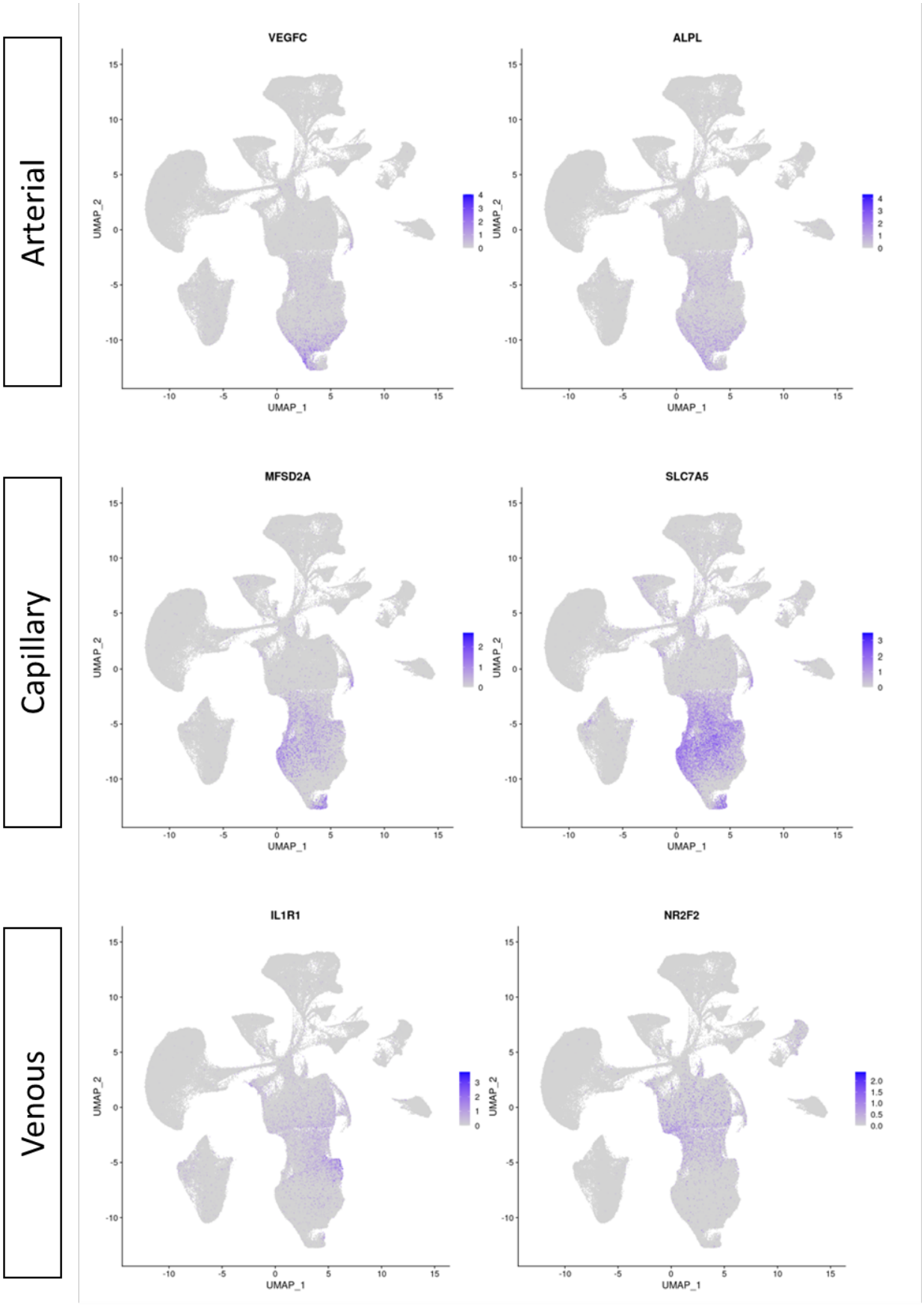
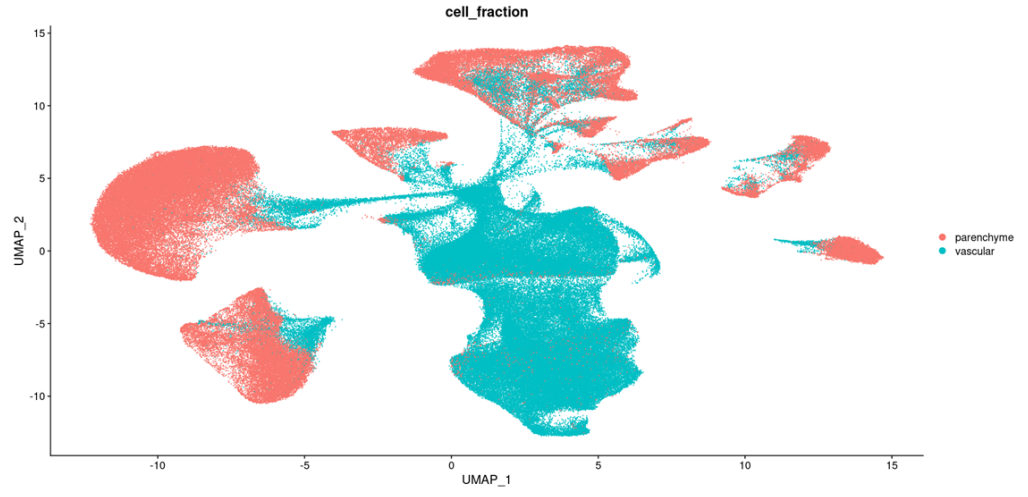


Figure 4.6– Endothelial cells possess distinct sub populations of arterial, capillary, and venous endothelial cells.

UMAP depicting individual endothelial cell sub-types based on marker expression. Arterial endothelial cells were identified through VEGFC and ALPL, capillary endothelial cells through MFSD2A and SLC7A5, and venous endothelial cells through IL1R1 and NR2F2.

An assessment of the UMAP plot, which separates nuclei from both parenchymal and vascular fractions, affirms the success of the isolation protocol in enriching the vascular fraction with distinct vascular cell types (Figure 4.7A). The success of vascular isolation was corroborated by assessing the proportion of vascular nuclei in each isolated compartment, including endothelial, pericyte, and smooth muscle cell nuclei. Vascular preparations demonstrated an average of 74.76 +/- 21.26% of vascular nuclei, whereas parenchymal nuclei preparations contained 1.27 +/- 0.80% of vascular nuclei (Figure 4.7B, $p<0.0001$, $n=44$, paired student's t-test).



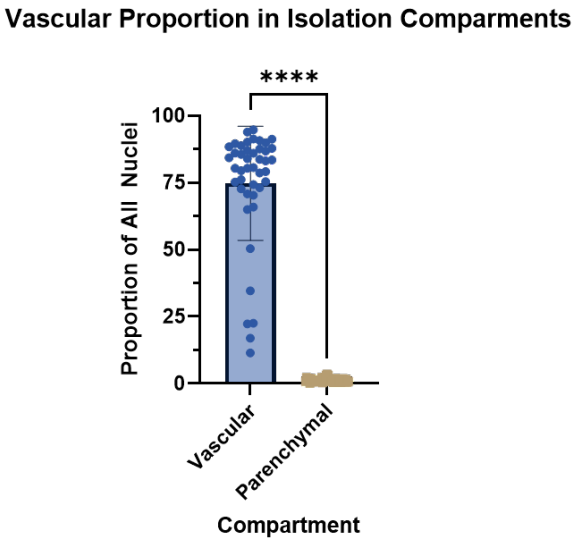


Figure 4.7– Validation of Vessel-Isolation protocol corroborated through snRNA-seq
A- UMAP depicting source compartment of each sequenced nuclei indicates high proportion of cells in vascular compartment cluster together away from parenchyma cells, and vice-versa.
B- Proportion of nuclei in vascular samples that sequenced to either endothelial cells, pericytes, or smooth muscle cells. Vascular samples had an average of 74.76+/- 21.26% sequence to a vascular fate, while proportion of vascular nuclei in parenchymal samples was significantly lower at 1.273+/-0.80%. ($p<0.0001$, $n=44$, paired student's t-test)

Donor Clinical Details

I obtained extended clinical data from the brain banks where this was available including prescription medication details. 9 donors who were annotated as non-hypertense in the online brain bank database (from Bristol and Netherlands) were discovered to have been diagnosed with hypertension upon checking their medical records. There were no incorrect annotations of diabetes diagnosis. Samples were therefore corrected for clinical diagnosis.

3 diabetic donors were noted to not be taking any diabetic medication (including insulin, metformin, thiazolidinediones, and sulfonylureas). There were no donors that were not on diabetic medication that did take diabetic medication. 4 donors that were not diagnosed with hypertension were taking ant-hypertensive medicine at time of death.

The prescription data allowed two sets of analysis – firstly a comparison of diabetic vs non-diabetic based on clinical diagnosis and that based on diabetics on medication (n=15) vs non diabetic (n=26) (Table 4.2). Similarly for hypertension, this was analysed based on clinical diagnosis (n=25 with hypertension vs n = 19 control) on medication (n=29 on medication vs n = 12 control; 3 donors omitted as they lacked prescription data). Patients stratified by medication with detailed information on medical regimen can be found in table 4.3.

Table 4.2 – Modified cohort based on corrected medical diagnosis of diabetes and hypertension patients. Yellow cells denote donors corrected as having a clinical diagnosis of hypertension. Orange denotes a donor misdiagnosed as diabetic.

Grouping by Diagnosis							
DIABETIC				CONTROL			
Sample	Age	Sex	Bank	Sample	Age	Sex	Bank
6	74	M	Newcastle	2	87	F	Bristol
10	69	F	Newcastle	5	89	F	Newcastle
16	86	F	Newcastle	11	99	F	Newcastle
19	80	F	Newcastle	25	86	M	Netherlands
20	70	M	Bristol	26	82	M	Bristol
21	88	M	Newcastle	29	78	F	Newcastle
23	75	M	Newcastle	34	65	F	Newcastle
38	82	F	Bristol	37	101	F	Netherlands
46	65	M	Newcastle	41	64	M	Newcastle
				42	67	M	Newcastle
DIABETIC/HYPERTENSION				CONTROL/HYPERTENSION			
3	83	M	Bristol	7	91	M	Newcastle
8	84	M	Edinburgh	12	92	F	Bristol
17	73	M	Newcastle	13	71	F	Newcastle
27	71	M	Newcastle	14	78	M	Bristol
31	69	M	Edinburgh	15	68	M	Edinburgh
32	71	F	Edinburgh	22	97	M	Newcastle
36	60	M	Edinburgh	24	84	F	Netherlands
39	85	F	Netherlands	28	82	M	Netherlands
43	89	F	Netherlands	30	73	M	Bristol
44	84	M	Newcastle	33	73	F	Edinburgh
50	91	M	Newcastle	35	61	M	Edinburgh
				40	86	F	Newcastle
				47	85	M	Bristol
				48	60	M	Edinburgh

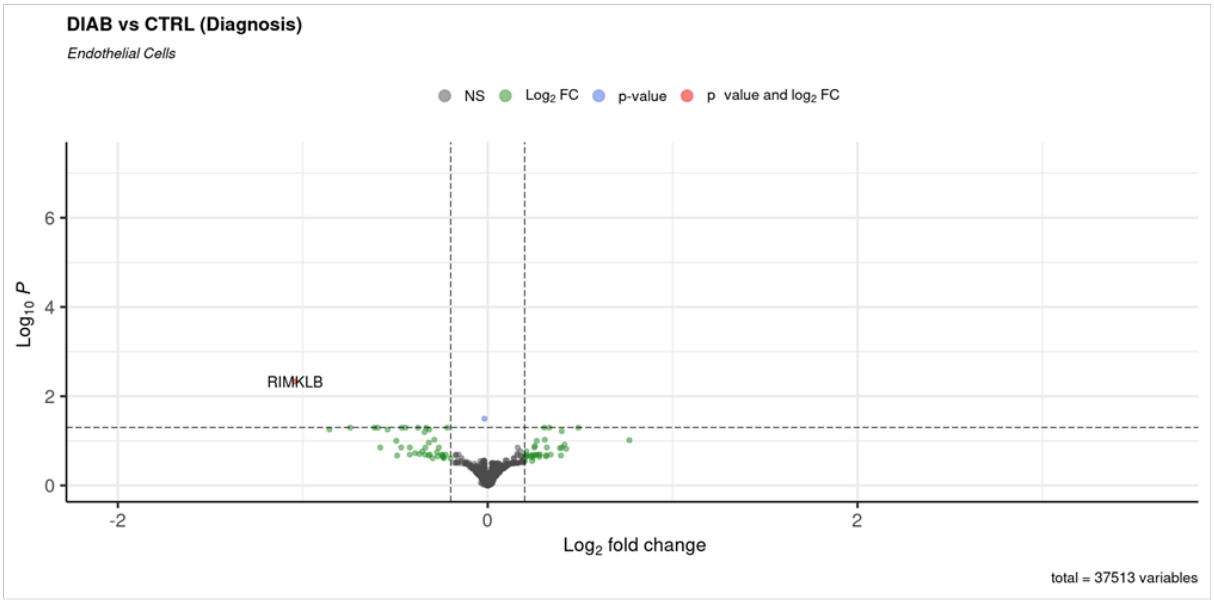
Table 4.3 – Modified cohort based on medication intake for each patient. Yellow: non-hypertense donors that were found to take hypertension medication. Orange: diabetic donors not taking any diabetic medication. Red: non-hypertense diabetic donors not taking diabetic medication and taking hypertension medication. There was no medical information available for patients 10, 11, and 30.

GROUPING BY MEDICATION					
DIABETIC			CONTROL		
Sample	**Diabetic Medication**	**Hypertension Medication**	**Sample**	**Diabetic Medication**	**Hypertension Medication**
19	Metformin	None	2	None	None
20	Sulfonylureas	None	5	None	None
6	Metformin, Sulfonylureas	None	23	None	None
			25	None	None
			26	None	None
			34	None	None
			37	None	None
			41	None	None
			42	None	None
DIABETIC/HYPERTENSION			CONTROL/HYPERTENSION		
3	Sulfonylureas	β-blocker, calcium channel blocker, statin	7	None	β -blocker, ACE-I/ARB, Alpha blocker, statin
8	Insulin	β -blocker	12	None	β -blocker, calcium channel blocker
17	Insulin	β -blocker, ACE-I/ARB, Alpha Blocker, statin	13	None	β -blocker, ACE-I/ARB
31	Metformin, sulfonylureas	Calcium-channel blocker	14	None	β -blocker, statin, thiazide
32	Insulin, metformin, sulfonylureas	ACE-I/ARB, statin	15	None	β -blocker, ACE-I/ARB
36	Insulin, Metformin	Calcium-channel blocker, ACE-I/ARB, statin, thiazide	16	None	ACE-I/ARB, statin
38	Insulin, Sulfonylureas	Calcium-channel blocker	21	None	Statin
39	Insulin, Metformin	β -blocker	22	None	ACE-I/ARB
43	Metformin	β -blocker, ACE-I/ARB, thiazide	24	None	β -blocker, ACE-I/ARB
44	Sulfonylureas	ACE-I/ARB	27	None	β -blocker, ACE-I/ARB, statin
46	Insulin	β -blocker, ACE-I/ARB, statin	28	None	ACE-I/ARB
50	Insulin, thiazolidine, sulfonylureas	Calcium channel blocker, alpha-blocker, statin	29	None	ACE-I/ARB, statin
			33	None	ACE-I/ARB
			35	None	Thiazide
			40	None	None available, hypertension confirmed via medical records
			47	None	β -blocker, ACE-I/ARB, statin, thiazide
			48	None	Calcium channel blocker, statin

Differential Gene Expression and Pathway Analysis

DEG analyses were conducted for endothelial cells in diabetic donors, considering both diagnosis and medication statuses. Strikingly, both the diagnosis-based or diabetic medication use analysis revealed a very limited differential gene expression. The diagnosis-based DEG showed only two genes exhibiting significant downregulation in diabetic donors relative to controls (Figure 4.8A). Specifically, RIMKLB displayed a downregulation with a log2 fold change of -1.04 (adjusted p value of 0.0047), whereas IL1RL1 exhibited a slight downregulation with a log2 fold change of -0.017 (adjusted p-value of 0.032). There were no up-regulated genes. DEG analysis of diabetic donors based on medication intake showed no discernible DEGs (Figure 4.8B).

A



B

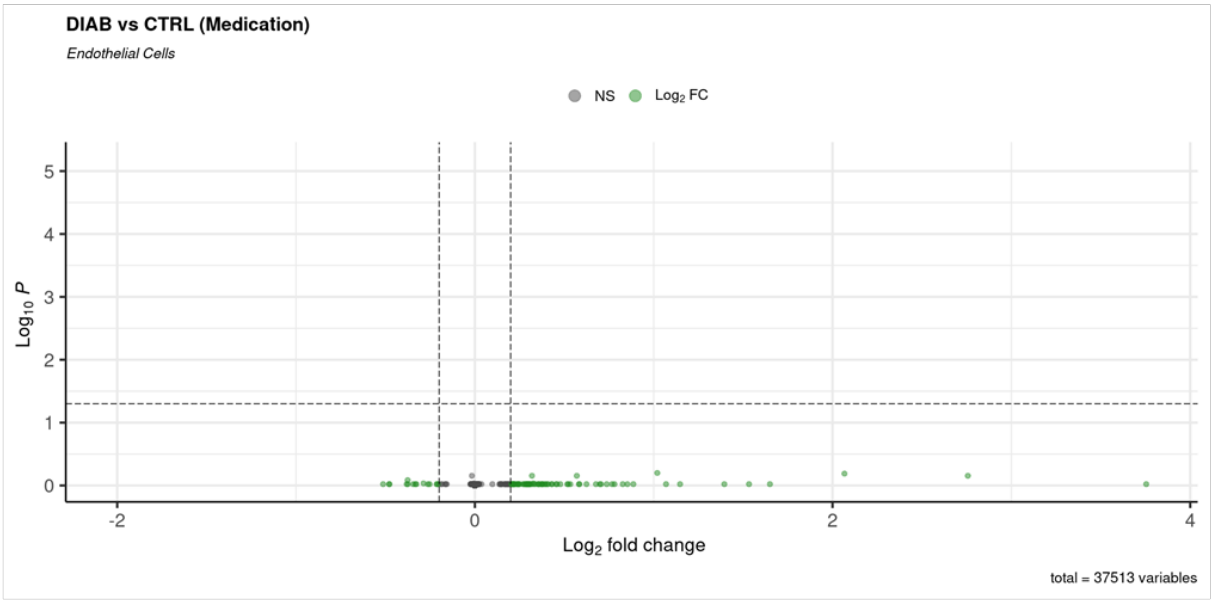


Figure 4.8– Differentially expressed genes (DEG) analysis in diabetic donors stratified by medical diagnosis or medication taken

A- Volcano plot of donors stratified based on original medical diagnosis reveals 2 significantly downregulated genes with adjusted p-value<0.05. (RIMKLB, -1.04 log2 fold change, 0.0047 adjusted p value, and IL1RL1, -0.017 log2 fold change, 0.032 adjusted p-value.

B-Volcano plot of donors stratified by medication reveal no significant DEGs across type II diabetics and controls.

The DEG analysis for hypertension produced notably different outcomes. Examination by diagnosis identified 8 upregulated genes and 36 downregulated genes (Figure 4.9A). The most pronounced log2 fold changes among the downregulated genes were observed in SAGE1 (-2.145 log2 fold change), ONECUT3 (-2.10 log2 fold change), and ADGRG7 (-1.66 log2 fold change). Conversely, the most prominent changes in the upregulated genes featured SELE (2.89 log2 fold change), NR4A2 (1.9 log2 fold change), and NALF1 (0.72 log2 fold change).

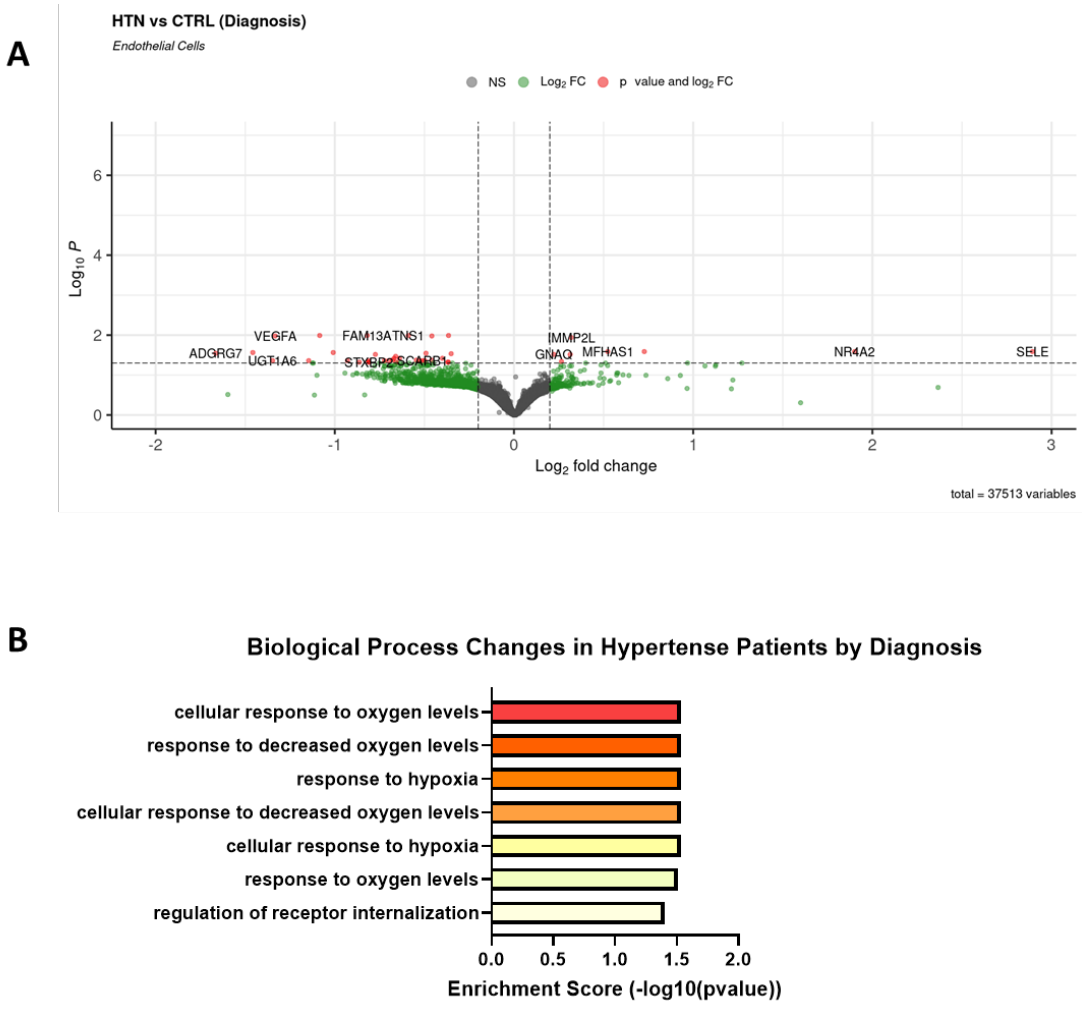


Figure 4.9– Differentially expressed genes (DEG) analysis in brain endothelial cells of hypertense donors stratified by diagnosis
A- Volcano plot of donors stratified based on original medical diagnosis reveals 8 significantly upregulated genes and 36 significantly downregulated genes
B-GO Analysis yields hypoxia-related pathways are significantly altered in hypertension

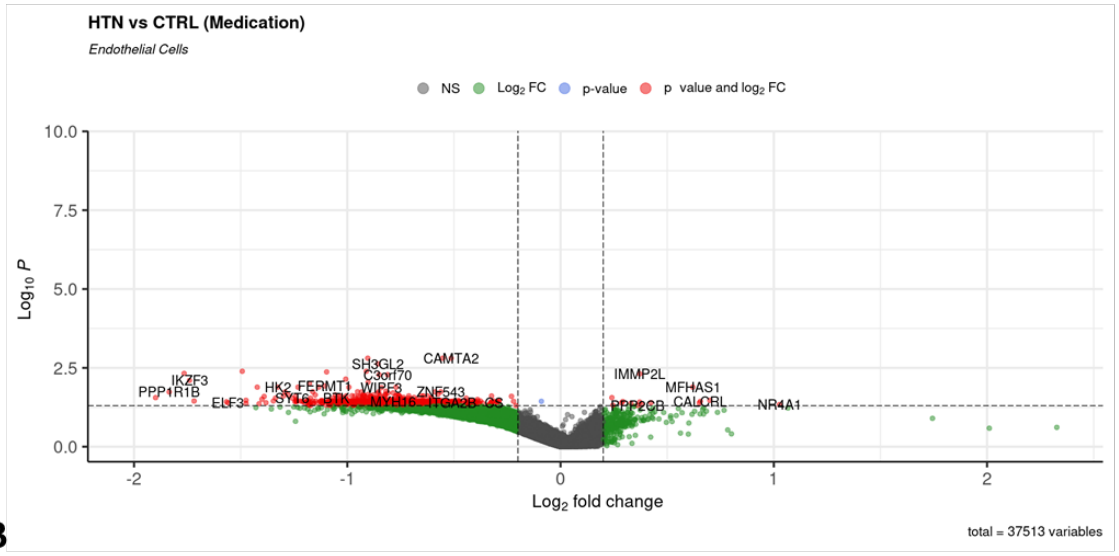
The analysis of KEGG and GO pathways revealed few distinct alterations in the hypertensive by diagnosis cohort. Regarding biological processes, hypoxia and regulation of receptor internalization emerged as significant hits (Figure 4.9B). Notably, the pathway analysis did not unveil any pathways that reached statistical significance. However, the glycosaminoglycan biosynthesis pathway, specifically keratan sulfate, approached significance with an adjusted p-value of 0.06.

DEG Analysis for hypertension based on medication had significantly more DEGs than by diagnosis (Figure 4.10A). 15 genes were significantly upregulated while 993 genes were downregulated. Highest log2 fold changes in downregulated genes included SLC18A2 (-2.95 log2 fold change), SAGE1 (-2.14 log2 fold change) and FOXN4 (-1.57 log2 fold change), while highest changes in upregulated genes included ANKRD37 (1.14 log2 fold change), CALCRL (0.75 log2 fold change), and NALF1 (0.68 log2 fold change).

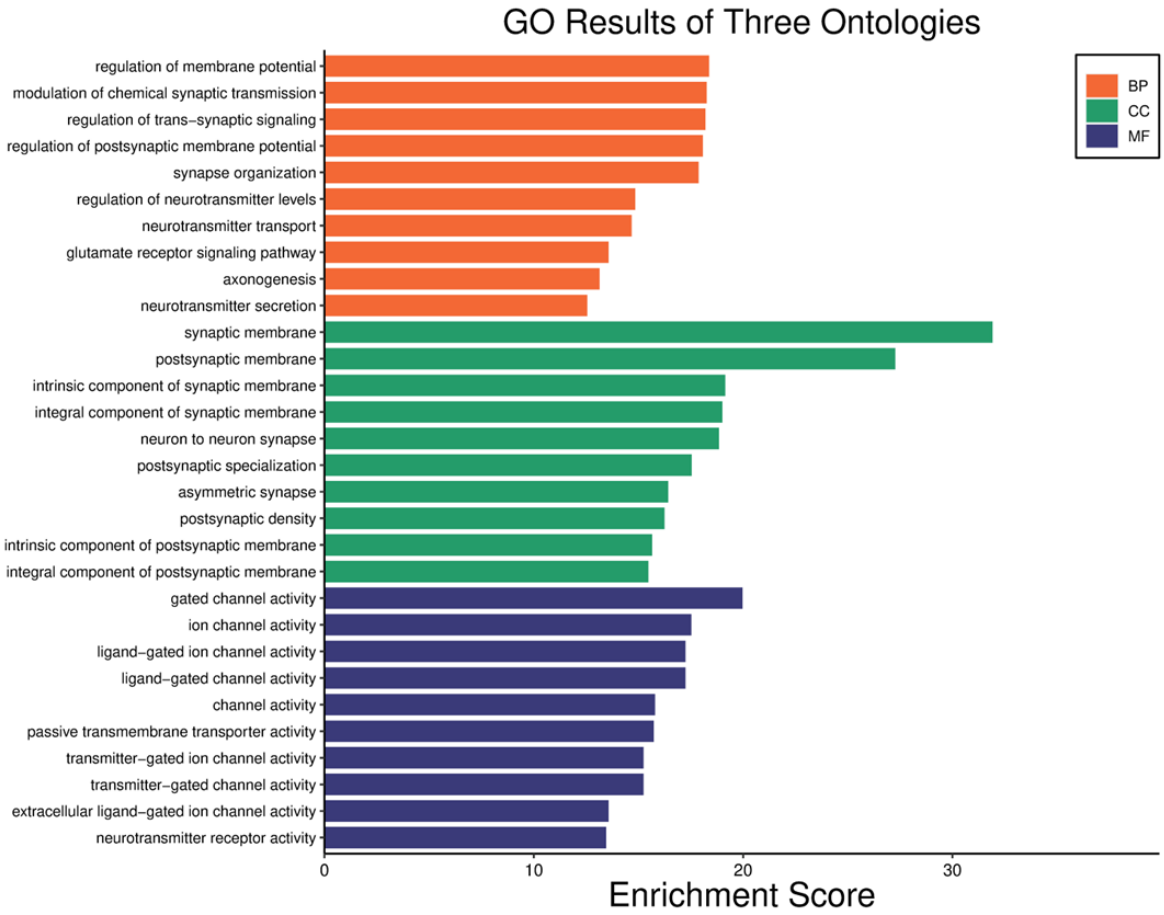
The KEGG and GO pathway analyses conducted on the hypertension by medication cohort unveiled a myriad of significant alterations in various biological processes. Among the 271 significantly changed processes, the top 10 encompassed fundamental neuronal activities, including membrane potential, synaptic signalling, synapse organization, neurotransmitter transport, and axonogenesis. In cellular component analysis, 104 significantly changed components were identified, with the top 10 predominantly associated with synapses. Molecular function revealed 98 significant changes, with the top 10 functions highlighting modification in channel activity. (Figure 4.10B)

Moreover, the pathway analysis identified 25 significant pathways that underwent alterations. Noteworthy findings include nicotine addiction, glutamatergic synapse, neuroactive ligand-receptor interaction, GABAergic synapse, and axon guidance as the top five significant hits (Figure 4.10C). In the realm of vascular-related pathways, significant hits were observed in cell-adhesion molecules, focal adhesion, and vascular smooth muscle contraction. Intriguingly, insulin secretion emerged as a significant hit, and although not reaching statistical significance, Type II Diabetes exhibited a notable trend at p=0.09.

A


HTN vs CTRL (Medication)
Endothelial Cells
NS
Log2 FC
p-value
p value and log2 FC
10.0
7.5
5.0
2.5
0.0
Log10 P
-2
-1
0
1
2
Log2 fold change
total = 37513 variables
IKZF3
PPP1R1B
ELF3
HK2
FERMT1
SYT6
SH3GL2
C3orf70
WIPF3
BTK
CAMTA2
ZNF543
MYH10
ITGA2B
GS
IMMP2L
PPP2CB
MFHAS1
CALCRL
NR4A1

B


GO Results of Three Ontologies
BP
CC
MF
regulation of membrane potential
modulation of chemical synaptic transmission
regulation of trans−synaptic signaling
regulation of postsynaptic membrane potential
synapse organization
regulation of neurotransmitter levels
neurotransmitter transport
glutamate receptor signaling pathway
axonogenesis
neurotransmitter secretion
synaptic membrane
postsynaptic membrane
intrinsic component of synaptic membrane
integral component of synaptic membrane
neuron to neuron synapse
postsynaptic specialization
asymmetric synapse
postsynaptic density
intrinsic component of postsynaptic membrane
integral component of postsynaptic membrane
gated channel activity
ion channel activity
ligand−gated ion channel activity
ligand−gated channel activity
channel activity
passive transmembrane transporter activity
transmitter−gated ion channel activity
transmitter−gated channel activity
extracellular ligand−gated ion channel activity
neurotransmitter receptor activity
0
10
20
30
Enrichment Score

C

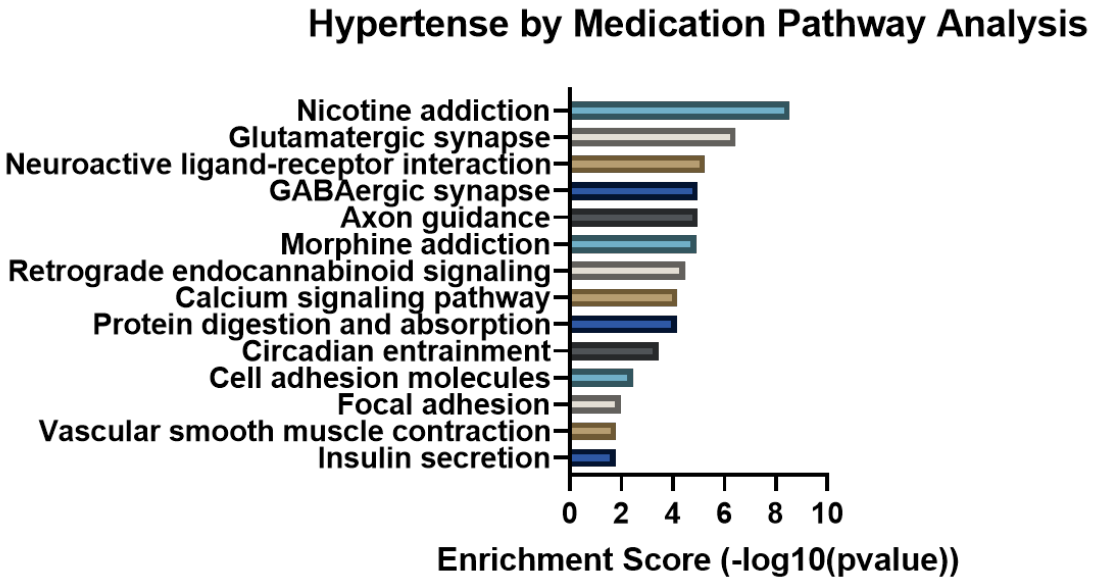


Figure 4.10– Differentially expressed genes (DEG) analysis in brain endothelial cells of hypertense donors stratified by diagnosis

A- Volcano plot of donors stratified based on hypertension medication intake reveals 15 significantly upregulated genes and 993 significantly downregulated genes

B- Top 10 pathways altered as identified in GO analysis for biological processes (orange), cellular compartment (green), and molecular function (purple). Results highlight several altered neuronal pathways including synaptic signalling, channel activity, and axonogenesis

C- Top 10 significantly altered pathways in brain endothelial cells of hypertension donors highlight key neuronal pathways are impaired. Further, focal adhesion, vascular smooth muscle contraction, and insulin secretion (not top 10) are included as they may play key roles in hypertension mediated endothelial impairment.

Discussion

In this chapter, I have employed a novel microvessel isolation protocol designed for the extraction of nuclei from vascular and parenchymal compartments in donors with type II diabetes, hypertension, and control donors. Nuclei were then prepared for sequencing using SPLiT-seq, which I confirmed yielded sequencing outcomes comparable to those achieved by the 10X technology, thus validating its efficacy for snRNA-seq. The success of vascular enrichment was substantiated by the results of the snRNAseq, with 74.76 +/- 21.26% of cells in the vascular fraction being composed of endothelial cells, pericytes, and SMCs while only 1.27+/- 0.8% of vascular cells populating the parenchymal fraction. This represents a significant advance of current methods for undertaking snRNAseq of human post-mortem brain tissue with respect to the ability to sequence both vascular and parenchymal nuclei at high yield.

The results challenges the prevailing notion that diabetes exerts a substantive impact on endothelial cells of the brain, contradicting findings from *in vitro* studies and results from post-mortem study carried out by Bury et al. [159]. Analysis performed either based on diagnosis or medication taken revealed no differentially expressed genes in diabetic patients compared to controls. In contrast to the DEG analysis reported by Bury et al., which implicated diabetes-associated pathways, including insulin signalling and AGE-RAGE pathways, the present study indicates that endothelial cells either remain unaffected by diabetes, or possess inherent protective mechanisms that deter transcriptional changes and maintain blood-brain barrier integrity. Despite abundant evidence linking type II diabetes to an elevated risk of dementia, the current investigation suggests that the progression of dementia may not be mediated through endothelial cells.

Efforts to stratify disease cohorts based on medication intake did not yield significant alterations in DEG results. However, this underscores a critical limitation in post-mortem tissue processing, namely the reliance on prior diagnoses and medical records. The variability in the availability of detailed medication histories, along with the absence of Hba1C measurements,

preclude an in-depth analysis of diabetes progression. Additionally, the complexity of diabetic patients' co-morbidities, coupled with the inherent environmental and lifestyle noise in the samples, suggests that a larger donor pool might be necessary to mitigate potential noise and achieve statistical significance. Nevertheless, the study cautions that even with an increased sample size, the observed changes may be subtle, and the biological relevance could be questionable. These findings emphasize the considerable challenges associated with post-mortem tissue studies, underscoring the need for meticulous consideration of sample characteristics, diagnostic information, and associated limitations when interpreting results.

The choice of using the pre-frontal cortex for tissue analysis was done based on published data indicating atrophy and associated decline in cognitive function in diabetics [109, 154-156], as well because of tissue availability. only previous single cell RNA-seq study specifically on diabetic subjects was performed in the temporal cortex, and their results indicated typical diabetes-modified pathways such as AGE-RAGE and insulin signalling. Research has shown that age-related neuron extracellular vesicle insulin signalling decrease is seen in the temporal cortex, but not frontal, parietal, or occipital cortices [330]. This indicates that insulin signalling in the temporal cortex may be governed by different mechanisms than to the frontal cortex, and therefore may be more vulnerable to diabetic insults.

A recent human transcriptomic study utilised expression data (GTEx) from 13 brain regions to identify differences between 302 diabetics and 608 controls.[324, 331] The study identified 2939 DEGs in the caudate , 486 DEGs in the hippocampus, 6 DEGs in the amygdala, 2 DEGs in the cerebellar hemisphere, and 1 DEG in the anterior cingulate cortex and hypothalamus. No DEGs were detected in the cerebellum, temporal cortex, frontal cortex, nucleus accumbens, putamen, and substantia nigra. Gene Ontology (GO) biological processes significantly altered in both caudate and hippocampus involved synaptic functions. KEGG pathway analysis identified that DEGs in caudate were enriched in neurodegenerative processes such as Alzheimer's disease, Huntington's disease,

and Parkinson's disease. The hippocampus has been thoroughly described as experiencing atrophy in T2DM [332, 333] as well as impaired neurogenesis, dendritic remodelling, and increased apoptosis [334, 335].While some research shows reduced functional connectivity and blood flow in the caudate nucleus of diabetic patients [336] [337], no molecular examination of caudate tissue has been explored.

The white matter mostly represents myelinated axons and the grey matter represents cell bodies, and this results in different environmental cues for nutrient demand. Due to the higher energy demand of grey matter, microvessels in the grey matter are denser. However, it has been noted in multiple sclerosis [338], HIV [339], and dementia[340, 341] there is preferential damage to white matter microvessels over grey matter [340]. Further, previous description of the neuropathology of diabetes in the brain indicated increase white matter hyperintensities, confirming that these vessels are vulnerable to diabetic insults. This suggests that targeting white matter endothelial cells should be explored in future studies.

Despite the original focus of analysing transcriptional changes in the diabetic BBB, the significant co-morbidity with hypertension prompted a concurrent investigation into transcriptional changes in the hypertensive BBB. Results from diagnosed hypertensive patients revealed 44 differentially expressed genes, while analysis of hypertension-medicated patients unveiled a more extensive set of 1008 DEGs.

Pathways analysis of the DEGs of hypertension by diagnosis suggests that a primary challenge faced by endothelial cells in hypertension is hypoxia. This pathway was constituted by downregulation of key genes including VEGFA, BMP7, AK4, EGLN3, and BNIP3L. Previous studies have reported the upregulation of VEGFA in various cell types (such as oligodendrocyte progenitor cells [342], smooth muscle cells [343], and in bovine aortic endothelial cells in culture [344]) under hypoxic conditions. Our findings of downregulation of VEGF in brain endothelial cells may suggest that human brain endothelial cells respond differently under hypoxia, or that other factors than

hypoxia are suppressing VEGF. Given that non-endothelial cells release VEGF, a comprehensive analysis of transcriptional changes across all cell types in our dataset will be required in future work to better understand how VEGF signalling is changing and potential effects on angiogenesis, cell migration, and vascular permeability [345].

The observed reduction in EGLN3 in brain endothelial cells could induce Erk3 degradation [346], a protein known to upregulate expression of VEGF receptors and promote endothelial cell function [347]. Consequently, the diminished EGLN3 levels in brain endothelial cells may contribute to altered VEGF receptor expression which combined with downregulated VEGF, could then impair endothelial function in the context of hypertension.

Under hypoxia, BMP7 and AK4 have been shown to be released in arterial cells and HEK293, respectively, and have been suggested to prevent endothelial to mesenchymal transition (EMT) and cellular stress [348, 349]. These factors are typically mobilized to counteract hypoxic stress and maintain cellular homeostasis. Downregulation of these genes in hypertension may suggests a compromised ability of endothelial cells to cope with hypoxic stress, potentially leading to heightened cellular stress and increased likelihood of EMT. Additionally, the significant downregulation of BNIP3L, a crucial factor in hypoxia-mediated autophagy [350], implies a potential impairment in essential endothelial autophagy, allowing cells that would typically undergo autophagy to persist.

It has been established that chronic hypoxia induces hypertension in humans [351], with hypertense patients experiencing higher concentrations of blood lactate than healthy controls. Low oxygen availability in the brainstem activates sympathetic circuits to release ATP and lactate from rat rostral ventrolateral medulla neurons [352]. Further, lactate can act as a GPR81 agonist, activating the endothelin pathway to increase blood pressure systemically [353]. Therefore, the hypertension seen in the patients included in the study may have been a result of chronic subclinical hypoxia

throughout their lifetime (for example, through vessel atherosclerosis)- with the pathway analysis highlighting hypoxia as a potential causal factor for hypertension rather than a response.

Collectively, these findings shed light on the intricate molecular dynamics involved in the endothelial cell response to hypoxic conditions during hypertension, pointing towards potential disruptions in cellular stress management and autophagic processes.

Stratification by medication status revealed a significantly broader spectrum of altered biological processes, cellular compartments, molecular functions, and pathways. Notably, an abundance of glutamatergic synaptic genes exhibited downregulation in endothelial cells, encompassing GRIA1, SLC17A7, GRIN2B, GRIN3A GRIK4 and GRM1. Furthermore, GABAergic synaptic genes, including GAD1, GAD2, GABBR2, GABRG1, GABRA5, and SLC6A11, also displayed downregulation. While it is noteworthy that several of these GABAergic synaptic genes are implicated in nicotine addiction, the highest significantly altered pathway identified via KEGG analysis, smoking history among donors may have contributed to this outcome. Interestingly, nicotine addiction triples the risk of hypertension [354].

The substantial downregulation of conventionally neuronal genes in endothelial cells was unexpected. However, recent studies have highlighted that mouse endothelial cells, across various tissues, exhibit the capability to express genes from adjacent tissues, including the brain, heart, and lung [355]. Specifically, brain endothelial cells have been identified to express genes associated with synapse organization and neurotransmitter transport, such as Ptdgs, Atp1a2, Bsg, Apoe, Glul, and Ptn. Another study corroborated this by identifying that brain endothelial cells express neurexin (NRXN) and neuroligin (NGLN), two transmembrane synaptic proteins [356]. This suggests that endothelial cells possess multifaceted functions beyond supplying nutrients to the brain, adapting to neighbouring cells for tailored cross-talk and maintenance. Subsequent analyses of other cell types captured in the single-nucleus RNAseq dataset may unveil novel interactions between endothelial synaptic genes and SMC and neuronal function. Lastly, epigenetic research done on both human and

high-fat diet T2D mice show an elevation in histone deacetylases (HDACs) class IIa in their brain, which is associated with heightened insult from amyloid-β-induced synaptic dysfunction [357], suggesting a potential source of synaptic dysfunction identified in this study.

The downregulation of axon guidance genes, including SEMA4D, EPHA5, PLXNB3, EPHB2, EPHB1, DCC, and ROBO2, is noteworthy, considering their significant implications in endothelial tip cells associated with vascular patterning and angiogenesis [358, 359]. Particularly, SEMA4D reduction and inhibition have been linked to the protection of the BBB and neurovascular coupling [360, 361]. This downregulation may suggest a potential protective effect on endothelial cells under hypertension, albeit at the expense of dysregulated angiogenesis. Aberrant angiogenesis has been validated in hypertensive patients [362], and the reduction in axon guidance proteins provides a plausible explanation for this phenomenon.

Several other pathways exhibited significant changes in hypertension, including cell adhesion molecules, focal adhesion, and vascular smooth muscle contraction. Notably, NRXN2 and NLGN4X, previously highlighted as crucial regulators of endothelial angiogenesis, were downregulated in the cell adhesion pathway, potentially influencing the cross-talk between endothelial cells and neurons. Additional differentially expressed genes in the cell adhesion pathway, such as NECTIN1, CDH15, CLDN10, and NEGR1, are implicated in cell-cell adhesion and junction processes, indicating that barrier properties of the BBB may be compromised. The focal adhesion pathway was significantly downregulated including several extracellular matrix genes from both the laminin and collagen families, including LAMC2, LAMA1, LAMB4, COL9A2, COL6A5, COL4A6, and COL4A5. Given that hypertension induces shear stress and rarefaction in blood vessel walls [363], these results may reflect alterations in the focal extracellular matrix of endothelial cells.

Furthermore, the smooth muscle contraction pathway was altered in endothelial cells, with a substantial proportion of differently expressed genes of this pathway related to calcium signalling, such as KCNMB2, ADCY8, ADCY1, KCNMA1, CACNA1D, IRAG1. Additionally, receptors for calcitonin

gene-related peptide (CGRP), CALCRL and CALCB, were downregulated, which is involved in reflex vasodilation and is a major therapeutic target in migraine [364].

There remains a substantial amount of analysis to be conducted to comprehensively investigate the transcriptomic landscape of both diabetes and hypertension in the brain vasculature and parenchyma. While the initial examination did not reveal differentially expressed genes in endothelial cells of diabetic donors, exploring other cell types may unveil important insights.

However, it is crucial to acknowledge that the hypertensive analysis was conducted without accounting for diabetic status, resulting in a cohort that includes both diabetic and non-diabetic donors. Future analyses should incorporate both a multi-variable approach, considering variables such as diabetic status, type of medication, age, and sex. This comprehensive analysis will help discern the specific contributions of each variable to DEG significance, providing a more nuanced understanding of the molecular landscape in the context of diabetes and hypertension.

Furthermore, the identification of several neuronal DEGs in the hypertension cohort highlights the need for DEG analysis in neurons. This focused analysis will enhance our understanding of the specific cross-talk and consequences of endothelial synaptic dysfunction in the neuronal context. Additionally, investigating pericytes and mural cells could unveil specific changes associated with endothelial synaptic dysfunction or calcium signalling impairment. Given that contractile activity in pericytes and smooth muscle cells is regulated by cytosolic concentrations of calcium [365], dysfunction in endothelial calcium signalling may indeed have profound effects on mural cell contraction, potentially resulting in impaired vasoreactivity of endothelial cells. These future analyses hold the potential to unravel the intricate molecular mechanisms underlying the pathophysiology of diabetes and hypertension in the brain, contributing to a more comprehensive understanding of vascular and neuronal interactions in these conditions.

Comparing both stratifications prompts a critical evaluation of the most suitable approach for future analyses. The reliance on third-party resources for accurate information input into

databases is pivotal for analysis fidelity. Examining medical records directly may enhance confidence in diagnoses, given that these records are meticulously curated by dedicated healthcare professionals for each patient. In contrast, the inputting of disease codes into brain bank databases, as exemplified by the misdiagnosis instances in the Netherlands Brain Bank and several misclassified hypertension patients, is susceptible to errors. Since hypertension may not be classified as a classically "neurological condition," there is a potential for oversight or reduced vigilance during code input. However, analysing the data stratified by medication also has its limitations. While some donors have detailed information on when medication was taken throughout their life, many do not declare if medication was being taken at time of death or in previous years. Further, analysing the effects of medications in the transcriptome is dependent on donors actively taking the medication, which cannot be corroborated. Despite these limitations, I propose that future analyses to account for prescription data to enhance robustness of the analysis. This approach avoids potential inaccuracies in diagnosis (such as non-hypertense donors taking hypertension medication).

In conclusion, this chapter challenges the notion of diabetes exerting a discernible impact on brain endothelial cells. In hypertension, the observed downregulation of key genes associated with hypoxia, synaptic function, and extracellular matrix reveals intricate molecular dynamics and potential implications for endothelial cell function. Despite limitations in post-mortem tissue studies, including the challenges in stratifying cohorts based on available clinical data, this investigation highlights the need for meticulous consideration of sample characteristics and diagnostic and prescription information. Future analyses of other cell types in mural and parenchymal cells incorporating a multi-variable approach, will help to unravel the intricate molecular mechanisms underlying the pathophysiology hypertension in the brain, contributing to a better understanding of vascular and neuronal interactions in these conditions.

Concluding Remarks:

My research has revealed many unexpected findings. Foremost is that despite diabetes being widely recognised as a vasculopathy affecting multiple organs through macro- and microangiopathic pathology – the brain vasculature appears to be relatively protected. Contrary to previous reports, both murine *in* vitro brain microvascular endothelial cells and human post-mortem brain endothelial cells show negligible gene expression changes in the face of hyperglycaemia (in the case of the moues cells) or the presence of diabetes for the human study. Investigations yielded results that suggest endothelial cells are not gravely affected by hyperglycaemia and diabetic injury. There are limitations to my studies and reasons to interpret this result with caution. Firstly, the study using mouse primary cells required the inclusion of supplemental media additives -cAMP, dexamethasone, and RO-20-1724- which may have masked cellular inflammation in response to hyperglycaemia. Further research is required perhaps using live mice administered with glucose after which brain endothelial cells could be isolated to assess for any inflammatory or other responses.

The surprising findings from the human post-mortem transcriptomic analyses could have arisen for several reasons: (i) the frontal cortex endothelial cells are protected from diabetes unlike other brain regions such as the temporal cortex, which have shown abnormalities, (ii) the transcriptomic changes identified in bulk RNA sequencing studies or the laser capture microdissection study may have come from mural cells rather than endothelial cells, (iii) previous research may not have had enough patients to appropriately power the results of the investigation leading to false positive findings, or (iv) further errors in disease and medication labelling could have confounded my data; (v) my dataset may have not been sufficiently powered to detect subtle differences.

Irrespective, the single nuclei RNA sequencing dataset I have generated will represent a valuable resource in the broader field. This will open new avenues for researchers to perform their own analyses on disease targets of different brain cell types. This was highlighted by the profound

changes in gene expression associated with hypertension. Donors defined as hypertensive either by diagnosis or on the basis of the medication they were taking, a range of interesting pathway perturbations including response to hypoxia, synaptic function, axon guidance, and calcium signalling changes. Differential gene expression of neuronal genes in endothelial cells was unexpected but expression of such genes in vascular cells have been established for some time including mechanistic explorations of the implications of neuronal genes on vascular network formation. The results from my work pave a way for novel hypertension disease targets in endothelial cells. Further work is needed to account for diabetic status in both normo and hypertensive patients, but the current database will provide significant information for future explorations of hypertension in the brain.

My work also has advanced methods for IPSC differentiation to brain microvascular endothelial cells by inducing expression of transcription factors LEF1, ETS1, and MRTFB. This protocol yields endothelial cells expressing key markers VE-CADHERIN, PECAM1, and CLDN5. Crucially, these cells do not have an epithelial phenotype, with the absence of expression of E-CADHERIN. This provides a significant step towards the acquisition of true differentiated endothelial cells rather than epithelial hybrids commonly used in the field. Further research is needed to induce tight junction expression of OCLN, which is currently lacking in these cells, and CLDN5. This may then lead to improved barrier integrity of this *in vitro* model. Attempts to improve the differentiation through CRISPR activation of the transcription factors yielded a significantly smaller proportion of endothelial cells, indicating that high expression of the transcription factors may be necessary for accurate endothelial acquisition. Further, future experiments are necessary to determine the contribution of each transcription factor to the differentiation and the duration of the expression that will be required.

In conclusion, my research provides new data suggesting relative protection of brain endothelium to hyperglycaemia and diabetes in mouse and human cells. It also identifies novel targets to hypertension in human brain endothelial cells not previously reported. An *in vitro human*

cellular model has been progressed and with further development has the potential to provide a suitable platform to test targets identified in diabetes, hypertension, or other neurological diseases.

Methods:

Chapter 1

Polyclonal Cell Line (BMEC TFx3) Generation for IPSC-BMEC Differentiation

A polyclonal IPSC cell line was generated via lentiviral delivery of a dox-inducible cassette for the expression of LEF1, ETS1, and MRTFB. Briefly, IPSCs were seeded with mTeSR (100-0276, STEMCell) + rock inhibitor (1254, Tocris) at 22K/cm2 in 24 well plates and transduced with 2ul of lentivirus in mTeSR the following day. Cells were allowed to grow to 80% confluence with daily media changes, and then split via accutase (07920, STEMCell) to allow for single cell seeding and selection. The day after seeding, media was changed to mTeSR with 4ug/ml Blasticidin (A1113903, Thermo) with daily media changes. Upon confluency, the selection was continued for two more accutase splits, a process lasting around two weeks. The resulting cell line, named "BMEC TFx3" was validated by performing a qPCR on Blasticidin resistance gene (BSD), as well as ICC after induction of the three transcription factors (LEF1, ETS1, MRTFB).

Differentiation of IPSCs to Brain Microvascular Endothelial Cells

BMEC TFx3 IPSCs were maintained in mTeSR media and split via EDTA (15575-038, Invitrogen) passaging, seeding them at a ratio of 1:8. Once ready for differentiation, cells were split via accutase and seeded at 30k/cm2 in mTeSR + rock inhibitor. The next day, media was changed to TeSR-E6 media (05946, STEMCell) with BMP4 (10ng/ml) (314-BP/CF, R&D Systems), LY294002 (10uM) (L9908, Sigma), bFGF (20ng/ml) (233-FB-025, R&D Systems), and doxycycline (4ug/ml) (J60422.06, Thermo). One and a half days after, media was changed to TeSR-E6 with LY294002 (10uM), bFGF (20ng/ml), SB43154 (1uM) (S4317, Sigma), and doxycycline (4ug/ml). Two days later, media was changed to TeSR-E6 with LY294002 (10uM), bFGF (20ng/ml), and doxycycline (4ug/ml). One and a half days later, media was changed to endothelial induction media, consisting of human ESFM (11111044, Thermo) with VEGF (200ng/ml) (100-20, Peprotech), bFGF (20ng/ml), wnt7A (10ng/ml) (120-31, Peprotech),

Forskolin (2uM) (1099, Tocris), Retinoic Acid (10uM) (R2625, Sigma), and doxycycline (4ug/ml). The media was changed for two more days with endothelial induction media, and at this point large BMEC-producing clumps have been assembled in the culture plate.

To enrich for these BMEC-producing clumps, the cells were split using a gentle dissociation reagent, ReleSR (05872, STEMCELL), to detach single cells but keep clumps intact. ReleSR was added to the culture for 45 seconds, and then aspirated to leave a thin film of liquid behind and placed in a 37C incubator for 5 minutes. The small amount of ReleSR was aspirated, and 1 ml of DMEM/F12 was added gently to the culture plate. The vessel was then hit on its side thirty times, and released clumps were placed in a 15 ml tube. To dislodge remaining clumps, quickly eject DMEM/F12 over them and place them in the 15 ml tube. Repeat as necessary until all clumps have been removed from the vessel. Fill up the 15 ml tube up to 10 ml with DMEM/F12 and spin at 35g for 1 minute to separate single cells and clumps. Resuspend the clump pellet with 10 ml DMEM/F12 and repeat this process twice. After the last spin, seed the clumps at a 1:3 ratio in endothelial maintenance media consisting of ESFM with bFGF (20ng/ml), wnt7A (10ng/ml) Forskolin (2uM), Retinoic Acid (10uM), doxycycline (4ug/ml), and rock inhibitor (10uM). For the next three days, media was changed to endothelial maintenance media without rock inhibitor. BMEC cells should be visible and growing out of the clump-enriched culture at this point. To further purify the culture, perform a MACS sort for CD144 (VE-Cadherin) (130-097-857, Miltenyi Biotec) by following the manufacturer's instructions. After separation, seed ISPC-BMEC cells at 200K/cm2 with endothelial maintenance media with Rock inhibitor either in cell culture plates (ICC, RNA, WB), transwells (TEER), or GFR Matrigel (vessels). Media was changed every day for 4 days, after then cells were ready for analyses.

Immunocytochemistry

Cells were washed with PBS and fixed for 10 minutes at room temperature using 4% PFA. They were then permeabilized with 0.2% Triton-X for 15 minutes, and blocked with 10% goat serum at 4C for 1 hour. They were then exposed to primary antibody diluted in blocking buffer at 4C overnight. The

next days, cells were washed 3X with 1% goat serum, and then exposed to secondary antibodies for 2 hours at room temperature. The cells were then washed 3X with 1% goat serum, and incubated with 1ug/ml DAPI for 10 minutes at room temperature. Finally, cells were washed 3X with PBS and kept covered with foil at 4C until imaged.

Vessel Formation Assay

To produce vessels from the MACS sorted BMEC cells, resuspend 75K cells per well of a 96wp in equal volumes of GFR Matrigel (CLS354230-1EA, Sigma) and endothelial maintenance media+ rock inhibitor. Seed the GFR-Matrigel matrix onto the plate and leave in the incubator for 15 minutes to harden. Then, add endothelial maintenance media over the Matrigel matrix, and change that media every day.

Vessels were fixed with 2%PFA for one hour at room temperature to maintain the Matrigel intact. Staining was performed as described above.

QPCR

RNA was obtained by adding 300ul Trizol directly into culture plates and immediately isolated using Direct-zol RNA Microprep Kits (R2062) with DNase digestion. cDNA was synthesized using Superscript IV (18090010), Random Hexamers (N8080127), dNTPs (18427013), and 300ng RNA. qPCR was performed by diluting cDNA 1:20 (for endothelial differentiation experiments) and using SYBR Green (4309155) as a detection reagent. Results were calculated by averaging the control condition cT value and normalizing all cT values to this averaged value and then performing the $2^{-\Delta\,\Delta Ct}$ method.

Western Blotting

Protein was isolated by giving cells a wash with 1X DPBS, and then placing 150ul RIPA (89900, Thermo) buffer with Halt protease (1862209, Thermo) on a 24 well plate. The cells were scraped, moved to an eppendorf tube, and immediately placed on ice for 30 minutes, vortexing every 10 minutes. The homogenate was then spun at 13,200g for 5 minutes at 4C, and the supernatant was

retained. Protein concentration was performed using Pierce BCA assay (23227, Thermo), and final aliquots of 10ug protein were prepared in 0.6ml eppendorf tubes and frozen.

Western blot was performed by adding loading buffer (NP0004, Thermo) to each sample and run through a (NP0336BOX) pre-cast gels. Low molecular weight target CLDN5 was run for 35 minutes. The protein was then transferred to a blot (1704158, Thermo) with the Turbo machine. Once transferred, antibody binding was performed with the fluorescent iBlot 3 Western Blot Transfer System, using LICOR secondary antibodies (ab216779 and ab216774) for fluorescent detection. CLDN5 was used at 1:500, while b-actin was used at 1:5000.

Trans-Endothelial Electrical Resistance (TEER) Measurements

TEER measurements were performed with EVOM2 Epithelial Voltohmeter (World Precision Instruments). Probes and vessels were sterilized 3x with ethanol and washed 3x with water before and after measurements.

Chapter 2

gRNA Cloning and Plasmid Assembly

Plasmids were obtained by Dr. David Knapp and expanded using NEB-10b bacteria (C3020K, NEB). Forward and reverse DNA oligos were ordered from IDT and resuspended at 100uM. 1uL of each was added to 1uL of T4 DNA ligase buffer (M0202S, NEB), 0.25uL T4 PNK (M0201S, NEB), and 6.75uL H2O. The solution was incubated at 37C for 30 minutes, 95C for 5 minutes, and then ramped down to 25C at a rate of 0.1C/s. Digestion was done by preparing 1000ng of the p222 placeholder vector in 30uL total reaction volume in 1x FastDigest Green Buffer (B72, Thermo) with 1uL Bpil-FD (FD1014, Thermo). Incubate at 37C for 1 hour and load on a 1% agarose gel. The band was then cut with a scalpel and purified with QIAquick Gel Extraction Kit (28704, Thermo).

Ligation was done with 1uL 1:50 diluted annealed spacer, 1uL p222 vector, 1uL 10X T4 DNA ligase buffer, 0.25uL T4 DNA ligase, and 6.75uL H2O. The solution was incubated for 10 minutes at room temperature, and then 10 minutes at 65C. 1 uL was added to 10uL of DH5a (C2987H, NEB) competent bacteria and left on ice for 30 minutes. The bacteria were then heat shocked at 42C for 30 seconds and placed on ice for 2 minutes. 200uL of SOC medium was added, incubated at 37C with shaking, and plated onto LB agar plates with 100 ug/ml ampicillin left to grow overnight at 37C. Colonies were picked and placed into 5mL LB broth with 100ug/ml ampicillin and grown overnight again at 37C. Plasmids were extracted with Zippy™ Plasmid Miniprep Kit (D4036, Zymo).

gRNA Screening for CRISPR Activation

Transfection optimizations were done according to manufacturer's protocol for LT-1 (MIR2304, Mirus) and LipoSTEM (STEM00015, Thermo). gRNA screening was performed by plating iPSCs at 45k cells/cm2 per well and transfecting according to LT-1 forward transfection protocol with p222 (gRNA) and p284 (MS2 scaffold) summing to 500ng plasmid total at equimolar amounts. The media was changed 8-12 hours after, and the media was changed daily until 96 hours from transfection, in which the cells were resuspended in 300ul Trizol. RNA isolation was done in accordance with the Directzol Kit. The cDNA was synthesized using Superscript IV (18090010, Thermo). Finally, qPCR was performed with SYBR-Green, and primers designed for each specific gene. Housekeeping gene actin was used to normalize loading. The results were analysed with the ΔΔCt method.

CRISPR Activation Cell Line Generation

A monoclonal cell line was generated for CRISPR activation, including dCas9, activating proteins VP64, p65, MS2, HSF-1, and Csy4 which cuts the gRNA sequences so they can have their effect on the gene of interest. IPSCs were seeded at 45K/cm2 and transfected with LT-1, the sleeping beauty construct, and the transposase (provided by Dr. David Knapp). The resulting culture was allowed to

grow to confluency and seeded at a low density of 10K/cm2 and exposed to 0.2ug/ml puromycin (P7255, Merck) for selection. After four days of selection, individual colonies were picked and seeded individually in wells to allow for monoclonal generation of the stable cells line. Validation of the stable cell line was done by ICC and qPCR of dCas9 in all individual colonies. The three colonies with highest signal were further expanded and frozen.

Chapter 3

Murine Brain Capillary and Primary Cell Isolation and Culture

Culture plates were coated with collagen (c5533, Sigma) at 10ug/ml overnight at room temperature. Plates were washed three times with PBS, and further coated with 10ug/ml Fibronectin (F1056, Sigma) for 30 minutes at room temperature.

Isolation of mouse capillaries were followed by a previously published protocol [261]. Four week old male and female C56Bl/6J mice were purchased from Charles Rivers Ltd. and housed in the Oxford animal facility. Three male and female mice were anesthetized under isoflurane for three minutes, cervically dislocated, and decapitated for brain retrieval. Brains were placed in ice cold petri dish with DMEM/F12 (D8437), and cortices were isolated by removing the hippocampus, midbrain, basal ganglia, and its connective tissues. Two at a time, the cortices were rolled on blotting paper to remove meninges, and dounced with a 7ml dounce homogenizer (D9063), 10 times with large clearance pestle (pestle A) and 5 with small clearance pestle (pestle B). The resulting homogenate was pooled between all mice and mixed and vortexed 1:3 with 24% dextran (A1847, BioChemica) for a final composition of 16% dextran. The resulting solution was spun at 3,800g, 20 minutes, 4C. The supernatant and floating myelin were removed, and the resulting pellets and tube were washed with DMEM-Complete (DMEM+Glutamax (10566016), 10% FBS (17256336, Gibco), MEM-NEAA (11140-035, Gibco), and Penicillin/Streptomycin (15140122, Gibco), and spun down at 800g, 10 minutes, 4C.

The pellet was resuspended in DMEM-Complete and filtered through a 40um filter (Pluristrainer, 43-50040-03). The resulting capillary-containing filter was cut using a scalpel and washed by submerging the filter in 2ml DMEM-Complete to release trapped capillaries. The capillaries were spun at 800g, 10 minutes, 4C, and resuspended in 5 ml digestion medium made up of DMEM-Complete, trypsin TRL (90 U/ml) (LS003702, Worthington), collagenase II (200U/ml) (STEMCELL, #07418), and DNase I ((170U/ml) (LS0066344, Worthington) for 40 minutes at 37C. Enzyme treatment was halted by dilution in 30ml DMEM-complete, and the isolated capillaries were spun at 500g, 5 minutes, RT, resuspended in DMEM-complete, and seeded to collagen/fibronectin coated plates. The capillaries were incubated for three hours at 37C, 5% CO2, carefully washed once with PBS, and medium was changed to DMEM-Complete supplemented with 4ug/ml puromycin to purify the resulting culture from other contaminating cell types. Capillaries were cultured for 4-5 days, with a medium change of DMEM-complete (no puromycin) done every two days.

The resulting *ex-plant* culture was trypsinised with TrypLE Express (12604-013, Gibco) for 8 minutes, and neutralized with complete mouse endothelial media (M1168-kit) and spun at 500g, 5 minutes RT. Endothelial cells were seeded at 134,000 cells/cm2 in complete mouse endothelial media in 96 well plates for ICC, ROS, and RNS studies, transwell inserts (662641, Greiner) for TEER measurements, and 12 well plates for RNA analysis. Three days later, media was changed to experimental medium, consisting of low-glucose DMEM without NaHCO3 (31600-083, Gibco), supplemented with 10% FBS, 8-(4-CPT)-cyclic adenose monophosphate (CAMP)(#c3912, Sigma) at 312.5uM, dexamethasone (D4902, Sigma) at 0.5uM, RO-20-1724 (17.5uM) (0415, Tocris), and N-[tris(hydrozymethyl)methyl]-2-aminoethanesulfonic acid (TES) (T5691, Sigma) at 50mM (pH adjusted to 7.4). This media was additionally supplemented with glucose (A24940-01, Gibco) for conditions with 15mM or 25mM glucose concentrations. Cells were incubated in experimental media for four days, where assays were then performed and RNA extracted, with a medium change at day 2.

Glucose Concentration Measurements

Glucose concentration readings were taken prior from experimental media before and after culturing using the GlucCell meter (GC01000, KDBio) in accordance with the manufacturer's instructions.

Trans-Endothelial Electrical Resistance (TEER) Measurements

TEER measurements were performed with EVOM2 Epithelial Voltohmeter (World Precision Instruments). Probes and vessels were sterilized 3x with ethanol and washed 3x with water before and after measurements.

Lactate Assay

Lactate was measured using the colorimetric Lactate Assay Kit (Sigma, MAK064-1KT) and following in accordance with the manufacturer's instructions. Snap-frozen cell culture medium from different glucose conditions was thawed, and spun at 14,000g, 10 minutes, room temperature in an Amicon Ultra 0.5ml Centrifugal Filter Units (UFC501024, Millipore) to separate lactate from lactate dehydrogenase present in serum. The flow-through was retained and 2ul of media was used per well for lactate detection.

RNA Isolation and qPCR

RNA was isolated with Direct-zol RNA Microprep kit (R2062) by adding Trizol directly to cell culture plates and following the manufacturer's instructions, including DNase digestion and nanodropped to ensure sufficient RNA yield and quality via A260/A280 and A260/A230 readings. Following isolation, 300ng RNA was used and synthesised to cDNA with Superscript IV reverse transcriptase (18090010), random hexamers (100026484, Invitrogen), and dNTPs (D75295, Sigma). The resulting cDNA was diluted 1:5 with DEPC treated H2O and qPCR was run with SYBR green reagent (4309155, Thermo).

Mitochondrial ROS Assay

Endothelial cells were seeded in black 96-well plates with glass bottom for optimal imaging. Mitochondrial ROS was measured by live-staining MitoSOX Red (M36008, Thermo) at 1uM for 15 minutes, 37C, followed by Mitotracker Green FM (M7514, Thermo) at 20nM and Hoechst (10ug/ml) (62249, Thermo) for 10 minutes, 37C, in PBS Ca2+/Mg2+ (14040141, Thermo). Images were captured with an EVOS fluorescent microscope at 40X, and analysed by overlaying Mitotracker and MitoSOX signals to detect true mitochondrial staining rather than artifacts. Puncta were counted with ImageJ.

Nitric Oxide Assay

Nitric Oxide was measured with ROS-ID ROS/RNS detection kit (ENZ-51001-200, Enzo) in accordance with the manufacturer's instructions.

Chapter 4

Diabetic and Control Brain Donor Selection

Diabetic and control frontal cortex donors were selected by searching "Type II diabetes" and "control" in the UK MRC Biobank, consisting of several different bank locations in the UK. Potential candidates were compiled in an excel list form, and individually checked for confounding factors (co-morbidities) that would immediately exclude donors, such as Alzheimer's, Parkinson's, progressive supranuclear palsy, multiple sclerosis, sepsis, brain cancer, infarcts in the frontal cortex, and moderate or severe small-vessel disease. Remaining donors were further stratified to hypertense and non-hypertense groups for analysis on the effects of this co-morbidity commonly seen with diabetic patients. Control patients were then selected to age and sex-match diabetic donors. Due to the lack of availability of tissues, age matching was not exact, but is on average within 3 years difference from diabetic donors.

Human Capillary Isolation Sample Preparation

Frozen frontal cortex tissue was placed on a petri dish on dry ice for sample preparation. In short, 1-1.2 grams of tissue was cut from the frozen block and scraped with a scalpel to remove meninges and any remaining blood on the tissue. It was then extensively diced using a 3D printed razor holder developed in lab by Dr. Hannah Sleven, until the tissue was well minced. The prepped tissue was then moved to a 50ml tube and frozen at -80 until the experiment day.

Human Capillary and Parenchyma Nuclei Isolation

A list of buffer ingredients can be found in supplementary materials table.

All spin steps were performed at 4C.

Vascular Nuclei Isolation

The minced tissue was retrieved from -80 and 5ml Buffer A was added to the 50ml tube. The tissue was homogenised with 60 strokes using a motorized pestle, filled up with buffer A, and spun at 35g to pellet material not fully homogenised. The supernatant was set aside, and the remaining pellet was homogenised again. This process was repeated three times. The final homogenates were spun at 35g for 3 minutes. While retaining the supernatant, pellets were further homogenised using a 7ml dounce (D9063-1SET, Sigma), and spun at 204g for 3 minutes to ensure all vessels pellet in this spin. Three to five ml of supernatant was retained to process for parenchymal cells (see below), while the pellets were resuspended in 4% dextran and overlayed on top of a 16%-12% double-layer dextran solution and spun at 2600g for 6 minutes. Following the spin, the supernatant was removed until the 10ml mark, and 10ml buffer A was added for a final concentration of 8% dextran. The tube was thoroughly washed to ensure vessels washed off from the sides of the tube. Finally, 20ml of 20% dextran was underlaid below the 8% dextran homogenate. The tube was allowed to sit on ice for 10 minutes, and then spun at 4200g for 20 minutes.

Following the spin, the vessels were resuspended in buffer C, ensuring to thoroughly wash the sides of the tubes again. The remaining solution was put through a 100um filter (43-57100-051,

pluriSelect) to get rid of any large unhomogenized tissue. The resulting filtrate was spun at 800g for 8 minutes. The pellet was resuspended in buffer C and put through a 40um filter (43-50040-01, pluriSelect). Vessels trapped on the filter were then flushed by turning the filter upside down on a new tube and washing the filter with buffer C. The resulting solution now is highly enriched for microvessels and is spun at 800g for 8 minutes. The resulting pellet was resuspended in buffer C and put through a 20um filter (43-50020-01, pluriSelect) fit with a connector ring (41-50000-01, pluriSelect). With the lock open, then vessels were placed and washed on the 20um filter three times (once with buffer I), and then with the lock closed, collagenase II (07418, STEMCell) diluted with HBSS (14025-050, Gibco) was put on the filter for a 15-minute incubation. After the incubation, the lock was opened, and the vessels washed with buffer I. The filter was moved onto a 3D printed funnel system connected to a low-bind 1.5ml eppendorf tube (022431021, Eppendorf). The vessels on the filter were then homogenized with a motorized pestle, disrupting the basement membrane of vessels, and freeing the nuclei into suspension down the eppendorf below. The eppendorf tubes were spun at 500g for 10 minutes, resuspended in PBS/BSA with DAPI (D1306, Thermo), and taken to FACS sorting for DAPI+ nuclei.

Parenchymal Nuclei Isolation

Parenchymal cells were taken from the supernatant after the 204g spin. An equal volume of 2% Triton was added to the homogenate for a final concentration of 1% Triton (93443, Sigma), and allowed to incubate for five minutes on ice. The solution was then spun at 500g for 5 minutes. The pellet was resuspended and homogenized with a 2ml dounce (D8938-1SET, Sigma), and put through a 20um filter onto a low-bind 1.5ml eppendorf. The eppendorf tubes were spun at 500g for 10 minutes, resuspended in PBS/BSA with DAPI, and taken to FACS sorting for DAPI+ nuclei.

Nuclei Fixation and Preparation for snRNA-seq

The FACS-sorted parenchymal and vascular nuclei were fixed using the Parse Fixation kit (WN300, Parse Biosciences) with a few modifications. The nuclei were fixed, permeabilized, and neutralized as

instructed. Due to high vascular nuclei clumping, the resulting nuclei were filtered with a 5um filter rather than a 40um filter. Nuclei were counted using EVOS Analysis software through the DAPI channel. Clumped nuclei for the optimizations were counted using “Split Cells – Shape” or “Split Cells – None” to differentiate individual nuclei with clumped. One microliter was taken from the sample for counting and the resulting nuclei solution was frozen in a -80 freezer by adding 5% DMSO and placing tubes in a Mr. Frosty.

Nuclei Barcoding and Sequencing

Nuclei barcoding was done using a WT Mega kit (NC2373631) from Parse Biosciences following the instructions in the manual. Sequencing was performed by using Nextseq500 and NovaSeq 6000.

scRNA-seq Analysis

Hope Han conducted a differential gene expression (DEG) analysis utilizing DESeq2 with pseudobulk measurements [366] provided by Dr. Cesar Prada at Novo Nordisk. The procedure involved the estimation of size factors using ‘estimateSizeFactors()’ function, imposition of a count threshold (10) for gene filtering, and application of the ‘lfcShrink(type=’apeglm’) methodology for noise reduction while preserving substantial gene expression differences.

Supplemental Methods

Primers

Gene	Target	Forward	Reverse
Il1b	Mouse	ATGGCAACTGTTCCTGAACTCAACT	CAGGACAGGTATAGATTCTTTCCTTT
Il1a	Mouse	CAAGATGGCCAAAGTTCGTGAC	GTCTCATGAAGTGAGCCATAGC
Il6	Mouse	CAAGAGACTTCCATCCAGTTGC	TTGCCGAGTTCTCAAAGTGAC
Ifny	Mouse	GGCCATCAGCAACAACATAAGCGT	TGGGTTGTTGACCTCAAACTTGGC
TNF-a	Mouse	ATGAGCACAGAAAGCATGATCCG	CCAAAGTAGACCTGCCCGGACTC
Inos	Mouse	AATGGCAACATCAGGTCGGCCATCACT	GCTGTGTGTCACAGAAGTCTCGAACTC
Gapdh	Mouse	ATCCCATCACCATCTTCCAG	CCTGCTTCACCACCTTCTTG
Icam	Mouse	GGCATTGTTCTCTAATGTCTCCG	CCGCTCAGAAGAACCACCTTGG
Vcam	Mouse	TACTCCCGTCATTGAGGATATTGG	CTCCTTCACACACATAGACTCC
Crp	Mouse	CGCAGCTTCAGTGTCTTCTC	GATGTGTGTTGGAGCCTCA
Mcp1	Mouse	TGATCCCAATGAGTAGGCTGGAG	ATGTCTGGACCCATTCCTTCTTG
Pai1	Mouse	GACACCCTCAGCATGTTCATC	AGGGTTGCACTAAACATGTCAG
Actin	Mouse	AGGCATCCTCACCCTGAAGTA	CACACGCAGCTCATTGTAGA
VE-CADHERIN	Human	CGCAATAGACAAGGACATAACAC	GGTCAAACTGCCCATACTTG
PECAM1	Human	GAGTATTACTGCACAGCCTTCA	AACCACTGCAATAAGTCCTTTC
CLDN5	Human	GTTCGCCAACATTGTCGTCC	GTAGTTCTTCTTGTCGTAGTCGC
KDR	Human	TTTTTGCCCTTGTTCTGTCC	TCATTGTTCCCAGCATTTCA
VWF	Human	CCCGAAAGGCCAGGTGTA	AGCAAGCTTCCGGGGACT
SLC2A1	Human	AACTCTTCAGCCAGGGTCCAC	CACAGTGAAGATGATGAAGAC
OCLN	Human	GACTTCAGGCAGCCTCGTTAC	GCCAGTTGTGTAGTCCTCA
PGP	Human	CTCATCGTTTGTCTACAGTTC	AAGACATTTCCAAGGCATCA
LEF1	Human	CTTTATCCAGGCTGGTCTGC	TCGTTTTCCACCATGTTTCA
ETS1	Human	TTCACTAAAGAACAGCAAC	TGTCCCCAACAAAGTCTG
MRTFB	Human	CCTGTGACTACAAACACTCCAGC	CAGGCTTTGCTGAGGACACAGT
dCAS9	Human	CCCAAGAGGAACAGCGATAAG	GATAAGACACGACCACCACC
BSD (Blasticidin deaminase)	Human	AGCTGGCAACCTGACTTGTA	TTGGGATTCGTGAATTGCTGC
GAPDH	Human	GTCTCCTCTGACTTCAACAGCG	ACCACCCTGTTGCTGTAGCCAA
ACTIN	Human	GACCCAGATCATGTTTGAGACCT	GAGGCGTACAGGCATAGCAC

Antibodies

Gene	Dilution	Product Code
VE-CADHERIN	1:400	D87F2 (Cell Sig Tech)
PECAM1	1:400	MA3100 (Thermo)
PECAM1	1:100	RB-10333-PO (Neomarkers)
CLDN5	1:100	35-2500 (Invitrogen)
GLUT1 (SLC2A1)	1:1000	MA511315 (Thermo)
OCLN	1:200	OC-3F-10 (Affinity)
ZO1	1:400	402200 (Invitrogen)
JAM-A	1:100	361700 (LifeTech)
KI67	1:100	MAB4190 (Millipore)
E-CADHERIN	1:400	3195P (Cell Sig Tech)
B-CATENIN	1:100	9582S (Cell Sig Tech)
PGP	1:20	MA126529 (Thermo)
CCN1	1:10000	C2687 (Sigma)
LEF1	1:250	2230s (Cell Sig Tech)
ETS1	1:1000	14069s (Cell Sig Tech)
MRTFB	1:100	NBP1-46209 (Novus)
GFP	1:10000	AB13970 (Abcam)
dCAS9	1:1000	MA1-201 (Thermo)
bACTIN	1:5000	AB8224 (Abcam)

Plasmid Sequences

tagBFP-rtTA3

TTAATGTAGTCTTATGCAATACTCTTGTAGTCTTGCAACATGGTAACGATGAGTTAGCAACATGCCTTACAAGGAGAGAAAAAGCA
CCGTGCATGCCGATTGGTGGAAGTAAGGTGGTACGATCGTGCCTTATTAGGAAGGCAACAGACGGGTCTGACATGGATTGGACG
AACCACTGAATTGCCGCATTGCAGAGATATTGTATTTAAGTGCCTAGCTCGATACATAAACGGGTCTCTCTGGTTAGACCAGATCTG
AGCCTGGGAGCTCTCTGGCTAACTAGGGAACCCACTGCTTAAGCCTCAATAAAGCTTGCCTTGAGTGCTTCAAGTAGTGTGTGCCC
GTCTGTTGTGTGACTCTGGTAACTAGAGATCCCTCAGACCCTTTTAGTCAGTGTGGAAAATCTCTAGCAGTGGCGCCCGAACAGG
GACTTGAAAGCGAAAGGGAAACCAGAGGAGCTCTCTCGACGCAGGACTCGGCTTGCTGAAGCGCGCACGGCAAGAGGCGAGG
GGCGGCGACTGGTGAGTACGCCAAAAATTTTGACTAGCGGAGGCTAGAAGGAGAGAGATGGGTGCGAGAGCGTCAGTATTAAG
CGGGGGAGAATTAGATCGCGATGGGAAAAAATTCGGTTAAGGCCAGGGGGAAAGAAAAATATAAATTAAAACATATAGTATGG
GCAAGCAGGGAGCTAGAACGATTCGCAGTTAATCCTGGCCTGTTAGAAACATCAGAAGGCTGTAGACAAATACTGGGACAGCTA
CAACCATCCCTTCAGACAGGATCAGAAGAACTTAGATCATTATATAATACAGTAGCAACCCTCTATTGTGTGCATCAAAGGATAGAG
ATAAAAGACACCAAGGAAGCTTTAGACAAGATAGAGGAAGAGCAAAACAAAAGTAAGACCACCGCACAGCAAGCGGCCGCAG
GAGCTTTGTTCCTTGGGTTCTTGGGAGCAGCAGGAAGCACTATGGGCGCAGCGTCAATGACGCTGACGGTACAGGCCAGACAAT
TATTGTCTGGTATAGTGCAGCAGCAGAACAATTTGCTGAGGGCTATTGAGGCGCAACAGCATCTGTTGCAACTCACAGTCTGGGG
CATCAAGCAGCTCCAGGCAAGAATCCTGGCTGTGGAAAGATACCTAAAGGATCAACAGCTCCTTGAGACAAATGGCAGTATTCAT
CCACAATTTTAAAAGAAAAGGGGGGATTGGGGGGTACAGTGCAGGGGAAAGAATAGTAGACATAATAGCAACAGACATACAAA
CTAAAGAATTACAAAAACAAATTACAAAAATTCAAAATTTTGCGGCCGCGACTAGTTATTAATAGTAATCAATTACGGGGTCATT
AGTTCATAGCCCATATATGGAGTTCCGCGTTACATAACTTACGGTAAATGGCCCGCCTGGCTGACCGCCCAACGACCCCCGCCCATT
GACGTCAATAATGACGTATGTTCCCATAGTAACGCCAATAGGGACTTTCCATTGACGTCAATGGGTGGACTATTTACGGTAAACTGC
CCACTTGGCAGTACATCAAGTGTATCATATGCCAAGTACGCCCCCTATTGACGTCAATGACGGTAAATGGCCCGCCTGGCATTATGC
CCAGTACATGACCTTATGGGACTTTCCTACTTGGCAGTACATCTACGTATTAGTCATCGCTATTACCATGGGTCGAGGTGAGCCCCA
CGTTCTGCTTCACTCTCCCCATCTCCCCCCCCTCCCCACCCCCAATTTTGTATTTATTTATTTTTTAATTATTTTGTGCAGCGATGGGGG

CGGGGGGGGGGGGGGCGCGCGCCAGGCGGGGCGGGGCGGGGCGAGGGGCGGGGCGGGGCGAGGCGGAGAGGTGCGGCG
GCAGCCAATCAGAGCGGCGCGCTCCGAAAGTTTCCTTTTATGGCGAGGCGGCGGCGGCGGCGGCCCTATAAAAAGCGAAGCGC
GCGGCGGGCGGGAGTCGCTGCGTTGCCTTCGCCCCGTGCCCCGCTCCGCGCCGCCTCGCGCCGCCCGCCCCGGCTCTGACTGACC
GCGTTACTCCCACAGGTGAGCGGGCGGGACGGCCCTTCTCCTCCGGGCTGTAATTAGCGCTTGGTTTAATGACGGCTCGTTTCTTT
TCTGTGGCTGCGTGAAAGCCTTAAAGGGCTCCGGGAGGGCCCTTTGTGCGGGGGGGAGCGGCTCGGGGGGTGCGTGCGTGTGT
GTGTGCGTGGGGAGCGCCGCGTGCGGCCCGCGCTGCCCGGCGGCTGTGAGCGCTGCGGGCGCGGCGCGGGGCTTTGTGCGCTC
CGCGTGTGCGCGAGGGGAGCGCGGCCGGGGGCGGTGCCCCGCGGTGCGGGGGGGCTGCGAGGGGAACAAAGGCTGCGTGCG
GGGTGTGTGCGTGGGGGGGTGAGCAGGGGGTGTGGGCGCGGCGGTCGGGCTGTAACCCCCCCCTGCACCCCCCTCCCCGAGTT
GCTGAGCACGGCCCGGCTTCGGGTGCGGGGCTCCGTGCGGGGCGTGGCGCGGGGCTCGCCGTGCCGGGCGGGGGGTGGCGGC
AGGTGGGGGTGCCGGGCGGGGCGGGGCCGCCTCGGGCCGGGGAGGGCTCGGGGGAGGGGCGCGGCGGCCCCGGAGCGCCG
GCGGCTGTCGAGGCGCGGCGAGCCGCAGCCATTGCCTTTTATGGTAATCGTGCGAGAGGGCGCAGGGACTTCCTTTGTCCCAAA
TCTGGCGGAGCCGAAATCTGGGAGGCGCCGCCGCACCCCCTCTAGCGGGCGCGGGCGAAGCGGTGCGGCGCCGGCAGGAAGG
AAATGGGCGGGGAGGGCCTTCGTGCGTCGCCGCGCCGCCGTCCCCTTCTCCATCTCCAGCCTCGGGGCTGCCGCAGGGGGACGG
CTGCCTTCGGGGGGGACGGGGCAGGGCGGGGTTCGGCTTCTGGCGTGTGACCGGCGGCTCTAGAGCCTCTGCTAACCATGTTCA
TGCCTTCTTCTTTTTCCTACAGCTCCTGGGCAACGTGCTGGTTGTTGTGCTGTCTCATCATTTTGGCAAAGAATTACCCGCCGGGCG
CGCCCCACCATGTCTAGACTGGACAAGAGCAAAGTCATAAACGGAGCTCTGGAATTACTCAATGGTGTCGGTATCGAAGGCCTGA
CGACAAGGAAACTCGCTCAAAAGCTGGGAGTTGAGCAGCCTACCCTGTACTGGCACGTGAAGAACAAGCGGGCCCTGCTCGAT
GCCCTGCCAATCGAGATGCTGGACAGGCATCATACCCACTTCTGCCCCCTGGAAGGCGAGTCATGGCAAGACTTTCTGCGGAACA
ACGCCAAGTCATACCGCTGTGCTCTCCTCTCACATCGCGACGGGGCTAAAGTGCATCTCGGCACCCGCCCAACAGAGAAACAGTA
CGAAACCCTGGAAAATCAGCTCGCGTTCCTGTGTCAGCAAGGCTTCTCCCTGGAGAACGCACTGTACGCTCTGTCCGCCGTGGGC
CACTTTACACTGGGCTGCGTATTGGAGGAACAGGAGCATCAAGTAGCAAAAGAGGAAAGAGAGACACCTACCACCGATTCTATG
CCCCCACTTCTGAGACAAGCAATTGAGCTGTTCGACCGGCAGGGAGCCGAACCTGCCTTCCTTTTCGGCCTGGAACTAATCATATG
TGGCCTGGAGAAACAGCTAAAGTGCGAAAGCGGCGGGCCGACCGACGCCCTTGACGATTTTGACTTAGACATGCTCCCAGCCGA
TGCCCTTGACGACTTTGACCTTGATATGCTGCCTGCTGACGCTCTTGACGATTTTGACCTTGACATGCTCCCCGGGGGTTCCGGCG
CAACAAACTTCTCTCTGCTGAAACAAGCCGGAGATGTCGAAGAGAATCCTGGACCGATGACCGAGTACAAGCCCACGGTGCGCC
TCGCCACCCGCGACGACGTCCCCAGGGCCGTACGCACCCTCGCCGCCGCGTTCGCCGACTACCCCGCCACGCGCCACACCGTCGA
TCCGGACCGCCACATCGAGCGGGTCACCGAGCTGCAAGAACTCTTCCTCACGCGCGTCGGGCTCGACATCGGCAAGGTGTGGGT
CGCGGACGACGGCGCCGCGGTGGCGGTCTGGACCACGCCGGAGAGCGTCGAAGCGGGGGCGGTGTTCGCCGAGATCGGCCCG
CGCATGGCCGAGTTGAGCGGTTCCCGGCTGGCCGCGCAGCAACAGATGGAAGGCCTCCTGGCGCCGCACCGGCCCAAGGAGCC
CGCGTGGTTCCTGGCCACCGTCGGAGTCTCGCCCGACCACCAGGGCAAGGGTCTGGGCAGCGCCGTCGTGCTCCCCGGAGTGGA
GGCGGCCGAGCGCGCCGGGGTGCCCGCCTTCCTGGAGACCTCCGCGCCCCGCAACCTCCCCTTCTACGAGCGGCTCGGCTTCACC
GTCACCGCCGACGTCGAGGTGCCCGAAGGACCGCGCACCTGGTGCATGACCCGCAAGCCCGGTGCCGGTACCGGTTCCGGCGAG
GGCAGAGGAAGTCTTCTAACATGCGGTGACGTGGAGGAGAATCCCGGCCCTATGAGCGAGCTGATTAAGGAGAACATGCACATG
AAGCTGTACATGGAGGGCACCGTGGACAACCATCACTTCAAGTGCACATCCGAGGGCGAAGGCAAGCCCTACGAGGGCACCCA
GACCATGAGAATCAAGGTGGTCGAGGGCGGCCCTCTCCCCTTCGCCTTCGACATCCTGGCTACTAGCTTCCTCTACGGCAGCAAGA
CCTTCATCAACCACACCCAGGGCATCCCCGACTTCTTCAAGCAGTCCTTCCCTGAGGGCTTCACATGGGAGAGAGTCACCACATAC
GAAGACGGGGGCGTGCTGACCGCTACCCAGGACACCAGCCTCCAGGACGGCTGCCTCATCTACAACGTCAAGATCAGAGGGGTG
AACTTCACATCCAACGGCCCTGTGATGCAGAAGAAAACACTCGGCTGGGAGGCCTTCACCGAGACGCTGTACCCCGCTGACGGC
GGCCTGGAAGGCAGAAACGACATGGCCCTGAAGCTCGTGGGCGGGAGCCATCTGATCGCAAACATCAAGACCACATATAGATCC
AAGAAACCCGCTAAGAACCTCAAGATGCCTGGCGTCTACTATGTGGACTACAGACTGGAAAGAATCAAGGAGGCCAACAACGAG
ACCTACGTCGAGCAGCACGAGGTGGCAGTGGCCAGATACTGCGACCTCCCTAGCAAACTGGGGCACAAGCTTAATCCAAAGAAG
AAGCGGAAAGTCGGTACCTAATAGTGAACGCGTTAAGTCGACAATCAACCTCTGGATTACAAAATTTGTGAAAGATTGACTGGTA
TTCTTAACTATGTTGCTCCTTTTACGCTATGTGGATACGCTGCTTTAATGCCTTTGTATCATGCTATTGCTTCCCGTATGGCTTTCATTT
TCTCCTCCTTGTATAAATCCTGGTTGCTGTCTCTTTATGAGGAGTTGTGGCCCGTTGTCAGGCAACGTGGCGTGGTGTGCACTGTGT
TTGCTGACGCAACCCCCACTGGTTGGGGCATTGCCACCACCTGTCAGCTCCTTTCCGGGACTTTCGCTTTCCCCCTCCCTATTGCCA
CGGCGGAACTCATCGCCGCCTGCCTTGCCCGCTGCTGGACAGGGGCTCGGCTGTTGGGCACTGACAATTCCGTGGTGTTGTCGGG
GAAATCATCGTCCTTTCCTTGGCTGCTCGCCTGTGTTGCCACCTGGATTCTGCGCGGGACGTCCTTCTGCTACGTCCCTTCGGCCCT
CAATCCAGCGGACCTTCCTTCCCGCGGCCTGCTGCCGGCTCTGCGGCCTCTTCCGCGTCTTCGCCTTCGCCCTCAGACGAGTCGGA

TCTCCCTTTGGGCCGCCTCCCCGCGTCGACTTTAAGACCAATGACTTACAAGGCAGCTGTAGATCTTAGCCACTTTTTAAAAGAAA
AGGGGGGACTGGAAGGGCTAATTCACTCCCAACGAAGACAAGATCTGCTTTTTGCTTGTACTGGGTCTCTCTGGTTAGACCAGAT
CTGAGCCTGGGAGCTCTCTGGCTAACTAGGGAACCCACTGCTTAAGCCTCAATAAAGCTTGCCTTGAGTGCTTCAAGTAGTGTGT
GCCCGTCTGTTGTGTGACTCTGGTAACTAGAGATCCCTCAGACCCTTTTAGTCAGTGTGGAAAATCTCTAGCAGTACGTATAGTAGT
TCATGTCATCTTATTATTCAGTATTTATAACTTGCAAAGAAATGAATATCAGAGAGTGAGAGGAACTTGTTTATTGCAGCTTATAATG
GTTACAAATAAAGCAATAGCATCACAAATTTCACAAATAAAGCATTTTTTTCACTGCATTCTAGTTGTGGTTTGTCCAAACTCATCA
ATGTATCTTATCATGTCTGGCTCTAGCTATCCCGCCCCTAACTCCGCCCATCCCGCCCCTAACTCCGCCCAGTTCCGCCCATTCTCCGC
CCCATGGCTGACTAATTTTTTTTATTTATGCAGAGGCCGAGGCCGCCTCGGCCTCTGAGCTATTCCAGAAGTAGTGAGGAGGCTTT
TTTGGAGGCCTAGGGACGTACCCAATTCGCCCTATAGTGAGTCGTATTACGCGCGCTCACTGGCCGTCGTTTTACAACGTCGTGAC
TGGGAAAACCCTGGCGTTACCCAACTTAATCGCCTTGCAGCACATCCCCCTTTCGCCAGCTGGCGTAATAGCGAAGAGGCCCGCA
CCGATCGCCCTTCCCAACAGTTGCGCAGCCTGAATGGCGAATGGGACGCGCCCTGTAGCGGCGCATTAAGCGCGGCGGGTGTGG
TGGTTACGCGCAGCGTGACCGCTACACTTGCCAGCGCCCTAGCGCCCGCTCCTTTCGCTTTCTTCCCTTCCTTTCTCGCCACGTTCG
CCGGCTTTCCCCGTCAAGCTCTAAATCGGGGGCTCCCTTTAGGGTTCCGATTTAGTGCTTTACGGCACCTCGACCCCAAAAAACTT
GATTAGGGTGATGGTTCACGTAGTGGGCCATCGCCCTGATAGACGGTTTTTCGCCCTTTGACGTTGGAGTCCACGTTCTTTAATAG
TGGACTCTTGTTCCAAACTGGAACAACACTCAACCCTATCTCGGTCTATTCTTTTGATTTATAAGGGATTTTGCCGATTTCGGCCTAT
TGGTTAAAAAATGAGCTGATTTAACAAAAATTTAACGCGAATTTTAACAAAATATTAACGCTTACAATTTAGGTGGCACTTTTCGG
GGAAATGTGCGCGGAACCCCTATTTGTTTATTTTTCTAAATACATTCAAATATGTATCCGCTCATGAGACAATAACCCTGATAAATGC
TTCAATAATATTGAAAAAGGAAGAGTATGAGTATTCAACATTTCCGTGTCGCCCTTATTCCCTTTTTTGCGGCATTTTGCCTTCCTGT
TTTTGCTCACCCAGAAACGCTGGTGAAAGTAAAAGATGCTGAAGATCAGTTGGGTGCACGAGTGGGTTACATCGAACTGGATCTC
AACAGCGGTAAGATCCTTGAGAGTTTTCGCCCCGAAGAACGTTTTCCAATGATGAGCACTTTTAAAGTTCTGCTATGTGGCGCGG
TATTATCCCGTATTGACGCCGGGCAAGAGCAACTCGGTCGCCGCATACACTATTCTCAGAATGACTTGGTTGAGTACTCACCAGTCA
CAGAAAAGCATCTTACGGATGGCATGACAGTAAGAGAATTATGCAGTGCTGCCATAACCATGAGTGATAACACTGCGGCCAACTT
ACTTCTGACAACGATCGGAGGACCGAAGGAGCTAACCGCTTTTTTGCACAACATGGGGGATCATGTAACTCGCCTTGATCGTTGG
GAACCGGAGCTGAATGAAGCCATACCAAACGACGAGCGTGACACCACGATGCCTGTAGCAATGGCAACAACGTTGCGCAAACTA
TTAACTGGCGAACTACTTACTCTAGCTTCCCGGCAACAATTAATAGACTGGATGGAGGCGGATAAAGTTGCAGGACCACTTCTGC
GCTCGGCCCTTCCGGCTGGCTGGTTTATTGCTGATAAATCTGGAGCCGGTGAGCGTGGGTCTCGCGGTATCATTGCAGCACTGGG
GCCAGATGGTAAGCCCTCCCGTATCGTAGTTATCTACACGACGGGGAGTCAGGCAACTATGGATGAACGAAATAGACAGATCGCT
GAGATAGGTGCCTCACTGATTAAGCATTGGTAACTGTCAGACCAAGTTTACTCATATATACTTTAGATTGATTTAAAACTTCATTTTT
AATTTAAAAGGATCTAGGTGAAGATCCTTTTTGATAATCTCATGACCAAAATCCCTTAACGTGAGTTTTCGTTCCACTGAGCGTCAG
ACCCCGTAGAAAAGATCAAAGGATCTTCTTGAGATCCTTTTTTTCTGCGCGTAATCTGCTGCTTGCAAACAAAAAAACCACCGCTA
CCAGCGGTGGTTTGTTTGCCGGATCAAGAGCTACCAACTCTTTTTCCGAAGGTAACTGGCTTCAGCAGAGCGCAGATACCAAATA
CTGTTCTTCTAGTGTAGCCGTAGTTAGGCCACCACTTCAAGAACTCTGTAGCACCGCCTACATACCTCGCTCTGCTAATCCTGTTACC
AGTGGCTGCTGCCAGTGGCGATAAGTCGTGTCTTACCGGGTTGGACTCAAGACGATAGTTACCGGATAAGGCGCAGCGGTCGGG
CTGAACGGGGGGTTCGTGCACACAGCCCAGCTTGGAGCGAACGACCTACACCGAACTGAGATACCTACAGCGTGAGCTATGAGA
AAGCGCCACGCTTCCCGAAGGGAGAAAGGCGGACAGGTATCCGGTAAGCGGCAGGGTCGGAACAGGAGAGCGCACGAGGGA
GCTTCCAGGGGGAAACGCCTGGTATCTTTATAGTCCTGTCGGGTTTCGCCACCTCTGACTTGAGCGTCGATTTTTGTGATGCTCGTC
AGGGGGGCGGAGCCTATGGAAAAACGCCAGCAACGCGGCCTTTTTACGGTTCCTGGCCTTTTGCTGGCCTTTTGCTCACATGTTC
TTTCCTGCGTTATCCCCTGATTCTGTGGATAACCGTATTACCGCCTTTGAGTGAGCTGATACCGCTCGCCGCAGCCGAACGACCGAG
CGCAGCGAGTCAGTGAGCGAGGAAGCGGAAGAGCGCCCAATACGCAAACCGCCTCTCCCCGCGCGTTGGCCGATTCATTAATGC
AGCTGGCACGACAGGTTTCCCGACTGGAAAGCGGGCAGTGAGCGCAACGCAATTAATGTGAGTTAGCTCACTCATTAGGCACCC
CAGGCTTTACACTTTATGCTTCCGGCTCGTATGTTGTGTGGAATTGTGAGCGGATAACAATTTCACACAGGAAACAGCTATGACCA
TGATTACGCCAAGCGCGCAATTAACCCTCACTAAAGGGAACAAAAGCTGGAGCTGCAAGC

LEF1, ETS1, MRTFB Transcription Factor Overexpression Plasmid

TTAATGTAGTCTTATGCAATACTCTTGTAGTCTTGCAACATGGTAACGATGAGTTAGCAACATGCCTTACAAGGAGAGAAAAAGCA
CCGTGCATGCCGATTGGTGGAAGTAAGGTGGTACGATCGTGCCTTATTAGGAAGGCAACAGACGGGTCTGACATGGATTGGACG
AACCACTGAATTGCCGCATTGCAGAGATATTGTATTTAAGTGCCTAGCTCGATACATAAACGGGTCTCTCTGGTTAGACCAGATCTG
AGCCTGGGAGCTCTCTGGCTAACTAGGGAACCCACTGCTTAAGCCTCAATAAAGCTTGCCTTGAGTGCTTCAAGTAGTGTGTGCCC
GTCTGTTGTGTGACTCTGGTAACTAGAGATCCCTCAGACCCTTTTAGTCAGTGTGGAAAATCTCTAGCAGTGGCGCCCGAACAGG
GACTTGAAAGCGAAAGGGAAACCAGAGGAGCTCTCTCGACGCAGGACTCGGCTTGCTGAAGCGCGCACGGCAAGAGGCGAGG
GGCGGCGACTGGTGAGTACGCCAAAAATTTTGACTAGCGGAGGCTAGAAGGAGAGAGATGGGTGCGAGAGCGTCAGTATTAAG
CGGGGGAGAATTAGATCGCGATGGGAAAAAATTCGGTTAAGGCCAGGGGGAAAGAAAAAATATAAATTAAAACATATAGTATGG
GCAAGCAGGGAGCTAGAACGATTCGCAGTTAATCCTGGCCTGTTAGAAACATCAGAAGGCTGTAGACAAATACTGGGACAGCTA
CAACCATCCCTTCAGACAGGATCAGAAGAACTTAGATCATTATATAATACAGTAGCAACCCTCTATTGTGTGCATCAAAGGATAGAG
ATAAAAGACACCAAGGAAGCTTTAGACAAGATAGAGGAAGAGCAAAACAAAAGTAAGACCACCGCACAGCAAGCGGCCGCGC
TAGCAGGAGCTTTGTTCCTTGGGTTCTTGGGAGCAGCAGGAAGCACTATGGGCGCAGCGTCAATGACGCTGACGGTACAGGCCA
GACAATTATTGTCTGGTATAGTGCAGCAGCAGAACAATTTGCTGAGGGCTATTGAGGCGCAACAGCATCTGTTGCAACTCACAGT
CTGGGGCATCAAGCAGCTCCAGGCAAGAATCCTGGCTGTGGAAAGATACCTAAAGGATCAACAGCTCCTTGAGACAAATGGCAG
TATTCATCCACAATTTTAAAAGAAAAGGGGGGATTGGGGGGTACAGTGCAGGGGAAAGAATAGTAGACATAATAGCAACAGACA
TACAAACTAAAGAATTACAAAAACAAATTACAAAAATTCAAAATTTTACGGGGACAGCCCCCCCCCAAAGCCCCCAGGGATGTAA
TTACGTCCCTCCCCCGCTAGGGGGCAGCAGCGAGCCGCCCGGGGCTCCGCTCCGGTCCGGCGCTCCCCCCGCATCCCCGAGCCGG
CAGCGTGCGGGGACAGCCCGGGCACGGGGAAGGTGGCACGGGATCGCTTTCCTCTGAACGCTTCTCGCTGCTCTTTGAGCCTGC
AGACACCTGGGGGATACGGGGAAAGAGTTTACTCCCTATCAGTGATAGAGAACGTATGTCGAGTTTACTCCCTATCAGTGATAGA
GAACGATGTCGAGTTTACTCCCTATCAGTGATAGAGAACGTATGTCGAGTTTACTCCCTATCAGTGATAGAGAACGTATGTCGAGTT
TACTCCCTATCAGTGATAGAGAACGTATGTCGAGTTTATCCCTATCAGTGATAGAGAACGTATGTCGAGTTTACTCCCTATCAGTGAT
AGAGAACGTATGTCGAGGTAGGCGTGTACGGTGGGAGGCCTATATAAGCAGAGCTCGTTTAGTGAACCGTCAGATCGCCTGGAG
AATGCCACCATGGGATCCCAATTGCCCCAACTCTCCGGAGGAGGTGGCGGCGGCGGGGGGGACCCGGAACTCTGCGCCACGGA
CGAGATGATCCCCTTCAAGGACGAGGGCGATCCTCAGAAGGAAAAGATCTTCGCCGAGATCAGTCATCCCGAAGAGGAAGGCG
ATTTAGCTGACATCAAGTCTTCCTTGGTGAACGAGTCTGAAATCATCCCGGCCAGCAACGGACACGAGGTGGCCAGACAAGCAC
AAACCTCTCAGGAGCCCTACCACGACAAGGCCAGAGAACACCCCGATGACGGAAAGCATCCAGATGGAGGCCTCTACAACAAG
GGACCCTCCTACTCGAGTTATTCCGGGTACATAATGATGCCAAATATGAATAACGACCCATACATGTCAAATGGATCTCTTTCTCCAC
CCATCCCGAGAACATCAAATAAAGTGCCCGTGGTGCAGCCATCCCATGCGGTCCATCCTCTCACCCCCCTCATCACTTACAGTGACG
AGCACTTTTCTCCAGGATCACACCCGTCACACATCCCATCAGATGTCAACTCCAAACAAGGCATGTCCAGACATCCTCCAGCTCCTG
ATATCCCTACTTTTTATCCCTTGTCTCCGGGTGGTGTTGGACAGATCACCCCACCTCTTGGCTGGCAAGGTCAGCCTGTATATCCCAT
CACGGGTGGATTCAGGCAACCCTACCCATCCTCACTGTCAGTCGACACTTCCATGTCCAGGTTTTCCCATCATATGATTCCCGGTCCT
CCTGGTCCCCACACAACTGGCATCCCTCATCCAGCTATTGTAACACCTCAGGTCAAACAGGAACATCCCCACACTGACAGTGACCT
AATGCACGTGAAGCCTCAGCATGAACAGAGAAAGGAGCAGGAGCCAAAAAGACCTCACATTAAGAAGCCTCTGAATGCTTTTAT
GTTATACATGAAAGAAATGAGAGCGAATGTCGTTGCTGAGTGTACTCTAAAAGAAAGTGCAGCTATCAACCAGATTCTTGGCAGA
AGGTGGCATGCCCTCTCCCGTGAAGAGCAGGCTAAATATTATGAATTAGCACGGAAAGAAAGACAGCTACATATGCAGCTTTATCC
AGGCTGGTCTGCAAGAGACAATTATGGTAAGAAAAAGAAGAGGAAGAGAGAGAAACTACAGGAATCTGCATCAGGTACAGGTC
CAAGAATGACAGCTGCCTACATCGGTTCCGGGGAGGGCAGAGGAAGTCTTCTAACATGCGGTGACGTGGAGGAGAATCCCGGC
CCTATCGATAAGGCGGCCGTCGATCTCAAGCCGACTCTCACCATCATCAAGACGGAAAAAGTCGATCTGGAGCTTTTCCCCTCCCC
GGATATGGAATGTGCAGATGTCCCACTATTAACTCCAAGCAGCAAAGAAATGATGTCTCAAGCATTAAAAGCTACTTTCAGTGGTT
TCACTAAAGAACAGCAACGACTGGGCATCCCAAAAGACCCCCGGCAGTGGACAGAAACCCATGTTCGGGACTGGGTGATGTGG
GCTGTGAATGAATTCAGCCTGAAAGGTGTAGACTTCCAGAAGTTCTGTATGAATGGAGCAGCCCTCTGCGCCCTGGGTAAAGACT
GCTTTCTCGAGCTGGCCCCAGACTTTGTTGGGGACATCTTATGGGAACATCTAGAGATCCTGCAGAAAGAGGATGTGAAACCATA
TCAAGTTAATGGAGTCAACCCAGCCTATCCAGAATCCCGCTATACCTCGGATTACTTCATTAGCTATGGTATTGAGCATGCCCAGTGT
GTTCCACCATCGGAGTTCTCAGAGCCCAGCTTCATCACAGAGTCCTATCAGACGCTCCATCCCATCAGCTCGGAAGAGCTCCTCTCC
CTCAAGTATGAGAATGACTACCCCTCGGTCATTCTCCGAGACCCTCTCCAGACAGACACCTTGCAGAATGACTACTTTGCTATCAAA

CAAGAAGTCGTCACCCCAGACAACATGTGCATGGGGAGGACCAGTCGTGGTAAACTCGGGGGCCAGGACTCTTTTGAAAGCATA
GAGAGCTACGATAGTTGTGATCGCCTCACCCAGTCCTGGAGCAGCCAGTCATCTTTCAACAGCCTGCAGCGTGTTCCCTCCTATGA
CAGCTTCGACTCAGAGGACTATCCGGCTGCCCTGCCCAACCACAAGCCCAAGGGCACCTTCAAGGACTATGTGCGGGACCGTGCT
GACCTCAATAAGGACAAGCCTGTCATTCCTGCTGCTGCCCTAGCTGGCTACACAGGCAGTGGACCAATCCAGCTATGGCAGTTTCT
TCTGGAATTACTCACTGATAAATCCTGTCAGTCTTTTATCAGCTGGACAGGAGATGGCTGGGAATTCAAACTTTCTGACCCAGATG
AGGTGGCCAGGAGATGGGGAAAGAGGAAAAACAAACCTAAGATGAATTATGAGAAACTGAGCCGTGGCCTACGCTACTATTAC
GACAAAAACATCATCCACAAGACAGCGGGGAAACGCTACGTGTACCGCTTTGTGTGTGACCTGCAGAGCCTGCTGGGGTACACC
CCTGAGGAGCTGCACGCCATGCTGGACGTCAAGCCAGATGCCGACGAGGGGTCGGGCCAGTGCACCAACTACGCCCTCTTGAAG
CTGGCGGGCGACGTGGAGTCGAACCCCGGCCCGGGTACCACCGGTATGCATCGTACGGATCACACAGGGGCGATAGACACCGAG
GATGAAGTGGGACCTTTAGCCCATCTTGCTCCAAGTCCTCAGAGTGAAGCTGTGGCTCATGAATTCCAGGAACTCTCCTTGCAGTC
CAGTCAAAACTTACCCCCTCTGAACGAAAGGAAAAATGTGCTCCAGCTGAGGCTGCAACAAAGGAGGACGAGAGAACAACTCG
TGGACCAGGGCATCATGCCACCTTTGAAGAGCCCAGCGGCATTCCATGAACAGATAAAAAGCTTGGAACGAGCCAGAACTGAAA
ACTTTTTGAAACACAAGATTCGGAGTCGACCAGATCGTTCTGAACTTGTCAGGATGCACATTTTAGAAGAAACATTTGCAGAGCC
ATCCCTGCAGGCTACTCAGATGAAGTTGAAAAGAGCTCGACTAGCAGATGATCTGAATGAAAAGATTGCTCAAAGACCTGGTCCT
ATGGAGCTGGTAGAGAAAAACATCCTTCCTGTGGACTCCAGTGTTAAAGAAGCAATTATAGGCGTTGGGAAGGAGGACTATCCC
CACACTCAGGGCGATTTCTCATTTGATGAAGACAGCAGTGACGCTTTGTCTCCGGACCAGCCTGCGAGTCAGGAGTCACAGGGG
TCAGCCGCGTCCCCAAGTGAGCCAAAAGTTAGTGAATCGCCATCTCCTGTGACTACAAACACTCCAGCGCAGTTTGCTTCAGTGTC
CCCAACAGTTCCTGAATTCTTGAAAACTCCTCCAACTGCAGATCAGCCTCCCCCACGGCCTGCAGCTCCTGTCCTCCCCACAAACAC
TGTGTCCTCAGCAAAGCCTGGCCCAGCACTGGTGAAGCAAAGCCATCCCAAGAATCCAAATGACAAACACCGTAGCAAAAAGTG
CAAAGATCCCAAACCACGGGTAAAGAAGTTAAAGTACCACCAATACATTCCACCAGATCAGAAGGGTGAGAAGAATGAGCCGCA
GATGGACTCTAACTACGCCCGCCTGCTCCAGCAGCAGCAGCTGTTCCTGCAACTGCAGATCCTGAGTCAGCAGAAGCAGCACTAC
AACTACCAGACCATCCTGCCTGCACCATTCAAGCCACTCAATGACAAAAATAGTAACAGTGGGAATTCAGCTTTGAACAATGCCAC
ACCTAACACACCAAGACAGAATACATCTACTCCTGTGAGAAAGCCAGGACCTCTGCCTTCTAGCCTGGATGACTTAAAGGTATCAG
AACTGAAGACAGAACTGAAGTTAAGGGGTCTGCCAGTGTCAGGCACCAAACCGGACCTCATTGAGCGCCTAAAACCCTACCAGG
AAGTGAACAGCAGCGGCCTTGCTGCTGGGGGCATCGTGGCAGTGTCATCATCAGCCATTGTCACCAGTAACCCAGAAGTCACTGT
GGCCTTGCCGGTTACAACACTACACAACACTGTGACTAGCTCAGTCTCTACTCTCAAGGCAGAATTGCCACCTACAGGAACCAGCA
ACGCAACCCGTGTGGAAAATGTTCATTCCCCTCTGCCCATTTCACCATCTCCCTCCGAACAGTCCAGTCTCAGTACTGATGACACAA
ACATGGCAGACACTTTCACCGAGATTATGACCATGATGTCGCCTTCACAGTTCTTGAGTTCATCTCCTTTGAGAATGACAAATAATG
AAGACAGTCTGAGTCCCACCAGCAGCACTCTGTCAAACCTGGAACTGGATGCAGCCGAAAAGGATCGCAAGCTTCAGGAGAAA
GAGAAGCAAATCGAAGAGCTGAAGAGGAAACTGGAACAAGAGCAGAAGCTCGTGGAAGTGCTGAAAATGCAACTTGAGGTTG
AAAAACGAGGGCAGCAGCAGCGGCCCCTGGAAGCCCAGCCCAGTGCCCCAGGTCATTCTGTCAAGTCAGATCAGAAGCACGGC
AGCCTTGGCTCCTCCATCAAAGATGAGGCCTCACTCCCTGACTGCTCCAGCTCCAGGCAGCCCATCCCAGTAGCCAGCCACGCTGT
AGGCCAGCCCGTCTCTACAGGTGGCCAGACCCTTGTTGCCAAAAAGGCTGTAGTTATCAAGCAAGAGGTCCCTGTGGGCCAGGC
AGAGCAGCAGAGTGTCGTCTCGCAGTTTTATACTTCACCACAAGCAGGAATGCAGACTCAGCCTCAGATAGCAACTGCTGCACAA
ATACCAACTGCTGCCTTGGCCTCAGGCTTGGCCCCAACTGTACCTCAGACACAAGACACGTTCCCGCAGCATGTGCTCAGTCAGCC
TCAACAAGTCAGAAAGGTTTTCACAAACTCAGCATCATCAAATACAGTTCTTCCATATCAGAGACATCCTGCCCCAGCTGTCCAGC
AGCCCTTTATCAATAAGGCCTCCAACAGTGTTCTTCAATCCAGAAATGCTCCGCTTCCATCCCTGCAAAATGGACCTAACACACCCA
ACAAGCCTAGTTCACCCCCGCCACCCCAGCAATTTGTCGTCCAGCACTCTCTATTTGGGAGTCCAGTCGCCAAGACAAAAGATCCC
CCCCGCTATGAGGAGGCCATCAAGCAGACACGCAGCACACAGGCCCCTCTGCCAGAGATTTCCAACGCTCACAGTCAGCAGATG
GATGACCTCTTTGATATCCTCATTAAGAGTGGAGAGATCTCCCTCCCCATAAAAGAAGAACCTTCTCCTATTTCCAAAATGAGACCA
GTGACAGCCAGCATCACCACAATGCCAGTGAATACAGTGGTGTCCCGGCCACCACCCCAAGTCCAAATGGCACCACCTGTATCTTT
AGAACCTATGGGCAGTTTATCTGCCAGCTTAGAGAACCAACTAGAAGCTTTCTTGGATGGAACTTTACCCTCAGCCAATGAAATTC
CTCCACTACAAAGCAGCAGTGAAGACAGAGAGCCCTTCTCTCTGATCGAGGACCTCCAGAATGATCTGCTGAGTCACTCAGGTAT
GCTGGACCATTCACACTCACCCATGGAGACTTCCGAGACCCAGTTTGCTGCAGGTACTCCCTGTCTGTCTCTCGACCTGTCAGACTC
AAACTTGGACAACATGGAGTGGTTGGACATTACCATGCCCAACTCCTCTTCAGGACTCACTCCTCTCAGCACCACCGCGCCGAGCA
TGTTCTCTGCTGACTTTCTAGACCCACAGGACCTACCGCTGCCATGGGACGGCAGCGGGGCAACAAACTTCTCTCTGCTGAAACA
AGCCGGAGATGTCGAAGAGAATCCTGGACCGAGCGCTACTAGTTCCCTAAGGGGCAGCCTCTCGCGTCTCCTCCAGACGCGAGT
GCATTCCATCCTGAAGAAATCCATGGTGAGCAAGGGCGAGGAGCTGTTCACCGGGGTGGTGCCCATCCTGGTCGAGCTGGACGG

CGACGTAAACGGCCACAAGTTCAGCGTGTCCGGCGAGGGCGAGGGCGATGCCACCTACGGCAAGCTGACCCTGAAGCTGATCTG
CACCACCGGCAAGCTGCCCGTGCCCTGGCCCACCCTCGTGACCACCCTGGGCTACGGCCTGCAGTGCTTCGCCCGCTACCCCGACC
ACATGAAGCAGCACGACTTCTTCAAGTCCGCCATGCCCGAAGGCTACGTCCAGGAGCGCACCATCTTCTTCAAGGACGACGGCAA
CTACAAGACCCGCGCCGAGGTGAAGTTCGAGGGCGACACCCTGGTGAACCGCATCGAGCTGAAGGGCATCGACTTCAAGGAGG
ACGGCAACATCCTGGGGCACAAGCTGGAGTACAACTACAACAGCCACAACGTCTATATCACCGCCGACAAGCAGAAGAACGGCA
TCAAGGCCAACTTCAAGATCCGCCACAACATCGAGGACGGCGGCGTGCAGCTCGCCGACCACTACCAGCAGAACACCCCCATCG
GCGACGGCCCCGTGCTGCTGCCCGACAACCACTACCTGAGCTACCAGTCCAAGCTGAGCAAAGACCCCAACGAGAAGCGCGATC
ACATGGTCCTGCTGGAGTTCGTGACCGCCGCCGGGATCACTCTCGGCATGGACGAGCTGTACAAGTGATAAACGGGGACAGCCC
CCCCCCAAAGCCCCCAGGGATGTAATTACGTCCCTCCCCCGCTAGGGGGCAGCAGCGAGCCGCCCGGGGCTCCGCTCCGGTCCGG
CGCTCCCCCCGCATCCCCGAGCCGGCAGCGTGCGGGGACAGCCCGGGCACGGGGAAGGTGGCACGGGATCGCTTTCCTCTGAAC
GCTTCTCGCTGCTCTTTGAGCCTGCAGACACCTGGGGGATACGGGGAAAGGGCAGAGCGCACATCGCCCACAGTCCCCGAGAAG
TTGGGGGGGAGGGGTCGGCAAATTGATCCGGTGCCTAGAGAAGGTGGCGCGGGGTAAACTGGGAAAGTGATGTCGTGTACTGGC
TCCGCCTTTTTCCCGAGGGTGGGGGAGAACCGTATATAAGTGCAGTAGTCGCCGTGAACGTTCTTTTTCGCAACGGGTTTGCCGC
CAGAACACAGATGGCCAAGCCTTTGTCTCAAGAAGAATCCACCCTCATTGAAAGAGCAACGGCTACAATCAACAGCATCCCCATC
TCTGAAGACTACAGCGTCGCCAGCGCAGCTCTCTCTAGCGACGGCCGCATCTTCACTGGTGTCAATGTATATCATTTTACTGGGGG
ACCTTGTGCAGAACTCGTGGTGCTGGGCACTGCTGCTGCTGCGGCAGCTGGCAACCTGACTTGTATCGTCGCGATCGGAAATGAG
AACAGGGGCATCTTGAGCCCCTGCGGACGGTGCCGACAGGTGCTTCTCGATCTGCATCCTGGGATCAAAGCGATAGTGAAGGAC
AGTGATGGACAGCCGACGGCAGTTGGGATTCGTGAATTGCTGCCCTCTGGTTATGTGTGGGAGGGCTAATAGTGAACGCGTTAA
GTCGACAATCAACCTCTGGATTACAAAATTTGTGAAAGATTGACTGGTATTCTTAACTATGTTGCTCCTTTTACGCTATGTGGATACG
CTGCTTTAATGCCTTTGTATCATGCTATTGCTTCCCGTATGGCTTTCATTTTCTCCTCCTTGTATAAATCCTGGTTGCTGTCTCTTTATG
AGGAGTTGTGGCCCGTTGTCAGGCAACGTGGCGTGGTGTGCACTGTGTTTGCTGACGCAACCCCCACTGGTTGGGGCATTGCCA
CCACCTGTCAGCTCCTTTCCGGGACTTTCGCTTTCCCCCTCCCTATTGCCACGGCGGAACTCATCGCCGCCTGCCTTGCCCGCTGCT
GGACAGGGGCTCGGCTGTTGGGCACTGACAATTCCGTGGTGTTGTCGGGGAAATCATCGTCCTTTCCTTGGCTGCTCGCCTGTGT
TGCCACCTGGATTCTGCGCGGGACGTCCTTCTGCTACGTCCCTTCGGCCCTCAATCCAGCGGACCTTCCTTCCCGCGGCCTGCTGCC
GGCTCTGCGGCCTCTTCCGCGTCTTCGCCTTCGCCCTCAGACGAGTCGGATCTCCCTTTGGGCCGCCTCCCCGCGTCGACTTTAAG
ACCAATGACTTACAAGGCAGCTGTAGATCTTAGCCACTTTTTAAAAGAAAAGGGGGGACTGGAAGGGCTAATTCACTCCCAACG
AAGACAAGATCTGCTTTTTGCTTGTACTGGGTCTCTCTGGTTAGACCAGATCTGAGCCTGGGAGCTCTCTGGCTAACTAGGGAACC
CACTGCTTAAGCCTCAATAAAGCTTGCCTTGAGTGCTTCAAGTAGTGTGTGCCCGTCTGTTGTGTGACTCTGGTAACTAGAGATCCC
TCAGACCCTTTTAGTCAGTGTGGAAAATCTCTAGCAGTACGTATAGTAGTTCATGTCATCTTATTATTCAGTATTTATAACTTGCAAA
GAAATGAATATCAGAGAGTGAGAGGAACTTGTTTATTGCAGCTTATAATGGTTACAAATAAAGCAATAGCATCACAAATTTCACAA
ATAAAGCATTTTTTTCACTGCATTCTAGTTGTGGTTTGTCCAAACTCATCAATGTATCTTATCATGTCTGGCTCTAGCTATCCCGCCCC
TAACTCCGCCCATCCCGCCCCTAACTCCGCCCAGTTCCGCCCATTCTCCGCCCCATGGCTGACTAATTTTTTTTATTTATGCAGAGGC
CGAGGCCGCCTCGGCCTCTGAGCTATTCCAGAAGTAGTGAGGAGGCTTTTTTGGAGGCCTAGGGACGTACCCAATTCGCCCTATA
GTGAGTCGTATTACGCGCGCTCACTGGCCGTCGTTTTACAACGTCGTGACTGGGAAAACCCTGGCGTTACCCAACTTAATCGCCTT
GCAGCACATCCCCCTTTCGCCAGCTGGCGTAATAGCGAAGAGGCCCGCACCGATCGCCCTTCCCAACAGTTGCGCAGCCTGAATG
GCGAATGGGACGCGCCCTGTAGCGGCGCATTAAGCGCGGCGGGTGTGGTGGTTACGCGCAGCGTGACCGCTACACTTGCCAGCG
CCCTAGCGCCCGCTCCTTTCGCTTTCTTCCCTTCCTTTCTCGCCACGTTCGCCGGCTTTCCCCGTCAAGCTCTAAATCGGGGGCTCCC
TTTAGGGTTCCGATTTAGTGCTTTACGGCACCTCGACCCCAAAAAACTTGATTAGGGTGATGGTTCACGTAGTGGGCCATCGCCCT
GATAGACGGTTTTTCGCCCTTTGACGTTGGAGTCCACGTTCTTTAATAGTGGACTCTTGTTCCAAACTGGAACAACACTCAACCCT
ATCTCGGTCTATTCTTTTGATTTATAAGGGATTTTGCCGATTTCGGCCTATTGGTTAAAAAATGAGCTGATTTAACAAAAATTTAAC
GCGAATTTTAACAAAATATTAACGCTTACAATTTAGGTGGCACTTTTCGGGGAAATGTGCGCGGAACCCCTATTTGTTTATTTTTCT
AAATACATTCAAATATGTATCCGCTCATGAGACAATAACCCTGATAAATGCTTCAATAATATTGAAAAAGGAAGAGTATGAGTATTC
AACATTTCCGTGTCGCCCTTATTCCCTTTTTTGCGGCATTTTGCCTTCCTGTTTTTGCTCACCCAGAAACGCTGGTGAAAGTAAAAG
ATGCTGAAGATCAGTTGGGTGCACGAGTGGGTTACATCGAACTGGATCTCAACAGCGGTAAGATCCTTGAGAGTTTTCGCCCCGA
AGAACGTTTTCCAATGATGAGCACTTTTAAAGTTCTGCTATGTGGCGCGGTATTATCCCGTATTGACGCCGGGCAAGAGCAACTCG
GTCGCCGCATACACTATTCTCAGAATGACTTGGTTGAGTACTCACCAGTCACAGAAAAGCATCTTACGGATGGCATGACAGTAAGA
GAATTATGCAGTGCTGCCATAACCATGAGTGATAACACTGCGGCCAACTTACTTCTGACAACGATCGGAGGACCGAAGGAGCTAA
CCGCTTTTTTGCACAACATGGGGGATCATGTAACTCGCCTTGATCGTTGGGAACCGGAGCTGAATGAAGCCATACCAAACGACGA

GCGTGACACCACGATGCCTGTAGCAATGGCAACAACGTTGCGCAAACTATTAACTGGCGAACTACTTACTCTAGCTTCCCGGCAAC
AATTAATAGACTGGATGGAGGCGGATAAAGTTGCAGGACCACTTCTGCGCTCGGCCCTTCCGGCTGGCTGGTTTATTGCTGATAA
ATCTGGAGCCGGTGAGCGTGGGTCTCGCGGTATCATTGCAGCACTGGGGCCAGATGGTAAGCCCTCCCGTATCGTAGTTATCTACA
CGACGGGGAGTCAGGCAACTATGGATGAACGAAATAGACAGATCGCTGAGATAGGTGCCTCACTGATTAAGCATTGGTAACTGTC
AGACCAAGTTTACTCATATATACTTTAGATTGATTTAAAACTTCATTTTTAATTTAAAAGGATCTAGGTGAAGATCCTTTTTGATAAT
CTCATGACCAAAATCCCTTAACGTGAGTTTTCGTTCCACTGAGCGTCAGACCCCGTAGAAAAGATCAAAGGATCTTCTTGAGATCC
TTTTTTTCTGCGCGTAATCTGCTGCTTGCAAACAAAAAAACCACCGCTACCAGCGGTGGTTTGTTTGCCGGATCAAGAGCTACCAA
CTCTTTTTCCGAAGGTAACTGGCTTCAGCAGAGCGCAGATACCAAATACTGTTCTTCTAGTGTAGCCGTAGTTAGGCCACCACTTC
AAGAACTCTGTAGCACCGCCTACATACCTCGCTCTGCTAATCCTGTTACCAGTGGCTGCTGCCAGTGGCGATAAGTCGTGTCTTACC
GGGTTGGACTCAAGACGATAGTTACCGGATAAGGCGCAGCGGTCGGGCTGAACGGGGGGTTCGTGCACACAGCCCAGCTTGGA
GCGAACGACCTACACCGAACTGAGATACCTACAGCGTGAGCTATGAGAAAGCGCCACGCTTCCCGAAGGGAGAAAGGCGGACA
GGTATCCGGTAAGCGGCAGGGTCGGAACAGGAGAGCGCACGAGGGAGCTTCCAGGGGGAAACGCCTGGTATCTTTATAGTCCT
GTCGGGTTTCGCCACCTCTGACTTGAGCGTCGATTTTTGTGATGCTCGTCAGGGGGGCGGAGCCTATGGAAAAACGCCAGCAAC
GCGGCCTTTTTACGGTTCCTGGCCTTTTGCTGGCCTTTTGCTCACATGTTCTTTCCTGCGTTATCCCCTGATTCTGTGGATAACCGTA
TTACCGCCTTTGAGTGAGCTGATACCGCTCGCCGCAGCCGAACGACCGAGCGCAGCGAGTCAGTGAGCGAGGAAGCGGAAGAG
CGCCCAATACGCAAACCGCCTCTCCCCGCGCGTTGGCCGATTCATTAATGCAGCTGGCACGACAGGTTTCCCGACTGGAAAGCGG
GCAGTGAGCGCAACGCAATTAATGTGAGTTAGCTCACTCATTAGGCACCCCAGGCTTTACACTTTATGCTTCCGGCTCGTATGTTGT
GTGGAATTGTGAGCGGATAACAATTTCACACAGGAAACAGCTATGACCATGATTACGCCAAGCGCGCAATTAACCCTCACTAAAG
GGAACAAAAGCTGGAGCTGCAAGC

P284 SCAFFOLD FOR CRISPRA

GCTAGCGAGGGCCTATTTCCCATGATTCCTTCATATTTGCATATACGATACAAGGCTGTTAGAGAGATAATTGGAATTAATTTGACT
GTAAACACAAAGATATTAGTACAAAATACGTGACGTAGAAAGTAATAATTTCTTGGGTAGTTTGCAGTTTTAAAATTATGTTTTAAA
ATGGACTATCATATGCTTACCGTAACTTGAAAGTATTTCGATTTCTTGGCTTTATATATCTT**GTGGAAAGGACGAAACACC**GA
GCATAGCAAGTTAAAATAAGGCTAGTCCGTTATCAACTTGAAAAAGTGGCACCGAGTCGGTGCTTTGGGAGCACATGAGGATCAC
CCATGTGCGACTCCCACAGTCACTGGGGAGTCATCCCTTTTTTGAATTCTGATGCGGTATTTTCTCCTTACGCATCTGTGCGGTATT**T**
CACACCGCATACGTCAAAGCAACCATAGTACGCGCCCTGTAGCGGCGCATTAAGCGCGGCGGGTGTGGTGGTTACGCGCAGCGT
GACCGCTACACTTGCCAGCGCC**T**TAGCGCCCGCTCCTTTCGCTTTCTTCCCTTCCTTTCTCGCCACGTTCGCCGGCTTTCCCCGTCAA
GCTCTAAATCGGGGGCTCCCTTTAGGGTTCCGATTTAGTGCTTTACGGCACCTCGACCCCAAAAAACTTGATTTGGGTGATGGTTC
ACGTAGTGGGCCATCGCCCTGATAGACGGTTTTTCGCCCTTTGACGTTGGAGTCCACGTTCTTTAATAGTGGACTCTTGTTCCAAAC
TGGAACAACACTCAAC**T**CTATCTCGGGCTATTCTTTTGATTTATAAGGGATTTTGCCGATTTCGG**T**CTATTGGTTAAAAAATGAGCT
GATTTAACAAAAATTTAACGCGAATTTTAACAAAATATTAACGTTTACAATTTTATGGTGCACTCTCAGTACAATCTGCTCTGATGCC
GCATAGTTAAGCCAGCCCCGACACCCGCCAACACCCGCTGACGCGCCCTGACGGGCTTGTCTGCTCCCGGCATCCGCTTACAGAC
AAGCTGTGACCGTCTCCGGGAGCTGCATGTGTCAGAGGTTTTCACCGTCATCACCGAAACGCGCGAGACGAAAGGGCCTCGTGA
TACGCCTATTTTTATAGGTTAATGTCATGATAATAATGGTTTCTTAGACGTCAGGTGGCACTTTTCGGGGAAATGTGCGCGGAACCC
CTATTTGTTTATTTTTCTAAATACATTCAAATATGTATCCGCTCATGAGACAATAACCCTGATAAATGCTTCAATAATATTGAAAAAGG
AAGAGTATGAGTATTCAACATTTCCGTGTCGCCCTTATTCCCTTTTTTGCGGCATTTTGCCTTCCTGTTTTTGCTCACCCAGAAACGC
TGGTGAAAGTAAAAGATGCTGAAGATCAGTTGGGTGCACGAGTGGGTTACATCGAACTGGATCTCAACAGCGGTAAGATCCTTG
AGAGTTTTCGCCCCGAAGAACGTTTTCCAATGATGAGCACTTTTAAAGTTCTGCTATGTGGCGCGGTATTATCCCGTATTGACGCCG
GGCAAGAGCAACTCGGTCGCCGCATACACTATTCTCAGAATGACTTGGTTGAGTACTCACCAGTCACAGAAAAGCATCTTACGGA
TGGCATGACAGTAAGAGAATTATGCAGTGCTGCCATAACCATGAGTGATAACACTGCGGCCAACTTACTTCTGACAACGATCGGA
GGACCGAAGGAGCTAACCGCTTTTTTGCACAACATGGGGGATCATGTAACTCGCCTTGATCGTTGGGAACCGGAGCTGAATGAA
GCCATACCAAACGACGAGCGTGACACCACGATGCCTGTAGCAATGGCAACAACGTTGCGCAAACTATTAACTGGCGAACTACTTA
CTCTAGCTTCCCGGCAACAATTAATAGACTGGATGGAGGCGGATAAAGTTGCAGGACCACTTCTGCGCTCGGCCCTTCCGGCTGG
CTGGTTTATTGCTGATAAATCTGGAGCCGGTGAGCGTGG**AAGC**CGCGGTATCATTGCAGCACTGGGGCCAGATGGTAAGCCCTC
CCGTATCGTAGTTATCTACACGACGGGGAGTCAGGCAACTATGGATGAACGAAATAGACAGATCGCTGAGATAGGTGCCTCACTG
ATTAAGCATTGGTAACTGTCAGACCAAGTTTACTCATATATACTTTAGATTGATTTAAAACTTCATTTTTAATTTAAAAGGATCTAGG
TGAAGATCCTTTTTGATAATCTCATGACCAAAATCCCTTAACGTGAGTTTTCGTTCCACTGAGCGTCAGACCCCGTAGAAAAGATC

AAAGGATCTTCTTGAGATCCTTTTTTTCTGCGCGTAATCTGCTGCTTGCAAACAAAAAAACCACCGCTACCAGCGGTGGTTTGTTT
GCCGGATCAAGAGCTACCAACTCTTTTTCCGAAGGTAACTGGCTTCAGCAGAGCGCAGATACCAAATACTGTTCTTCTAGTGTAGC
CGTAGTTAGGCCACCACTTCAAGAACTCTGTAGCACCGCCTACATACCTCGCTCTGCTAATCCTGTTACCAGTGGCTGCTGCCAGTG
GCGATAAGTCGTGTCTTACCGGGTTGGACTCAAGACGATAGTTACCGGATAAGGCGCAGCGGTCGGGCTGAACGGGGGGTTCGT
GCACACAGCCCAGCTTGGAGCGAACGACCTACACCGAACTGAGATACCTACAGCGTGAGCTATGAGAAAGCGCCACGCTTCCCG
AAGGGAGAAAGGCGGACAGGTATCCGGTAAGCGGCAGGGTCGGAACAGGAGAGCGCACGAGGGAGCTTCCAGGGGGAAACG
CCTGGTATCTTTATAGTCCTGTCGGGTTTCGCCACCTCTGACTTGAGCGTCGATTTTTGTGATGCTCGTCAGGGGGGCGGAGCCTAT
GGAAAAACGCCAGCAACGCGGCCTTTTTACGGTTCCTGGCCTTTTGCTGGCCTTTTGCTCA

P326- ACTIVATOR PROTEINS FOR CRISPRA

GTCGACGGATCGGGAGATCTCCCGATCCCCTATGGTGCACTCTCAGTACAATCTGCTCTGATGCCGCATAGTTAAGCCAGTATCTGC
TCCCTGCTTGTGTGTTGGAGGTCGCTGAGTAGTGCGCGAGCAAAATTTAAGCTACAACAAGGCAAGGCTTGACCGACAATTGCAT
GAAGAATCTGCTTAGGGTTAGGCGTTTTGCGCTGCTTCGCGATGTACGGGCCAGATATACGCGTTGACATTGATTATTGACTAGTT
ATTAATAGTAATCAATTACGGGGTCATTAGTTCATAGCCCATATATGGAGTTCCGCGTTACATAACTTACGGTAAATGGCCCGCCTGG
CTGACCGCCCAACGACCCCCGCCCATTGACGTCAATAATGACGTATGTTCCCATAGTAACGCCAATAGGGACTTTCCATTGACGTCA
ATGGGTGGAGTATTTACGGTAAACTGCCCACTTGGCAGTACATCAAGTGTATCATATGCCAAGTACGCCCCCTATTGACGTCAATGA
CGGTAAATGGCCCGCCTGGCATTATGCCCAGTACATGACCTTATGGGACTTTCCTACTTGGCAGTACATCTACGTATTAGTCATCGCT
ATTACCATGGTGATGCGGTTTTGGCAGTACATCAATGGGCGTGGATAGCGGTTTGACTCACGGGGATTTCCAAGTCTCCACCCCAT
TGACGTCAATGGGAGTTTGTTTTGGCACCAAAATCAACGGGACTTTCCAAAATGTCGTAACAACTCCGCCCCATTGACGCAAATG
GGCGGTAGGCGTGTACGGTGGGAGGTCTATATAAGCAGCGCGTTTTGCCTGTACTGGGTCTCTCTGGTTAGACCAGATCTGAGCC
TGGGAGCTCTCTGGCTAACTAGGGAACCCACTGCTTAAGCCTCAATAAAGCTTGCCTTGAGTGCTTCAAGTAGTGTGTGCCCGTCT
GTTGTGTGACTCTGGTAACTAGAGATCCCTCAGACCCTTTTAGTCAGTGTGGAAAATCTCTAGCAGTGGCGCCCGAACAGGGACT
TGAAAGCGAAAGGGAAACCAGAGGAGCTCTCTCGACGCAGGACTCGGCTTGCTGAAGCGCGCACGGCAAGAGGCGAGGGGC
GGCGACTGGTGAGTACGCCAAAAATTTTGACTAGCGGAGGCTAGAAGGAGAGAGATGGGTGCGAGAGCGTCAGTATTAAGCGG
GGGAGAATTAGATCGCGATGGGAAAAAATTCGGTTAAGGCCAGGGGGAAAGAAAAAATATAAATTAAAACATATAGTATGGGCA
AGCAGGGAGCTAGAACGATTCGCAGTTAATCCTGGCCTGTTAGAAACATCAGAAGGCTGTAGACAAATACTGGGACAGCTACAA
CCATCCCTTCAGACAGGATCAGAAGAACTTAGATCATTATATAATACAGTAGCAACCCTCTATTGTGTGCATCAAAGGATAGAGATA
AAAGACACCAAGGAAGCTTTAGACAAGATAGAGGAAGAGCAAAACAAAAGTAAGACCACCGCACAGCAAGCGGCCGCTGATC
TTCAGACCTGGAGGAGGAGATATGAGGGACAATTGGAGAAGTGAATTATATAAATATAAAGTAGTAAAAATTGAACCATTAGGAG
TAGCACCCACCAAGGCAAAGAGAAGAGTGGTGCAGAGAGAAAAAAGAGCAGTGGGAATAGGAGCTTTGTTCCTTGGGTTCTTG
GGAGCAGCAGGAAGCACTATGGGCGCAGCGTCAATGACGCTGACGGTACAGGCCAGACAATTATTGTCTGGTATAGTGCAGCAG
CAGAACAATTTGCTGAGGGCTATTGAGGCGCAACAGCATCTGTTGCAACTCACAGTCTGGGGCATCAAGCAGCTCCAGGCAAGA
ATCCTGGCTGTGGAAAGATACCTAAAGGATCAACAGCTCCTGGGGATTTGGGGTTGCTCTGGAAAACTCATTTGCACCACTGCTG
TGCCTTGGAATGCTAGTTGGAGTAATAAATCTCTGGAACAGATTTGGAATCACACGACCTGGATGGAGTGGGACAGAGAAATTAA
CAATTACACAAGCTTAATACACTCCTTAATTGAAGAATCGCAAAACCAGCAAGAAAAGAATGAACAAGAATTATTGGAATTAGAT
AAATGGGCAAGTTTGTGGAATTGGTTTAACATAACAAATTGGCTGTGGTATATAAAATTATTCATAATGATAGTAGGAGGCTTGGT
AGGTTTAAGAATAGTTTTTGCTGTACTTTCTATAGTGAATAGAGTTAGGCAGGGATATTCACCATTATCGTTTCAGACCCACCTCCC
AACCCCGAGGGGACCCGACAGGCCCGAAGGAATAGAAGAAGAAGGTGGAGAGAGAGACAGAGACAGATCCATTCGATTAGTG
AACGGATCGGCACTGCGTGCGCCAATTCTGCAGACAAATGGCAGTATTCATCCACAATTTTAAAAGAAAAGGGGGGATTGGGGG
GTACAGTGCAGGGGAAAGAATAGTAGACATAATAGCAACAGACATACAAACTAAAGAATTACAAAAACAAATTACAAAAATTCA
AAATTTTCGGGTTTATTACAGGGACAGCAGAGATCCAGTTTGGTTAATTAATGCAAAGATGGATAAAGTTTTAAACAGAGAGGAA
TCTTTGCAGCTAATGGACCTTCTAGGTCTTGAAAGGAGTGGGAATTGGCTCCGGTGCCCGTCAGTGGGCAGAGCGCACATCGCCC
ACAGTCCCCGAGAAGTTGGGGGGAGGGGTCGGCAATTGAACCGGTGCCTAGAGAAGGTGGCGCGGGGTAAACTGGGAAAGTG
ATGTCGTGTACTGGCTCCGCCTTTTTCCCGAGGGTGGGGGAGAACCGTATATAAGTGCAGTAGTCGCCGTGAACGTTCTTTTTCGC
AACGGGTTTGCCGCCAGAACACAGGTAAGTGCCGTGTGTGGTTCCCGCGGGCCTGGCCTCTTTACGGGTTATGGCCCTTGCGTGC
CTTGAATTACTTCCACTGGCTGCAGTACGTGATTCTTGATCCCGAGCTTCGGGTTGGAAGTGGGTGGGAGAGTTCGAGGCCTTGC
GCTTAAGGAGCCCCTTCGCCTCGTGCTTGAGTTGAGGCCTGGCCTGGGCGCTGGGGCCGCCGCGTGCGAATCTGGTGGCACCTTC
GCGCCTGTCTCGCTGCTTTCGATAAGTCTCTAGCCATTTAAAATTTTTGATGACCTGCTGCGACGCTTTTTTTCTGGCAAGATAGTCT

TGTAAATGCGGGCCAAGATCTGCACACTGGTATTTCGGTTTTTGGGGCCGCGGGCGGCGACGGGGCCCGTGCGTCCCAGCGCAC
ATGTTCGGCGAGGCGGGGCCTGCGAGCGCGGCCACCGAGAATCGGACGGGGGTAGTCTCAAGCTGGCCGGCCTGCTCTGGTGC
CTGGCCTCGCGCCGCCGTGTATCGCCCCGCCCTGGGCGGCAAGGCTGGCCCGGTCGGCACCAGTTGCGTGAGCGGAAAGATGGC
CGCTTCCCGGCCCTGCTGCAGGGAGCTCAAAATGGAGGACGCGGCGCTCGGGAGAGCGGGCGGGTGAGTCACCCACACAAAG
GAAAAGGGCCTTTCCGTCCTCAGCCGTCGCTTCATGTGACTCCACGGAGTACCGGGCGCCGTCCAGGCACCTCGATTAGTTCTCG
AGCTTTTGGAGTACGTCGTCTTTAGGTTGGGGGGAGGGGTTTTATGCGATGGAGTTTCCCCACACTGAGTGGGTGGAGACTGAA
GTTAGGCCAGCTTGGCACTTGATGTAATTCTCCTTGGAATTTGCCCTTTTTGAGTTTGGATCTTGGTTCATTCTCAAGCCTCAGACA
GTGGTTCAAAGTTTTTTTCTTCCATTTCAGGTGTCGTGAC**GTACG**GCCACC**ATGGCTTCAAACTTTACTCAGTTCGTGCT**
CGTGGACAATGGTGGGACAGGGGATGTGACAGTGGCTCCTTCTAATTTCGCTAATGGGGTGGCAGAGTG
GATCAGCTCCAACTCACGGAGCCAGGCCTACAAGGTGACATGCAGCGTCAGGCAGTCTAGTGCCCAGAA
G**AGAAAGTATACCATCAAGGTGGAGGTCCCCAAAGTGGCTACCCAGACAGTGGGCGGAGTCGAACTGCC**
TGTCGCCGCTTGGAGGTCCTACCTGAACATGGAGCTCACTATCCCAATTTTCGCTACCAATTCTGACTGTGA
ACTCATCGTGAAGGCAATGCAGGGGCTCCTCAAAGACGGTAATCCTATCCCTTCCGCCATCGCCGCTAACT
CAGGTATCTACAGCGCT**GGAGGAGGTGGAAGCGGAGGAGGAGGAAGCGGAGGAGGAGGTAGC**GGACCTA
AGAAAAAGAGGAAGGTGGCGGCCGCTGGATCC**CCTTCAGGGCAGATCAGCAACCAGGCCCTGGCTCTGGCCCCT**
AGCTCCGCTCCAGTGCTGGCCCAGACTATGGTGCCCTCTAGTGCTATGGTGCCTCTGGCCCAGCCACCTGC
TCCAGCCCCTGTGCTGACCCCAGGACCACCCCAGTCACTGAGCGCTCCAGTGCCCAAGTCTACACAGGCC
GGCGAGGGGACTCTGAGTGAAGCTCTGCTGCACCTGCAGTTCGACGCTGATGAGGACCTGGGAGCTCTG
CTGGGGAACAGCACCGATCCCGGAGTGTTCACAGATCTGGCCTCCGTGGACAACTCTGAGTTTCAGCAGC
TGCTGAATCAGGGCGTGTCCATGTCTCATAGTACAGCCGAACCAATGCTGATGGAGTACCCCGAAGCCATT
ACCCGGCTGGTGACCGGCAGCCAGCGGCCCCCCGACCCCGCTCCAACTCCCCTGGGAACCAGCGGCCTG
CCTAATGGGCTGTCCGGAGATGAAGACTTCTCAAGCATCGCTGATATGGACTTTAGTGCCCTGCTGTCACA
GATTTCCTCTAGTGGGCAGGGAGGAGGTGGAAGCGGCTTCAGCGTGGACACCAGTGCCCTGCTGGACCT
GTTCAGCCCCTCGGTGACCGTGCCCGACATGAGCCTGCCTGACCTTGACAGCAGCCTGGCCAGTATCCAA
GAGCTCCTGTCTCCCCAGGAGCCCCCCAGGCCTCCCGAGGCAGAGAACAGCAGCCCGGATTCAGGGAAG
CAGCTGGTGCACTACACAGCGCAGCCGCTGTTCCTGCTGGACCCCGGCTCCGTGGACACCGGGAGCAAC
GACCTGCCGGTGCTGTTTGAGCTGGGAGAGGGCTCCTACTTCTCCGAAGGGGACGGCTTCGCCGAGGAC
CCCACCATCTCCCTGCTGACAGGCTCGGAGCCTCCCAAAGCCAAGGACCCCACTGTCTCCGCTAGC**GGCAG**
TGGAGCCACGAACTTCTCTCTGTTAAAGCAAGCAGGAGACGTGGAAGAAAACCCCGGTCCTATG**GCCCCA**
AAGAAGAAGCGGAAGGTCGGTATCCACGGAGTCCCAGCAGCCGAAAACCTGTACTTCCAATCCAATGCAGCTAGC
GACCACTATCTGGACATCAGACTGAGGCCCGATCCTGAGTTCCCTCCCGCCCAGCTGATGAGCGTGCTGTTTGGCAAGCTGCATCA
GGCTCTGGTCGCCCAAGGCGGAGACAGAATCGGCGTGTCCTTCCCCGACCTGGACGAGTCCCGGAGTCGCCTGGGCGAGCGGCT
GAGAATCCACGCCAGCGCAGACGATCTGCGCGCCCTGCTGGCCCGGCCTTGGCTGGAGGGCCTGCGGGATCATCTGCAGTTTGG
CGAGCCCGCCGTGGTGCCACACCCAACACCCTACCGCCAGGTGAGCCGCGTGCAGGCCAAGTCAAATCCCGAGAGACTGCGGCG
GAGGCTGATGAGGCGACATGATCTGAGCGAGGAGGAGGCCAGAAAGAGAATCCCCGACACAGTGGCCAGAGCCCTGGATCTGC
CATTTGTGACCCTGCGGAGCCAGAGCACTGGCCAGCATTTCAGACTGTTCATCAGACACGGGCCCCTGCAGGTGACAGCCGAGG
AGGGCGGATTTACATGCTATGGCCTGTCTAAAGGCGGCTTCGTGCCCTGGTTCGCTAGC**GGCAGTGGAGAGGGCAGAGG**
AAGTCTGCTAACATGCGGTGACGTCGAGGAGAATCCTGGCCCAATGGCCAAGTTGACCAGTGCCGTTCCGGTGCTC
ACCGCGCGCGACGTCGCCGGAGCGGTCGAGTTCTGGACCGACCGGCTCGGGTTCTCCCGGGACTTCGTGGAGGACGACTTCGCC
GGTGTGGTCCGGGACGACGTGACCCTGTTCATCAGCGCGGTCCAGGACCAGGTGGTGCCGGACAACACCCTGGCCTGGGTGTGG
GTGCGCGGCCTGGACGAGCTGTACGCCGAGTGGTCGGAGGTCGTGTCCACGAACTTCCGGGACGCCTCCGGGCCGGCCATGACC
GAGATCGGCGAGCAGCCGTGGGGGCGGGAGTTCGCCCTGCGCGACCCGGCCGGCAACTGCGTGCACTTCGTGGCCGAGGAGCA
GGACTGAGAATTCGATATCAAGCTTATCGATAATCAACCTCTGGATTACAAAATTTGTGAAAGATTGACTGGTATTCTTAACTATGT
TGCTCCTTTTACGCTATGTGGATACGCTGCTTTAATGCCTTTGTATCATGCTATTGCTTCCCGTATGGCTTTCATTTTCTCCTCCTTGTA
TAAATCCTGGTTGCTGTCTCTTTATGAGGAGTTGTGGCCCGTTGTCAGGCAACGTGGCGTGGTGTGCACTGTGTTTGCTGACGCAA
CCCCCACTGGTTGGGGCATTGCCACCACCTGTCAGCTCCTTTCCGGGACTTTCGCTTTCCCCCTCCCTATTGCCACGGCGGAACTCA
TCGCCGCCTGCCTTGCCCGCTGCTGGACAGGGGCTCGGCTGTTGGGCACTGACAATTCCGTGGTGTTGTCGGGGAAATCATCGTC
CTTTCCTTGGCTGCTCGCCTGTGTTGCCACCTGGATTCTGCGCGGGACGTCCTTCTGCTACGTCCCTTCGGCCCTCAATCCAGCGGA

CCTTCCTTCCCGCGGCCTGCTGCCGGCTCTGCGGCCTCTTCCGCGTCTTCGCCTTCGCCCTCAGACGAGTCGGATCTCCCTTTGGGC
CGCCTCCCCGCATCGATACCGTCGACCTCGAGACCTAGAAAAACATGGAGCAATCACAAGTAGCAATACAGCAGCTACCAATGCT
GATTGTGCCTGGCTAGAAGCACAAGAGGAGGAGGAGGTGGGTTTTCCAGTCACACCTCAGGTACCTTTAAGACCAATGACTTAC
AAGGCAGCTGTAGATCTTAGCCACTTTTTAAAAGAAAAGGGGGGACTGGAAGGGCTAATTCACTCCCAACGAAGACAAGATATC
CTTGATCTGTGGATCTACCACACACAAGGCTACTTCCCTGATTGGCAGAACTACACACCAGGGCCAGGGATCAGATATCCACTGAC
CTTTGGATGGTGCTACAAGCTAGTACCAGTTGAGCAAGAGAAGGTAGAAGAAGCCAATGAAGGAGAGAACACCCGCTTGTTAC
ACCCTGTGAGCCTGCATGGGATGGATGACCCGGAGAGAGAAGTATTAGAGTGGAGGTTTGACAGCCGCCTAGCATTTCATCACAT
GGCCCGAGAGCTGCATCCGGACTGTACTGGGTCTCTCTGGTTAGACCAGATCTGAGCCTGGGAGCTCTCTGGCTAACTAGGGAAC
CCACTGCTTAAGCCTCAATAAAGCTTGCCTTGAGTGCTTCAAGTAGTGTGTGCCCGTCTGTTGTGTGACTCTGGTAACTAGAGATCC
CTCAGACCCTTTTAGTCAGTGTGGAAAATCTCTAGCAGGGCCCGTTTAAACCCGCTGATCAGCCTCGACTGTGCCTTCTAGTTGCC
AGCCATCTGTTGTTTGCCCCTCCCCCGTGCCTTCCTTGACCCTGGAAGGTGCCACTCCCACTGTCCTTTCCTAATAAAATGAGGAAA
TTGCATCGCATTGTCTGAGTAGGTGTCATTCTATTCTGGGGGGTGGGGTGGGGCAGGACAGCAAGGGGGAGGATTGGGAAGAC
AATAGCAGGCATGCTGGGGATGCGGTGGGCTCTATGGCTTCTGAGGCGGAAAGAACCAGCTGGGGCTCTAGGGGGTATCCCCAC
GCGCCCTGTAGCGGCGCATTAAGCGCGGCGGGTGTGGTGGTTACGCGCAGCGTGACCGCTACACTTGCCAGCGCCCTAGCGCCC
GCTCCTTTCGCTTTCTTCCCTTCCTTTCTCGCCACGTTCGCCGGCTTTCCCCGTCAAGCTCTAAATCGGGGGCTCCCTTTAGGGTTCC
GATTTAGTGCTTTACGGCACCTCGACCCCAAAAAACTTGATTAGGGTGATGGTTCACGTAGTGGGCCATCGCCCTGATAGACGGTT
TTTCGCCCTTTGACGTTGGAGTCCACGTTCTTTAATAGTGGACTCTTGTTCCAAACTGGAACAACACTCAACCCTATCTCGGTCTAT
TCTTTTGATTTATAAGGGATTTTGCCGATTTCGGCCTATTGGTTAAAAAATGAGCTGATTTAACAAAAATTTAACGCGAATTAATTC
TGTGGAATGTGTGTCAGTTAGGGTGTGGAAAGTCCCCAGGCTCCCCAGCAGGCAGAAGTATGCAAAGCATGCATCTCAATTAGTC
AGCAACCAGGTGTGGAAAGTCCCCAGGCTCCCCAGCAGGCAGAAGTATGCAAAGCATGCATCTCAATTAGTCAGCAACCATAGTC
CCGCCCCTAACTCCGCCCATCCCGCCCCTAACTCCGCCCAGTTCCGCCCATTCTCCGCCCCATGGCTGACTAATTTTTTTTATTTATGC
AGAGGCCGAGGCCGCCTCTGCCTCTGAGCTATTCCAGAAGTAGTGAGGAGGCTTTTTTGGAGGCCTAGGCTTTTGCAAAAAGCT
CCCGGGAGCTTGTATATCCATTTTCGGATCTGATCAGCACGTGTTGACAATTAATCATCGGCATAGTATATCGGCATAGTATAATACG
ACAAGGTGAGGAACTAAACCATGGCCAAGTTGACCAGTGCCGTTCCGGTGCTCACCGCGCGCGACGTCGCCGGAGCGGTCGAGT
TCTGGACCGACCGGCTCGGGTTCTCCCGGGACTTCGTGGAGGACGACTTCGCCGGTGTGGTCCGGGACGACGTGACCCTGTTCA
TCAGCGCGGTCCAGGACCAGGTGGTGCCGGACAACACCCTGGCCTGGGTGTGGGTGCGCGGCCTGGACGAGCTGTACGCCGAG
TGGTCGGAGGTCGTGTCCACGAACTTCCGGGACGCCTCCGGGCCGGCCATGACCGAGATCGGCGAGCAGCCGTGGGGGCGGGA
GTTCGCCCTGCGCGACCCGGCCGGCAACTGCGTGCACTTCGTGGCCGAGGAGCAGGACTGACACGTGCTACGAGATTTCGATTC
CACCGCCGCCTTCTATGAAAGGTTGGGCTTCGGAATCGTTTTCCGGGACGCCGGCTGGATGATCCTCCAGCGCGGGGATCTCATG
CTGGAGTTCTTCGCCCACCCCAACTTGTTTATTGCAGCTTATAATGGTTACAAATAAAGCAATAGCATCACAAATTTCACAAATAAA
GCATTTTTTTCACTGCATTCTAGTTGTGGTTTGTCCAAACTCATCAATGTATCTTATCATGTCTGTATACCGTCGACCTCTAGCTAGAG
CTTGGCGTAATCATGGTCATAGCTGTTTCCTGTGTGAAATTGTTATCCGCTCACAATTCCACACAACATACGAGCCGGAAGCATAAA
GTGTAAAGCCTGGGGTGCCTAATGAGTGAGCTAACTCACATTAATTGCGTTGCGCTCACTGCCCGCTTTCCAGTCGGGAAACCTGT
CGTGCCAGCTGCATTAATGAATCGGCCAACGCGCGGGGAGAGGCGGTTTGCGTATTGGGCGCTCTTCCGCTTCCTCGCTCACTGA
CTCGCTGCGCTCGGTCGTTCGGCTGCGGCGAGCGGTATCAGCTCACTCAAAGGCGGTAATACGGTTATCCACAGAATCAGGGGAT
AACGCAGGAAAGAACATGTGAGCAAAAGGCCAGCAAAAGGCCAGGAACCGTAAAAAGGCCGCGTTGCTGGCGTTTTTCCATAG
GCTCCGCCCCCCTGACGAGCATCACAAAAATCGACGCTCAAGTCAGAGGTGGCGAAACCCGACAGGACTATAAAGATACCAGGC
GTTTCCCCCTGGAAGCTCCCTCGTGCGCTCTCCTGTTCCGACCCTGCCGCTTACCGGATACCTGTCCGCCTTTCTCCCTTCGGGAAG
CGTGGCGCTTTCTCATAGCTCACGCTGTAGGTATCTCAGTTCGGTGTAGGTCGTTCGCTCCAAGCTGGGCTGTGTGCACGAACCCC
CCGTTCAGCCCGACCGCTGCGCCTTATCCGGTAACTATCGTCTTGAGTCCAACCCGGTAAGACACGACTTATCGCCACTGGCAGCA
GCCACTGGTAACAGGATTAGCAGAGCGAGGTATGTAGGCGGTGCTACAGAGTTCTTGAAGTGGTGGCCTAACTACGGCTACACTA
GAAGAACAGTATTTGGTATCTGCGCTCTGCTGAAGCCAGTTACCTTCGGAAAAAGAGTTGGTAGCTCTTGATCCGGCAAACAAAC
CACCGCTGGTAGCGGTGGTTTTTTTGTTTGCAAGCAGCAGATTACGCGCAGAAAAAAAGGATCTCAAGAAGATCCTTTGATCTTT
TCTACGGGGTCTGACGCTCAGTGGAACGAAAACTCACGTTAAGGGATTTTGGTCATGAGATTATCAAAAAGGATCTTCACCTAGA
TCCTTTTAAATTAAAAATGAAGTTTTAAATCAATCTAAAGTATATATGAGTAAACTTGGTCTGACAGTTACCAATGCTTAATCAGTGA
GGCACCTATCTCAGCGATCTGTCTATTTCGTTCATCCATAGTTGCCTGACTCCCCGTCGTGTAGATAACTACGATACGGGAGGGCTTA
CCATCTGGCCCCAGTGCTGCAATGATACCGCGAGACCCACGCTCACCGGCTCCAGATTTATCAGCAATAAACCAGCCAGCCGGAA
GGGCCGAGCGCAGAAGTGGTCCTGCAACTTTATCCGCCTCCATCCAGTCTATTAATTGTTGCCGGGAAGCTAGAGTAAGTAGTTCG

CCAGTTAATAGTTTGCGCAACGTTGTTGCCATTGCTACAGGCATCGTGGTGTCACGCTCGTCGTTTGGTATGGCTTCATTCAGCTCC
GGTTCCCAACGATCAAGGCGAGTTACATGATCCCCCATGTTGTGCAAAAAAGCGGTTAGCTCCTTCGGTCCTCCGATCGTTGTCAG
AAGTAAGTTGGCCGCAGTGTTATCACTCATGGTTATGGCAGCACTGCATAATTCTCTTACTGTCATGCCATCCGTAAGATGCTTTTCT
GTGACTGGTGAGTACTCAACCAAGTCATTCTGAGAATAGTGTATGCGGCGACCGAGTTGCTCTTGCCCGGCGTCAATACGGGATA
ATACCGCGCCACATAGCAGAACTTTAAAAGTGCTCATCATTGGAAAACGTTCTTCGGGGCGAAAACTCTCAAGGATCTTACCGCT
GTTGAGATCCAGTTCGATGTAACCCACTCGTGCACCCAACTGATCTTCAGCATCTTTTACTTTCACCAGCGTTTCTGGGTGAGCAAA
AACAGGAAGGCAAAATGCCGCAAAAAAGGGAATAAGGGCGACACGGAAATGTTGAATACTCATACTCTTCCTTTTTCAATATTAT
TGAAGCATTTATCAGGGTTATTGTCTCATGAGCGGATACATATTTGAATGTATTTAGAAAAATAAACAAATAGGGGTTCCGCGCAC
ATTTCCCCGAAAAGTGCCACCTGAC

dCas9-VP64

GTCGACGGATCGGGAGATCTCCCGATCCCCTATGGTGCACTCTCAGTACAATCTGCTCTGATGCCGCATAGTTAAGCCAGTATCTGC
TCCCTGCTTGTGTGTTGGAGGTCGCTGAGTAGTGCGCGAGCAAAATTTAAGCTACAACAAGGCAAGGCTTGACCGACAATTGCAT
GAAGAATCTGCTTAGGGTTAGGCGTTTTGCGCTGCTTCGCGATGTACGGGCCAGATATACGCGTTGACATTGATTATTGACTAGTT
ATTAATAGTAATCAATTACGGGGTCATTAGTTCATAGCCCATATATGGAGTTCCGCGTTACATAACTTACGGTAAATGGCCCGCCTGG
CTGACCGCCCAACGACCCCCGCCCATTGACGTCAATAATGACGTATGTTCCCATAGTAACGCCAATAGGGACTTTCCATTGACGTCA
ATGGGTGGAGTATTTACGGTAAACTGCCCACTTGGCAGTACATCAAGTGTATCATATGCCAAGTACGCCCCCTATTGACGTCAATGA
CGGTAAATGGCCCGCCTGGCATTATGCCCAGTACATGACCTTATGGGACTTTCCTACTTGGCAGTACATCTACGTATTAGTCATCGCT
ATTACCATGGTGATGCGGTTTTGGCAGTACATCAATGGGCGTGGATAGCGGTTTGACTCACGGGGATTTCCAAGTCTCCACCCCAT
TGACGTCAATGGGAGTTTGTTTTGGCACCAAAATCAACGGGACTTTCCAAAATGTCGTAACAACTCCGCCCCATTGACGCAAATG
GGCGGTAGGCGTGTACGGTGGGAGGTCTATATAAGCAGCGCGTTTTGCCTGTACTGGGTCTCTCTGGTTAGACCAGATCTGAGCC
TGGGAGCTCTCTGGCTAACTAGGGAACCCACTGCTTAAGCCTCAATAAAGCTTGCCTTGAGTGCTTCAAGTAGTGTGTGCCCGTCT
GTTGTGTGACTCTGGTAACTAGAGATCCCTCAGACCCTTTTAGTCAGTGTGGAAAATCTCTAGCAGTGGCGCCCGAACAGGGACT
TGAAAGCGAAAGGGAAACCAGAGGAGCTCTCTCGACGCAGGACTCGGCTTGCTGAAGCGCGCACGGCAAGAGGCGAGGGGC
GGCGACTGGTGAGTACGCCAAAAATTTTGACTAGCGGAGGCTAGAAGGAGAGAGATGGGTGCGAGAGCGTCAGTATTAAGCGG
GGGAGAATTAGATCGCGATGGGAAAAAATTCGGTTAAGGCCAGGGGGAAAGAAAAAATATAAATTAAAACATATAGTATGGGCA
AGCAGGGAGCTAGAACGATTCGCAGTTAATCCTGGCCTGTTAGAAACATCAGAAGGCTGTAGACAAATACTGGGACAGCTACAA
CCATCCCTTCAGACAGGATCAGAAGAACTTAGATCATTATATAATACAGTAGCAACCCTCTATTGTGTGCATCAAAGGATAGAGATA
AAAGACACCAAGGAAGCTTTAGACAAGATAGAGGAAGAGCAAAACAAAAGTAAGACCACCGCACAGCAAGCGGCCGCTGATC
TTCAGACCTGGAGGAGGAGATATGAGGGACAATTGGAGAAGTGAATTATATAAATATAAAGTAGTAAAAATTGAACCATTAGGAG
TAGCACCCACCAAGGCAAAGAGAAGAGTGGTGCAGAGAGAAAAAAGAGCAGTGGGAATAGGAGCTTTGTTCCTTGGGTTCTTG
GGAGCAGCAGGAAGCACTATGGGCGCAGCGTCAATGACGCTGACGGTACAGGCCAGACAATTATTGTCTGGTATAGTGCAGCAG
CAGAACAATTTGCTGAGGGCTATTGAGGCGCAACAGCATCTGTTGCAACTCACAGTCTGGGGCATCAAGCAGCTCCAGGCAAGA
ATCCTGGCTGTGGAAAGATACCTAAAGGATCAACAGCTCCTGGGGATTTGGGGTTGCTCTGGAAAACTCATTTGCACCACTGCTG
TGCCTTGGAATGCTAGTTGGAGTAATAAATCTCTGGAACAGATTTGGAATCACACGACCTGGATGGAGTGGGACAGAGAAATTAA
CAATTACACAAGCTTAATACACTCCTTAATTGAAGAATCGCAAAACCAGCAAGAAAAGAATGAACAAGAATTATTGGAATTAGAT
AAATGGGCAAGTTTGTGGAATTGGTTTAACATAACAAATTGGCTGTGGTATATAAAATTATTCATAATGATAGTAGGAGGCTTGGT
AGGTTTAAGAATAGTTTTTGCTGTACTTTCTATAGTGAATAGAGTTAGGCAGGGATATTCACCATTATCGTTTCAGACCCACCTCCC
AACCCCGAGGGGACCCGACAGGCCCGAAGGAATAGAAGAAGAAGGTGGAGAGAGAGACAGAGACAGATCCATTCGATTAGTG
AACGGATCGGCACTGCGTGCGCCAATTCTGCAGACAAATGGCAGTATTCATCCACAATTTTAAAAGAAAAGGGGGGATTGGGGG
GTACAGTGCAGGGGAAAGAATAGTAGACATAATAGCAACAGACATACAAACTAAAGAATTACAAAAACAAATTACAAAAATTCA
AAATTTTCGGGTTTATTACAGGGACAGCAGAGATCCAGTTTGGTTAATTAATGCAAAGATGGATAAAGTTTTAAACAGAGAGGAA
TCTTTGCAGCTAATGGACCTTCTAGGTCTTGAAAGGAGTGGGAATTGGCTCCGGTGCCCGTCAGTGGGCAGAGCGCACATCGCCC
ACAGTCCCCGAGAAGTTGGGGGGAGGGGTCGGCAATTGAACCGGTGCCTAGAGAAGGTGGCGCGGGGTAAACTGGGAAAGTG
ATGTCGTGTACTGGCTCCGCCTTTTTCCCGAGGGTGGGGGAGAACCGTATATAAGTGCAGTAGTCGCCGTGAACGTTCTTTTTCGC
AACGGGTTTGCCGCCAGAACACAGGTAAGTGCCGTGTGTGGTTCCCGCGGGCCTGGCCTCTTTACGGGTTATGGCCCTTGCGTGC
CTTGAATTACTTCCACTGGCTGCAGTACGTGATTCTTGATCCCGAGCTTCGGGTTGGAAGTGGGTGGGAGAGTTCGAGGCCTTGC
GCTTAAGGAGCCCCTTCGCCTCGTGCTTGAGTTGAGGCCTGGCCTGGGCGCTGGGGCCGCCGCGTGCGAATCTGGTGGCACCTTC

GCGCCTGTCTCGCTGCTTTCGATAAGTCTCTAGCCATTTAAAATTTTTGATGACCTGCTGCGACGCTTTTTTTCTGGCAAGATAGTCT
TGTAAATGCGGGCCAAGATCTGCACACTGGTATTTCGGTTTTTGGGGCCGCGGGCGGCGACGGGGCCCGTGCGTCCCAGCGCAC
ATGTTCGGCGAGGCGGGGCCTGCGAGCGCGGCCACCGAGAATCGGACGGGGGTAGTCTCAAGCTGGCCGGCCTGCTCTGGTGC
CTGGCCTCGCGCCGCCGTGTATCGCCCCGCCCTGGGCGGCAAGGCTGGCCCGGTCGGCACCAGTTGCGTGAGCGGAAAGATGGC
CGCTTCCCGGCCCTGCTGCAGGGAGCTCAAAATGGAGGACGCGGCGCTCGGGAGAGCGGGCGGGTGAGTCACCCACACAAAG
GAAAAGGGCCTTTCCGTCCTCAGCCGTCGCTTCATGTGACTCCACGGAGTACCGGGCGCCGTCCAGGCACCTCGATTAGTTCTCG
AGCTTTTGGAGTACGTCGTCTTTAGGTTGGGGGGAGGGGTTTTATGCGATGGAGTTTCCCCACACTGAGTGGGTGGAGACTGAA
GTTAGGCCAGCTTGGCACTTGATGTAATTCTCCTTGGAATTTGCCCTTTTTGAGTTTGGATCTTGGTTCATTCTCAAGCCTCAGACA
GTGGTTCAAAGTTTTTTTCTTCCATTTCAGGTGTCGTGAC**GTACG**GCCACCATG**AGCCCCAAGAA**G**AAGAG**A**AAGGTG**
GAGGCCAGCGACAAGAAGTACAGCATCGGCCTGGCCATCGGCACCAACTCTGTGGGCTGGGCCGTGATC
ACCGACGAGTACAAGGTGCCCAGCAAGAAATTCAAGGTGCTGGGCAACACCGACCGGCACAGCATCAA
GAAGAACCTGATCGGAGCCCTGCTGTTCGACAGCGGCGAAACAGCCGAGGCCACCCGGCTGAAGAGAA
CCGCCAGAAGAAGATACACCAGACGGAAGAACCGGATCTGCTATCTGCAAGAGATCTTCAGCAACGAGA
TGGCCAAGGTGGACGACAGCTTCTTCCACAGACTGGAAGAGTCCTTCCTGGTGGAAGAGGATAAGAAGC
ACGAGCGGCACCCCATCTTCGGCAACATCGTGGACGAGGTGGCCTACCACGAGAAGTACCCCACCATCTA
CCACCTGAGAAAGAAACTGGTGGACAGCACCGACAAGGCCGACCTGCGGCTGATCTATCTGGCCCTGGC
CCACATGATCAAGTTCCGGGGCCACTTCCTGATCGAGGGCGACCTGAACCCCGACAACAGCGACGTGGA
CAAGCTGTTCATCCAGCTGGTGCAGACCTACAACCAGCTGTTCGAGGAAAACCCCATCAACGCCAGCGGC
GTGGACGCCAAGGCCATCCTGTCTGCCAGACTGAGCAAGAGCAGACGGCTGGAAAATCTGATCGCCCAG
CTGCCCGGCGAGAAGAAGAATGGCCTGTTCGGCAACCTGATTGCCCTGAGCCTGGGCCTGACCCCCAACT
TCAAGAGCAACTTCGACCTGGCCGAGGATGCCAAACTGCAGCTGAGCAAGGACACCTACGACGACGACC
TGGACAACCTGCTGGCCCAGATCGGCGACCAGTACGCCGACCTGTTTCTGGCCGCCAAGAACCTGTCCGA
CGCCATCCTGCTGAGCGACATCCTGAGAGTGAACACCGAGATCACCAAGGCCCCCCTGAGCGCCTCTATG
ATCAAGAGATACGACGAGCACCACCAGGACCTGACCCTGCTGAAAGCTCTCGTGCGGCAGCAGCTGCCT
GAGAAGTACAAAGAGATTTTCTTCGACCAGAGCAAGAACGGCTACGCCGGCTACATTGACGGCGGAGCC
AGCCAGGAAGAGTTCTACAAGTTCATCAAGCCCATCCTGGAAAAGATGGACGGCACCGAGGAACTGCTC
GTGAAGCTGAACAGAGAGGACCTGCTGCGGAAGCAGCGGACCTTCGACAACGGCAGCATCCCCCACCA
GATCCACCTGGGAGAGCTGCACGCCATTCTGCGGCGGCAGGAAGATTTTTACCCATTCCTGAAGGACAAC
CGGGAAAAGATCGAGAAGATCCTGACCTTCCGCATCCCCTACTACGTGGGCCCTCTGGCCAGGGGAAACA
GCAGATTCGCCTGGATGACCAGAAAGAGCGAGGAAACCATCACCCCCTGGAACTTCGAGGAAGTGGTG
GACAAGGGCGCTTCCGCCCAGAGCTTCATCGAGCGGATGACCAACTTCGATAAGAACCTGCCCAACGAG
AAGGTGCTGCCCAAGCACAGCCTGCTGTACGAGTACTTCACCGTGTATAACGAGCTGACCAAAGTGAAAT
ACGTGACCGAGGGAATGAGAAAGCCCGCCTTCCTGAGCGGCGAGCAGAAAAAGGCCATCGTGGACCTG
CTGTTCAAGACCAACCGGAAAGTGACCGTGAAGCAGCTGAAAGAGGACTACTTCAAGAAAATCGAGTG
CTTCGACTCCGTGGAAATCTCCGGCGTGGAAGATCGGTTCAACGCCTCCCTGGGCACATACCACGATCTGC
TGAAAATTATCAAGGACAAGGACTTCCTGGACAATGAGGAAAACGAGGACATTCTGGAAGATATCGTGC
TGACCCTGACACTGTTTGAGGACAGAGAGATGATCGAGGAACGGCTGAAAACCTATGCCCACCTGTTCG
ACGACAAAGTGATGAAGCAGCTGAAGCGGCGGAGATACACCGGCTGGGGCAGGCTGAGCCGGAAGCT
GATCAACGGCATCCGGGACAAGCAGTCCGGCAAGACAATCCTGGATTTCCTGAAGTCCGACGGCTTCGCC
AACAGAAACTTCATGCAGCTGATCCACGACGACAGCCTGACCTTTAAAGAGGACATCCAGAAAGCCCAG
GTGTCCGGCCAGGGCGATAGCCTGCACGAGCACATTGCCAATCTGGCCGGCAGCCCCGCCATTAAGAAG
GGCATCCTGCAGACAGTGAAGGTGGTGGACGAGCTCGTGAAAGTGATGGGCCGGCACAAGCCCGAGAA
CATCGTGATCGAAATGGCCAGAGAGAACCAGACCACCCAGAAGGGACAGAAGAACAGCCGCGAGAGA
ATGAAGCGGATCGAAGAGGGCATCAAAGAGCTGGGCAGCCAGATCCTGAAAGAACACCCCGTGGAAAA
CACCCAGCTGCAGAACGAGAAGCTGTACCTGTACTACCTGCAGAATGGGCGGGATATGTACGTGGACCAG
GAACTGGACATCAACCGGCTGTCCGACTACGATGTGGACGC**TATCGTGCCTCAGAGCTTTCTGAAGGACG**
ACTCCATCGACAACAAGGTGCTGACCAGAAGCGACAAGAACCGGGGCAAGAGCGACAACGTGCCCTCC
GAAGAGGTCGTGAAGAAGATGAAGAACTACTGGCGGCAGCTGCTGAACGCCAAGCTGATTACCCAGAG

AAAGTTCGACAATCTGACCAAGGCCGAGAGAGGCGGCCTGAGCGAACTGGATAAGGCCGGCTTCATCAA
GAGACAGCTGGTGGAAACCCGGCAGATCACAAAGCACGTGGCACAGATCCTGGACTCCCGGATGAACAC
TAAGTACGACGAGAATGACAAGCTGATCCGGGAAGTGAAAGTGATCACCCTGAAGTCCAAGCTGGTGTC
CGATTTCCGGAAGGATTTCCAGTTTTACAAAGTGCGCGAGATCAACAACTACCACCACGCCCACGACGCC
TACCTGAACGCCGTCGTGGGAACCGCCCTGATCAAAAAGTACCCTAAGCTGGAAAGCGAGTTCGTGTACG
GCGACTACAAGGTGTACGACGTGCGGAAGATGATCGCCAAGAGCGAGCAGGAAATCGGCAAGGCTACC
GCCAAGTACTTCTTCTACAGCAACATCATGAACTTTTTCAAGACCGAGATTACCCTGGCCAACGGCGAGAT
CCGGAAGCGGCCTCTGATCGAGACAAACGGCGAAACCGGGGAGATCGTGTGGGATAAGGGCCGGGATT
TTGCCACCGTGCGGAAAGTGCTGAGCATGCCCCAAGTGAATATCGTGAAAAAGACCGAGGTGCAGACAG
GCGGCTTCAGCAAAGAGTCTATCCTGCCCAAGAGGAACAGCGATAAGCTGATCGCCAGAAAGAAGGACT
GGGACCCTAAGAAGTACGGCGGCTTCGACAGCCCCACCGTGGCCTATTCTGTGCTGGTGGTGGCCAAAGT
GGAAAAGGGCAAGTCCAAGAAACTGAAGAGTGTGAAAGAGCTGCTGGGGATCACCATCATGGAAAGA
AGCAGCTTCGAGAAGAATCCCATCGACTTTCTGGAAGCCAAGGGCTACAAAGAAGTGAAAAAGGACCT
GATCATCAAGCTGCCTAAGTACTCCCTGTTCGAGCTGGAAAACGGCCGGAAGAGAATGCTGGCCTCTGCC
GGCGAACTGCAGAAGGGAAACGAACTGGCCCTGCCCTCCAAATATGTGAACTTCCTGTACCTGGCCAGCC
ACTATGAGAAGCTGAAGGGCTCCCCCGAGGATAATGAGCAGAAACAGCTGTTTGTGGAACAGCACAAGC
ACTACCTGGACGAGATCATCGAGCAGATCAGCGAGTTCTCCAAGAGAGTGATCCTGGCCGACGCTAATCT
GGACAAAGTGCTGTCCGCCTACAACAAGCACCGGGATAAGCCCATCAGAGAGCAGGCCGAGAATATCAT
CCACCTGTTTACCCTGACCAATCTGGGAGCCCCTGCCGCCTTCAAGTACTTTGACACCACCATCGACCGGA
AGAGGTACACCAGCACCAAAGAGGTGCTGGACGCCACCCTGATCCACCAGAGCATCACCGGCCTGTACG
AGACACGGATCGACCTGTCTCAGCTGGGAGGCGACAGCGCTGGAGGAGGTGGAAGCGGAGGAGGAGGA
AGCGGAGGAGGAGGTAGCGGACCTAAGAAAAAGAGGAAGGTGGCGGCCGCTGGATCCGGACGGGCTGACGCATT
GGACGATTTTGATCTGGATATGCTGGGAAGTGACGCCCTCGATGATTTTGACCTTGACATGCTTGGTTCGG
ATGCCCTTGATGACTTTGACCTCGACATGCTCGGCAGTGACGCCCTTGATGATTTCGACCTGGACATGCTG
ATTAACGCTAGCGGCAGTGGAGAGGGCAGAGGAAGTCTGCTAACATGCGGTGACGTCGAGGAGAATCCTGGCCCAATGAC
CGAGTACAAGCCCACGGTGCGCCTCGCCACCCGCGACGACGTCCCCAGGGCCGTACGCACCCTCGCCGCCGCGTTCGCCGACTAC
CCCGCCACGCGCCACACCGTCGATCCGGACCGCCACATCGAGCGGGTCACCGAGCTGCAAGAACTCTTCCTCACGCGCGTCGGGC
TCGACATCGGCAAGGTGTGGGTCGCGGACGACGGCGCCGCGGTGGCGGTCTGGACCACGCCGGAGAGCGTCGAAGCGGGGGC
GGTGTTCGCCGAGATCGGCCCGCGCATGGCCGAGTTGAGCGGTTCCCGGCTGGCCGCGCAGCAACAGATGGAAGGCCTCCTGGC
GCCGCACCGGCCCAAGGAGCCCGCGTGGTTCCTGGCCACCGTCGGAGTCTCGCCCGACCACCAGGGCAAGGGTCTGGGCAGCG
CCGTCGTGCTCCCCGGAGTGGAGGCGGCCGAGCGCGCCGGGGTGCCCGCCTTCCTGGAGACCTCCGCGCCCCGCAACCTCCCCT
TCTACGAGCGGCTCGGCTTCACCGTCACCGCCGACGTCGAGGTGCCCGAAGGACCGCGCACCTGGTGCATGACCCGCAAGCCCG
GTGCCTGAGAATTCGATATCAAGCTTATCGATAATCAACCTCTGGATTACAAAATTTGTGAAAGATTGACTGGTATTCTTAACTATGT
TGCTCCTTTTACGCTATGTGGATACGCTGCTTTAATGCCTTTGTATCATGCTATTGCTTCCCGTATGGCTTTCATTTTCTCCTCCTTGTA
TAAATCCTGGTTGCTGTCTCTTTATGAGGAGTTGTGGCCCGTTGTCAGGCAACGTGGCGTGGTGTGCACTGTGTTTGCTGACGCAA
CCCCCACTGGTTGGGGCATTGCCACCACCTGTCAGCTCCTTTCCGGGACTTTCGCTTTCCCCCTCCCTATTGCCACGGCGGAACTCA
TCGCCGCCTGCCTTGCCCGCTGCTGGACAGGGGCTCGGCTGTTGGGCACTGACAATTCCGTGGTGTTGTCGGGGAAATCATCGTC
CTTTCCTTGGCTGCTCGCCTGTGTTGCCACCTGGATTCTGCGCGGGACGTCCTTCTGCTACGTCCCTTCGGCCCTCAATCCAGCGGA
CCTTCCTTCCCGCGGCCTGCTGCCGGCTCTGCGGCCTCTTCCGCGTCTTCGCCTTCGCCCTCAGACGAGTCGGATCTCCCTTTGGGC
CGCCTCCCCGCATCGATACCGTCGACCTCGAGACCTAGAAAAACATGGAGCAATCACAAGTAGCAATACAGCAGCTACCAATGCT
GATTGTGCCTGGCTAGAAGCACAAGAGGAGGAGGAGGTGGGTTTTCCAGTCACACCTCAGGTACCTTTAAGACCAATGACTTAC
AAGGCAGCTGTAGATCTTAGCCACTTTTTAAAAGAAAAGGGGGGACTGGAAGGGCTAATTCACTCCCAACGAAGACAAGATATC
CTTGATCTGTGGATCTACCACACACAAGGCTACTTCCCTGATTGGCAGAACTACACACCAGGGCCAGGGATCAGATATCCACTGAC
CTTTGGATGGTGCTACAAGCTAGTACCAGTTGAGCAAGAGAAGGTAGAAGAAGCCAATGAAGGAGAGAACACCCGCTTGTTAC
ACCCTGTGAGCCTGCATGGGATGGATGACCCGGAGAGAGAAGTATTAGAGTGGAGGTTTGACAGCCGCCTAGCATTTCATCACAT
GGCCCGAGAGCTGCATCCGGACTGTACTGGGTCTCTCTGGTTAGACCAGATCTGAGCCTGGGAGCTCTCTGGCTAACTAGGGAAC
CCACTGCTTAAGCCTCAATAAAGCTTGCCTTGAGTGCTTCAAGTAGTGTGTGCCCGTCTGTTGTGTGACTCTGGTAACTAGAGATCC
CTCAGACCCTTTTAGTCAGTGTGGAAAATCTCTAGCAGGGCCCGTTTAAACCCGCTGATCAGCCTCGACTGTGCCTTCTAGTTGCC

AGCCATCTGTTGTTTGCCCCTCCCCCGTGCCTTCCTTGACCCTGGAAGGTGCCACTCCCACTGTCCTTTCCTAATAAAATGAGGAAA
TTGCATCGCATTGTCTGAGTAGGTGTCATTCTATTCTGGGGGGTGGGGTGGGGCAGGACAGCAAGGGGGAGGATTGGGAAGAC
AATAGCAGGCATGCTGGGGATGCGGTGGGCTCTATGGCTTCTGAGGCGGAAAGAACCAGCTGGGGCTCTAGGGGGTATCCCCAC
GCGCCCTGTAGCGGCGCATTAAGCGCGGCGGGTGTGGTGGTTACGCGCAGCGTGACCGCTACACTTGCCAGCGCCCTAGCGCCC
GCTCCTTTCGCTTTCTTCCCTTCCTTTCTCGCCACGTTCGCCGGCTTTCCCCGTCAAGCTCTAAATCGGGGGCTCCCTTTAGGGTTCC
GATTTAGTGCTTTACGGCACCTCGACCCCAAAAAACTTGATTAGGGTGATGGTTCACGTAGTGGGCCATCGCCCTGATAGACGGTT
TTTCGCCCTTTGACGTTGGAGTCCACGTTCTTTAATAGTGGACTCTTGTTCCAAACTGGAACAACACTCAACCCTATCTCGGTCTAT
TCTTTTGATTTATAAGGGATTTTGCCGATTTCGGCCTATTGGTTAAAAAATGAGCTGATTTAACAAAAATTTAACGCGAATTAATTC
TGTGGAATGTGTGTCAGTTAGGGTGTGGAAAGTCCCCAGGCTCCCCAGCAGGCAGAAGTATGCAAAGCATGCATCTCAATTAGTC
AGCAACCAGGTGTGGAAAGTCCCCAGGCTCCCCAGCAGGCAGAAGTATGCAAAGCATGCATCTCAATTAGTCAGCAACCATAGTC
CCGCCCCTAACTCCGCCCATCCCGCCCCTAACTCCGCCCAGTTCCGCCCATTCTCCGCCCCATGGCTGACTAATTTTTTTTATTTATGC
AGAGGCCGAGGCCGCCTCTGCCTCTGAGCTATTCCAGAAGTAGTGAGGAGGCTTTTTTGGAGGCCTAGGCTTTTGCAAAAAGCT
CCCGGGAGCTTGTATATCCATTTTCGGATCTGATCAGCACGTGTTGACAATTAATCATCGGCATAGTATATCGGCATAGTATAATACG
ACAAGGTGAGGAACTAAACCATGGCCAAGTTGACCAGTGCCGTTCCGGTGCTCACCGCGCGCGACGTCGCCGGAGCGGTCGAGT
TCTGGACCGACCGGCTCGGGTTCTCCCGGGACTTCGTGGAGGACGACTTCGCCGGTGTGGTCCGGGACGACGTGACCCTGTTCA
TCAGCGCGGTCCAGGACCAGGTGGTGCCGGACAACACCCTGGCCTGGGTGTGGGTGCGCGGCCTGGACGAGCTGTACGCCGAG
TGGTCGGAGGTCGTGTCCACGAACTTCCGGGACGCCTCCGGGCCGGCCATGACCGAGATCGGCGAGCAGCCGTGGGGGCGGGA
GTTCGCCCTGCGCGACCCGGCCGGCAACTGCGTGCACTTCGTGGCCGAGGAGCAGGACTGACACGTGCTACGAGATTTCGATTC
CACCGCCGCCTTCTATGAAAGGTTGGGCTTCGGAATCGTTTTCCGGGACGCCGGCTGGATGATCCTCCAGCGCGGGGATCTCATG
CTGGAGTTCTTCGCCCACCCCAACTTGTTTATTGCAGCTTATAATGGTTACAAATAAAGCAATAGCATCACAAATTTCACAAATAAA
GCATTTTTTTCACTGCATTCTAGTTGTGGTTTGTCCAAACTCATCAATGTATCTTATCATGTCTGTATACCGTCGACCTCTAGCTAGAG
CTTGGCGTAATCATGGTCATAGCTGTTTCCTGTGTGAAATTGTTATCCGCTCACAATTCCACACAACATACGAGCCGGAAGCATAAA
GTGTAAAGCCTGGGGTGCCTAATGAGTGAGCTAACTCACATTAATTGCGTTGCGCTCACTGCCCGCTTTCCAGTCGGGAAACCTGT
CGTGCCAGCTGCATTAATGAATCGGCCAACGCGCGGGGAGAGGCGGTTTGCGTATTGGGCGCTCTTCCGCTTCCTCGCTCACTGA
CTCGCTGCGCTCGGTCGTTCGGCTGCGGCGAGCGGTATCAGCTCACTCAAAGGCGGTAATACGGTTATCCACAGAATCAGGGGAT
AACGCAGGAAAGAACATGTGAGCAAAAGGCCAGCAAAAGGCCAGGAACCGTAAAAAGGCCGCGTTGCTGGCGTTTTTCCATAG
GCTCCGCCCCCCTGACGAGCATCACAAAAATCGACGCTCAAGTCAGAGGTGGCGAAACCCGACAGGACTATAAAGATACCAGGC
GTTTCCCCCTGGAAGCTCCCTCGTGCGCTCTCCTGTTCCGACCCTGCCGCTTACCGGATACCTGTCCGCCTTTCTCCCTTCGGGAAG
CGTGGCGCTTTCTCATAGCTCACGCTGTAGGTATCTCAGTTCGGTGTAGGTCGTTCGCTCCAAGCTGGGCTGTGTGCACGAACCCC
CCGTTCAGCCCGACCGCTGCGCCTTATCCGGTAACTATCGTCTTGAGTCCAACCCGGTAAGACACGACTTATCGCCACTGGCAGCA
GCCACTGGTAACAGGATTAGCAGAGCGAGGTATGTAGGCGGTGCTACAGAGTTCTTGAAGTGGTGGCCTAACTACGGCTACACTA
GAAGAACAGTATTTGGTATCTGCGCTCTGCTGAAGCCAGTTACCTTCGGAAAAAGAGTTGGTAGCTCTTGATCCGGCAAACAAAC
CACCGCTGGTAGCGGTGGTTTTTTTGTTTGCAAGCAGCAGATTACGCGCAGAAAAAAAGGATCTCAAGAAGATCCTTTGATCTTT
TCTACGGGGTCTGACGCTCAGTGGAACGAAAACTCACGTTAAGGGATTTTGGTCATGAGATTATCAAAAAGGATCTTCACCTAGA
TCCTTTTAAATTAAAAATGAAGTTTTAAATCAATCTAAAGTATATATGAGTAAACTTGGTCTGACAGTTACCAATGCTTAATCAGTGA
GGCACCTATCTCAGCGATCTGTCTATTTCGTTCATCCATAGTTGCCTGACTCCCCGTCGTGTAGATAACTACGATACGGGAGGGCTTA
CCATCTGGCCCCAGTGCTGCAATGATACCGCGAGACCCACGCTCACCGGCTCCAGATTTATCAGCAATAAACCAGCCAGCCGGAA
GGGCCGAGCGCAGAAGTGGTCCTGCAACTTTATCCGCCTCCATCCAGTCTATTAATTGTTGCCGGGAAGCTAGAGTAAGTAGTTCG
CCAGTTAATAGTTTGCGCAACGTTGTTGCCATTGCTACAGGCATCGTGGTGTCACGCTCGTCGTTTGGTATGGCTTCATTCAGCTCC
GGTTCCCAACGATCAAGGCGAGTTACATGATCCCCCATGTTGTGCAAAAAAGCGGTTAGCTCCTTCGGTCCTCCGATCGTTGTCAG
AAGTAAGTTGGCCGCAGTGTTATCACTCATGGTTATGGCAGCACTGCATAATTCTCTTACTGTCATGCCATCCGTAAGATGCTTTTCT
GTGACTGGTGAGTACTCAACCAAGTCATTCTGAGAATAGTGTATGCGGCGACCGAGTTGCTCTTGCCCGGCGTCAATACGGGATA
ATACCGCGCCACATAGCAGAACTTTAAAAGTGCTCATCATTGGAAAACGTTCTTCGGGGCGAAAACTCTCAAGGATCTTACCGCT
GTTGAGATCCAGTTCGATGTAACCCACTCGTGCACCCAACTGATCTTCAGCATCTTTTACTTTCACCAGCGTTTCTGGGTGAGCAAA
AACAGGAAGGCAAAATGCCGCAAAAAAGGGAATAAGGGCGACACGGAAATGTTGAATACTCATACTCTTCCTTTTTCAATATTAT
TGAAGCATTTATCAGGGTTATTGTCTCATGAGCGGATACATATTTGAATGTATTTAGAAAAATAAACAAATAGGGGTTCCGCGCAC
ATTTCCCCGAAAAGTGCCACCTGAC

FINAL GRNA ASSEMBLY FOR CRISPRA

GTCGACGGATCGGGAGATCTCCCGATCCCCTATGGTGCACTCTCAGTACAATCTGCTCTGATGCCGCATAGTTAAGCCAGTATCTGC
TCCCTGCTTGTGTGTTGGAGGTCGCTGAGTAGTGCGCGAGCAAAATTTAAGCTACAACAAGGCAAGGCTTGACCGACAATTGCAT
GAAGAATCTGCTTAGGGTTAGGCGTTTTGCGCTGCTTCGCGATGTACGGGCCAGATATACGCGTTGACATTGATTATTGACTAGTT
ATTAATAGTAATCAATTACGGGGTCATTAGTTCATAGCCCATATATGGAGTTCCGCGTTACATAACTTACGGTAAATGGCCCGCCTGG
CTGACCGCCCAACGACCCCCGCCCATTGACGTCAATAATGACGTATGTTCCCATAGTAACGCCAATAGGGACTTTCCATTGACGTCA
ATGGGTGGAGTATTTACGGTAAACTGCCCACTTGGCAGTACATCAAGTGTATCATATGCCAAGTACGCCCCCTATTGACGTCAATGA
CGGTAAATGGCCCGCCTGGCATTATGCCCAGTACATGACCTTATGGGACTTTCCTACTTGGCAGTACATCTACGTATTAGTCATCGCT
ATTACCATGGTGATGCGGTTTTGGCAGTACATCAATGGGCGTGGATAGCGGTTTGACTCACGGGGATTTCCAAGTCTCCACCCCAT
TGACGTCAATGGGAGTTTGTTTTGGCACCAAAATCAACGGGACTTTCCAAAATGTCGTAACAACTCCGCCCCATTGACGCAAATG
GGCGGTAGGCGTGTACGGTGGGAGGTCTATATAAGCAGCGCGTTTTGCCTGTACTGGGTCTCTCTGGTTAGACCAGATCTGAGCC
TGGGAGCTCTCTGGCTAACTAGGGAACCCACTGCTTAAGCCTCAATAAAGCTTGCCTTGAGTGCTTCAAGTAGTGTGTGCCCGTCT
GTTGTGTGACTCTGGTAACTAGAGATCCCTCAGACCCTTTTAGTCAGTGTGGAAAATCTCTAGCAGTGGCGCCCGAACAGGGACT
TGAAAGCGAAAGGGAAACCAGAGGAGCTCTCTCGACGCAGGACTCGGCTTGCTGAAGCGCGCACGGCAAGAGGCGAGGGGC
GGCGACTGGTGAGTACGCCAAAAATTTTGACTAGCGGAGGCTAGAAGGAGAGAGATGGGTGCGAGAGCGTCAGTATTAAGCGG
GGGAGAATTAGATCGCGATGGGAAAAAATTCGGTTAAGGCCAGGGGGAAAGAAAAAATATAAATTAAAACATATAGTATGGGCA
AGCAGGGAGCTAGAACGATTCGCAGTTAATCCTGGCCTGTTAGAAACATCAGAAGGCTGTAGACAAATACTGGGACAGCTACAA
CCATCCCTTCAGACAGGATCAGAAGAACTTAGATCATTATATAATACAGTAGCAACCCTCTATTGTGTGCATCAAAGGATAGAGATA
AAAGACACCAAGGAAGCTTTAGACAAGATAGAGGAAGAGCAAAACAAAAGTAAGACCACCGCACAGCAAGCGGCCGCTGATC
TTCAGACCTGGAGGAGGAGATATGAGGGACAATTGGAGAAGTGAATTATATAAATATAAAGTAGTAAAAATTGAACCATTAGGAG
TAGCACCCACCAAGGCAAAGAGAAGAGTGGTGCAGAGAGAAAAAAGAGCAGTGGGAATAGGAGCTTTGTTCCTTGGGTTCTTG
GGAGCAGCAGGAAGCACTATGGGCGCAGCGTCAATGACGCTGACGGTACAGGCCAGACAATTATTGTCTGGTATAGTGCAGCAG
CAGAACAATTTGCTGAGGGCTATTGAGGCGCAACAGCATCTGTTGCAACTCACAGTCTGGGGCATCAAGCAGCTCCAGGCAAGA
ATCCTGGCTGTGGAAAGATACCTAAAGGATCAACAGCTCCTGGGGATTTGGGGTTGCTCTGGAAAACTCATTTGCACCACTGCTG
TGCCTTGGAATGCTAGTTGGAGTAATAAATCTCTGGAACAGATTTGGAATCACACGACCTGGATGGAGTGGGACAGAGAAATTAA
CAATTACACAAGCTTAATACACTCCTTAATTGAAGAATCGCAAAACCAGCAAGAAAAGAATGAACAAGAATTATTGGAATTAGAT
AAATGGGCAAGTTTGTGGAATTGGTTTAACATAACAAATTGGCTGTGGTATATAAAATTATTCATAATGATAGTAGGAGGCTTGGT
AGGTTTAAGAATAGTTTTTGCTGTACTTTCTATAGTGAATAGAGTTAGGCAGGGATATTCACCATTATCGTTTCAGACCCACCTCCC
AACCCCGAGGGGACCCGACAGGCCCGAAGGAATAGAAGAAGAAGGTGGAGAGAGAGACAGAGACAGATCCATTCGATTAGTG
AACGGATCGGCACTGCGTGCGCCAATTCTGCAGACAAATGGCAGTATTCATCCACAATTTTAAAAGAAAAGGGGGGATTGGGGG
GTACAGTGCAGGGGAAAGAATAGTAGACATAATAGCAACAGACATACAAACTAAAGAATTACAAAAACAAATTACAAAAATTCA
AAATTTTCGGGTTTATTACAGGGACAGCAGAGATCCAGTTTGGTTAATTAATGCAAAGATGGATAAAGTTTTAAACAGAGAGGAA
TCTTTGCAGCTAATGGACCTTCTAGGTCTTGAAAGGAGTGGGAATTGGCTCCGGTGCCCGTCAGTGGGCAGAGCGCACATCGCCC
ACAGTCCCCGAGAAGTTGGGGGGAGGGGTCGGCAATTGAACCGGTGCCTAGAGAAGGTGGCGCGGGGTAAACTGGGAAAGTG
ATGTCGTGTACTGGCTCCGCCTTTTTCCCGAGGGTGGGGGAGAACCGTATATAAGTGCAGTAGTCGCCGTGAACGTTCTTTTTCGC
AACGGGTTTGCCGCCAGAACACAGGTAAGTGCCGTGTGTGGTTCCCGCGGGCCTGGCCTCTTTACGGGTTATGGCCCTTGCGTGC
CTTGAATTACTTCCACTGGCTGCAGTACGTGATTCTTGATCCCGAGCTTCGGGTTGGAAGTGGGTGGGAGAGTTCGAGGCCTTGC
GCTTAAGGAGCCCCTTCGCCTCGTGCTTGAGTTGAGGCCTGGCCTGGGCGCTGGGGCCGCCGCGTGCGAATCTGGTGGCACCTTC
GCGCCTGTCTCGCTGCTTTCGATAAGTCTCTAGCCATTTAAAATTTTTGATGACCTGCTGCGACGCTTTTTTTCTGGCAAGATAGTCT
TGTAAATGCGGGCCAAGATCTGCACACTGGTATTTCGGTTTTTGGGGCCGCGGGCGGCGACGGGGCCCGTGCGTCCCAGCGCAC
ATGTTCGGCGAGGCGGGGCCTGCGAGCGCGGCCACCGAGAATCGGACGGGGGTAGTCTCAAGCTGGCCGGCCTGCTCTGGTGC
CTGGCCTCGCGCCGCCGTGTATCGCCCCGCCCTGGGCGGCAAGGCTGGCCCGGTCGGCACCAGTTGCGTGAGCGGAAAGATGGC
CGCTTCCCGGCCCTGCTGCAGGGAGCTCAAAATGGAGGACGCGGCGCTCGGGAGAGCGGGCGGGTGAGTCACCCACACAAAG
GAAAAGGGCCTTTCCGTCCTCAGCCGTCGCTTCATGTGACTCCACGGAGTACCGGGCGCCGTCCAGGCACCTCGATTAGTTCTCG
AGCTTTTGGAGTACGTCGTCTTTAGGTTGGGGGGAGGGGTTTTATGCGATGGAGTTTCCCCACACTGAGTGGGTGGAGACTGAA
GTTAGGCCAGCTTGGCACTTGATGTAATTCTCCTTGGAATTTGCCCTTTTTGAGTTTGGATCTTGGTTCATTCTCAAGCCTCAGACA
GTGGTTCAAAGTTTTTTTCTTCCATTTCAGGTGTCGTGA**CCGCCGCCACCATGGCCAAGCCTTTGTCTCAAGAAGAAT**

CCACCCTCATTGAAAGAGCAACGGCTACAATCAACAGCATCCCCATCTCTGAAGACTACAGCGTCGCCAGC
GCAGCTCTCTCTAGCGACGGCCGCATCTTCACTGGTGTCAATGTATATCATTTTACTGGGGGACCTTGTGCA
GAACTCGTGGTGCTGGGCACTGCTGCTGCTGCGGCAGCTGGCAACCTGACTTGTATCGTCGCGATCGGAA
ATGAGAACAGGGGCATCTTGAGCCCCTGCGGACGGTGCCGACAGGTGCTTCTCGATCTGCATCCTGGGAT
CAAAGCCATAGTGAAGGACAGTGATGGACAGCCGACGGCAGTTGGGATTCGTGAATTGCTGCCCTCTGG
TTATGTGTGGGAGGGCTAGAAAAAAAGCATAGCTCTAAAACCCCTCTAGCTCTCCTTGGCAGGTTCCACC
GAGATTTGAACTCGGATCGCTGGATTCAGAGTCCAGAGTGCTAACCATTACACCATGGAACCTGGATCAG
TAGCTCGATAGCTATCATACAACCCAGCCGTGACTAACGCATCATAAATTGCAAAAAAGCATAGCTCTAAA
ACAGCACCGCGGCCAATCTCCTTCCCTGACCGGGAATCGAACCCGGGCCGCGGCGGTGAGAGCGCCGAA
TCCTAACCACTAGACCACCAGGGAAAAAAAGGGATGACTCCCCAGTGACTGTGGGAGTCGCACATGGGT
GATCCTCATGTGCTCCCAAAGCACCGACTCGGTGCCACTTTTTCAAGTTGATAACGGACTAGCCTTATTTTA
ACTTGCTATGCTGGTGTTTCGTCCTTTCCACAAGATATATAAAGCCAAGAAATCGAAATACTTTCAAGTTAC
GGTAAGCATATGATAGTCCATTTTAAAACATAATTTTAAAACTGCAAACTACCCAAGAAATTATTACTTTCT
ACGTCACGTATTTTGTACTAATATCTTTGTGTTTACAGTCAAATTAATTCCAATTATCTCTCTAACAGCCTTGT
ATCGTATATGCAAATATGAAGGAATCATGGGAAATAGGCCCTCAAAAAAGCATAGCTCTAAAACAGGCTA
GAAGCGGCTCGGCGGGCTCGTCCGGGATTTGAACCCGGGACCTCTCGCACCCTAAGCGAGAATCATACCC
CTAGACCAACGAGCCCGATATCAAGCTTATCGATAATCAACCTCTGGATTACAAAATTTGTGAAAGATTGACTGGTA
TTCTTAACTATGTTGCTCCTTTTACGCTATGTGGATACGCTGCTTTAATGCCTTTGTATCATGCTATTGCTTCCCGTATGGCTTTCATTT
TCTCCTCCTTGTATAAATCCTGGTTGCTGTCTCTTTATGAGGAGTTGTGGCCCGTTGTCAGGCAACGTGGCGTGGTGTGCACTGTGT
TTGCTGACGCAACCCCCACTGGTTGGGGCATTGCCACCACCTGTCAGCTCCTTTCCGGGACTTTCGCTTTCCCCCTCCCTATTGCCA
CGGCGGAACTCATCGCCGCCTGCCTTGCCCGCTGCTGGACAGGGGCTCGGCTGTTGGGCACTGACAATTCCGTGGTGTTGTCGGG
GAAATCATCGTCCTTTCCTTGGCTGCTCGCCTGTGTTGCCACCTGGATTCTGCGCGGGACGTCCTTCTGCTACGTCCCTTCGGCCCT
CAATCCAGCGGACCTTCCTTCCCGCGGCCTGCTGCCGGCTCTGCGGCCTCTTCCGCGTCTTCGCCTTCGCCCTCAGACGAGTCGGA
TCTCCCTTTGGGCCGCCTCCCCGCATCGATACCGTCGACCTCGAGACCTAGAAAAACATGGAGCAATCACAAGTAGCAATACAGCA
GCTACCAATGCTGATTGTGCCTGGCTAGAAGCACAAGAGGAGGAGGAGGTGGGTTTTCCAGTCACACCTCAGGTACCTTTAAGA
CCAATGACTTACAAGGCAGCTGTAGATCTTAGCCACTTTTTAAAAGAAAAGGGGGGACTGGAAGGGCTAATTCACTCCCAACGA
AGACAAGATATCCTTGATCTGTGGATCTACCACACACAAGGCTACTTCCCTGATTGGCAGAACTACACACCAGGGCCAGGGATCA
GATATCCACTGACCTTTGGATGGTGCTACAAGCTAGTACCAGTTGAGCAAGAGAAGGTAGAAGAAGCCAATGAAGGAGAGAAC
ACCCGCTTGTTACACCCTGTGAGCCTGCATGGGATGGATGACCCGGAGAGAGAAGTATTAGAGTGGAGGTTTGACAGCCGCCTA
GCATTTCATCACATGGCCCGAGAGCTGCATCCGGACTGTACTGGGTCTCTCTGGTTAGACCAGATCTGAGCCTGGGAGCTCTCTGG
CTAACTAGGGAACCCACTGCTTAAGCCTCAATAAAGCTTGCCTTGAGTGCTTCAAGTAGTGTGTGCCCGTCTGTTGTGTGACTCTG
GTAACTAGAGATCCCTCAGACCCTTTTAGTCAGTGTGGAAAATCTCTAGCAGGGCCCGTTTAAACCCGCTGATCAGCCTCGACTGT
GCCTTCTAGTTGCCAGCCATCTGTTGTTTGCCCCTCCCCCGTGCCTTCCTTGACCCTGGAAGGTGCCACTCCCACTGTCCTTTCCTAA
TAAAATGAGGAAATTGCATCGCATTGTCTGAGTAGGTGTCATTCTATTCTGGGGGGTGGGGTGGGGCAGGACAGCAAGGGGGA
GGATTGGGAAGACAATAGCAGGCATGCTGGGGATGCGGTGGGCTCTATGGCTTCTGAGGCGGAAAGAACCAGCTGGGGCTCTA
GGGGGTATCCCCACGCGCCCTGTAGCGGCGCATTAAGCGCGGCGGGTGTGGTGGTTACGCGCAGCGTGACCGCTACACTTGCCA
GCGCCCTAGCGCCCGCTCCTTTCGCTTTCTTCCCTTCCTTTCTCGCCACGTTCGCCGGCTTTCCCCGTCAAGCTCTAAATCGGGGGC
TCCCTTTAGGGTTCCGATTTAGTGCTTTACGGCACCTCGACCCCAAAAAACTTGATTAGGGTGATGGTTCACGTAGTGGGCCATCG
CCCTGATAGACGGTTTTTCGCCCTTTGACGTTGGAGTCCACGTTCTTTAATAGTGGACTCTTGTTCCAAACTGGAACAACACTCAA
CCCTATCTCGGTCTATTCTTTTGATTTATAAGGGATTTTGCCGATTTCGGCCTATTGGTTAAAAAATGAGCTGATTTAACAAAAATTT
AACGCGAATTAATTCTGTGGAATGTGTGTCAGTTAGGGTGTGGAAAGTCCCCAGGCTCCCCAGCAGGCAGAAGTATGCAAAGCA
TGCATCTCAATTAGTCAGCAACCAGGTGTGGAAAGTCCCCAGGCTCCCCAGCAGGCAGAAGTATGCAAAGCATGCATCTCAATTA
GTCAGCAACCATAGTCCCGCCCCTAACTCCGCCCATCCCGCCCCTAACTCCGCCCAGTTCCGCCCATTCTCCGCCCCATGGCTGACTA
ATTTTTTTTATTTATGCAGAGGCCGAGGCCGCCTCTGCCTCTGAGCTATTCCAGAAGTAGTGAGGAGGCTTTTTTGGAGGCCTAGG
CTTTTGCAAAAAGCTCCCGGGAGCTTGTATATCCATTTTCGGATCTGATCAGCACGTGTTGACAATTAATCATCGGCATAGTATATCG
GCATAGTATAATACGACAAGGTGAGGAACTAAACCATGGCCAAGTTGACCAGTGCCGTTCCGGTGCTCACCGCGCGCGACGTCGC
CGGAGCGGTCGAGTTCTGGACCGACCGGCTCGGGTTCTCCCGGGACTTCGTGGAGGACGACTTCGCCGGTGTGGTCCGGGACG
ACGTGACCCTGTTCATCAGCGCGGTCCAGGACCAGGTGGTGCCGGACAACACCCTGGCCTGGGTGTGGGTGCGCGGCCTGGACG

AGCTGTACGCCGAGTGGTCGGAGGTCGTGTCCACGAACTTCCGGGACGCCTCCGGGCCGGCCATGACCGAGATCGGCGAGCAGC
CGTGGGGGCGGGAGTTCGCCCTGCGCGACCCGGCCGGCAACTGCGTGCACTTCGTGGCCGAGGAGCAGGACTGACACGTGCTA
CGAGATTTCGATTCCACCGCCGCCTTCTATGAAAGGTTGGGCTTCGGAATCGTTTTCCGGGACGCCGGCTGGATGATCCTCCAGCG
CGGGGATCTCATGCTGGAGTTCTTCGCCCACCCCAACTTGTTTATTGCAGCTTATAATGGTTACAAATAAAGCAATAGCATCACAAA
TTTCACAAATAAAGCATTTTTTTCACTGCATTCTAGTTGTGGTTTGTCCAAACTCATCAATGTATCTTATCATGTCTGTATACCGTCGA
CCTCTAGCTAGAGCTTGGCGTAATCATGGTCATAGCTGTTTCCTGTGTGAAATTGTTATCCGCTCACAATTCCACACAACATACGAG
CCGGAAGCATAAAGTGTAAAGCCTGGGGTGCCTAATGAGTGAGCTAACTCACATTAATTGCGTTGCGCTCACTGCCCGCTTTCCAG
TCGGGAAACCTGTCGTGCCAGCTGCATTAATGAATCGGCCAACGCGCGGGGAGAGGCGGTTTGCGTATTGGGCGCTCTTCCGCTT
CCTCGCTCACTGACTCGCTGCGCTCGGTCGTTCGGCTGCGGCGAGCGGTATCAGCTCACTCAAAGGCGGTAATACGGTTATCCACA
GAATCAGGGGATAACGCAGGAAAGAACATGTGAGCAAAAGGCCAGCAAAAGGCCAGGAACCGTAAAAAGGCCGCGTTGCTGG
CGTTTTTCCATAGGCTCCGCCCCCCTGACGAGCATCACAAAAATCGACGCTCAAGTCAGAGGTGGCGAAACCCGACAGGACTATA
AAGATACCAGGCGTTTCCCCCTGGAAGCTCCCTCGTGCGCTCTCCTGTTCCGACCCTGCCGCTTACCGGATACCTGTCCGCCTTTCT
CCCTTCGGGAAGCGTGGCGCTTTCTCATAGCTCACGCTGTAGGTATCTCAGTTCGGTGTAGGTCGTTCGCTCCAAGCTGGGCTGTG
TGCACGAACCCCCCGTTCAGCCCGACCGCTGCGCCTTATCCGGTAACTATCGTCTTGAGTCCAACCCGGTAAGACACGACTTATCG
CCACTGGCAGCAGCCACTGGTAACAGGATTAGCAGAGCGAGGTATGTAGGCGGTGCTACAGAGTTCTTGAAGTGGTGGCCTAAC
TACGGCTACACTAGAAGAACAGTATTTGGTATCTGCGCTCTGCTGAAGCCAGTTACCTTCGGAAAAAGAGTTGGTAGCTCTTGATC
CGGCAAACAAACCACCGCTGGTAGCGGTGGTTTTTTTGTTTGCAAGCAGCAGATTACGCGCAGAAAAAAAGGATCTCAAGAAG
ATCCTTTGATCTTTTCTACGGGGTCTGACGCTCAGTGGAACGAAAACTCACGTTAAGGGATTTTGGTCATGAGATTATCAAAAAGG
ATCTTCACCTAGATCCTTTTAAATTAAAAATGAAGTTTTAAATCAATCTAAAGTATATATGAGTAAACTTGGTCTGACAGTTACCAAT
GCTTAATCAGTGAGGCACCTATCTCAGCGATCTGTCTATTTCGTTCATCCATAGTTGCCTGACTCCCCGTCGTGTAGATAACTACGAT
ACGGGAGGGCTTACCATCTGGCCCCAGTGCTGCAATGATACCGCGAGACCCACGCTCACCGGCTCCAGATTTATCAGCAATAAACC
AGCCAGCCGGAAGGGCCGAGCGCAGAAGTGGTCCTGCAACTTTATCCGCCTCCATCCAGTCTATTAATTGTTGCCGGGAAGCTAG
AGTAAGTAGTTCGCCAGTTAATAGTTTGCGCAACGTTGTTGCCATTGCTACAGGCATCGTGGTGTCACGCTCGTCGTTTGGTATGG
CTTCATTCAGCTCCGGTTCCCAACGATCAAGGCGAGTTACATGATCCCCCATGTTGTGCAAAAAAGCGGTTAGCTCCTTCGGTCCT
CCGATCGTTGTCAGAAGTAAGTTGGCCGCAGTGTTATCACTCATGGTTATGGCAGCACTGCATAATTCTCTTACTGTCATGCCATCC
GTAAGATGCTTTTCTGTGACTGGTGAGTACTCAACCAAGTCATTCTGAGAATAGTGTATGCGGCGACCGAGTTGCTCTTGCCCGGC
GTCAATACGGGATAATACCGCGCCACATAGCAGAACTTTAAAAGTGCTCATCATTGGAAAACGTTCTTCGGGGCGAAAACTCTCA
AGGATCTTACCGCTGTTGAGATCCAGTTCGATGTAACCCACTCGTGCACCCAACTGATCTTCAGCATCTTTTACTTTCACCAGCGTT
TCTGGGTGAGCAAAAACAGGAAGGCAAAATGCCGCAAAAAAGGGAATAAGGGCGACACGGAAATGTTGAATACTCATACTCTT
CCTTTTTCAATATTATTGAAGCATTTATCAGGGTTATTGTCTCATGAGCGGATACATATTTGAATGTATTTAGAAAAATAAACAAATA
GGGGTTCCGCGCACATTTCCCCGAAAAGTGCCACCTGAC

Microvessel Isolation Buffers

Buffer A

Reagent	Amount	Product Code
PBS	500ml	D8662, Sigma
KCl	467.5ul	AM9640G, Invitrogen
CaCl2	360ul	21115, Sigma
Glucose	0.5g	A24940-01, Gibco

Buffer C

Reagent	Amount	Product Code
Buffer A	567.5ml	n/A
BSA	0.5%	A7979, Merck

Buffer I

Reagent	Amount	Product Code
Sucrose	250mM	D8662, Sigma
KCl	25mM	AM9640G, Invitrogen
MgCl2	5mM	AM9530G, Invitrogen
Tris Buffer, pH 8.0	10mM	AM9855G, Invitrogen
DTT	1uM	P117A, Promega
Nuclease Free Water	40mL	MA9932, Thermo

DNAse/RNAse Inhibitors

Reagent	Amount	Product Code
RNAsin Plus	250mM	N261B, Promega
RNAse OUT	25mM	10777019, Invitrogen
Protector RNAse	5mM	03335399001, Roche
DNAse	10mM	04716728001, Roche
DNAse	1uM	E1010, Zymo

Collaboration Declaration / Acknowledgements

The research undertaken in this report was primarily performed by me, Gabriel Rocha. However, single nuclei RNA-seq was performed with the collaboration of the following colleagues:

Dr. Anandhakumar Chandran performed the barcoding and sequencing of fixed nuclei at Novo Nordisk from both 10X and SPLiT-Seq platforms.

Dr. Robert Kitchen performed bioinformatic analysis including quality check and clustering of 10X vs SPLiT-Seq pilot experiment.

Dr. Cesar Prada performed initial bioinformatic analyses of sequenced nuclei, including quality check, normalization, and deconvolution.

Dr. Hannah Sleven performed the initial clustering and annotation prior to omitting QC-failed samples.

Hope Han performed clustering and DEG analysis from pseudobulk measurements.

This study was funded by the IM2PACT consortium which has received funding from the Innovative Medicines Initiative 2 Joint Undertaking under grant agreement No 807015. This Join Undertaking receives support from the European Union's Horizon 2020 research and innovation programme EFPIA.

I would like to personally acknowledge a few people who were instrumental in my experimental success throughout my time in Oxford.

My (now) husband Parker Johnson who dropped everything and moved across the Atlantic to let me pursue my PhD. He was my go-to when I needed someone the most, always providing open arms for a hug, or a nice shoulder to cry on. He showed me that resiliency is the most important trait any professional should have. He travelled several times during COVID to come see me, despite me not being able to travel to him. I love you.

My mum, dad, brother, and sister in law, Marta, Bruno, Lucas, and Bia Rocha for pampering me every time I came to London to escape Oxford for a bit. They reminded me every time that family was just around the corner and would always be there for me.

My London friends: my best friend Kylee Mansfield who I had the joy of enjoying one year close by while she studied at Cambridge. She became a foundation of support and a person I knew I could rely on if I needed a giggle. Kanika Chandaria, Freddie Archer, Elliot Briery, Alessandro Magliani, Sandra Nuoramo, and Marcus Ward, my tight London crew who provided me with a space to relax and have fun when I was not taking care of my cells. You were all imperative to my mental health not deteriorating.

My close Oxford friends: Lampros Bisdounis, my first (yes my first) actual friend in Oxford who became my closest ally in lab. I miss waddling over to his desk and talking about our problems and laughing at ourselves. Lizzie Casey, who listened to *all* of my problems and even gave me a condolence card when my cells died; meeting you was one of the best gifts Oxford gave me. Markella Zormpa, who came short of teaching me Greek but provided me with so many laughs during some tough times, Shobhan Dhir, for being so relatable in our research struggles, Elizabeth Rees for some well-deserved Friday kitchen dance parties during deep COVID, Fran Rigby for always playing games with me and generally slaying, Amy Ryder for being the funniest Gen-Z girl I'll ever meet, Ziski Putz and Jake Stein for being the loveliest couple who endured that cold blast in 2022 with me, and lastly Elisa Serra, the friend that entered my life a bit too late in my Ph.D but taught me that quality friendships don't need years to develop.

My lab-mates: Dr. Zameel Cader who pushed me to keep going with my experiments and providing all resources needed for my experiments. Dr. Hannah Sleven who despite us having some "language barrier" moments, provided me with the most direct help for my experiments out of anyone and I truly could not have don't it without her. Dr. Tanya Singh, my closest lab mate who quickly became a person I could trust in helping me with both scientific and interpersonal issues, as well as talking

about our true crime obsession. Dr. Florian Zirpel, who became a doctor a mere two days after me, it was a shame we only found out that we were so similar towards the end of our journey at Oxford. Dr. Tina Wei, Xinyu Li, and Shaan Baig for being amazing lab mates who also provided me with so much help and guidance.

And everyone else I met along the way. Big or small impact, I'm here because of you.

References

1. Kaiser, A.B., N. Zhang, and W.V. Der Pluijm, *Global Prevalence of Type 2 Diabetes over the Next Ten Years (2018-2028).* Diabetes, 2018. **67**(Supplement 1): p. 202-LB.
2. Suckale, J. and M. Solimena, *Pancreas islets in metabolic signaling--focus on the beta-cell.* Front Biosci, 2008. **13**: p. 7156-71.
3. Berger, C. and D. Zdzieblo, *Glucose transporters in pancreatic islets.* Pflugers Arch, 2020. **472**(9): p. 1249-1272.
4. Wilcox, G., *Insulin and insulin resistance.* Clin Biochem Rev, 2005. **26**(2): p. 19-39.
5. Klec, C., et al., *Calcium Signaling in ß-cell Physiology and Pathology: A Revisit.* Int J Mol Sci, 2019. **20**(24).
6. Matschinsky, F.M., *Glucokinase as glucose sensor and metabolic signal generator in pancreatic beta-cells and hepatocytes.* Diabetes, 1990. **39**(6): p. 647-52.
7. Newsholme, P., et al., *Amino acid metabolism, insulin secretion and diabetes.* Biochem Soc Trans, 2007. **35**(Pt 5): p. 1180-6.
8. Newsholme, P., et al., *Life and death decisions of the pancreatic beta-cell: the role of fatty acids.* Clin Sci (Lond), 2007. **112**(1): p. 27-42.
9. Fu, Z., E.R. Gilbert, and D. Liu, *Regulation of insulin synthesis and secretion and pancreatic Beta-cell dysfunction in diabetes.* Curr Diabetes Rev, 2013. **9**(1): p. 25-53.
10. Smith, U., *Impaired ('diabetic') insulin signaling and action occur in fat cells long before glucose intolerance--is insulin resistance initiated in the adipose tissue?* Int J Obes Relat Metab Disord, 2002. **26**(7): p. 897-904.
11. Wheatcroft, S.B., et al., *Pathophysiological implications of insulin resistance on vascular endothelial function.* Diabet Med, 2003. **20**(4): p. 255-68.
12. Stockhorst, U., et al., *Insulin and the CNS: effects on food intake, memory, and endocrine parameters and the role of intranasal insulin administration in humans.* Physiol Behav, 2004. **83**(1): p. 47-54.
13. Nagasaka, Y. and T. Kaneko, *[Molecular biology of regulation of renal function--structure, function and distribution of the receptor--insulin, glucagon].* Nihon Rinsho, 1992. **50**(12): p. 2921-4.
14. Poretsky, L. and M.F. Kalin, *The gonadotropic function of insulin.* Endocr Rev, 1987. **8**(2): p. 132-41.
15. Thomas, D.M., et al., *Insulin receptor expression in primary and cultured osteoclast-like cells.* Bone, 1998. **23**(3): p. 181-6.
16. Havrankova, J., J. Roth, and M. Brownstein, *Insulin receptors are widely distributed in the central nervous system of the rat.* Nature, 1978. **272**(5656): p. 827-829.
17. Kido, Y., J. Nakae, and D. Accili, *Clinical review 125: The insulin receptor and its cellular targets.* J Clin Endocrinol Metab, 2001. **86**(3): p. 972-9.
18. Merz, K.E. and D.C. Thurmond, *Role of Skeletal Muscle in Insulin Resistance and Glucose Uptake.* Compr Physiol, 2020. **10**(3): p. 785-809.
19. Meng, Z.X., et al., *Glucose Sensing by Skeletal Myocytes Couples Nutrient Signaling to Systemic Homeostasis.* Mol Cell, 2017. **66**(3): p. 332-344.e4.
20. Konishi, M., et al., *Endothelial insulin receptors differentially control insulin signaling kinetics in peripheral tissues and brain of mice.* Proc Natl Acad Sci U S A, 2017. **114**(40): p. E8478-e8487.
21. Rhea, E.M., C. Rask-Madsen, and W.A. Banks, *Insulin transport across the blood-brain barrier can occur independently of the insulin receptor.* J Physiol, 2018. **596**(19): p. 4753-4765.
22. Yu, Y., A.J. Kastin, and W. Pan, *Reciprocal interactions of insulin and insulin-like growth factor I in receptor-mediated transport across the blood-brain barrier.* Endocrinology, 2006. **147**(6): p. 2611-5.

23. Watson, L.S., et al., *Hyperinsulinemia alters insulin receptor presentation and internalization in brain microvascular endothelial cells.* Diab Vasc Dis Res, 2022. **19**(4): p. 14791641221118626.
24. Katakam, P.V., et al., *Cerebrovascular responses to insulin in rats.* J Cereb Blood Flow Metab, 2009. **29**(12): p. 1955-67.
25. Faber, C.L., et al., *Distinct Neuronal Projections From the Hypothalamic Ventromedial Nucleus Mediate Glycemic and Behavioral Effects.* Diabetes, 2018. **67**(12): p. 2518-2529.
26. Meek, T.H., et al., *Leptin action in the ventromedial hypothalamic nucleus is sufficient, but not necessary, to normalize diabetic hyperglycemia.* Endocrinology, 2013. **154**(9): p. 3067-76.
27. Reno, C.M., Y. Ding, and R. Sherwin, *Leptin acts in the brain to influence hypoglycemic counterregulation: disparate effects of acute and recurrent hypoglycemia on glucagon release.* Am J Physiol Endocrinol Metab, 2015. **309**(12): p. E960-7.
28. Larrabee, M.G., *Lactate metabolism and its effects on glucose metabolism in an excised neural tissue.* J Neurochem, 1995. **64**(4): p. 1734-41.
29. Silver, I.A. and M. Erecińska, *Extracellular glucose concentration in mammalian brain: continuous monitoring of changes during increased neuronal activity and upon limitation in oxygen supply in normo-, hypo-, and hyperglycemic animals.* J Neurosci, 1994. **14**(8): p. 5068-76.
30. Blázquez, E., et al., *Insulin in the brain: its pathophysiological implications for States related with central insulin resistance, type 2 diabetes and Alzheimer's disease.* Front Endocrinol (Lausanne), 2014. **5**: p. 161.
31. Amin, A.M., H. Mostafa, and H.M.J. Khojah, *Insulin resistance in Alzheimer's disease: The genetics and metabolomics links.* Clinica Chimica Acta, 2023. **539**: p. 215-236.
32. Lee, S.H., et al., *Insulin in the nervous system and the mind: Functions in metabolism, memory, and mood.* Mol Metab, 2016. **5**(8): p. 589-601.
33. van der Heide, L.P., G.M.J. Ramakers, and M.P. Smidt, *Insulin signaling in the central nervous system: Learning to survive.* Progress in Neurobiology, 2006. **79**(4): p. 205-221.
34. Li, Y., et al., *Diabetic vascular diseases: molecular mechanisms and therapeutic strategies.* Signal Transduction and Targeted Therapy, 2023. **8**(1): p. 152.
35. Jacob, M., D. Chappell, and B.F. Becker, *Regulation of blood flow and volume exchange across the microcirculation.* Critical Care, 2016. **20**(1): p. 319.
36. Freeman, K., et al., *In situ three-dimensional reconstruction of mouse heart sympathetic innervation by two-photon excitation fluorescence imaging.* Journal of Neuroscience Methods, 2014. **221**: p. 48-61.
37. Polovina, M., et al., *Type 2 diabetes increases the long-term risk of heart failure and mortality in patients with atrial fibrillation.* European Journal of Heart Failure, 2020. **22**(1): p. 113-125.
38. Grubić Rotkvić, P., et al., *The Mystery of Diabetic Cardiomyopathy: From Early Concepts and Underlying Mechanisms to Novel Therapeutic Possibilities.* International Journal of Molecular Sciences, 2021. **22**(11): p. 5973.
39. Kenny, H.C. and E.D. Abel, *Heart Failure in Type 2 Diabetes Mellitus.* Circulation Research, 2019. **124**(1): p. 121-141.
40. Jia, G., V.G. DeMarco, and J.R. Sowers, *Insulin resistance and hyperinsulinaemia in diabetic cardiomyopathy.* Nature Reviews Endocrinology, 2016. **12**(3): p. 144-153.
41. Jia, G., A. Whaley-Connell, and J.R. Sowers, *Diabetic cardiomyopathy: a hyperglycaemia- and insulin-resistance-induced heart disease.* Diabetologia, 2018. **61**(1): p. 21-28.
42. Song, S., et al., *Sirtuin 3 deficiency exacerbates diabetic cardiomyopathy via necroptosis enhancement and NLRP3 activation.* Acta Pharmacologica Sinica, 2021. **42**(2): p. 230-241.
43. Papadopoulou-Marketou, N., et al., *Biomarkers of diabetic nephropathy: A 2017 update.* Critical Reviews in Clinical Laboratory Sciences, 2017. **54**(5): p. 326-342.
44. Deng, Y., et al., *Global, Regional, and National Burden of Diabetes-Related Chronic Kidney Disease From 1990 to 2019.* Frontiers in Endocrinology, 2021. **12**.

45. Bidani, A.K., et al., *Renal microvascular dysfunction, hypertension and CKD progression.* Current Opinion in Nephrology and Hypertension, 2013. **22**(1): p. 1-9.
46. Roman, R.J. and F. Fan, *Genetic Susceptibility to Hypertension-Induced Renal Injury.* Hypertension, 2018. **71**(4): p. 559-560.
47. Jeansson, M., et al., *Angiopoietin-1 is essential in mouse vasculature during development and in response to injury.* J Clin Invest, 2011. **121**(6): p. 2278-89.
48. Undas, A., et al., *Hyperglycemia is associated with enhanced thrombin formation, platelet activation, and fibrin clot resistance to lysis in patients with acute coronary syndrome.* Diabetes Care, 2008. **31**(8): p. 1590-5.
49. Boels, M.G.S., et al., *Atrasentan Reduces Albuminuria by Restoring the Glomerular Endothelial Glycocalyx Barrier in Diabetic Nephropathy.* Diabetes, 2016. **65**(8): p. 2429-2439.
50. Navarro-González, J.F. and C. Mora-Fernández, *The Role of Inflammatory Cytokines in Diabetic Nephropathy.* Journal of the American Society of Nephrology, 2008. **19**(3): p. 433-442.
51. Ducos, C., et al., *Diabetic retinopathy in well-controlled type 2 diabetes: Role of glycaemic memory.* Diabetes Metab, 2021. **47**(1): p. 101156.
52. Wang, W. and A.C.Y. Lo, *Diabetic Retinopathy: Pathophysiology and Treatments.* International Journal of Molecular Sciences, 2018. **19**(6): p. 1816.
53. Fickweiler, W., et al., *Elevated Retinol Binding Protein 3 Concentrations Are Associated With Decreased Vitreous Inflammatory Cytokines, VEGF, and Progression of Diabetic Retinopathy.* Diabetes Care, 2022. **45**(9): p. 2159-2162.
54. Yokomizo, H., et al., *Retinol binding protein 3 is increased in the retina of patients with diabetes resistant to diabetic retinopathy.* Science Translational Medicine, 2019. **11**(499): p. eaau6627.
55. Giblin, M.J., C.D. Ontko, and J.S. Penn, *Effect of cytokine-induced alterations in extracellular matrix composition on diabetic retinopathy-relevant endothelial cell behaviors.* Scientific Reports, 2022. **12**(1): p. 12955.
56. Liu, X., et al., *IL-1β Induces IL-6 production in retinal Müller cells predominantly through the activation of P38 MAPK/NF-κB signaling pathway.* Experimental Cell Research, 2015. **331**(1): p. 223-231.
57. Liu, Y., et al., *TNF-α released from retinal Müller cells aggravates retinal pigment epithelium cell apoptosis by upregulating mitophagy during diabetic retinopathy.* Biochem Biophys Res Commun, 2021. **561**: p. 143-150.
58. Aday, A.W. and K. Matsushita, *Epidemiology of Peripheral Artery Disease and Polyvascular Disease.* Circulation Research, 2021. **128**(12): p. 1818-1832.
59. Sen, S., et al., *Neuropathy May Be an Independent Risk Factor for Amputation After Lower-Extremity Burn in Adults With Diabetes.* Clin Diabetes, 2019. **37**(4): p. 352-356.
60. Penno, A., et al., *Hereditary sensory neuropathy type 1 is caused by the accumulation of two neurotoxic sphingolipids.* J Biol Chem, 2010. **285**(15): p. 11178-87.
61. Lim, A.K., *Diabetic nephropathy - complications and treatment.* International journal of nephrology and renovascular disease, 2014. **7**: p. 361-381.
62. Martín-Timón, I., et al., *Type 2 diabetes and cardiovascular disease: Have all risk factors the same strength?* World journal of diabetes, 2014. **5**(4): p. 444-470.
63. Verma, S., et al., *Cardiovascular Outcomes and Safety of Empagliflozin in Patients With Type 2 Diabetes Mellitus and Peripheral Artery Disease.* Circulation, 2018. **137**(4): p. 405-407.
64. Ehrlich, P., *Das Sauerstoff-Bedürfniss des Organismus; eine farbenanalytische Studie.* Berlin : August Hirschwald, 1885.
65. Bield A., K.R., *Uber eine bisher unbekannte toxische Wirkung der Gallensauren auf das Zentralnervensystem.* Zhl Inn Med, 1898. **19**: p. 1185-1200.
66. Lewandowsky, M., *Zur Lehre der Zerebrospinalflussigkeit.* Z Klin Med, 1900. **40**: p. 480-484.

67. Karnovsky, M.J., *The ultrastructural basis of capillary permeability studied with peroxidase as a tracer.* J Cell Biol, 1967. **35**(1): p. 213-36.
68. Shivers, R.R., A.L. Betz, and G.W. Goldstein, *Isolated rat brain capillaries possess intact, structurally complex, interendothelial tight junctions; freeze-fracture verification of tight junction integrity.* Brain Res, 1984. **324**(2): p. 313-22.
69. Nagy, Z., H. Peters, and I. Hüttner, *Fracture faces of cell junctions in cerebral endothelium during normal and hyperosmotic conditions.* Lab Invest, 1984. **50**(3): p. 313-22.
70. Davson, H. and W.H. Oldendorf, *Symposium on membrane transport. Transport in the central nervous system.* Proc R Soc Med, 1967. **60**(4): p. 326-9.
71. Tao-Cheng, J.H., Z. Nagy, and M.W. Brightman, *Tight junctions of brain endothelium in vitro are enhanced by astroglia.* J Neurosci, 1987. **7**(10): p. 3293-9.
72. Xu, L., A. Nirwane, and Y. Yao, *Basement membrane and blood-brain barrier.* Stroke Vasc Neurol, 2019. **4**(2): p. 78-82.
73. Yao, Y., et al., *Astrocytic laminin regulates pericyte differentiation and maintains blood brain barrier integrity.* Nat Commun, 2014. **5**: p. 3413.
74. Gautam, J., X. Zhang, and Y. Yao, *The role of pericytic laminin in blood brain barrier integrity maintenance.* Sci Rep, 2016. **6**: p. 36450.
75. Katsuno, T., et al., *Deficiency of zonula occludens-1 causes embryonic lethal phenotype associated with defected yolk sac angiogenesis and apoptosis of embryonic cells.* Mol Biol Cell, 2008. **19**(6): p. 2465-75.
76. Umeda, K., et al., *Establishment and characterization of cultured epithelial cells lacking expression of ZO-1.* J Biol Chem, 2004. **279**(43): p. 44785-94.
77. Dickens, D., S. Radisch, and M. Pirmohamed, *Drug transporters at the blood-brain barrier*. 2016. p. 151-183.
78. Daneman, R., et al., *The mouse blood-brain barrier transcriptome: a new resource for understanding the development and function of brain endothelial cells.* PLoS One, 2010. **5**(10): p. e13741.
79. Georgieff, M.K., *Nutrition and the developing brain: nutrient priorities and measurement2.* The American Journal of Clinical Nutrition, 2007. **85**(2): p. 614S-620S.
80. De Vivo, D.C., et al., *Defective glucose transport across the blood-brain barrier as a cause of persistent hypoglycorrhachia, seizures, and developmental delay.* N Engl J Med, 1991. **325**(10): p. 703-9.
81. Tărlungeanu, D.C., et al., *Impaired Amino Acid Transport at the Blood Brain Barrier Is a Cause of Autism Spectrum Disorder.* Cell, 2016. **167**(6): p. 1481-1494.e18.
82. Schinkel, A.H., *P-Glycoprotein, a gatekeeper in the blood-brain barrier.* Adv Drug Deliv Rev, 1999. **36**(2-3): p. 179-194.
83. Storck, S.E., et al., *Endothelial LRP1 transports amyloid-β(1-42) across the blood-brain barrier.* J Clin Invest, 2016. **126**(1): p. 123-36.
84. Sweeney, M.D., S. Ayyadurai, and B.V. Zlokovic, *Pericytes of the neurovascular unit: key functions and signaling pathways.* Nat Neurosci, 2016. **19**(6): p. 771-83.
85. Ben-Zvi, A., et al., *Mfsd2a is critical for the formation and function of the blood–brain barrier.* Nature, 2014. **509**(7501): p. 507-511.
86. Montagne, A., et al., *Pericyte degeneration causes white matter dysfunction in the mouse central nervous system.* Nat Med, 2018. **24**(3): p. 326-337.
87. Kisler, K., et al., *Acute Ablation of Cortical Pericytes Leads to Rapid Neurovascular Uncoupling.* Front Cell Neurosci, 2020. **14**: p. 27.
88. Melgar, M.A., et al., *Postischemic reperfusion: ultrastructural blood-brain barrier and hemodynamic correlative changes in an awake model of transient forebrain ischemia.* Neurosurgery, 2005. **56**(3): p. 571-81.

89. Nikolakopoulou, A.M., et al., *Regional early and progressive loss of brain pericytes but not vascular smooth muscle cells in adult mice with disrupted platelet-derived growth factor receptor-β signaling.* PLoS One, 2017. **12**(4): p. e0176225.
90. Takahashi, S., *Metabolic Contribution and Cerebral Blood Flow Regulation by Astrocytes in the Neurovascular Unit.* Cells, 2022. **11**(5): p. 813.
91. Zhou, J., et al., *Altered blood–brain barrier integrity in adult aquaporin-4 knockout mice.* NeuroReport, 2008. **19**(1): p. 1-5.
92. Jeon, H., et al., *Upregulation of AQP4 Improves Blood-Brain Barrier Integrity and Perihematomal Edema Following Intracerebral Hemorrhage.* Neurotherapeutics, 2021. **18**(4): p. 2692-2706.
93. Wolburg, H., et al., *Agrin, aquaporin-4, and astrocyte polarity as an important feature of the blood-brain barrier.* Neuroscientist, 2009. **15**(2): p. 180-93.
94. Gaillard, P.J., et al., *Astrocytes Increase the Functional Expression of P-Glycoprotein in an In Vitro Model of The Blood-Brain Barrier.* Pharmaceutical Research, 2000. **17**(10): p. 1198-1205.
95. Martinez-Lozada, Z. and M.B. Robinson, *Reciprocal communication between astrocytes and endothelial cells is required for astrocytic glutamate transporter 1 (GLT-1) expression.* Neurochem Int, 2020. **139**: p. 104787.
96. Cabezas, R., et al., *Astrocytic modulation of blood brain barrier: perspectives on Parkinson's disease.* Front Cell Neurosci, 2014. **8**: p. 211.
97. Heithoff, B.P., et al., *Astrocytes are necessary for blood-brain barrier maintenance in the adult mouse brain.* Glia, 2021. **69**(2): p. 436-472.
98. Biessels, G.J., et al., *Risk of dementia in diabetes mellitus: a systematic review.* Lancet Neurol, 2006. **5**(1): p. 64-74.
99. Biessels, G.J. and Y.D. Reijmer, *Brain changes underlying cognitive dysfunction in diabetes: what can we learn from MRI?* Diabetes, 2014. **63**(7): p. 2244-52.
100. Thomassen, J.Q., et al., *Type-2 diabetes and risk of dementia: observational and Mendelian randomisation studies in 1 million individuals.* Epidemiol Psychiatr Sci, 2020. **29**: p. e118.
101. Cheng, G., et al., *Diabetes as a risk factor for dementia and mild cognitive impairment: a meta-analysis of longitudinal studies.* Internal Medicine Journal, 2012. **42**(5): p. 484-491.
102. Sanahuja, J., et al., *Increased Burden of Cerebral Small Vessel Disease in Patients With Type 2 Diabetes and Retinopathy.* Diabetes Care, 2016. **39**(9): p. 1614.
103. Liu, J., et al., *Causal Impact of Type 2 Diabetes Mellitus on Cerebral Small Vessel Disease: A Mendelian Randomization Analysis.* Stroke, 2018. **49**(6): p. 1325-1331.
104. Williams, O.A., et al., *Predicting Dementia in Cerebral Small Vessel Disease Using an Automatic Diffusion Tensor Image Segmentation Technique.* Stroke, 2019. **50**(10): p. 2775-2782.
105. Moran, C., et al., *Brain Atrophy in Type 2 Diabetes.* Diabetes Care, 2013. **36**(12): p. 4036.
106. van Elderen, S.G.C., et al., *Progression of brain atrophy and cognitive decline in diabetes mellitus.* Neurology, 2010. **75**(11): p. 997.
107. Espeland, M.A., et al., *Influence of Type 2 Diabetes on Brain Volumes and Changes in Brain Volumes.* Diabetes Care, 2013. **36**(1): p. 90.
108. Akisaki, T., et al., *Cognitive dysfunction associates with white matter hyperintensities and subcortical atrophy on magnetic resonance imaging of the elderly diabetes mellitus Japanese elderly diabetes intervention trial (J-EDIT).* Diabetes Metab Res Rev, 2006. **22**(5): p. 376-84.
109. Roy, B., et al., *Regional Brain Gray Matter Changes in Patients with Type 2 Diabetes Mellitus.* Scientific Reports, 2020. **10**(1): p. 9925.
110. Korf, E.S.C., et al., *Brain Aging in Very Old Men With Type 2 Diabetes.* Diabetes Care, 2006. **29**(10): p. 2268.
111. Abner, E.L., et al., *Diabetes is associated with cerebrovascular but not Alzheimer's disease neuropathology.* Alzheimers Dement, 2016. **12**(8): p. 882-9.

112. Arvanitakis, Z., et al., *Diabetes is related to cerebral infarction but not to AD pathology in older persons.* Neurology, 2006. **67**(11): p. 1960-5.
113. Schneider, A.L.C., et al., *Diabetes, Prediabetes, and Brain Volumes and Subclinical Cerebrovascular Disease on MRI: The Atherosclerosis Risk in Communities Neurocognitive Study (ARIC-NCS).* Diabetes Care, 2017. **40**(11): p. 1514-1521.
114. Thorand, B., et al., *C-Reactive Protein as a Predictor for Incident Diabetes Mellitus Among Middle-aged Men: Results From the MONICA Augsburg Cohort Study, 1984-1998.* Archives of Internal Medicine, 2003. **163**(1): p. 93-99.
115. van Dijk, E.J., et al., *C-reactive protein and cerebral small-vessel disease: the Rotterdam Scan Study.* Circulation, 2005. **112**(6): p. 900-5.
116. Spranger, J., et al., *Inflammatory Cytokines and the Risk to Develop Type 2 Diabetes: Results of the Prospective Population-Based European Prospective Investigation into Cancer and Nutrition (EPIC)-Potsdam Study.* Diabetes, 2003. **52**(3): p. 812-817.
117. Staszewski, J., et al., *IL-1α and IL-6 predict vascular events or death in patients with cerebral small vessel disease-Data from the SHEF-CSVD study.* Adv Med Sci, 2019. **64**(2): p. 258-266.
118. Rehman, K., et al., *Role of Interleukin-6 in Development of Insulin Resistance and Type 2 Diabetes Mellitus.* Crit Rev Eukaryot Gene Expr, 2017. **27**(3): p. 229-236.
119. Song, Y., et al., *Circulating levels of endothelial adhesion molecules and risk of diabetes in an ethnically diverse cohort of women.* Diabetes, 2007. **56**(7): p. 1898-1904.
120. Rouhl, R.P., et al., *Vascular inflammation in cerebral small vessel disease.* Neurobiol Aging, 2012. **33**(8): p. 1800-6.
121. Kawamura, T., et al., *Soluble adhesion molecules and C-reactive protein in the progression of silent cerebral infarction in patients with type 2 diabetes mellitus.* Metabolism, 2006. **55**(4): p. 461-6.
122. Kanai, A., et al., *Association between future events of brain infarction and soluble levels of intercellular adhesion molecule-1 and C-reactive protein in patients with type 2 diabetes mellitus.* Diabetes Res Clin Pract, 2008. **82**(2): p. 157-64.
123. Klassen, A.C., R.B. Loewenson, and J.A. Resch, *Cerebral atherosclerosis in selected chronic disease states.* Atherosclerosis, 1973. **18**(2): p. 321-36.
124. Luoto, T.M., et al., *Large vessel cerebral atherosclerosis is not in direct association with neuropathological lesions of Alzheimer's disease.* Eur Neurol, 2009. **62**(2): p. 93-8.
125. Itoh, Y., et al., *Atherosclerosis is not implicated in association of APOE epsilon4 with AD.* Neurology, 1999. **53**(1): p. 236-7.
126. Yarchoan, M., et al., *Cerebrovascular atherosclerosis correlates with Alzheimer pathology in neurodegenerative dementias.* Brain, 2012. **135**(Pt 12): p. 3749-56.
127. Beach, T.G., et al., *Circle of Willis atherosclerosis: association with Alzheimer's disease, neuritic plaques and neurofibrillary tangles.* Acta Neuropathol, 2007. **113**(1): p. 13-21.
128. Wisse, L.E.M., et al., *Global brain atrophy but not hippocampal atrophy is related to type 2 diabetes.* Journal of the Neurological Sciences, 2014. **344**(1): p. 32-36.
129. Last, D., et al., *Global and Regional Effects of Type 2 Diabetes on Brain Tissue Volumes and Cerebral Vasoreactivity.* Diabetes Care, 2007. **30**(5): p. 1193.
130. Manschot, S.M., et al., *Brain Magnetic Resonance Imaging Correlates of Impaired Cognition in Patients With Type 2 Diabetes.* Diabetes, 2006. **55**(4): p. 1106.
131. Saczynski, J.S., et al., *Glycemic Status and Brain Injury in Older Individuals.* Diabetes Care, 2009. **32**(9): p. 1608.
132. Shenkin, S.D., et al., *Maximum (prior) brain size, not atrophy, correlates with cognition in community-dwelling older people: a cross-sectional neuroimaging study.* BMC Geriatrics, 2009. **9**(1): p. 12.
133. Ruscheweyh, R., et al., *Executive performance is related to regional gray matter volume in healthy older individuals.* Hum Brain Mapp, 2013. **34**(12): p. 3333-46.

134. Dong, C., et al., *Cognitive correlates of white matter lesion load and brain atrophy: the Northern Manhattan Study.* Neurology, 2015. **85**(5): p. 441-9.
135. Tan, Z.S., et al., *Association of Metabolic Dysregulation With Volumetric Brain Magnetic Resonance Imaging and Cognitive Markers of Subclinical Brain Aging in Middle-Aged Adults.* Diabetes Care, 2011. **34**(8): p. 1766.
136. Willette, A.A., et al., *Insulin resistance, brain atrophy, and cognitive performance in late middle-aged adults.* Diabetes Care, 2013. **36**(2): p. 443-9.
137. Dhikav, V. and K. Anand, *Potential predictors of hippocampal atrophy in Alzheimer's disease.* Drugs Aging, 2011. **28**(1): p. 1-11.
138. Hempel, R., R. Onopa, and A. Convit, *Type 2 diabetes affects hippocampus volume differentially in men and women.* Diabetes Metab Res Rev, 2012. **28**(1): p. 76-83.
139. Gold, S., et al., *Hippocampal damage and memory impairments as possible early brain complications of type 2 diabetes.* Diabetologia, 2007. **50**: p. 711-9.
140. Salameh, T.S., et al., *Disruption of the hippocampal and hypothalamic blood–brain barrier in a diet-induced obese model of type II diabetes: prevention and treatment by the mitochondrial carbonic anhydrase inhibitor, topiramate.* Fluids and Barriers of the CNS, 2019. **16**(1): p. 1.
141. Kanoski, S.E., et al., *The effects of a high-energy diet on hippocampal function and blood-brain barrier integrity in the rat.* Journal of Alzheimer's disease : JAD, 2010. **21**(1): p. 207-219.
142. Yoo, D.Y., et al., *Chronic type 2 diabetes reduces the integrity of the blood-brain barrier by reducing tight junction proteins in the hippocampus.* J Vet Med Sci, 2016. **78**(6): p. 957-62.
143. Koshiyama, H., et al., *Hypothalamic pathogenesis of type 2 diabetes.* Medical Hypotheses, 2006. **67**(2): p. 307-310.
144. Burgos-Ramos, E., et al., *Differential insulin receptor substrate-1 (IRS1)-related modulation of neuropeptide Y and proopiomelanocortin expression in nondiabetic and diabetic IRS2-/- mice.* Endocrinology, 2012. **153**(3): p. 1129-40.
145. Posey, K.A., et al., *Hypothalamic proinflammatory lipid accumulation, inflammation, and insulin resistance in rats fed a high-fat diet.* Am J Physiol Endocrinol Metab, 2009. **296**(5): p. E1003-12.
146. Valdearcos, M., et al., *Microglia dictate the impact of saturated fat consumption on hypothalamic inflammation and neuronal function.* Cell reports, 2014. **9**(6): p. 2124-2138.
147. De Souza, C.T., et al., *Consumption of a fat-rich diet activates a proinflammatory response and induces insulin resistance in the hypothalamus.* Endocrinology, 2005. **146**(10): p. 4192-9.
148. Tsaousidou, E., et al., *Distinct Roles for JNK and IKK Activation in Agouti-Related Peptide Neurons in the Development of Obesity and Insulin Resistance.* Cell Rep, 2014. **9**(4): p. 1495-506.
149. Schriever, S.C., et al., *Type 2 diabetes risk gene Dusp8 regulates hypothalamic Jnk signaling and insulin sensitivity.* The Journal of Clinical Investigation, 2020. **130**(11): p. 6093-6108.
150. Ciofi, P., et al., *Brain-endocrine interactions: a microvascular route in the mediobasal hypothalamus.* Endocrinology, 2009. **150**(12): p. 5509-5519.
151. Haddad-Tóvolli, R., et al., *Development and Function of the Blood-Brain Barrier in the Context of Metabolic Control.* Frontiers in neuroscience, 2017. **11**: p. 224-224.
152. Gao, Y., Matthias H. Tschöp, and S. Luquet, *Hypothalamic Tanycytes: Gatekeepers to Metabolic Control.* Cell Metabolism, 2014. **19**(2): p. 173-175.
153. Balland, E., et al., *Hypothalamic Tanycytes Are an ERK-Gated Conduit for Leptin into the Brain.* Cell Metabolism, 2014. **19**(2): p. 293-301.
154. Fuster, J.n.M., *The Prefrontal Cortex—An Update: Time Is of the Essence.* Neuron, 2001. **30**(2): p. 319-333.
155. Holtzer, R., et al., *The effect of diabetes on prefrontal cortex activation patterns during active walking in older adults.* Brain and Cognition, 2018. **125**: p. 14-22.

156. Choi, S.E., et al., *Prefrontal cortex brain damage and glycemic control in patients with type 2 diabetes.* Journal of Diabetes, 2020. **12**(6): p. 465-473.
157. Abdul-Rahman, O., et al., *Altered gene expression profiles in the hippocampus and prefrontal cortex of type 2 diabetic rats.* BMC Genomics, 2012. **13**(1): p. 81.
158. Piątkowska-Chmiel, I., et al., *Regulation of Neuroinflammatory Signaling by PPARγ Agonist in Mouse Model of Diabetes.* Int J Mol Sci, 2022. **23**(10).
159. Bury, J.J., et al., *Type 2 diabetes mellitus-associated transcriptome alterations in cortical neurones and associated neurovascular unit cells in the ageing brain.* Acta Neuropathologica Communications, 2021. **9**(1): p. 5.
160. Nguyen, T.T., et al., *Type 3 Diabetes and Its Role Implications in Alzheimer's Disease.* Int J Mol Sci, 2020. **21**(9).
161. Chung, S.J., et al., *Association of type 2 diabetes GWAS loci and the risk of Parkinson's and Alzheimer's diseases.* Parkinsonism Relat Disord, 2015. **21**(12): p. 1435-40.
162. Heitner, J. and D. Dickson, *Diabetics do not have increased Alzheimer-type pathology compared with age-matched control subjects.* Neurology, 1997. **49**(5): p. 1306.
163. Peila, R., B.L. Rodriguez, and L.J. Launer, *Type 2 Diabetes, APOE Gene, and the Risk for Dementia and Related Pathologies.* Diabetes, 2002. **51**(4): p. 1256.
164. Beeri, M.S., et al., *Type 2 diabetes is negatively associated with Alzheimer's disease neuropathology.* J Gerontol A Biol Sci Med Sci, 2005. **60**(4): p. 471-5.
165. Madsen-Bouterse, S., G. Mohammad, and R.A. Kowluru, *Glyceraldehyde-3-phosphate dehydrogenase in retinal microvasculature: implications for the development and progression of diabetic retinopathy.* Investigative ophthalmology & visual science, 2010. **51**(3): p. 1765-1772.
166. Du, X., et al., *Inhibition of GAPDH activity by poly(ADP-ribose) polymerase activates three major pathways of hyperglycemic damage in endothelial cells.* The Journal of clinical investigation, 2003. **112**(7): p. 1049-1057.
167. Kanwar, M. and R.A. Kowluru, *Role of glyceraldehyde 3-phosphate dehydrogenase in the development and progression of diabetic retinopathy.* Diabetes, 2009. **58**(1): p. 227-234.
168. Nicholls, C., H. Li, and J.P. Liu, *GAPDH: a common enzyme with uncommon functions.* Clin Exp Pharmacol Physiol, 2012. **39**(8): p. 674-9.
169. Rodríguez-Pascual, F., et al., *Glyceraldehyde-3-phosphate dehydrogenase regulates endothelin-1 expression by a novel, redox-sensitive mechanism involving mRNA stability.* Mol Cell Biol, 2008. **28**(23): p. 7139-55.
170. Du, X.-L., et al., *Hyperglycemia-induced mitochondrial superoxide overproduction activates the hexosamine pathway and induces plasminogen activator inhibitor-1 expression by increasing Sp1 glycosylation.* Proceedings of the National Academy of Sciences, 2000. **97**(22): p. 12222.
171. Shivashankar, G., J.C. Lim, and M.L. Acosta, *Glyceraldehyde-3-phosphate dehydrogenase and glutamine synthetase inhibition in the presence of pro-inflammatory cytokines contribute to the metabolic imbalance of diabetic retinopathy.* Experimental Eye Research, 2021. **213**: p. 108845.
172. Giacco, F. and M. Brownlee, *Oxidative stress and diabetic complications.* Circulation research, 2010. **107**(9): p. 1058-1070.
173. Yao, D., et al., *High glucose increases angiopoietin-2 transcription in microvascular endothelial cells through methylglyoxal modification of mSin3A.* J Biol Chem, 2007. **282**(42): p. 31038-45.
174. Eshaq, R.S. and N.R. Harris, *The role of tumor necrosis factor-α and interferon-γ in the hyperglycemia-induced ubiquitination and loss of platelet endothelial cell adhesion molecule-1 in rat retinal endothelial cells.* Microcirculation, 2021. **28**(7): p. e12717.

175. Li, W., R.E. Maloney, and T.Y. Aw, *High glucose, glucose fluctuation and carbonyl stress enhance brain microvascular endothelial barrier dysfunction: Implications for diabetic cerebral microvasculature.* Redox Biol, 2015. **5**: p. 80-90.
176. Lander, H.M., et al., *Activation of the receptor for advanced glycation end products triggers a p21(ras)-dependent mitogen-activated protein kinase pathway regulated by oxidant stress.* J Biol Chem, 1997. **272**(28): p. 17810-4.
177. Vlassara, H. and J. Uribarri, *Advanced glycation end products (AGE) and diabetes: cause, effect, or both?* Current diabetes reports, 2014. **14**(1): p. 453-453.
178. Yamamoto, Y., et al., *Development and prevention of advanced diabetic nephropathy in RAGE-overexpressing mice.* J Clin Invest, 2001. **108**(2): p. 261-8.
179. Gao, X., et al., *AGE/RAGE produces endothelial dysfunction in coronary arterioles in type 2 diabetic mice.* Am J Physiol Heart Circ Physiol, 2008. **295**(2): p. H491-8.
180. Yao, D. and M. Brownlee, *Hyperglycemia-induced reactive oxygen species increase expression of the receptor for advanced glycation end products (RAGE) and RAGE ligands.* Diabetes, 2010. **59**(1): p. 249-55.
181. Stillwell, W., *An Introduction to Biological Membranes: Composition, Structure and Function: Second Edition*. 2016. 1-597.
182. Geraldes, P. and G.L. King, *Activation of protein kinase C isoforms and its impact on diabetic complications.* Circulation research, 2010. **106**(8): p. 1319-1331.
183. Shiba, T., et al., *Correlation of diacylglycerol level and protein kinase C activity in rat retina to retinal circulation.* Am J Physiol, 1993. **265**(5 Pt 1): p. E783-93.
184. Inoguchi, T., et al., *Preferential elevation of protein kinase C isoform beta II and diacylglycerol levels in the aorta and heart of diabetic rats: differential reversibility to glycemic control by islet cell transplantation.* Proceedings of the National Academy of Sciences of the United States of America, 1992. **89**(22): p. 11059-11063.
185. Geraldes, P., et al., *Activation of PKC-delta and SHP-1 by hyperglycemia causes vascular cell apoptosis and diabetic retinopathy.* Nature medicine, 2009. **15**(11): p. 1298-1306.
186. Tang, Y., et al., *Protein kinase C-delta inhibition protects blood-brain barrier from sepsis-induced vascular damage.* Journal of Neuroinflammation, 2018. **15**(1): p. 309.
187. Li, J., et al., *Nephroprotective effects of diacylglycerol on diabetic nephropathy in type 2 diabetic rats.* Exp Ther Med, 2018. **15**(2): p. 1918-1926.
188. Akimoto, Y., et al., *Hyperglycemia and the O-GlcNAc Transferase in Rat Aortic Smooth Muscle Cells: Elevated Expression and Altered Patterns of O-GlcNAcylation.* Archives of biochemistry and biophysics, 2001. **389**: p. 166-75.
189. Laczy, B., et al., *Protein O-GlcNAcylation: a new signaling paradigm for the cardiovascular system.* Am J Physiol Heart Circ Physiol, 2009. **296**(1): p. H13-28.
190. Fülöp, N., R.B. Marchase, and J.C. Chatham, *Role of protein O-linked N-acetyl-glucosamine in mediating cell function and survival in the cardiovascular system.* Cardiovascular Research, 2007. **73**(2): p. 288-297.
191. Rajapakse, A.G., et al., *The hexosamine biosynthesis inhibitor azaserine prevents endothelial inflammation and dysfunction under hyperglycemic condition through antioxidant effects.* Am J Physiol Heart Circ Physiol, 2009. **296**(3): p. H815-22.
192. Chung, S.S., et al., *Contribution of polyol pathway to diabetes-induced oxidative stress.* J Am Soc Nephrol, 2003. **14**(8 Suppl 3): p. S233-6.
193. Oates, P.J. and B.L. Mylari, *Aldose reductase inhibitors: therapeutic implications for diabetic complications.* Expert Opin Investig Drugs, 1999. **8**(12): p. 2095-2119.
194. Hogan, K.A., et al., *The neural tube patterns vessels developmentally using the VEGF signaling pathway.* Development, 2004. **131**(7): p. 1503-13.
195. Duan, L.J., A. Nagy, and G.H. Fong, *Gastrulation and angiogenesis, not endothelial specification, is sensitive to partial deficiency in vascular endothelial growth factor-a in mice.* Biol Reprod, 2003. **69**(6): p. 1852-8.

196. Hellström, M., L.K. Phng, and H. Gerhardt, *VEGF and Notch signaling: the yin and yang of angiogenic sprouting.* Cell Adh Migr, 2007. **1**(3): p. 133-6.
197. James, J.M., C. Gewolb, and V.L. Bautch, *Neurovascular development uses VEGF-A signaling to regulate blood vessel ingression into the neural tube.* Development, 2009. **136**(5): p. 833-41.
198. Stenman, J.M., et al., *Canonical Wnt signaling regulates organ-specific assembly and differentiation of CNS vasculature.* Science, 2008. **322**(5905): p. 1247-50.
199. Gilbert, S.F., J.M. Opitz, and R.A. Raff, *Resynthesizing Evolutionary and Developmental Biology.* Developmental Biology, 1996. **173**(2): p. 357-372.
200. Marín-Padilla, M., *The human brain intracerebral microvascular system: development and structure.* Front Neuroanat, 2012. **6**: p. 38.
201. Mito, T., et al., *Immunohistochemical study of the vasculature in the developing brain.* Pediatr Neurol, 1991. **7**(1): p. 18-22.
202. Gerhardt, H., et al., *VEGF guides angiogenic sprouting utilizing endothelial tip cell filopodia.* J Cell Biol, 2003. **161**(6): p. 1163-77.
203. Gerhardt, H., et al., *Neuropilin-1 is required for endothelial tip cell guidance in the developing central nervous system.* Dev Dyn, 2004. **231**(3): p. 503-9.
204. Aguilera, K.Y. and R.A. Brekken, *Recruitment and retention: factors that affect pericyte migration.* Cell Mol Life Sci, 2014. **71**(2): p. 299-309.
205. Koyano-Nakagawa, N. and D.J. Garry, *Etv2 as an essential regulator of mesodermal lineage development.* Cardiovascular Research, 2017. **113**(11): p. 1294-1306.
206. Liu, F., et al., *ER71 specifies Flk-1+ hemangiogenic mesoderm by inhibiting cardiac mesoderm and Wnt signaling.* Blood, 2012. **119**(14): p. 3295-305.
207. Liu, F., et al., *Induction of hematopoietic and endothelial cell program orchestrated by ETS transcription factor ER71/ETV2.* EMBO Rep, 2015. **16**(5): p. 654-69.
208. Hayashi, H. and T. Kume, *Foxc transcription factors directly regulate Dll4 and Hey2 expression by interacting with the VEGF-Notch signaling pathways in endothelial cells.* PLoS One, 2008. **3**(6): p. e2401.
209. Hayashi, H. and T. Kume, *Foxc2 transcription factor as a regulator of angiogenesis via induction of integrin beta3 expression.* Cell Adh Migr, 2009. **3**(1): p. 24-6.
210. De Val, S., et al., *Combinatorial regulation of endothelial gene expression by ets and forkhead transcription factors.* Cell, 2008. **135**(6): p. 1053-64.
211. Shi, X., et al., *Cooperative interaction of Etv2 and Gata2 regulates the development of endothelial and hematopoietic lineages.* Dev Biol, 2014. **389**(2): p. 208-18.
212. Becker, P.W., et al., *An Intronic Flk1 Enhancer Directs Arterial-Specific Expression via RBPJ-Mediated Venous Repression.* Arterioscler Thromb Vasc Biol, 2016. **36**(6): p. 1209-19.
213. Song, H., et al., *Critical role for GATA3 in mediating Tie2 expression and function in large vessel endothelial cells.* J Biol Chem, 2009. **284**(42): p. 29109-24.
214. Payne, S., A. Neal, and S. De Val, *Transcription factors regulating vasculogenesis and angiogenesis.* Dev Dyn, 2024. **253**(1): p. 28-58.
215. Lan, Y., et al., *Essential role of endothelial Smad4 in vascular remodeling and integrity.* Mol Cell Biol, 2007. **27**(21): p. 7683-92.
216. Moya, I.M., et al., *Stalk cell phenotype depends on integration of Notch and Smad1/5 signaling cascades.* Dev Cell, 2012. **22**(3): p. 501-14.
217. Gutierrez, M.E.C., et al., *Defining the Transcriptional and Epigenetic Basis of Organotypic Endothelial Diversity in the Developing and Adult Mouse.* bioRxiv, 2021: p. 2021.11.15.468651.
218. Olsen, J.J., et al., *The Role of Wnt Signalling in Angiogenesis.* Clin Biochem Rev, 2017. **38**(3): p. 131-142.
219. Ortiz, A., et al., *Angiomotin is a novel component of cadherin-11/β-catenin/p120 complex and is critical for cadherin-11-mediated cell migration.* Faseb j, 2015. **29**(3): p. 1080-91.

220. Jho, E.-h., et al., *Wnt/β-Catenin/Tcf Signaling Induces the Transcription of Axin2, a Negative Regulator of the Signaling Pathway.* Molecular and Cellular Biology, 2002. **22**(4): p. 1172-1183.
221. Vattulainen-Collanus, S., et al., *Bone morphogenetic protein signaling is required for RAD51-mediated maintenance of genome integrity in vascular endothelial cells.* Communications Biology, 2018. **1**(1): p. 149.
222. Praça, C., et al., *Derivation of Brain Capillary-like Endothelial Cells from Human Pluripotent Stem Cell-Derived Endothelial Progenitor Cells.* Stem cell reports, 2019. **13**(4): p. 599-611.
223. Lippmann, E.S., et al., *Derivation of blood-brain barrier endothelial cells from human pluripotent stem cells.* Nat Biotechnol, 2012. **30**(8): p. 783-91.
224. Workman, M.J. and C.N. Svendsen, *Recent advances in human iPSC-derived models of the blood-brain barrier.* Fluids Barriers CNS, 2020. **17**(1): p. 30.
225. Panula, P., F. Joó, and L. Rechardt, *Evidence for the presence of viable endothelial cells in cultures derived from dissociated rat brain.* Experientia, 1978. **34**(1): p. 95-97.
226. Prieto, I., et al., *Metabolic adaptations in spontaneously immortalized PGC-1α knock-out mouse embryonic fibroblasts increase their oncogenic potential.* Redox Biol, 2020. **29**: p. 101396.
227. Lippmann, E.S., et al., *A retinoic acid-enhanced, multicellular human blood-brain barrier model derived from stem cell sources.* Scientific Reports, 2014. **4**(1): p. 4160.
228. Neal, E.H., et al., *A Simplified, Fully Defined Differentiation Scheme for Producing Blood-Brain Barrier Endothelial Cells from Human iPSCs.* Stem Cell Reports, 2019. **12**(6): p. 1380-1388.
229. Qian, T., et al., *Directed differentiation of human pluripotent stem cells to blood-brain barrier endothelial cells.* Science Advances, 2017. **3**(11): p. e1701679.
230. Hollmann, E.K., et al., *Accelerated differentiation of human induced pluripotent stem cells to blood–brain barrier endothelial cells.* Fluids and Barriers of the CNS, 2017. **14**(1): p. 9.
231. Lu, T.M., et al., *Human induced pluripotent stem cell-derived neuroectodermal epithelial cells mistaken for blood-brain barrier-forming endothelial cells.* bioRxiv, 2019: p. 699173.
232. Lippmann, E.S., et al., *Commentary on human pluripotent stem cell-based blood–brain barrier models.* Fluids and Barriers of the CNS, 2020. **17**(1): p. 64.
233. Qian, T., et al., *Directed differentiation of human pluripotent stem cells to blood-brain barrier endothelial cells.* Sci Adv, 2017. **3**(11): p. e1701679.
234. Lu, T.M., et al., *Pluripotent stem cell-derived epithelium misidentified as brain microvascular endothelium requires ETS factors to acquire vascular fate.* Proceedings of the National Academy of Sciences, 2021. **118**(8): p. e2016950118.
235. Ginsberg, M., et al., *Direct conversion of human amniotic cells into endothelial cells without transitioning through a pluripotent state.* Nature Protocols, 2015. **10**(12): p. 1975-1985.
236. Ginsberg, M., et al., *Efficient Direct Reprogramming of Mature Amniotic Cells into Endothelial Cells by ETS Factors and TGFβ Suppression.* Cell, 2012. **151**(3): p. 559-575.
237. Patsch, C., et al., *Generation of vascular endothelial and smooth muscle cells from human pluripotent stem cells.* Nat Cell Biol, 2015. **17**(8): p. 994-1003.
238. Yang, Y., et al., *Endogenous IGF Signaling Directs Heterogeneous Mesoderm Differentiation in Human Embryonic Stem Cells.* Cell Reports, 2019. **29**(11): p. 3374-3384.e5.
239. Wang, M.K., et al., *Different roles of TGF-β in the multi-lineage differentiation of stem cells.* World J Stem Cells, 2012. **4**(5): p. 28-34.
240. Gastfriend, B.D., et al., *Wnt signaling mediates acquisition of blood–brain barrier properties in naïve endothelium derived from human pluripotent stem cells.* eLife, 2021. **10**: p. e70992.
241. Bonney, S., et al., *Retinoic Acid Regulates Endothelial β-catenin Expression and Pericyte Numbers in the Developing Brain Vasculature.* Frontiers in Cellular Neuroscience, 2018. **12**.
242. Perrot, C.Y., J. Sawada, and M. Komatsu, *Prolonged activation of cAMP signaling leads to endothelial barrier disruption via transcriptional repression of RRAS.* Faseb j, 2018. **32**(11): p. fj201700818RRR.

243. Fukuhara, S., et al., *Cyclic AMP potentiates vascular endothelial cadherin-mediated cell-cell contact to enhance endothelial barrier function through an Epac-Rap1 signaling pathway.* Mol Cell Biol, 2005. **25**(1): p. 136-46.
244. Ge, Q., et al., *VEGF secreted by mesenchymal stem cells mediates the differentiation of endothelial progenitor cells into endothelial cells via paracrine mechanisms.* Mol Med Rep, 2018. **17**(1): p. 1667-1675.
245. Namkoong, S., et al., *Forskolin increases angiogenesis through the coordinated cross-talk of PKA-dependent VEGF expression and Epac-mediated PI3K/Akt/eNOS signaling.* Cell Signal, 2009. **21**(6): p. 906-15.
246. Guo, D., et al., *VEGF stimulated the angiogenesis by promoting the mitochondrial functions.* Oncotarget, 2017. **8**(44): p. 77020-77027.
247. Saharinen, P., L. Eklund, and K. Alitalo, *Therapeutic targeting of the angiopoietin–TIE pathway.* Nature Reviews Drug Discovery, 2017. **16**(9): p. 635-661.
248. Xing, G., et al., *Astrocytic Sonic Hedgehog Alleviates Intracerebral Hemorrhagic Brain Injury via Modulation of Blood-Brain Barrier Integrity.* Front Cell Neurosci, 2020. **14**: p. 575690.
249. Okawa, S., et al., *Transcriptional synergy as an emergent property defining cell subpopulation identity enables population shift.* Nat Commun, 2018. **9**(1): p. 2595.
250. Vanlandewijck, M., et al., *A molecular atlas of cell types and zonation in the brain vasculature.* Nature, 2018. **554**(7693): p. 475-480.
251. Planutiene, M., K. Planutis, and R.F. Holcombe, *Lymphoid enhancer-binding factor 1, a representative of vertebrate-specific Lef1/Tcf1 sub-family, is a Wnt-beta-catenin pathway target gene in human endothelial cells which regulates matrix metalloproteinase-2 expression and promotes endothelial cell invasion.* Vascular Cell, 2011. **3**(1): p. 28.
252. Hupe, M., et al., *Gene expression profiles of brain endothelial cells during embryonic development at bulk and single-cell levels.* Science Signaling, 2017. **10**(487): p. eaag2476.
253. Hübner, K., et al., *Wnt signaling positively regulates endothelial cell fate specification in the Fli1a-positive progenitor population via Lef1.* Developmental Biology, 2017. **430**(1): p. 142-155.
254. Wei, G., et al., *Ets1 and Ets2 are required for endothelial cell survival during embryonic angiogenesis.* Blood, 2009. **114**(5): p. 1123-1130.
255. Hashiya, N., et al., *In vivo evidence of angiogenesis induced by transcription factor Ets-1: Ets-1 is located upstream of angiogenesis cascade.* Circulation, 2004. **109**(24): p. 3035-41.
256. Iwasaka, C., et al., *Ets-1 regulates angiogenesis by inducing the expression of urokinase-type plasminogen activator and matrix metalloproteinase-1 and the migration of vascular endothelial cells.* J Cell Physiol, 1996. **169**(3): p. 522-31.
257. Luo, Y., et al., *Endothelial ETS1 inhibition exacerbate blood-brain barrier dysfunction in multiple sclerosis through inducing endothelial-to-mesenchymal transition.* Cell Death Dis, 2022. **13**(5): p. 462.
258. Trembley, M.A., et al., *Myocardin-related transcription factors control the motility of epicardium-derived cells and the maturation of coronary vessels.* Development, 2015. **142**(1): p. 21-30.
259. Menendez, M.T., et al., *BRG1 (Brahma-Related Gene 1) Promotes Endothelial Mrtf Transcription to Establish Embryonic Capillary Integrity.* Arteriosclerosis, thrombosis, and vascular biology, 2017. **37**(9): p. 1674-1682.
260. Davis, H.E., J.R. Morgan, and M.L. Yarmush, *Polybrene increases retrovirus gene transfer efficiency by enhancing receptor-independent virus adsorption on target cell membranes.* Biophys Chem, 2002. **97**(2-3): p. 159-72.
261. Hinca, S.B., et al., *Brain endothelial cells metabolize glutamate via glutamate dehydrogenase to replenish TCA-intermediates and produce ATP under hypoglycemic conditions.* J Neurochem, 2021. **157**(6): p. 1861-1875.

262. Hersom, M., et al., *Validation of reference genes for normalization of real-time quantitative PCR studies of gene expression in brain capillary endothelial cells cultured in vitro.* Molecular and Cellular Neuroscience, 2018. **93**: p. 27-35.
263. Patel, R. and A.J. Alahmad, *Growth-factor reduced Matrigel source influences stem cell derived brain microvascular endothelial cell barrier properties.* Fluids Barriers CNS, 2016. **13**: p. 6.
264. Srinivasan, B., et al., *TEER measurement techniques for in vitro barrier model systems.* J Lab Autom, 2015. **20**(2): p. 107-26.
265. Crone, C. and S.P. Olesen, *Electrical resistance of brain microvascular endothelium.* Brain Res, 1982. **241**(1): p. 49-55.
266. Olesen, S.P., *A calcium-dependent reversible permeability increase in microvessels in frog brain, induced by serotonin.* J Physiol, 1985. **361**: p. 103-13.
267. Butt, A.M., H.C. Jones, and N.J. Abbott, *Electrical resistance across the blood-brain barrier in anaesthetized rats: a developmental study.* J Physiol, 1990. **429**: p. 47-62.
268. Dasgupta, K. and J. Jeong, *Developmental biology of the meninges.* Genesis, 2019. **57**(5): p. e23288.
269. Appelt-Menzel, A., et al., *Establishment of a Human Blood-Brain Barrier Co-culture Model Mimicking the Neurovascular Unit Using Induced Pluri- and Multipotent Stem Cells.* Stem Cell Reports, 2017. **8**(4): p. 894-906.
270. Yunhui, D., D. Yanru, and Z. Shihan, *The Role of Occludin in Vascular Endothelial Protection*, in *Endothelial Dysfunction*, A. Alaeddin and F. Christopher, Editors. 2022, IntechOpen: Rijeka. p. Ch. 4.
271. Engelhardt, B., *β1-integrin/matrix interactions support blood-brain barrier integrity.* J Cereb Blood Flow Metab, 2011. **31**(10): p. 1969-71.
272. Calabria, A.R., et al., *Puromycin-purified rat brain microvascular endothelial cell cultures exhibit improved barrier properties in response to glucocorticoid induction.* J Neurochem, 2006. **97**(4): p. 922-33.
273. Jinek, M., et al., *A programmable dual-RNA-guided DNA endonuclease in adaptive bacterial immunity.* Science, 2012. **337**(6096): p. 816-21.
274. Konermann, S., et al., *Genome-scale transcriptional activation by an engineered CRISPR-Cas9 complex.* Nature, 2015. **517**(7536): p. 583-588.
275. Heigwer, F., G. Kerr, and M. Boutros, *E-CRISP: fast CRISPR target site identification.* Nature Methods, 2014. **11**(2): p. 122-123.
276. Liu, S., et al., *Neuronal Cell-type Engineering by Transcriptional Activation.* Front Genome Ed, 2021. **3**: p. 715697.
277. Liu, Y., et al., *CRISPR Activation Screens Systematically Identify Factors that Drive Neuronal Fate and Reprogramming.* Cell Stem Cell, 2018. **23**(5): p. 758-771.e8.
278. Wu, Q., et al., *Massively parallel characterization of CRISPR activator efficacy in human induced pluripotent stem cells and neurons.* Mol Cell, 2023. **83**(7): p. 1125-1139.e8.
279. Sun, J., et al., *Comparative studies between the murine immortalized brain endothelial cell line (bEnd.3) and induced pluripotent stem cell-derived human brain endothelial cells for paracellular transport.* PLOS ONE, 2022. **17**(5): p. e0268860.
280. Urrutia-Cabrera, D., et al., *Combinatorial Approach of Binary Colloidal Crystals and CRISPR Activation to Improve Induced Pluripotent Stem Cell Differentiation into Neurons.* ACS Applied Materials & Interfaces, 2022. **14**(7): p. 8669-8679.
281. Taïlé, J., et al., *Hyperglycemic Condition Causes Pro-Inflammatory and Permeability Alterations Associated with Monocyte Recruitment and Deregulated NFκB/PPARγ Pathways on Cerebral Endothelial Cells: Evidence for Polyphenols Uptake and Protective Effect.* Int J Mol Sci, 2021. **22**(3).

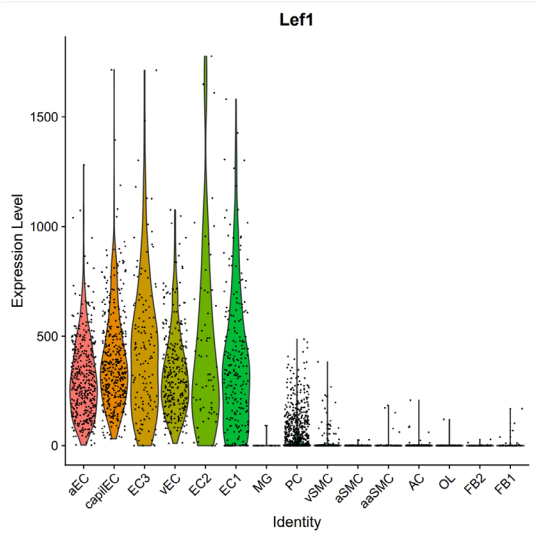
282. Sajja, R.K., S. Prasad, and L. Cucullo, *Impact of altered glycaemia on blood-brain barrier endothelium: an in vitro study using the hCMEC/D3 cell line.* Fluids Barriers CNS, 2014. **11**(1): p. 8.
283. Song, J., S.R. Yoon, and O.Y. Kim, *miR-Let7A Controls the Cell Death and Tight Junction Density of Brain Endothelial Cells under High Glucose Condition.* Oxidative Medicine and Cellular Longevity, 2017. **2017**: p. 6051874.
284. Barberio, C., et al., *A human-derived neurovascular unit in vitro model to study the effects of cellular cross-talk and soluble factors on barrier integrity.* Frontiers in Cellular Neuroscience, 2022. **16**.
285. Patel, H., et al., *Hyperglycemia induces differential change in oxidative stress at gene expression and functional levels in HUVEC and HMVEC.* Cardiovascular Diabetology, 2013. **12**(1): p. 142.
286. Cosentino, F., et al., *High Glucose Increases Nitric Oxide Synthase Expression and Superoxide Anion Generation in Human Aortic Endothelial Cells.* Circulation, 1997. **96**(1): p. 25-28.
287. Srinivasan, S., et al., *Hyperglycaemia-induced superoxide production decreases eNOS expression via AP-1 activation in aortic endothelial cells.* Diabetologia, 2004. **47**(10): p. 1727-1734.
288. Bogush, M., N.A. Heldt, and Y. Persidsky, *Blood Brain Barrier Injury in Diabetes: Unrecognized Effects on Brain and Cognition.* J Neuroimmune Pharmacol, 2017. **12**(4): p. 593-601.
289. Prakash, R., et al., *Cerebral Neovascularization and Remodeling Patterns in Two Different Models of Type 2 Diabetes.* PLOS ONE, 2013. **8**(2): p. e56264.
290. Prasad, S., et al., *Diabetes Mellitus and Blood-Brain Barrier Dysfunction: An Overview.* Journal of pharmacovigilance, 2014. **2**(2): p. 125.
291. Raker, V.K., C. Becker, and K. Steinbrink, *The cAMP Pathway as Therapeutic Target in Autoimmune and Inflammatory Diseases.* Frontiers in Immunology, 2016. **7**.
292. Noreen, S., I. Maqbool, and A. Madni, *Dexamethasone: Therapeutic potential, risks, and future projection during COVID-19 pandemic.* Eur J Pharmacol, 2021. **894**: p. 173854.
293. Tenor, H., et al., *Pharmacology, clinical efficacy, and tolerability of phosphodiesterase-4 inhibitors: impact of human pharmacokinetics.* Handb Exp Pharmacol, 2011(204): p. 85-119.
294. Rom, S., et al., *Hyperglycemia-Driven Neuroinflammation Compromises BBB Leading to Memory Loss in Both Diabetes Mellitus (DM) Type 1 and Type 2 Mouse Models.* Molecular Neurobiology, 2019. **56**(3): p. 1883-1896.
295. Chehade, J.M., M.J. Haas, and A.D. Mooradian, *Diabetes-related changes in rat cerebral occludin and zonula occludens-1 (ZO-1) expression.* Neurochem Res, 2002. **27**(3): p. 249-52.
296. Liu, L.P., et al., *Upregulation of RAGE at the blood-brain barrier in streptozotocin-induced diabetic mice.* Synapse, 2009. **63**(8): p. 636-642.
297. Price, T.O., et al., *Topiramate treatment protects blood-brain barrier pericytes from hyperglycemia-induced oxidative damage in diabetic mice.* Endocrinology, 2012. **153**(1): p. 362-72.
298. Deeds, M.C., et al., *Single dose streptozotocin-induced diabetes: considerations for study design in islet transplantation models.* Laboratory Animals, 2011. **45**(3): p. 131-140.
299. Bu, S., et al., *Endothelial cell-specific loss of eNOS differentially affects endothelial function.* PLoS One, 2022. **17**(9): p. e0274487.
300. Chakravarthy, U., et al., *Constitutive nitric oxide synthase expression in retinal vascular endothelial cells is suppressed by high glucose and advanced glycation end products.* Diabetes, 1998. **47**(6): p. 945-52.
301. Banks, W.A., et al., *Nitric oxide isoenzymes regulate lipopolysaccharide-enhanced insulin transport across the blood-brain barrier.* Endocrinology, 2008. **149**(4): p. 1514-23.
302. Tso, M.K., et al., *Gene expression profiling of brain endothelial cells after experimental subarachnoid haemorrhage.* Scientific Reports, 2021. **11**(1): p. 7818.

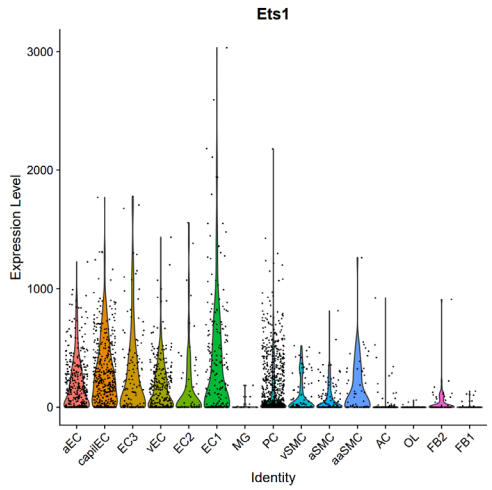
303. Mäe, M.A., et al., *Prolonged systemic hyperglycemia does not cause pericyte loss and permeability at the mouse blood-brain barrier.* Scientific Reports, 2018. **8**(1): p. 17462.
304. van Etten, R.W., et al., *Intensive lipid lowering by statin therapy does not improve vasoreactivity in patients with type 2 diabetes.* Arterioscler Thromb Vasc Biol, 2002. **22**(5): p. 799-804.
305. Tonyan, Z.N., et al., *Overview of Transcriptomic Research on Type 2 Diabetes: Challenges and Perspectives.* Genes (Basel), 2022. **13**(7).
306. Wang, C., et al., *Comparative gene expression profile and DNA methylation status in diabetic patients of Kazak and Han people.* Medicine (Baltimore), 2018. **97**(36): p. e11982.
307. Saxena, A., et al., *Transcriptome profiling reveals association of peripheral adipose tissue pathology with type-2 diabetes in Asian Indians.* Adipocyte, 2019. **8**(1): p. 125-136.
308. Noreen, Z., et al., *Transcriptional Profiling and Biological Pathway(s) Analysis of Type 2 Diabetes Mellitus in a Pakistani Population.* Int J Environ Res Public Health, 2020. **17**(16).
309. Lv, B., et al., *Transcriptome Sequencing Analysis of Peripheral Blood of Type 2 Diabetes Mellitus Patients With Thirst and Fatigue.* Front Endocrinol (Lausanne), 2020. **11**: p. 558344.
310. Segerstolpe, Å., et al., *Single-Cell Transcriptome Profiling of Human Pancreatic Islets in Health and Type 2 Diabetes.* Cell Metab, 2016. **24**(4): p. 593-607.
311. Xin, Y., et al., *RNA Sequencing of Single Human Islet Cells Reveals Type 2 Diabetes Genes.* Cell Metab, 2016. **24**(4): p. 608-615.
312. Gong, R., et al., *A comparison of gene expression profiles in patients with coronary artery disease, type 2 diabetes, and their coexisting conditions.* Diagn Pathol, 2017. **12**(1): p. 44.
313. Lin, Q., et al., *Abnormal Peripheral Neutrophil Transcriptome in Newly Diagnosed Type 2 Diabetes Patients.* J Diabetes Res, 2020. **2020**: p. 9519072.
314. Kleinstein, S.E., et al., *Transcriptomics of type 2 diabetic and healthy human neutrophils.* BMC Immunol, 2021. **22**(1): p. 37.
315. Beckman, J.A., et al., *Comparative Transcriptomics of Ex Vivo, Patient-Derived Endothelial Cells Reveals Novel Pathways Associated With Type 2 Diabetes Mellitus.* JACC Basic Transl Sci, 2019. **4**(5): p. 567-574.
316. Elzinga, S., et al., *2285-PUB: Hippocampal Transcriptomic Changes Due to High-Fat Diet in Prediabetic Mice.* Diabetes, 2020. **69**(Supplement 1): p. 2285-PUB.
317. Goto, Y., M. Kakizaki, and N. Masaki, *Production of Spontaneous Diabetic Rats by Repetition of Selective Breeding.* The Tohoku Journal of Experimental Medicine, 1976. **119**(1): p. 85-90.
318. Tran, M.N., et al., *Single-nucleus transcriptome analysis reveals cell-type-specific molecular signatures across reward circuitry in the human brain.* Neuron, 2021. **109**(19): p. 3088-3103.e5.
319. Del-Aguila, J.L., et al., *A single-nuclei RNA sequencing study of Mendelian and sporadic AD in the human brain.* Alzheimer's Research & Therapy, 2019. **11**(1): p. 71.
320. Mohammad, D., et al., *Single-nucleus RNA-sequencing reveals oligodendrocytes and their progenitors as vulnerable cell types in prefrontal cortex and anterior cingulate of brains with Parkinson's disease.* bioRxiv, 2023: p. 2023.05.11.540329.
321. Al-Majdoub, Z.M., et al., *Proteomic Quantification of Human Blood-Brain Barrier SLC and ABC Transporters in Healthy Individuals and Dementia Patients.* Mol Pharm, 2019. **16**(3): p. 1220-1233.
322. Garcia, F.J., et al., *Single-cell dissection of the human brain vasculature.* Nature, 2022. **603**(7903): p. 893-899.
323. Song, H.W., et al., *Transcriptomic comparison of human and mouse brain microvessels.* Scientific Reports, 2020. **10**(1): p. 12358.
324. Zhou, Z., et al., *Comprehensive transcriptomic analysis indicates brain regional specific alterations in type 2 diabetes.* Aging, 2019. **11**(16): p. 6398-6421.
325. Rosenberg, A.B., et al., *Single-cell profiling of the developing mouse brain and spinal cord with split-pool barcoding.* Science, 2018. **360**(6385): p. 176-182.

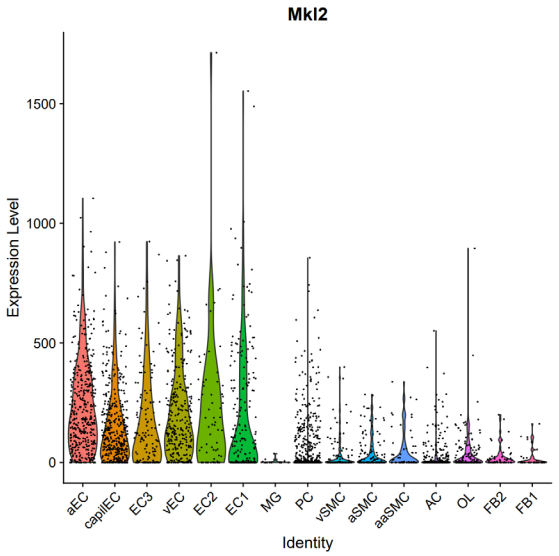
326. Hafemeister, C. and R. Satija, *Normalization and variance stabilization of single-cell RNA-seq data using regularized negative binomial regression.* Genome Biology, 2019. **20**(1): p. 296.
327. Amamoto, R., et al., *Probe-Seq enables transcriptional profiling of specific cell types from heterogeneous tissue by RNA-based isolation.* eLife, 2019. **8**: p. e51452.
328. Kishi, J.Y., et al., *SABER enables highly multiplexed and amplified detection of DNA and RNA in cells and tissues.* bioRxiv, 2018: p. 401810.
329. Franzén, O., L.M. Gan, and J.L.M. Björkegren, *PanglaoDB: a web server for exploration of mouse and human single-cell RNA sequencing data.* Database (Oxford), 2019. **2019**.
330. Walker, K.A., et al., *Neuronal insulin signaling and brain structure in nondemented older adults: the Atherosclerosis Risk in Communities Study.* Neurobiol Aging, 2021. **97**: p. 65-72.
331. Lonsdale, J., et al., *The Genotype-Tissue Expression (GTEx) project.* Nature Genetics, 2013. **45**(6): p. 580-585.
332. Monereo-Sánchez, J., et al., *The association of prediabetes and type 2 diabetes with hippocampal subfields volume: The Maastricht study.* NeuroImage: Clinical, 2023. **39**: p. 103455.
333. Li, M., et al., *Changes in the structure, perfusion, and function of the hippocampus in type 2 diabetes mellitus.* Frontiers in Neuroscience, 2023. **16**.
334. Ho, N., M.S. Sommers, and I. Lucki, *Effects of diabetes on hippocampal neurogenesis: links to cognition and depression.* Neurosci Biobehav Rev, 2013. **37**(8): p. 1346-62.
335. McIntyre, R.S., et al., *Brain volume abnormalities and neurocognitive deficits in diabetes mellitus: points of pathophysiological commonality with mood disorders?* Adv Ther, 2010. **27**(2): p. 63-80.
336. Fu, Y., et al., *Abnormal functional connectivity of the frontostriatal circuits in type 2 diabetes mellitus.* Front Aging Neurosci, 2022. **14**: p. 1055172.
337. Liu, J., et al., *Cerebral Blood Flow Alterations in Type 2 Diabetes Mellitus: A Systematic Review and Meta-Analysis of Arterial Spin Labeling Studies.* Frontiers in Aging Neuroscience, 2022. **14**.
338. Taheri, S., et al., *Quantitative measurement of blood-brain barrier permeability in human using dynamic contrast-enhanced MRI with fast T1 mapping.* Magn Reson Med, 2011. **65**(4): p. 1036-42.
339. Dallasta, L.M., et al., *Blood-brain barrier tight junction disruption in human immunodeficiency virus-1 encephalitis.* Am J Pathol, 1999. **155**(6): p. 1915-27.
340. Hase, Y., et al., *White matter capillaries in vascular and neurodegenerative dementias.* Acta Neuropathologica Communications, 2019. **7**(1): p. 16.
341. Ding, R., et al., *Loss of capillary pericytes and the blood-brain barrier in white matter in poststroke and vascular dementias and Alzheimer's disease.* Brain Pathol, 2020. **30**(6): p. 1087-1101.
342. Manukjan, N., et al., *Hypoxic oligodendrocyte precursor cell-derived VEGFA is associated with blood–brain barrier impairment.* Acta Neuropathologica Communications, 2023. **11**(1): p. 128.
343. Brogi, E., et al., *Indirect angiogenic cytokines upregulate VEGF and bFGF gene expression in vascular smooth muscle cells, whereas hypoxia upregulates VEGF expression only.* Circulation, 1994. **90**(2): p. 649-52.
344. Liu, Y., et al., *Hypoxia Regulates Vascular Endothelial Growth Factor Gene Expression in Endothelial Cells.* Circulation Research, 1995. **77**(3): p. 638-643.
345. Shibuya, M., *Vascular Endothelial Growth Factor (VEGF) and Its Receptor (VEGFR) Signaling in Angiogenesis: A Crucial Target for Anti- and Pro-Angiogenic Therapies.* Genes Cancer, 2011. **2**(12): p. 1097-105.
346. Jin, Y., et al., *Inactivation of EGLN3 hydroxylase facilitates Erk3 degradation via autophagy and impedes lung cancer growth.* Oncogene, 2022. **41**(12): p. 1752-1766.

347. Wang, W., et al., *ERK3 Promotes Endothelial Cell Functions by Upregulating SRC-3/SP1-Mediated VEGFR2 Expression.* Journal of Cellular Physiology, 2014. **229**(10): p. 1529-1537.
348. Zhang, H., et al., *Bone morphogenetic protein-7 inhibits endothelial-mesenchymal transition in pulmonary artery endothelial cell under hypoxia.* Journal of Cellular Physiology, 2018. **233**(5): p. 4077-4090.
349. Kong, F., et al., *Differential expression of adenylate kinase 4 in the context of disparate stress response strategies of HEK293 and HepG2 cells.* Archives of Biochemistry and Biophysics, 2013. **533**(1): p. 11-17.
350. Bellot, G., et al., *Hypoxia-induced autophagy is mediated through hypoxia-inducible factor induction of BNIP3 and BNIP3L via their BH3 domains.* Mol Cell Biol, 2009. **29**(10): p. 2570-81.
351. Calbet, J.A., *Chronic hypoxia increases blood pressure and noradrenaline spillover in healthy humans.* J Physiol, 2003. **551**(Pt 1): p. 379-86.
352. Marina, N., et al., *Brainstem hypoxia contributes to the development of hypertension in the spontaneously hypertensive rat.* Hypertension, 2015. **65**(4): p. 775-83.
353. Jones, N.K., et al., *Endothelin-1 Mediates the Systemic and Renal Hemodynamic Effects of GPR81 Activation.* Hypertension, 2020. **75**(5): p. 1213-1222.
354. Pipe, A., *Tobacco addiction and hypertension.* J Hum Hypertens, 1996. **10 Suppl 2**: p. S13-6.
355. Jambusaria, A., et al., *Endothelial heterogeneity across distinct vascular beds during homeostasis and inflammation.* Elife, 2020. **9**.
356. Bottos, A., et al., *The synaptic proteins neurexins and neuroligins are widely expressed in the vascular system and contribute to its functions.* Proc Natl Acad Sci U S A, 2009. **106**(49): p. 20782-7.
357. Wang, J., et al., *Epigenetic mechanisms linking diabetes and synaptic impairments.* Diabetes, 2014. **63**(2): p. 645-54.
358. Adams, R.H. and A. Eichmann, *Axon guidance molecules in vascular patterning.* Cold Spring Harb Perspect Biol, 2010. **2**(5): p. a001875.
359. Zhou, H., Y.H. Yang, and J.R. Basile, *Characterization of the Effects of Semaphorin 4D Signaling on Angiogenesis.* Methods Mol Biol, 2017. **1493**: p. 429-441.
360. Smith, E.S., et al., *SEMA4D compromises blood–brain barrier, activates microglia, and inhibits remyelination in neurodegenerative disease.* Neurobiology of Disease, 2015. **73**: p. 254-268.
361. Wu, J.H., et al., *Inhibition of Sema4D/PlexinB1 signaling alleviates vascular dysfunction in diabetic retinopathy.* EMBO Mol Med, 2020. **12**(2): p. e10154.
362. Humar, R., L. Zimmerli, and E. Battegay, *Angiogenesis and hypertension: an update.* Journal of Human Hypertension, 2009. **23**(12): p. 773-782.
363. Martinez-Quinones, P., et al., *Hypertension Induced Morphological and Physiological Changes in Cells of the Arterial Wall.* Am J Hypertens, 2018. **31**(10): p. 1067-1078.
364. Durham, P.L., *Calcitonin gene-related peptide (CGRP) and migraine.* Headache, 2006. **46 Suppl 1**(Suppl 1): p. S3-8.
365. Burdyga, T. and L. Borysova, *Ca(2+) Signalling in Pericytes.* Adv Exp Med Biol, 2018. **1109**: p. 95-109.
366. Love, M.I., W. Huber, and S. Anders, *Moderated estimation of fold change and dispersion for RNA-seq data with DESeq2.* Genome Biology, 2014. **15**(12): p. 550.

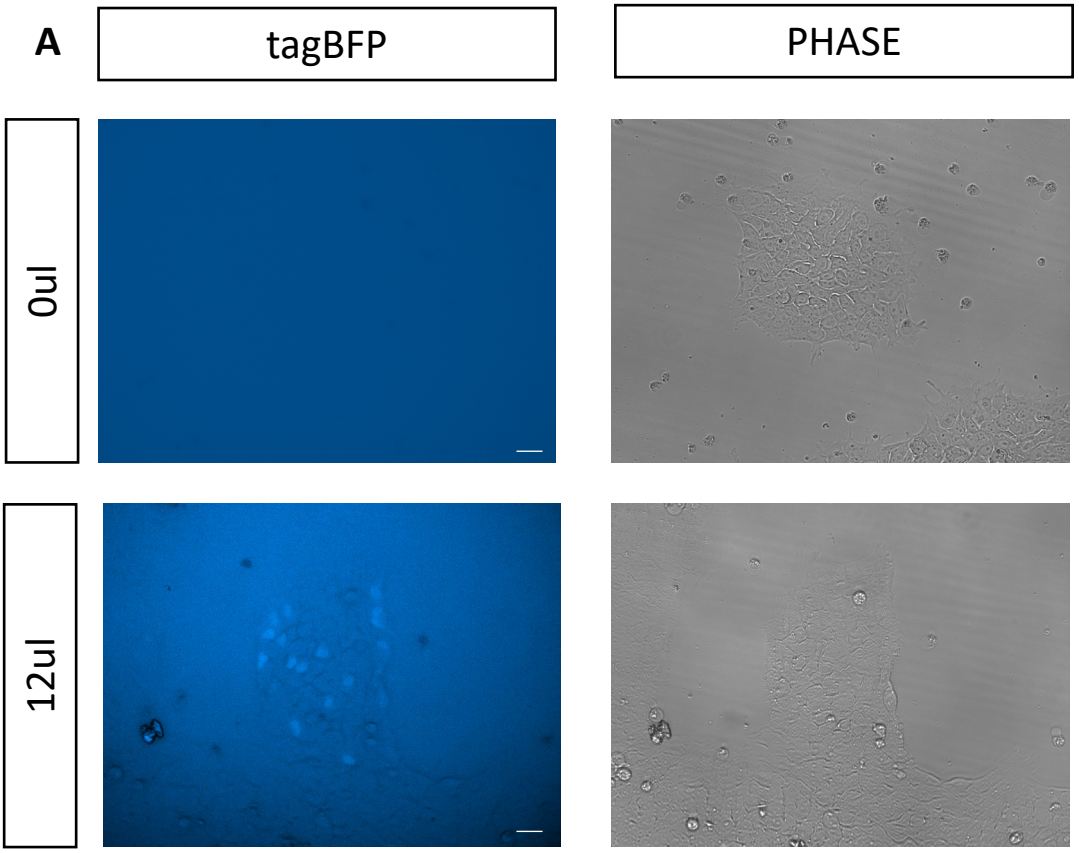
Supplementary Figures – Chapter 1



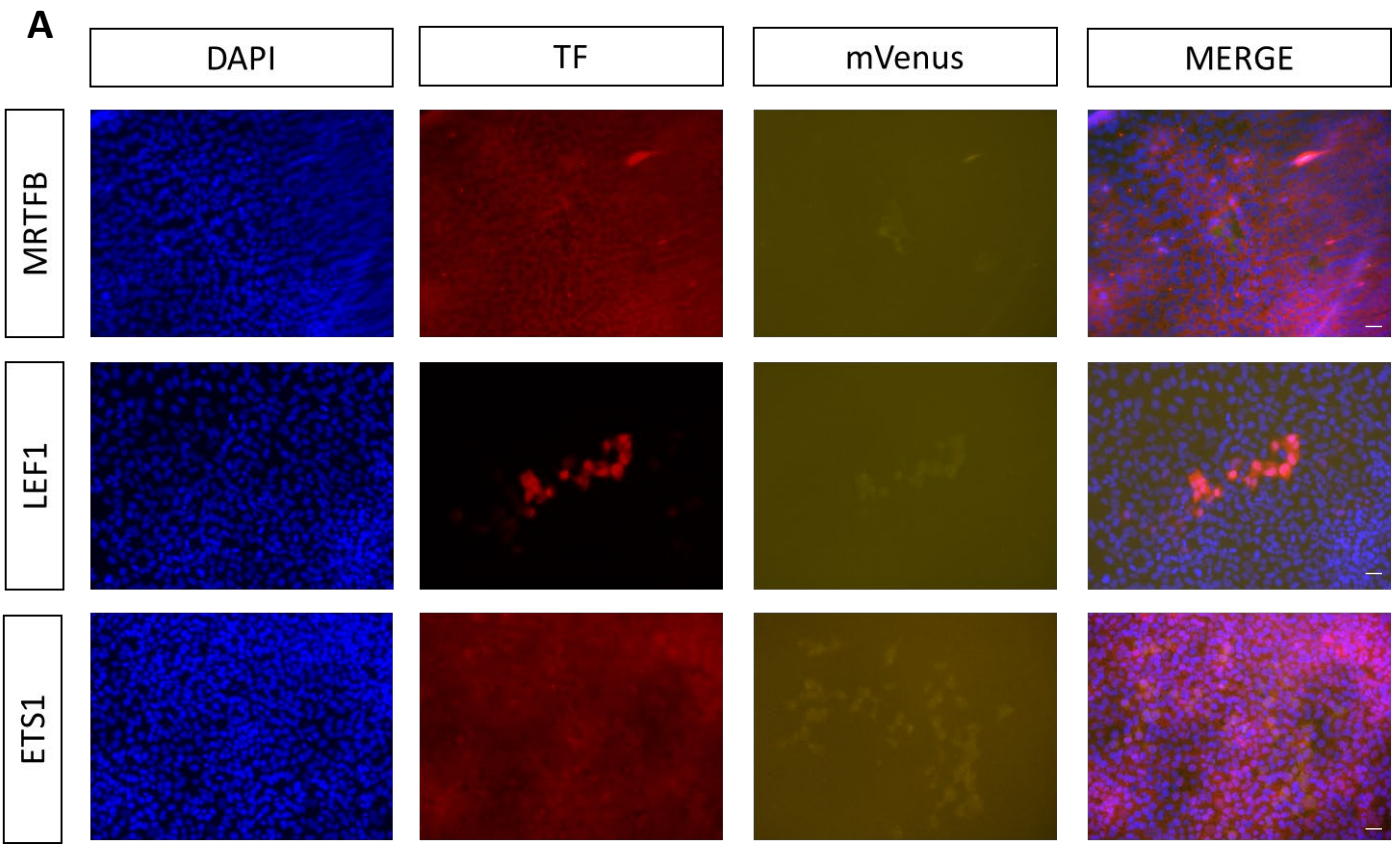




Supplementary Figure 1.1 – Expression of identified transcription factors in capillary endothelial cells based on scRNA-seq from Vanlandewijck et al.



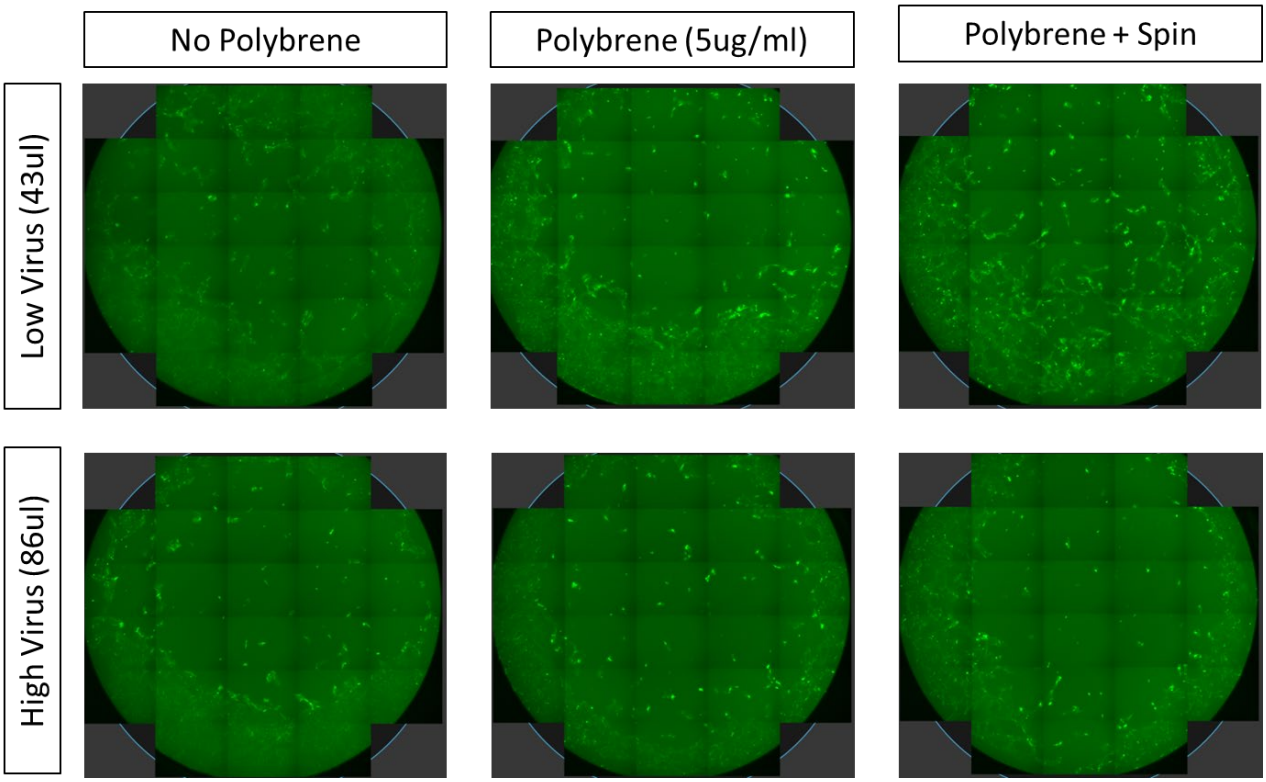
Supplementary Figure 1.2 – tagBFP transduction and expression in IPSCs
A- Live cell imaging of IPSCs 5 days post transduction of control (0ul) and infected (12ul) cells. At the high volume of 12ul, there is still only a subset of cells that faintly express tagBFP fluorescent protein. Scale bar, 50um. (n=3 biological replicates)



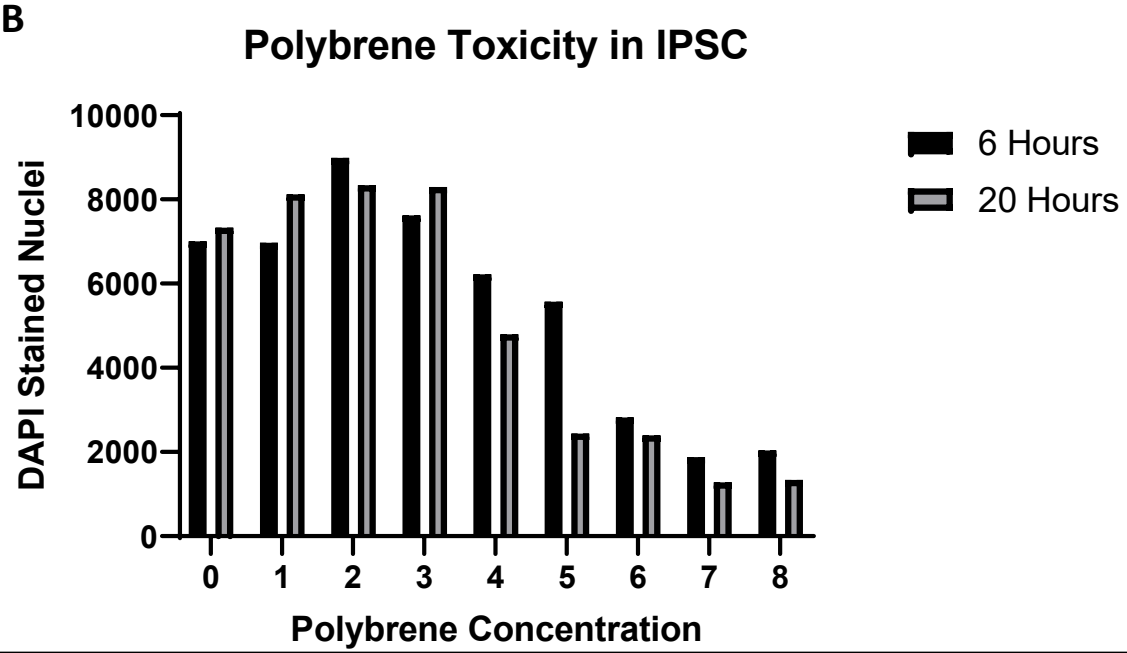
Supplementary Figure 1.3 – mVenus Signal Co-Localizes with LEF1

A- Immunocytochemistry IPSCs stained for each transcription factor five days after transduction of polycistronic TF and tagBFP rtTA virus. Visualising co-localization of mVenus and MRTFB or ETS1 proves to be challenging due to widespread expression of these two transcription factors in mVenus- cells. In the other hand, LEF1 perfectly co-localizes with the mVenus signal, indicating LEF1 is a more reliable marker of transduction success than ETS1 and MRTFB. Scale bars, 50um. (n=2 biological replicates)

A



B

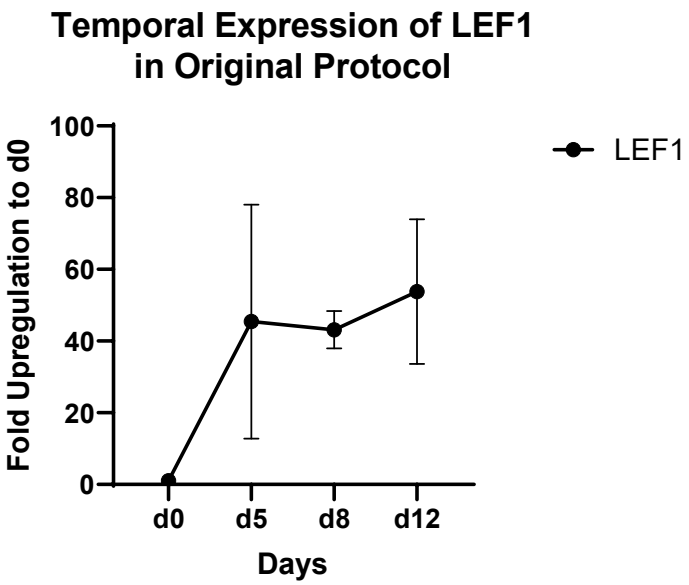


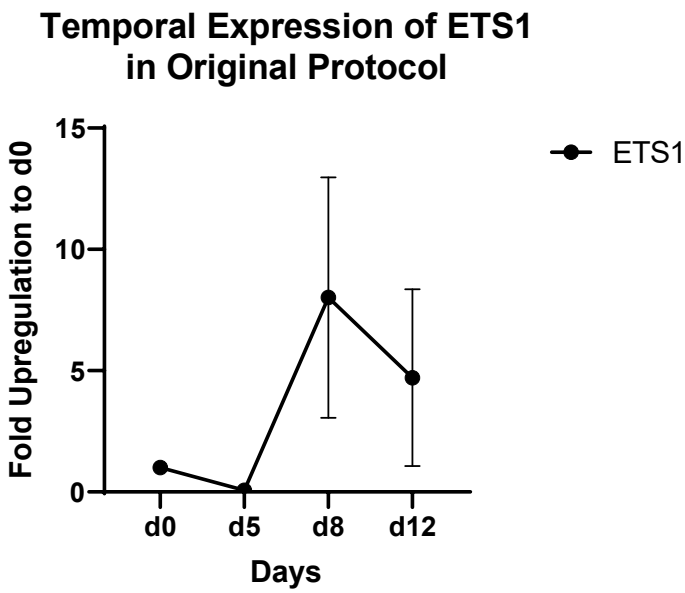
Supplementary Figure 1.4 – Effects of polybrene on virus transduction

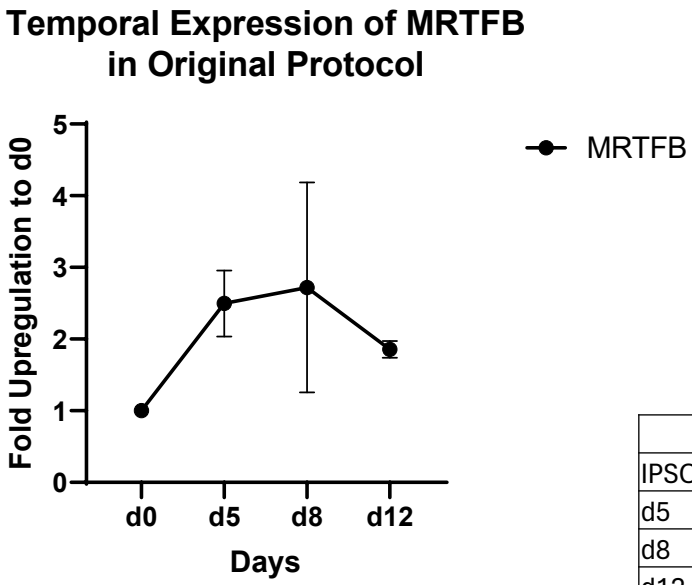
A- IPSCS transduced with 43ul or 86ul of CMV-GFP virus supernatant show increased GFP expression upon addition of polybrene. Further, adding a spin after transduction for 1 minute at 200g further increased GFP signal in the low virus condition. Images were taken at 10X and stitched to overview whole well.

B- Number of nuclei remaining after polybrene (5ug/ml) exposure at either 6 or 20 hours. (n=1 biological replicate)

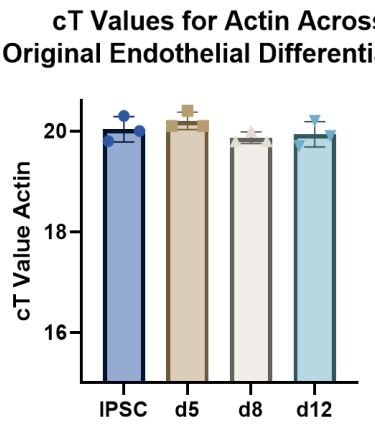
A







B



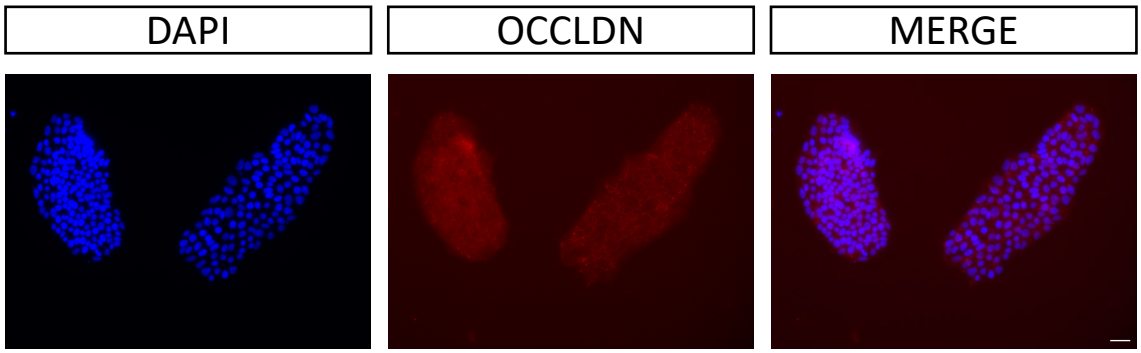
	1	2	3	St Dev
IPSC	20.3	19.8	20	0.251661
d5	20.4	20.1	20.1	0.173205
d8	19.8	20	19.8	0.11547
d12	19.9	19.7	20.2	0.251661

Supplementary Figure 1.5 – Endogenous RNA Expression Throughout Original BMEC Differentiation Protocol

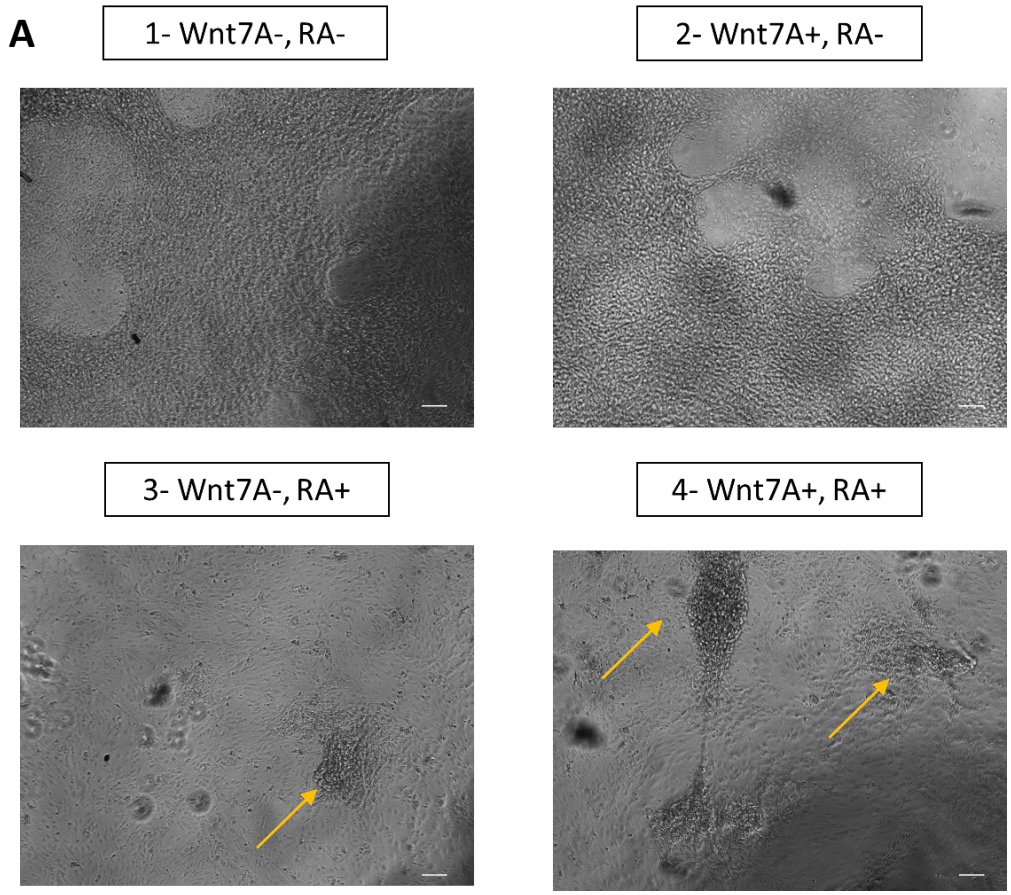
A- RNA obtained from different timepoints indicate that the protocol drastically upregulates LEF1 throughout the differentiation (d5,45.43+/-32.61, d8, 43.13+/- 5.20, d12, 53.78+/-20.13). On the other hand, ETS1 expression is reduced at the mesodermal stage (d5, 0.075+/-0.056), before spiking up during endothelial specification (d8, 8.01+/-4.96 and d12, 4.70+/-3.64). MRTFB is upregulated slightly upon differentiation to mesoderm (d5, 2.50+/- 0.46) and remains well expressed through the rest of the protocol (d8, 2.72+/- 1.46 and d12, 1.86+/- 0.12). (Values indicate average fold upregulation in comparison to day 0 +/- S.D. n=3 biological replicates, 3 technical replicates each)

B- cT values of housekeeping gene β-Actin demonstrating no significant changes in expression through the differentiation. (n=3 biological replicates)

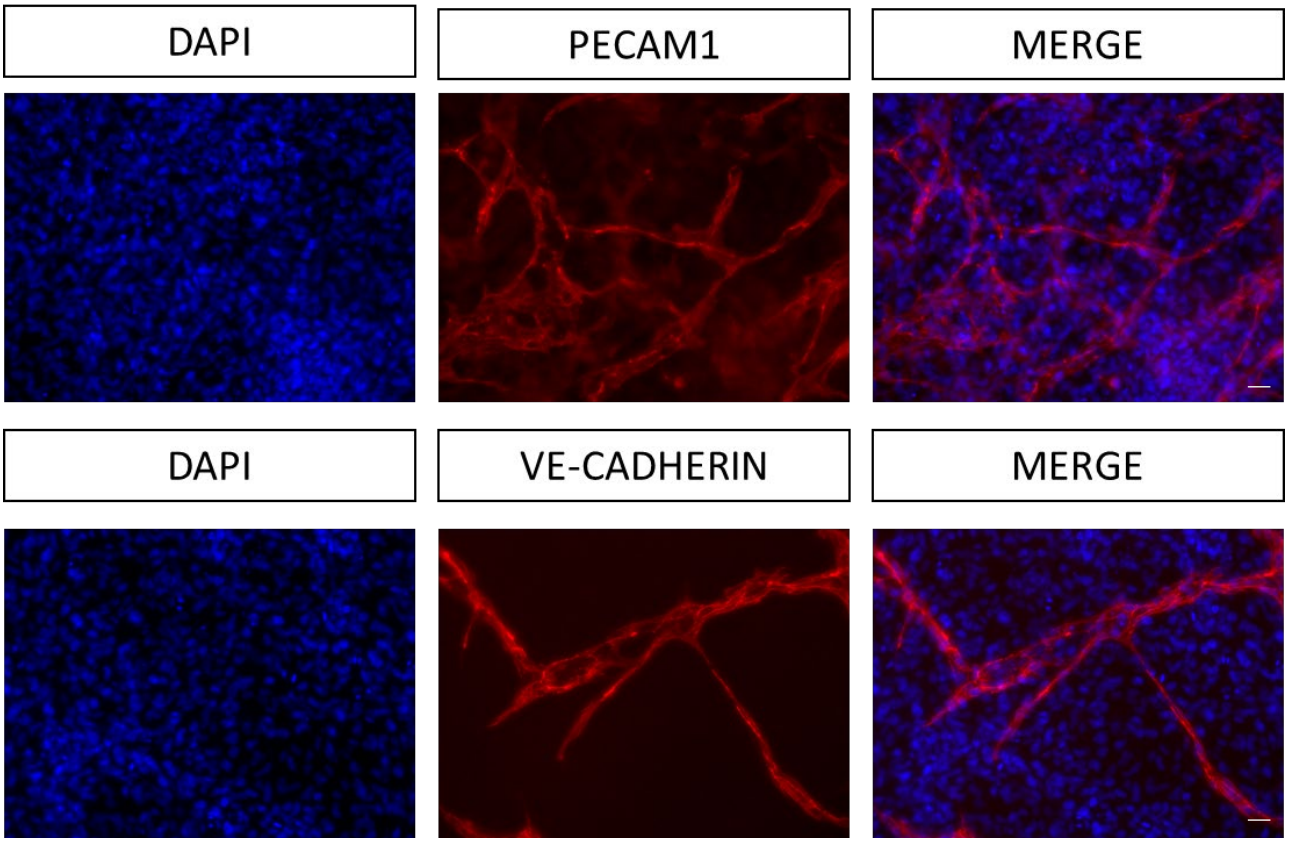
A



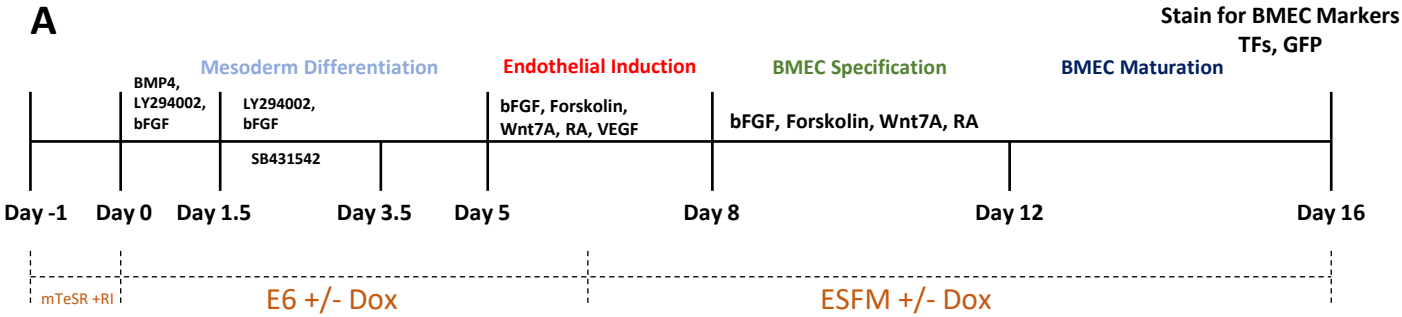
Supplementary Figure 1.6 – Endogenous OCCLDN Expression in immature IPSCs. Scale bar, 50um. (n=1 biological replicate)

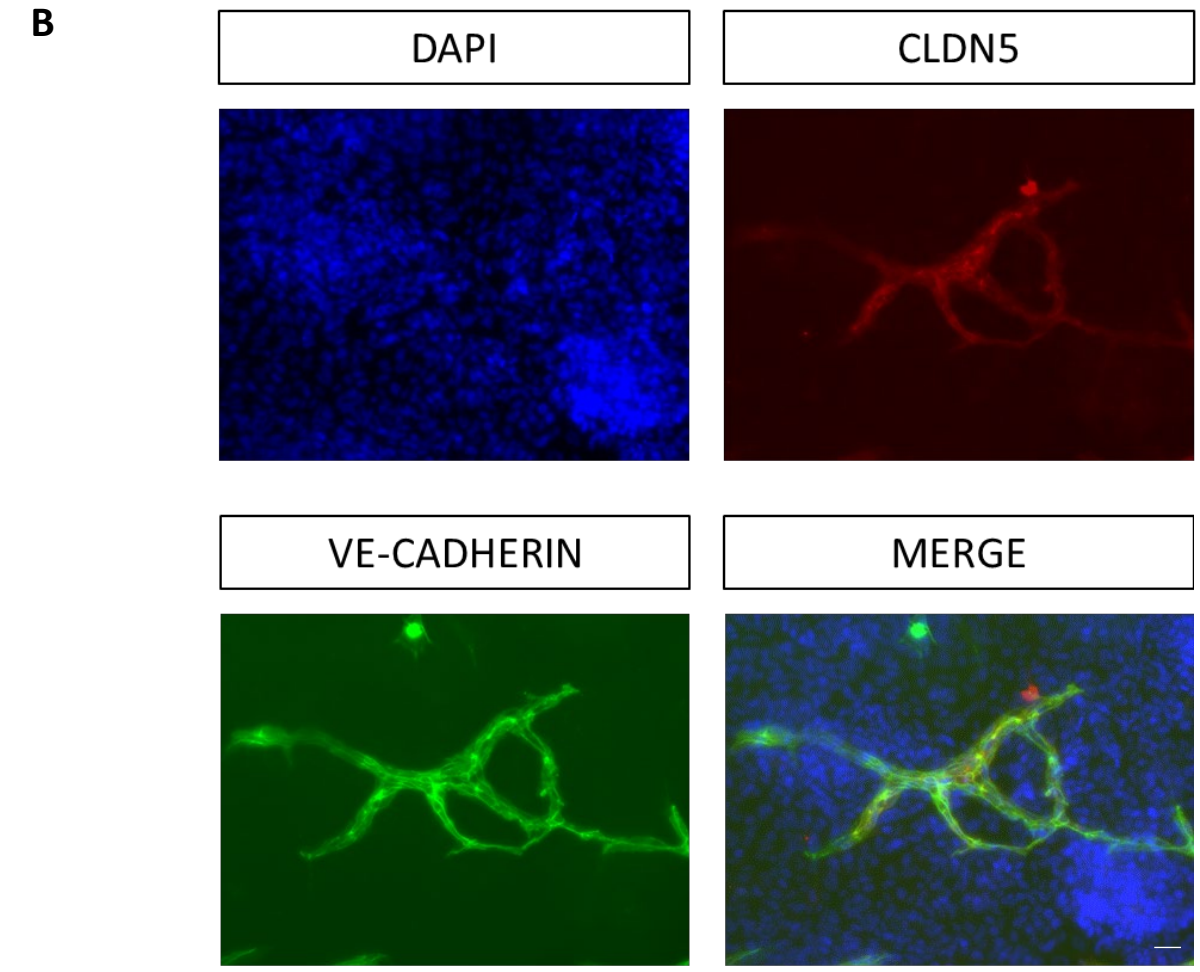


Supplementary Figure 1.7 – RA changes layer formation of BMEC differentiation
A – Phase contrast images of clumps formed by day 8 of BMEC differentiation. Cultures without RA were unable to form clumps and resulted in overcrowded cultures composed of two separate layers. Upon addition of RA (medias 3 and 4) the culture flattens to a single layer with clumps spread throughout. Scale bars, 50um. (n=2 biological replicates)

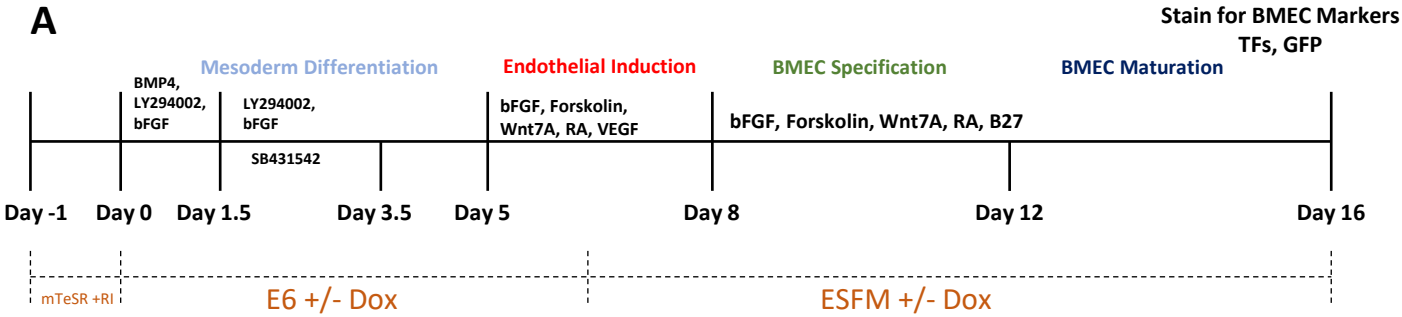


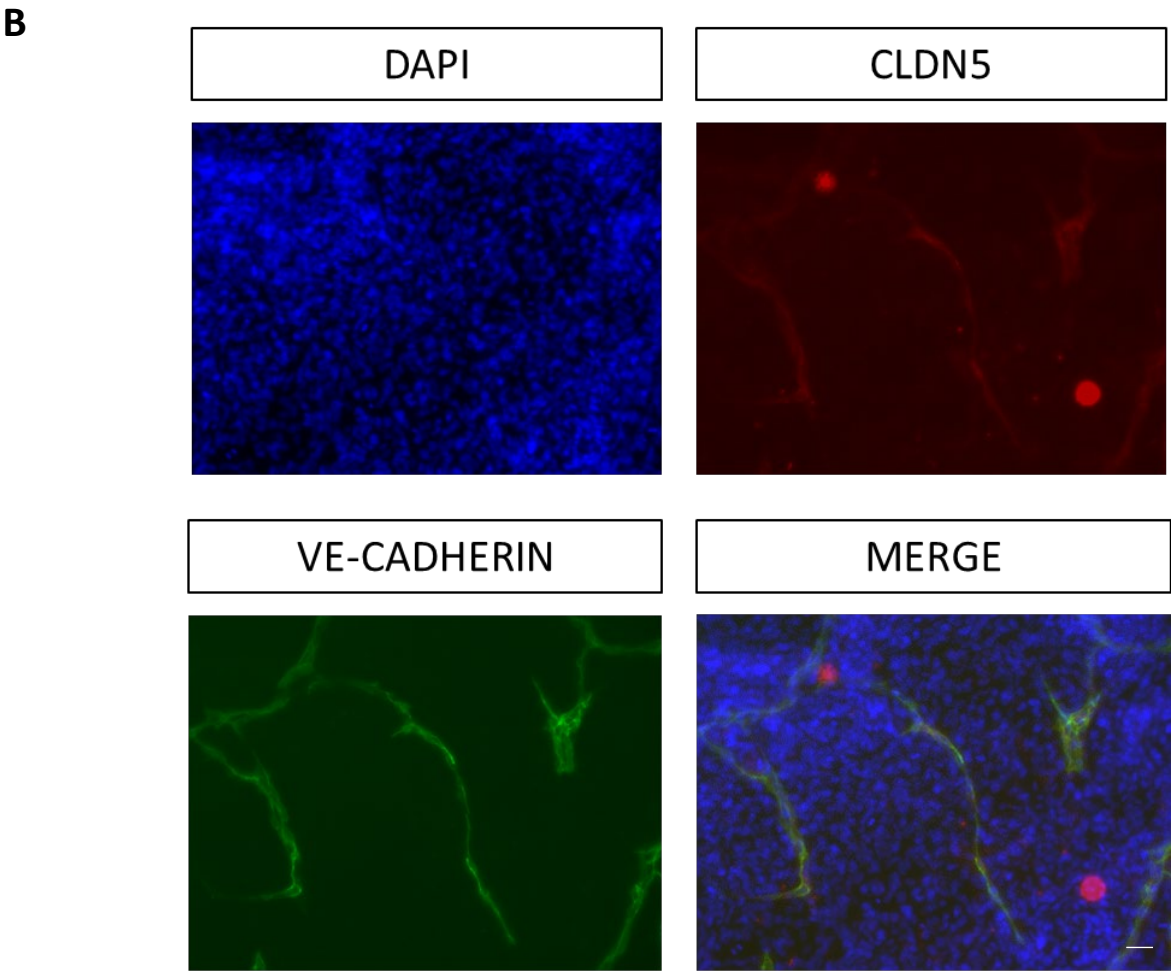
Supplementary Figure 1.8 – Single cells separated from clumps ay day 8 do not form a homogenous monolayer of differentiated BMEC cells as indicated by PECAM1 and VE-CADHERIN expression. Scale bars, 50um. (n= 2 biological replicates)



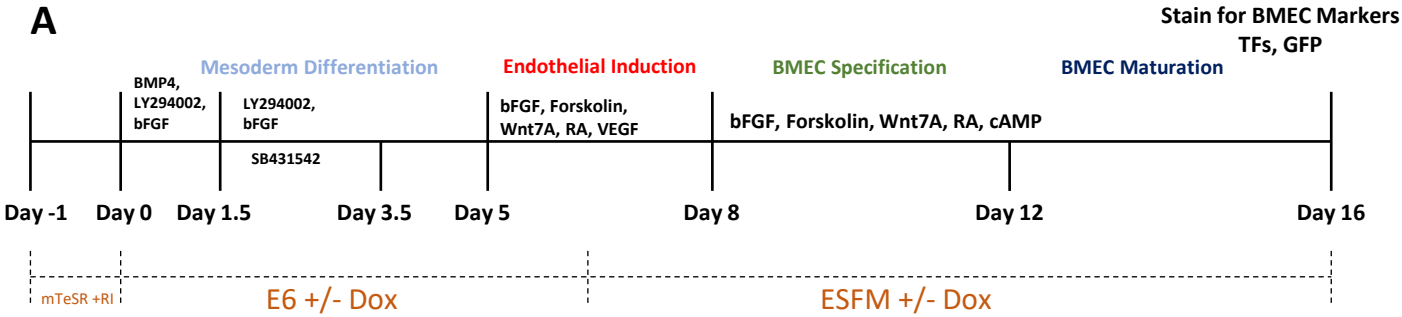


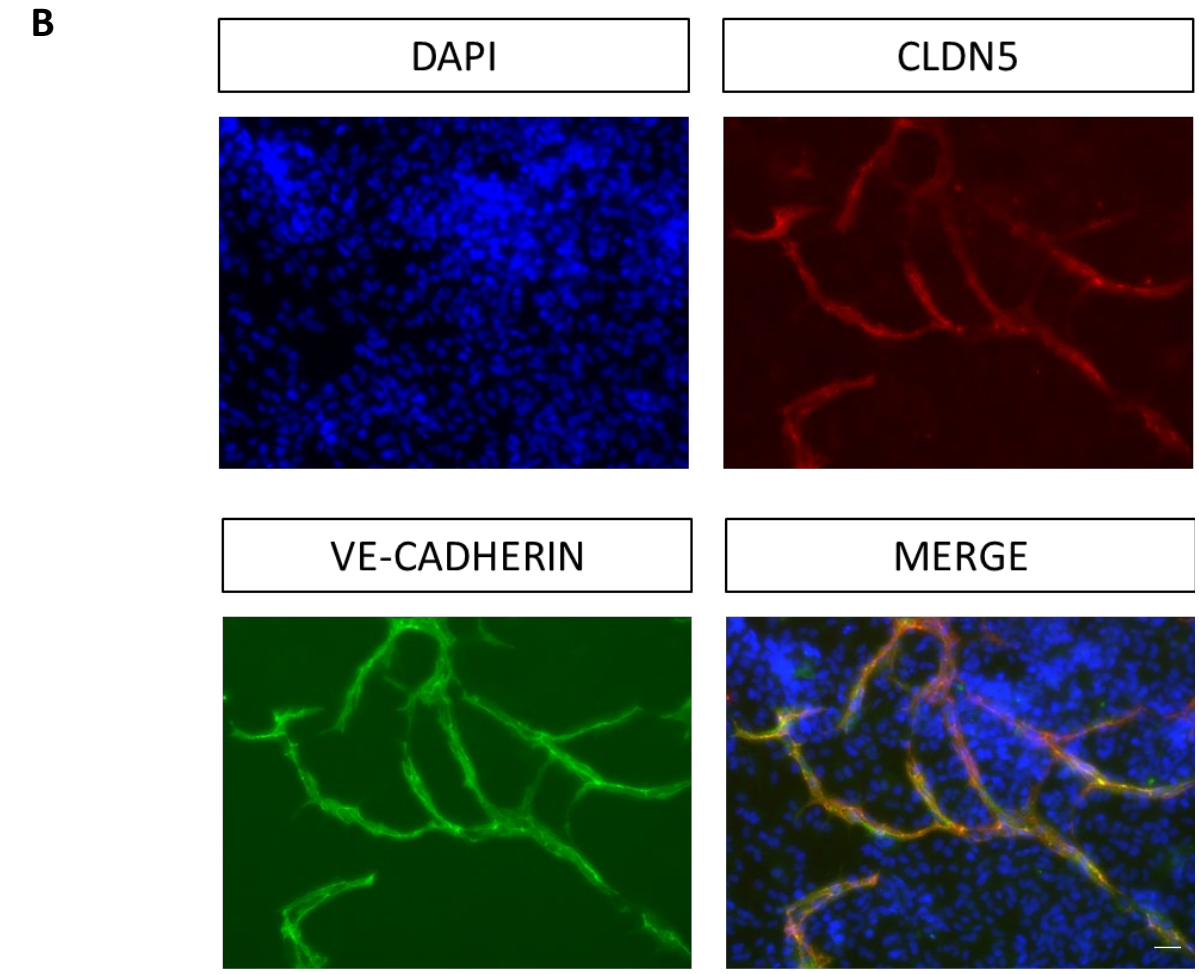
Supplementary Figure 1.9 – Further Optimizations to Endothelial Maturation (Control media)
A-Schematic of protocol used
B- Immunocytochemistry of CLDN5 and VE-CADHERIN for control media (no additives). Despite low endothelial enrichment, BMEC cells express CLDN5 and VE-CADHERIN. Scale bars, 50um. (n=2 biological replicates)



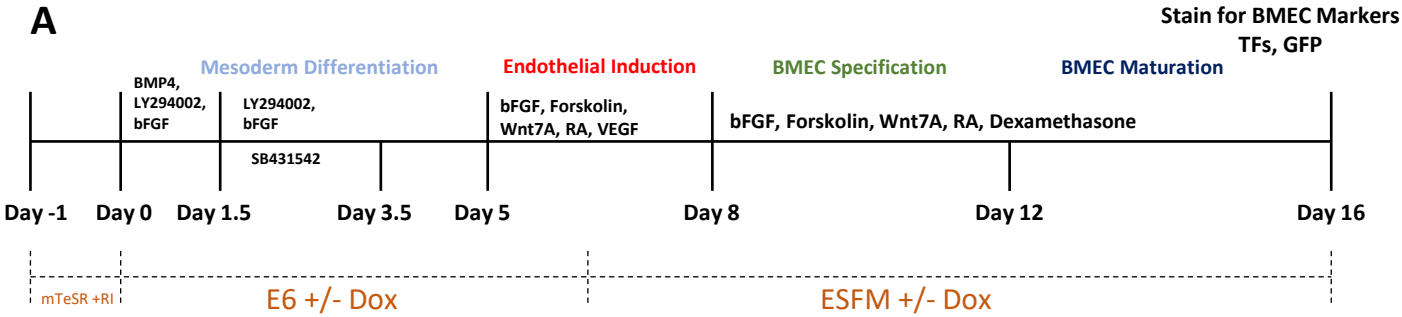


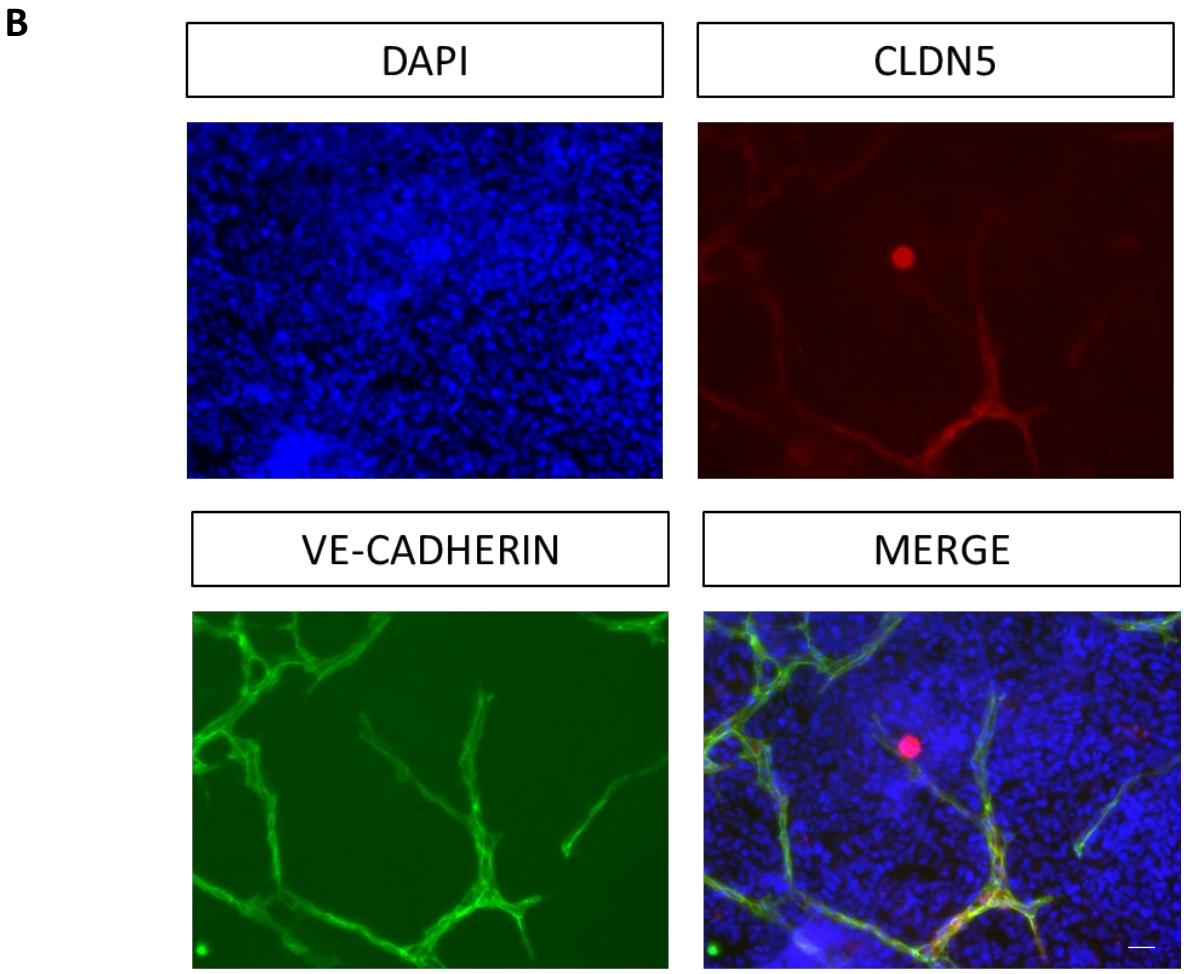
Supplementary Figure 1.10 – Further Optimizations to Endothelial Maturation (B27)
A-Schematic of protocol used
B- Immunocytochemistry of CLDN5 and VE-CADHERIN for media including B27. Despite low endothelial enrichment, BMEC cells express CLDN5 (albeit, at a reduced expression compared to other conditions) and VE-CADHERIN. Scale bars, 50um. (n=2 biological replicates)



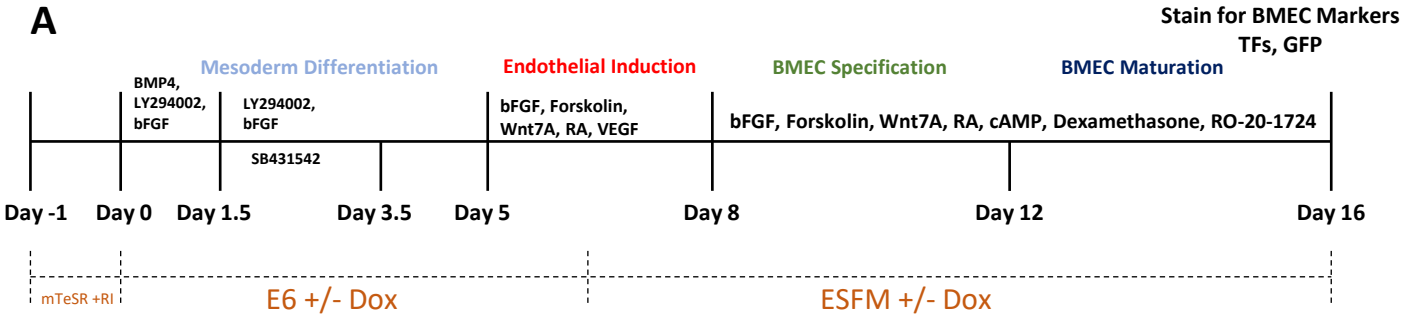


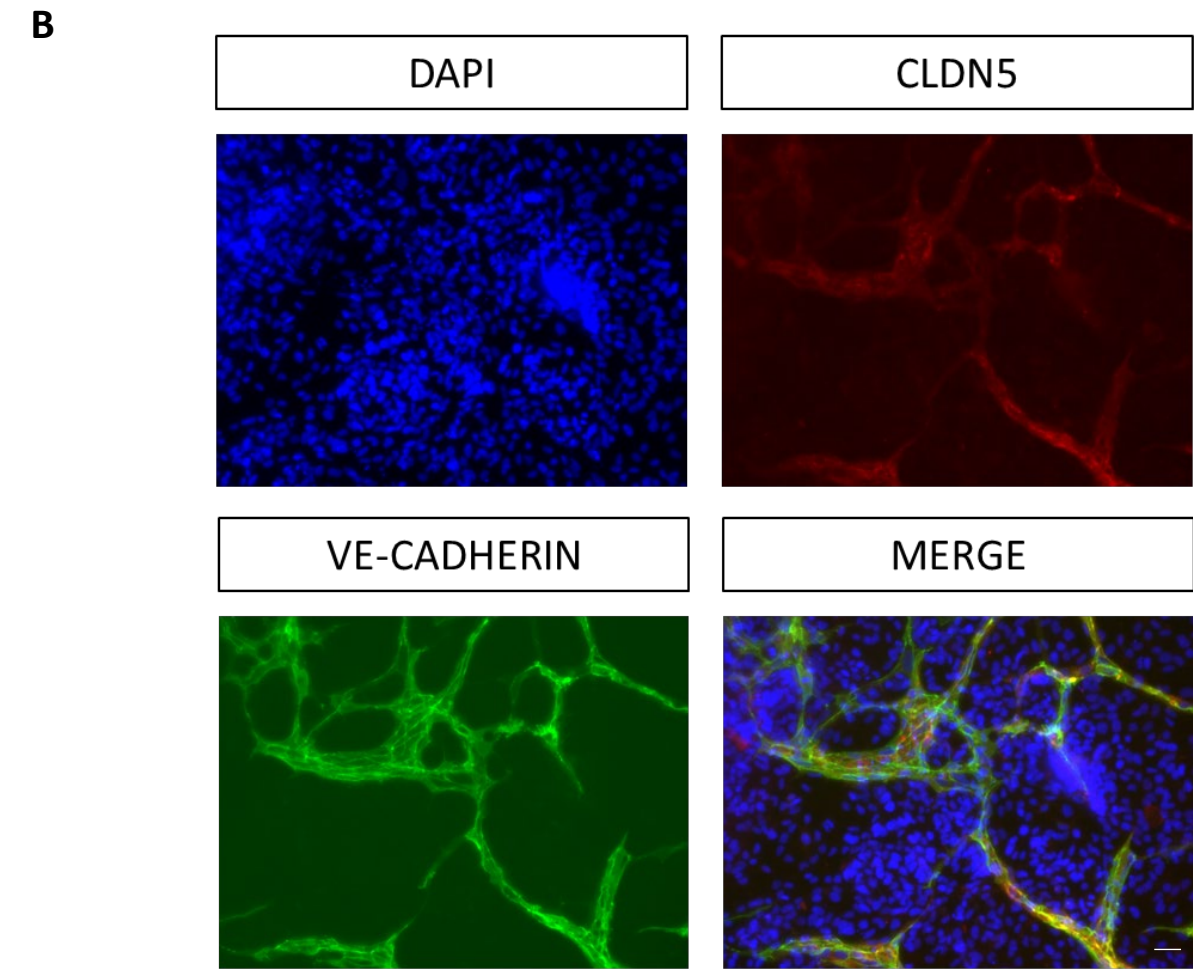
Supplementary Figure 1.11 – Further Optimizations to Endothelial Maturation (cAMP)
A-Schematic of protocol used
B- Immunocytochemistry of CLDN5 and VE-CADHERIN for media including cAMP. Despite low endothelial enrichment, BMEC cells express CLDN5 and VE-CADHERIN. Scale bar, 50um. (n=2 biological replicates)





Supplementary Figure 1.12 – Further Optimizations to Endothelial Maturation (Dexamethasone)
A-Schematic of protocol used
B- Immunocytochemistry of CLDN5 and VE-CADHERIN for media including dexamethasone. Despite low endothelial enrichment, BMEC cells express CLDN5 and VE-CADHERIN. Scale bars, 50um. (n=2 biological replicates)





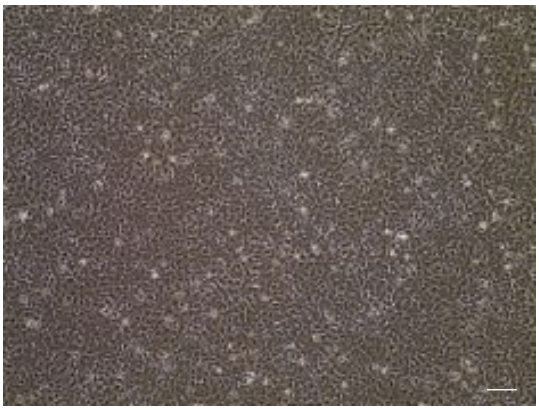
Supplementary Figure 1.13 – Further Optimizations to Endothelial Maturation (cAMP, dexamethasone, RO-20-1724

A-Schematic of protocol used

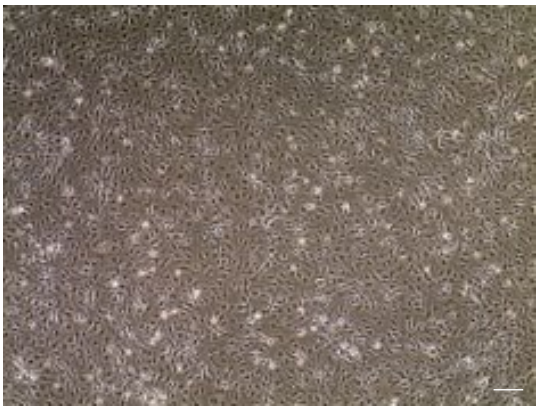
B- Immunocytochemistry of CLDN5 and VE-CADHERIN for media 4 including cAMP, Dexamethasone, and RO-20-1724. Despite low endothelial enrichment, BMEC cells express CLDN5 and VE-CADHERIN. Scale bars, 50um. (n=2 biological replicates)

.

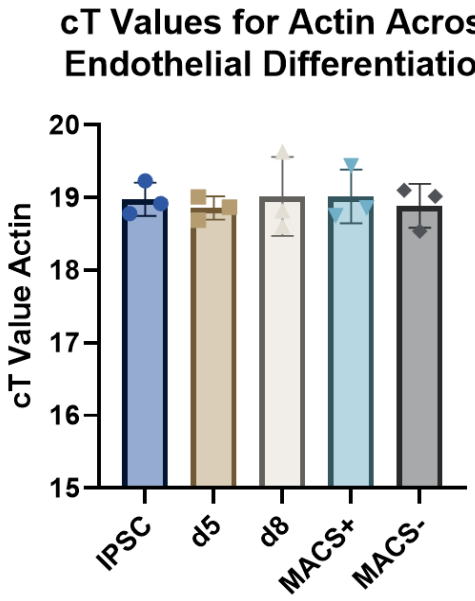
MACS VE-CADHERIN-



MACS VE-CADHERIN+



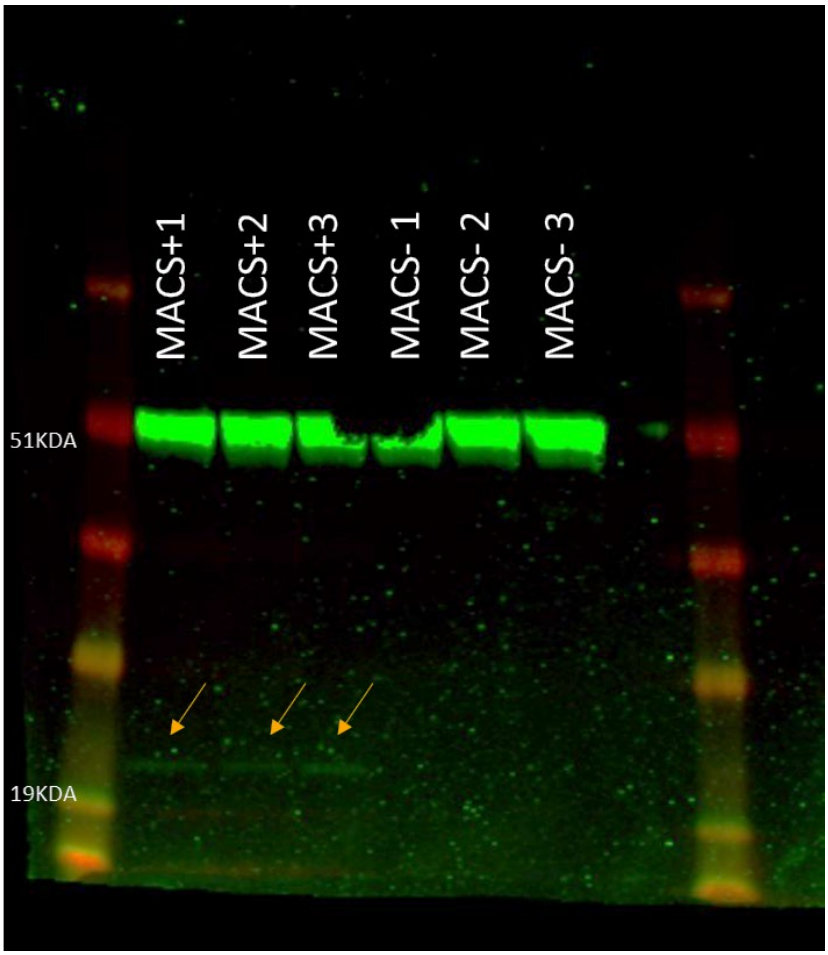
Supplementary Figure 1.14 – Phase images of MACS separation.
Cells on left panel represent the negative fraction that were not stained with VE-CADHERIN during separation process. Cells in right panel represent positive fraction of cells stained with VE-CADHERIN. Cells in VE-CADHERIN+ panel show a distinct morphological difference from VE-CADHERIN-, depicting an elongated cell body, whereas VE-CADHERIN- cells show a compact shape. (n=3 biological replicates)



	Diff1	Diff2	Diff3	St Dev
IPSC	18.78	19.23	18.92	0.23029
d5	19.01	18.87	18.69	0.160416
d8	18.6	19.63	18.82	0.542433
MACS+	18.86	18.75	19.44	0.37072
MACS-	18.54	19.02	19.1	0.302875

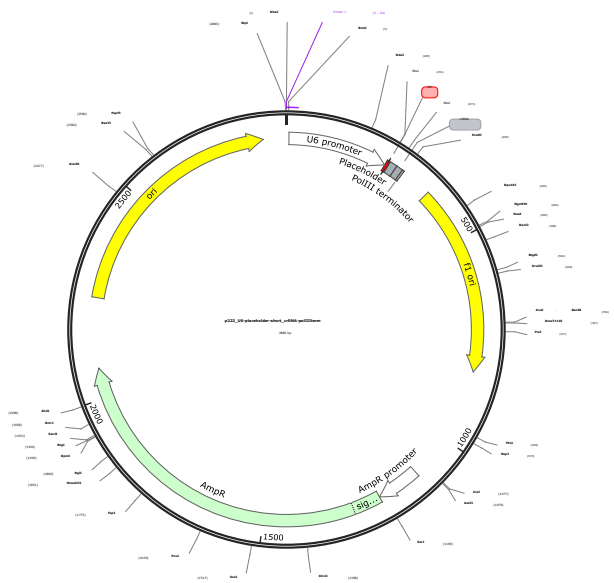
Supplementary Figure 1.15 –cT Values for β-Actin Throughout Differentiation Protocol

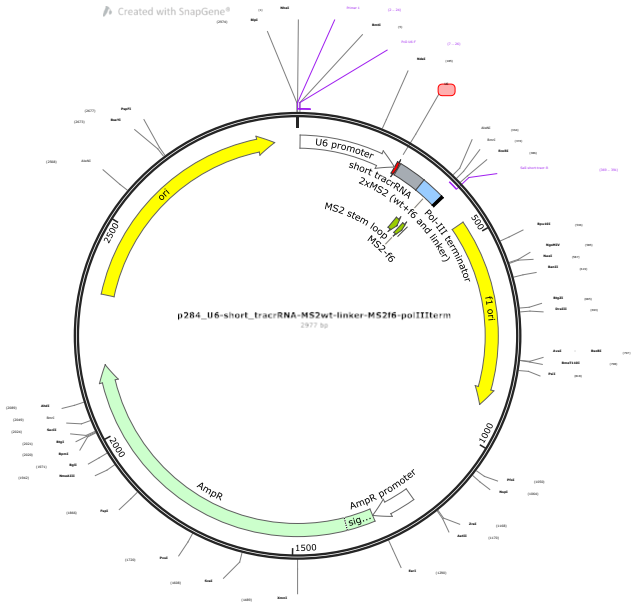
cT values for β-Actin do not significantly change as IPSCs differentiate towards an endothelial (or non-endothelial) fate, warranting Actin as a suitable housekeeping gene. (n=3 biological replicates, with 3 technical replicates each)

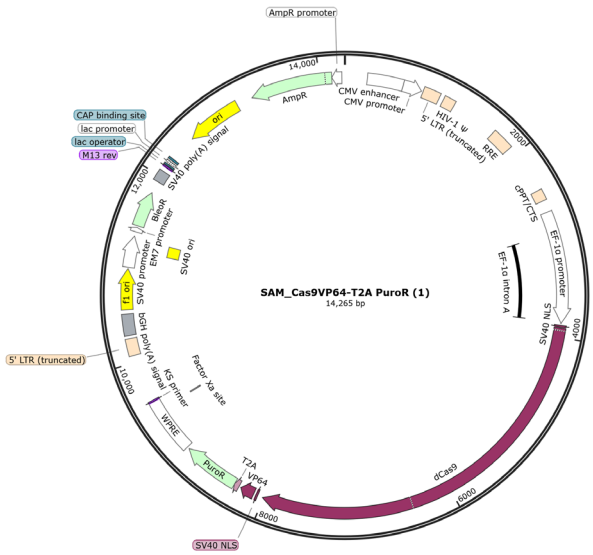


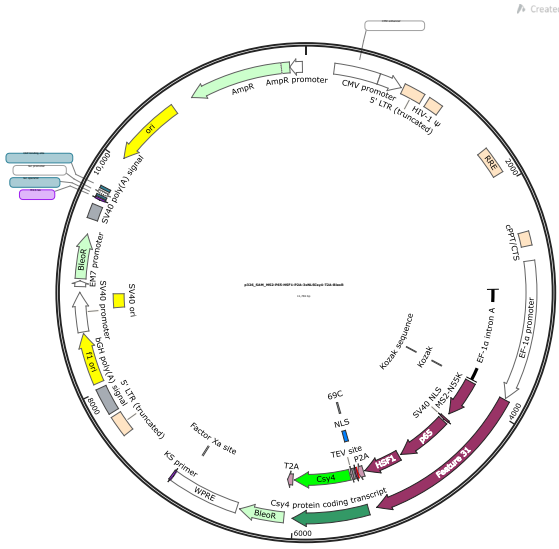
Supplementary Figure 1.16
A- Western Blot of CLDN5 in MACS+ and MACS- cultures. A faint band shows up in MACS+ lanes but not MACS-. Each lane is a separate biological replicate (n=3). Green band at 51kDa represents expression of housekeeping gene b-Actin. Faint green bands at 22kDa represent CLDN5 expression. (n=1 biological replicate)

Supplementary Figures – Chapter 2



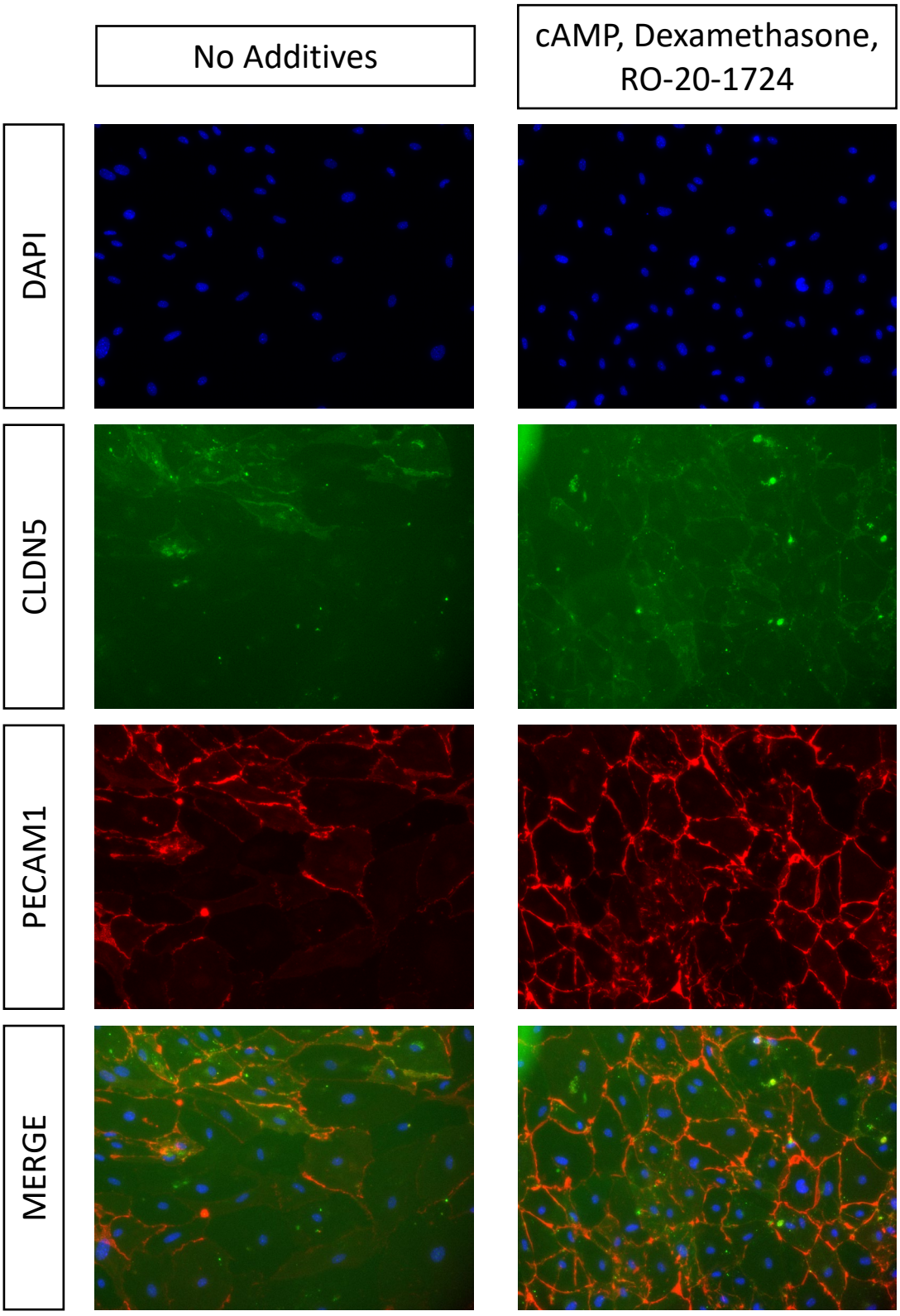




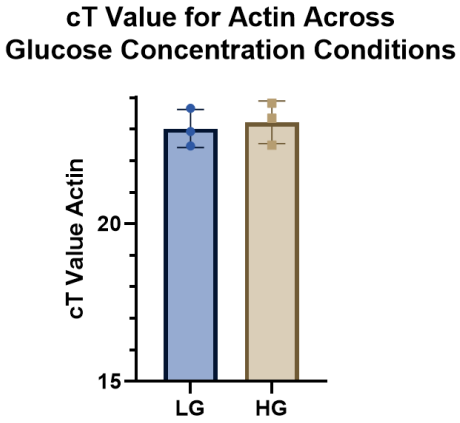


Supplementary Figure 2.1 – Plasmid maps of CRISPRa components.
P222_U6_Placeholder_crRNA-polIIIterm serves as the backbone to insert custom gRNAs for optimization experiments (top left)
P284_U6-short_tracrRNA-MS2wt-linker-MS2f6-polIIIterm codes for scaffold proteins for optimization experiments (top right)
SAM_Cas9VP64-T2A PuroR codes for dCAS9 and activator protein VP64 (bottom left)
P326_SAM_MS2-HSF1-P2A-3xNLSCCsy4-T2A-BleoR codes for SAM proteins for increased gene activation (bottom right)

Supplementary Figures – Chapter 3



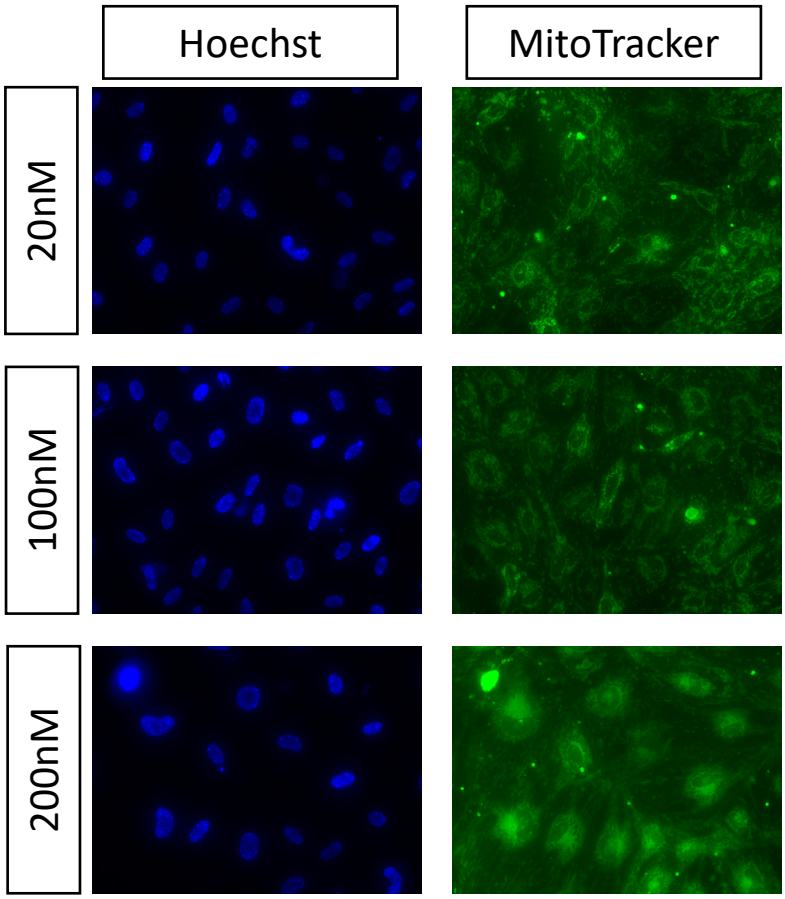
Supplementary Figure 3.1 Addition of cAMP, dexamethasone, and RO-20-1724 are imperative for murine brain endothelial cell marker expression
Immunocytochemistry for BMEC markers CLDN5 and PECAM1 show reduced staining without the added factors (n=1 biological replicate).



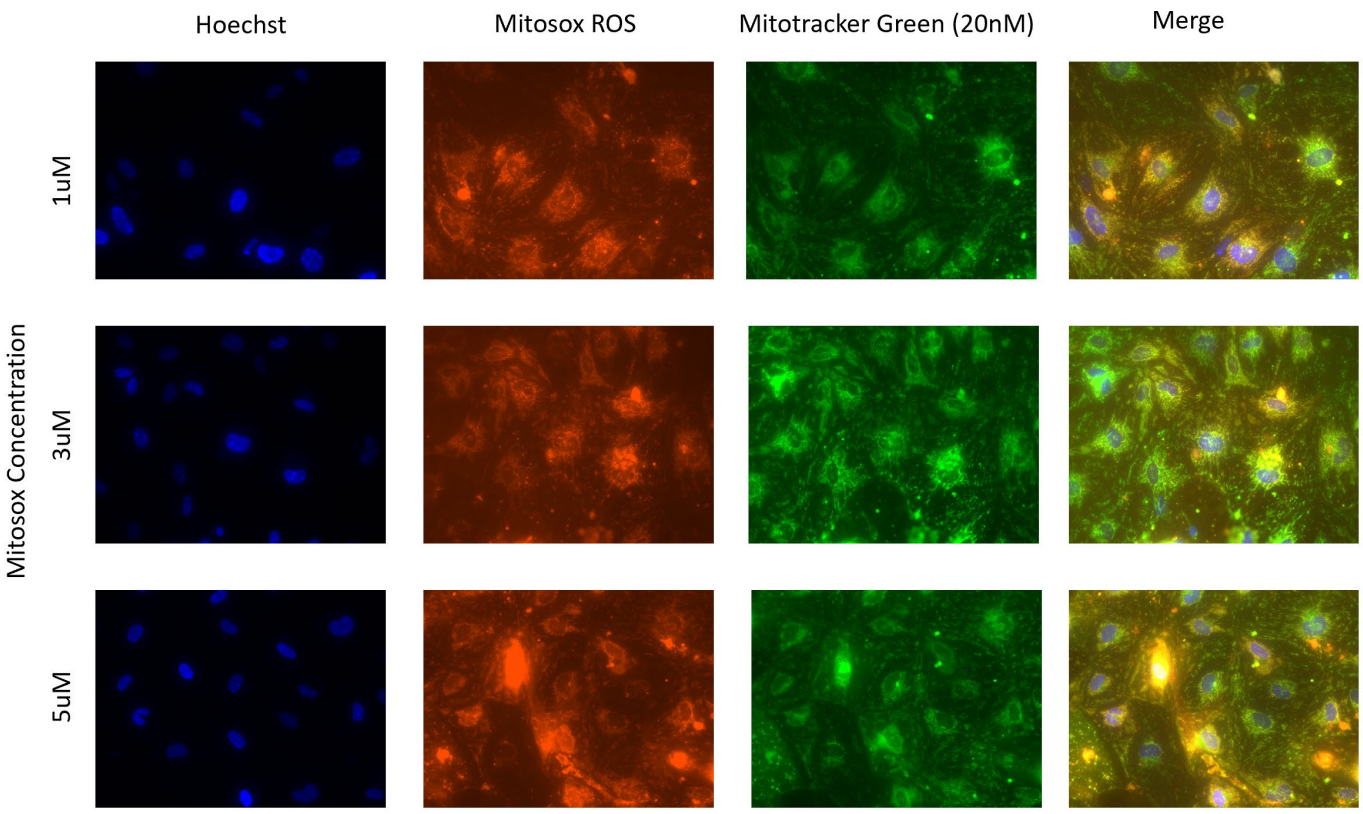
	1	2	3	St Dev
LG	23.66	22.47	22.92	0.60086
HG	23.82	22.49	23.34	0.673523

Supplementary Figure 3.2- cT Values for β-Actin Across Different Glycaemic Conditions

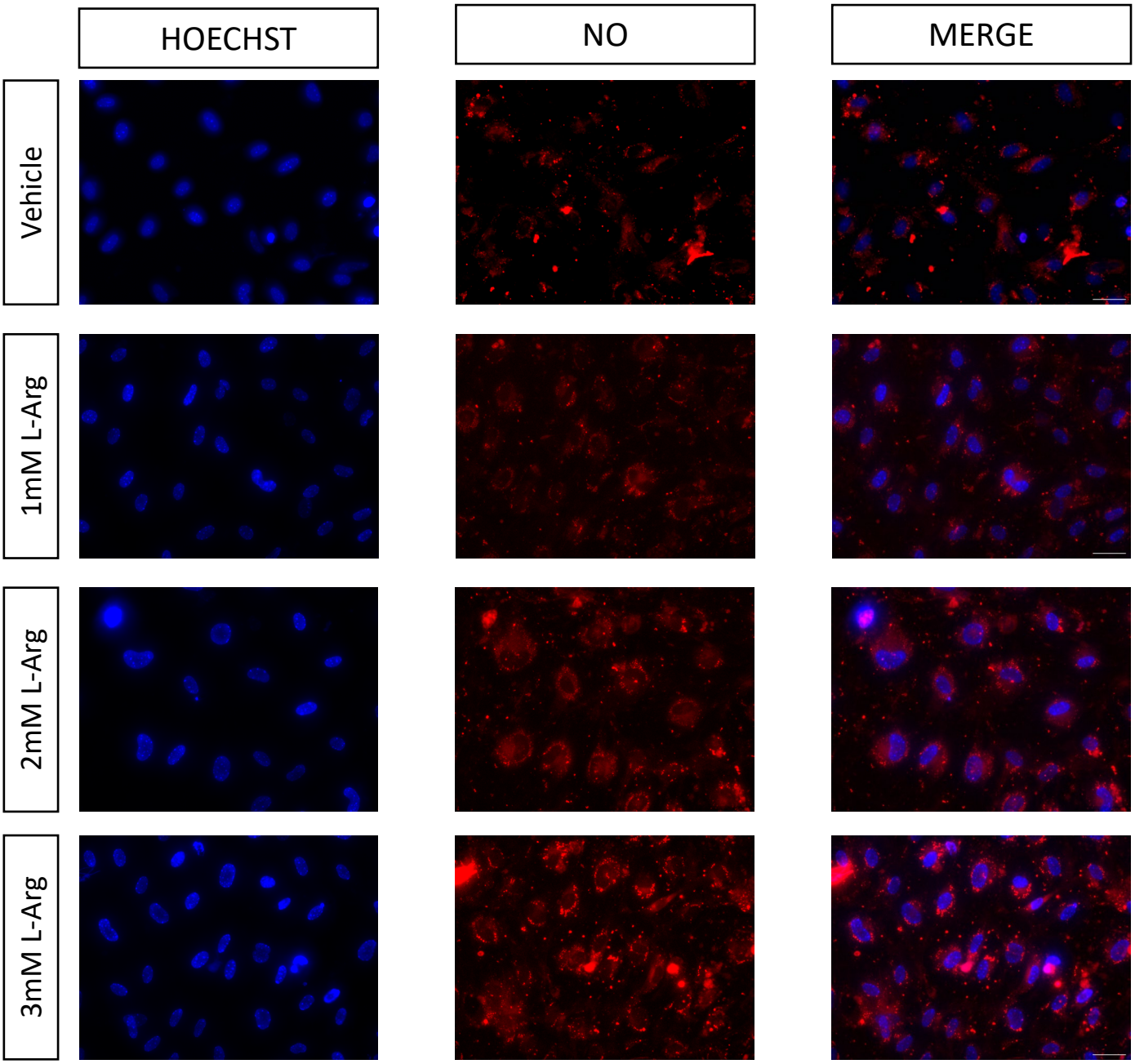
CT values for β-Actin do not significantly change when mouse endothelial cells are exposed to 5.5mM or 15mM glucose, warranting this housekeeping gene suitable for gene expression analysis (n=3 biological replicates, with 3 technical replicates each)

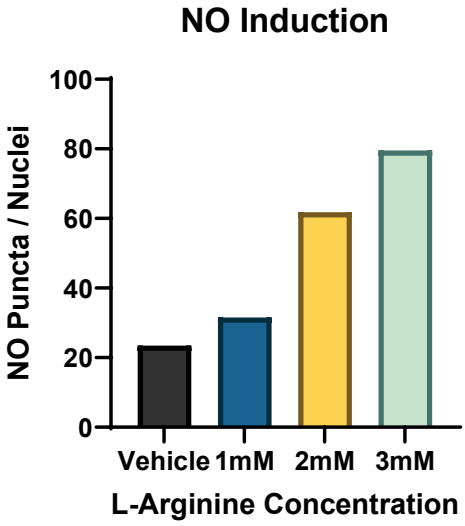


Supplementary Figure 3.3- MitoTracker Green Optimization
Murine brain endothelial cells given 20nM and 100nM MitoTracker show clear and distinct mitochondrial staining on cells' cytoplasm. Cells given 200nM MitoTracker show nuclei staining and diffuse cytoplasmic signal. (n=1 biological replicate)



Supplementary Figure 3.4- MitoSox Mitochondrial ROS Optimization
Murine brain endothelial cells given MitoSox at 1 and 3uM show distinct puncta that co-localizes with MitoTracker Green signal. Cells given MitoSox at 5uM start showing cellular toxicity via high-intensity signal in cells' nucleus. (n=1 biological replicate)

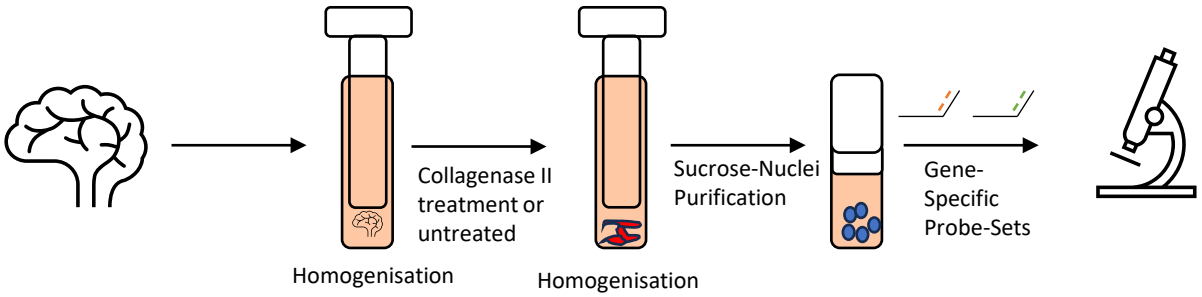


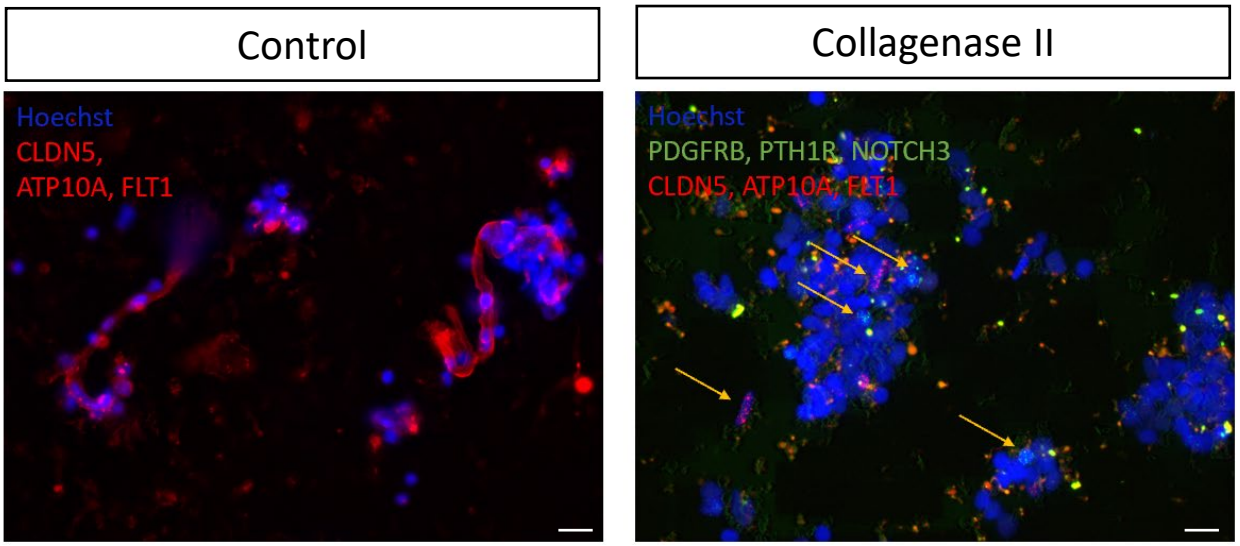


Supplementary Figure 3.5 – NO Assay optimization

Murine brain endothelial cells given vehicle, 1mM, 2mM, or 3mM L-Arginine show increased NO puncta counts/nuclei with increasing L-Arginine concentration. Scale bars=50um (n=1 biological replicate)

Supplementary Figures – Chapter 4

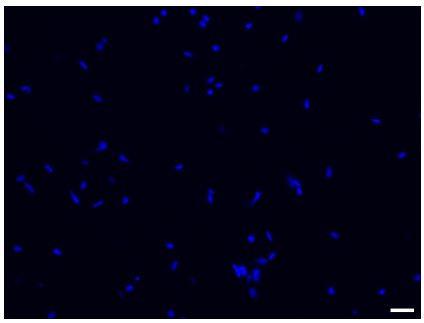




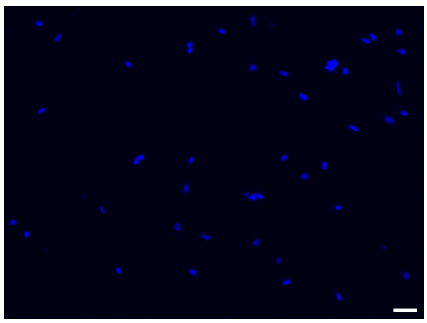
Supplementary Figure 4.1– Collagenase II Digestion Allows for Endothelial Nuclei Release
A- Experimental design of homogenisation followed by SABER-FISH staining
B- Control –vessels do not release nuclei and show staining for CLDN5, ATP10A, and FLT1 on vessel walls. Collagenase II – vessels digested for 15 minutes on ice followed by homogenisation allow for successful release of nuclei as evidenced by red nuclear staining of CLDN5, ATP10A, and FLT1, in absence of any vessel walls. Green nuclear staining represents pericyte nuclei stained by PDGFRB, PTH1B, and NOTCH3. Scale bar = 50um. (n=2 biological replicates)

VASCULAR			
NUCLEI	Total Nuclei Count	Total Individual Nuclei	% Clumped
Start of Fixation	66500	56080	15.6%
End of Fixation	36410	32240	11.4%
Retention	54.75%%	57.48%	

Start of Fixation

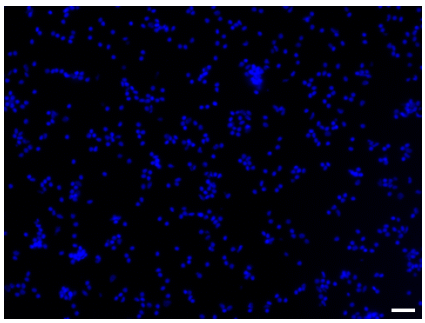


End of Fixation

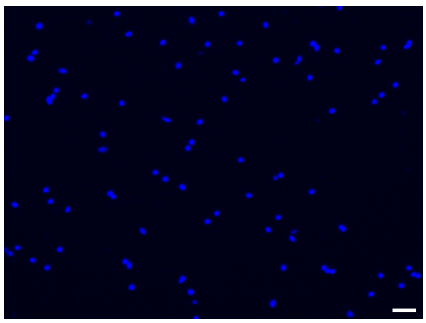


PARENCHYMA			
NUCLEI	Total Nuclei Count	Total Individual Nuclei	% Clumped
Start of Fixation	618730	438910	29%
End of Fixation	65330	58060	11.1%
Retention	10.55%	13.2%	

Start of Fixation

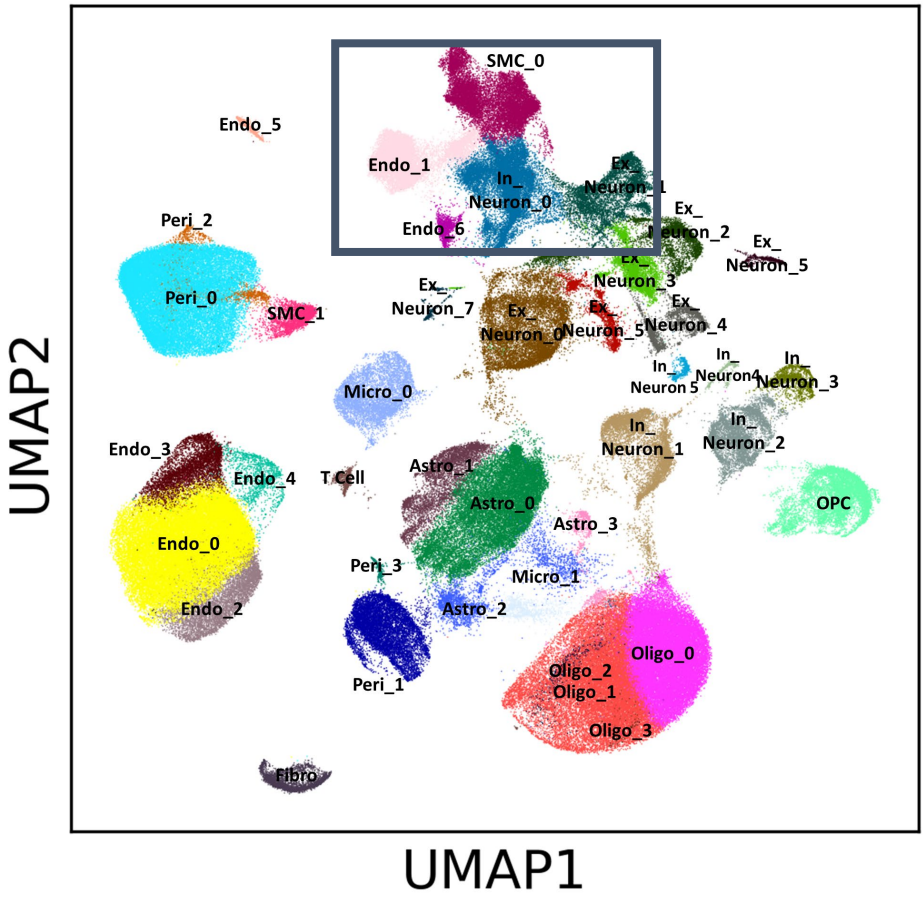


End of Fixation



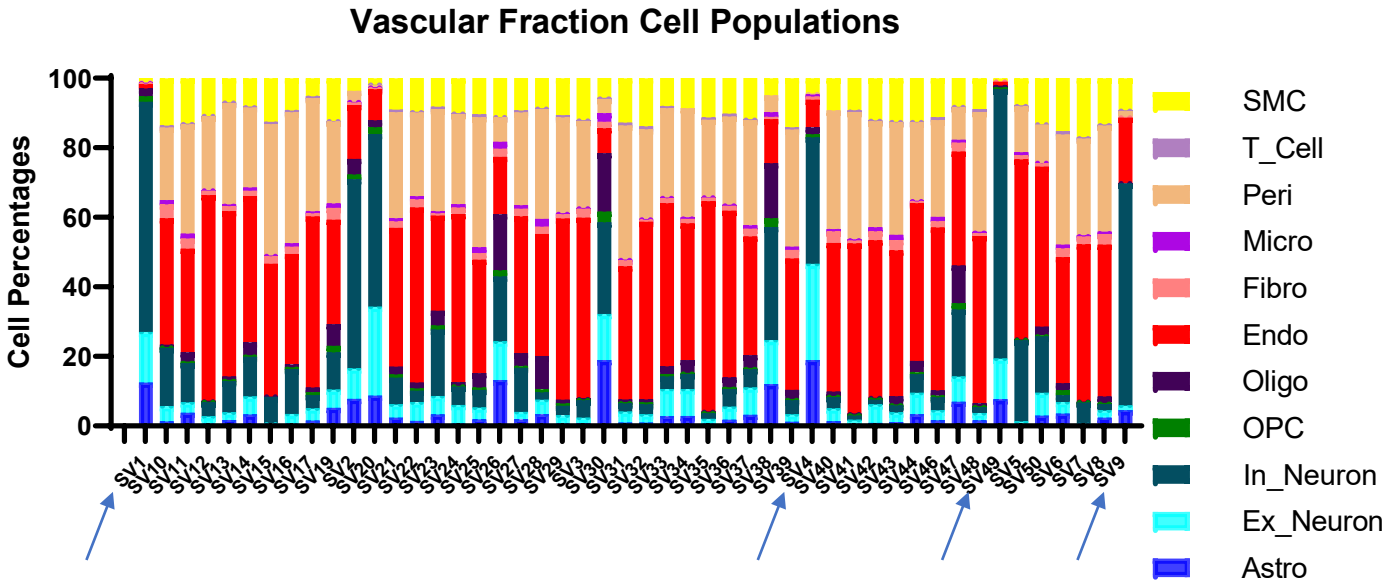
Supplementary Figure 4.2–Yield and Nuclei Clumping Quantification of Parse Fixation following Microvessel isolation protocol

Nuclei stained with DAPI for both vascular and parenchymal nuclei preparations following Parse fixation. Nuclei were counted using the EVOS automated counter, both with and without segregation of single nuclei from clumps to obtain counts counting clumps as 1 nuclei, or several. Vascular retention of individual nuclei (excluding clumps) was 57.58%, and 54.75% including clumps. Parenchymal retention of individual nuclei was 13.2% and 10.55% including clumps. Proportion of clumped nuclei in vascular fraction was 11.4%, while in parenchyma it was 11.1%. (n=1, scale bars = 50um)

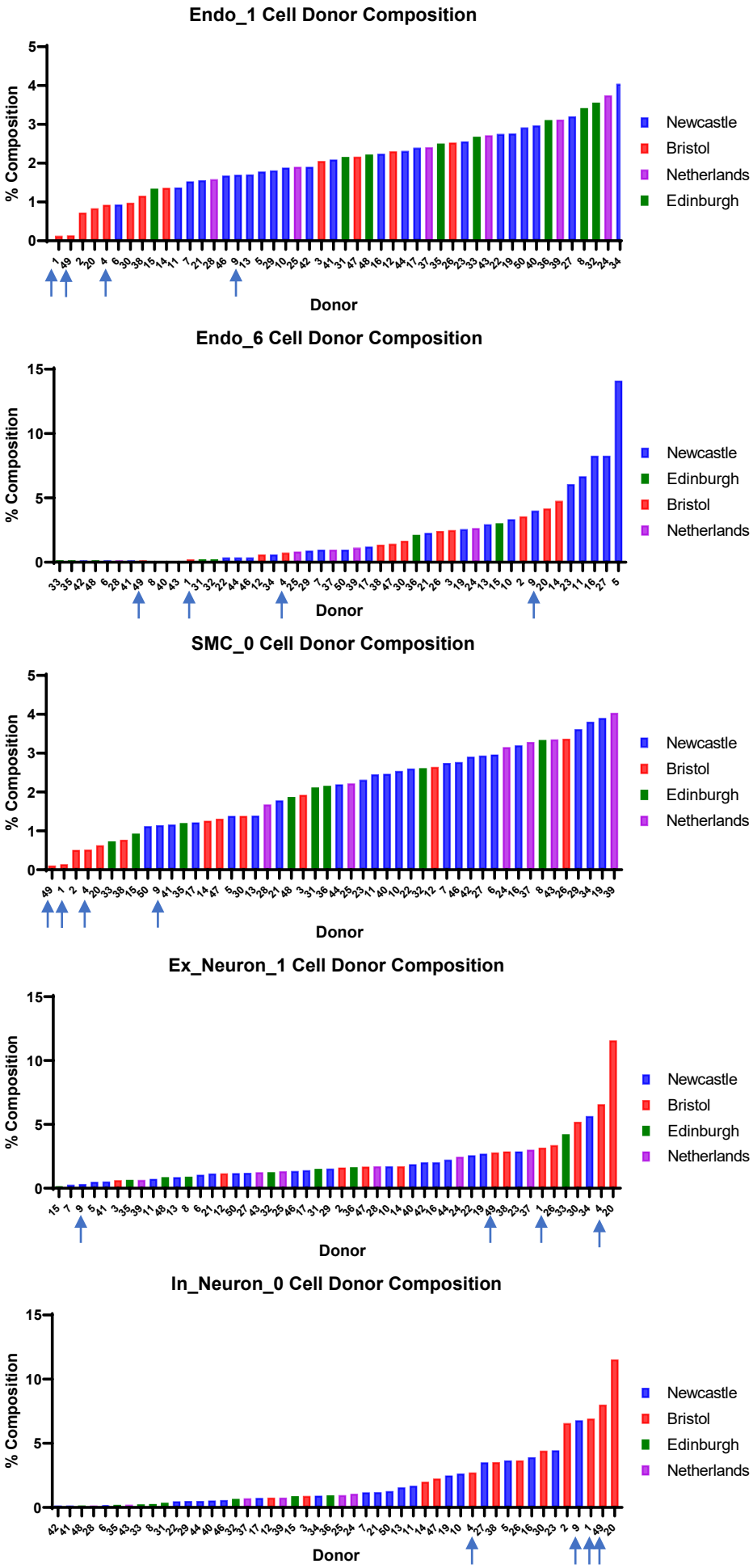


Supplementary Figure 4.3– Initial UMAP plot with annotations for all vascular and parenchymal samples across all samples.

11 cell types with 40 sub clusters were identified at a 1.0 resolution. Boxed clusters indicate cell identities with little annotation fidelity due to lack of specific marker expression.

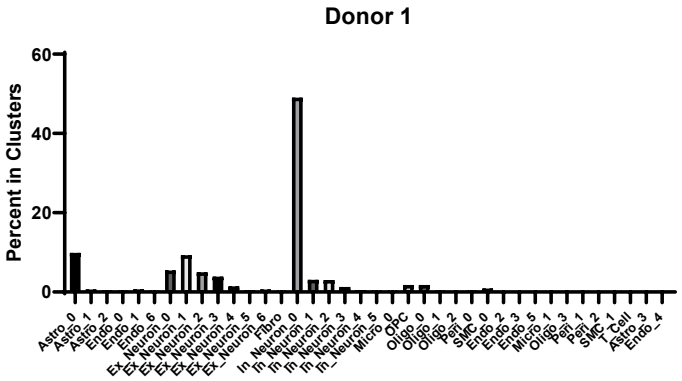


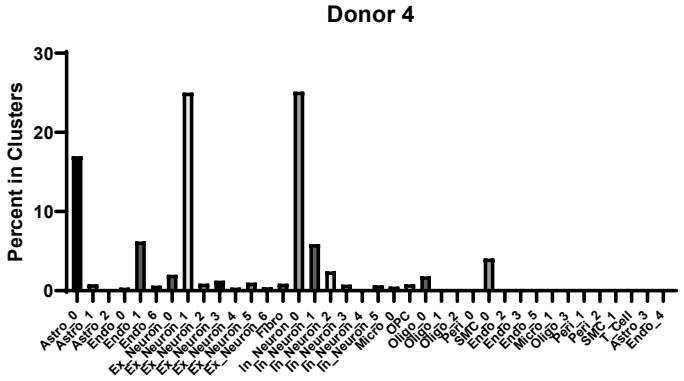
Supplementary Figure 4.4– Populational Analysis of identified cell types across all vascular compartments
Vascular samples were enriched with vascular cell types: endothelial cells, pericytes, and smooth muscle cells. 9 samples had an enrichment of less than 50% for vascular cell types, 4 of these being samples that did not pass QC (samples 1, 4, 9, and 49, denoted by arrows) (Figure 2.3).

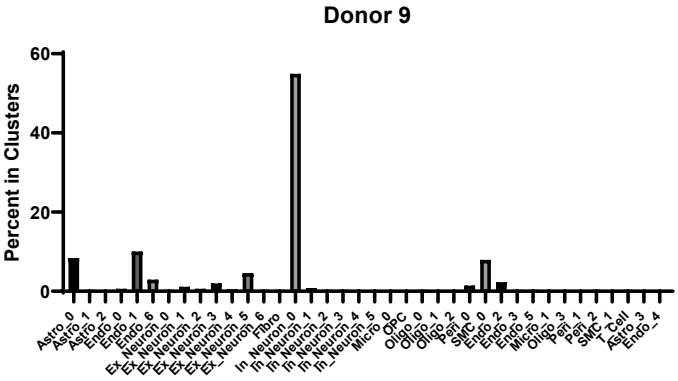


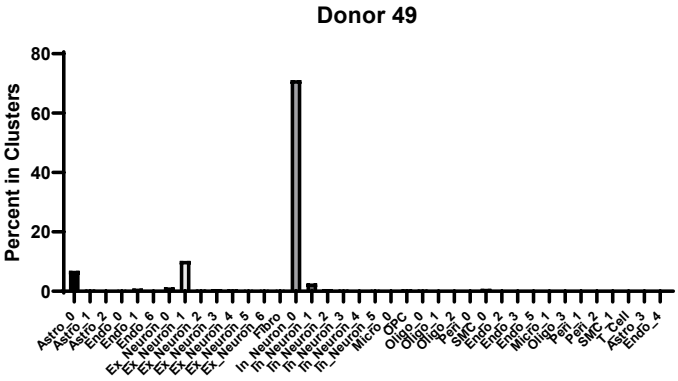
Supplementary Figure 4.5– Boxed Sub-cluster donor composition

Sub cluster endo_1, endo_6, and SMC_0 are not predominantly populated by 4 QC-failed samples. In the other hand, sub-cluster ex_neuron_1 has high proportion of nuclei arising from samples 1, 4, and 49 (12.87%). Sub cluster in_neuron_0 also shows high proportion (24.42%) of nuclei arising from all four QC-failed samples (1, 4, 9, 49).



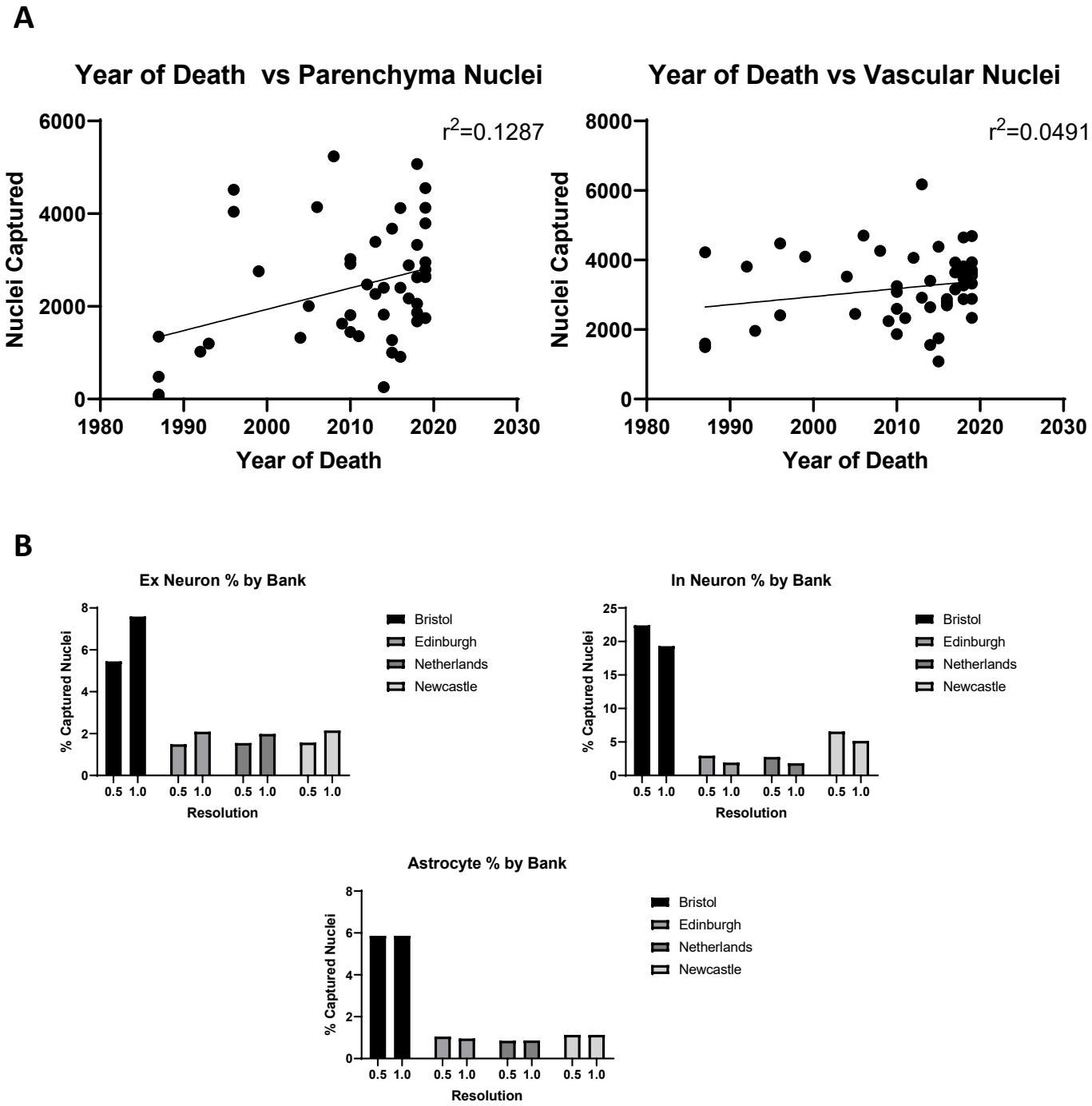






Supplementary Figure 4.6– QC-failed samples sub-cluster composition

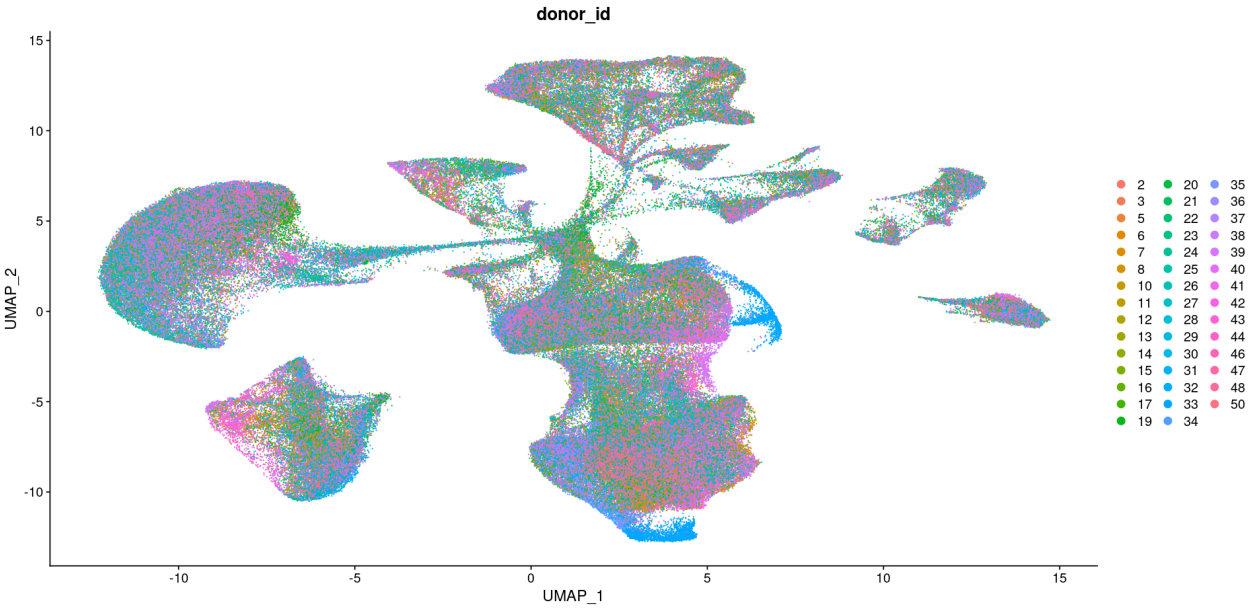
Proportion of nuclei from samples 1,4,9, and 49 show a high skew towards non-vascular clusters, indicating high contamination during nuclei preparations. Donors 1, 9, and 49 show high proportion of sequenced nuclei annotated to in_neuron_0 sub cluster, while donor 4 skewed towards in_neuron_0, ex_neuron_0, and astro_0.



Supplementary Figure 4.7– Year of Death and Brain Bank Effects on Sequencing and Annotation Quality

A- X/Y graph for parenchymal/vascular nuclei captured versus donor year of death. While recently-deceased (<15 years) tissues are prone to low parenchymal nuclei captured (<1500), samples retrieved from the 1990's had a considerably higher proportion of donors with low counts. There is no association between vascular nuclei captured and year of death.

B- Analysis of Ex-neuron, In_neuron, and astrocyte clusters in vascular compartment show high parenchymal contamination in the vascular compartment from samples sourced from Bristol brain bank.



Supplementary Figure 4.8 – No donor bias identified over UMAP plot